SANDIA REPORT

SAND2004-1057
Unlimited Release
Printed May 2004

Analytical Investigation of $AlCl_3/SO_2Cl_2$ Catholyte Materials for Secondary Fuze Reserve Batteries

T. J. Boyle, T. M. Alam, J. M. Segall, B. R. Cherry, D. R. Tallant, M. A. Rodriguez, M. Garcia, R. Simpson, L. A. Malizia, Jr., N. L. Andrews, D. Ingersoll, N. Clark, and P. Butler

Prepared by
Sandia National Laboratories
Albuquerque, New Mexico 87185 and Livermore, California 94550

Sandia is a multiprogram laboratory operated by Sandia Corporation,
a Lockheed Martin Company, for the United States Department of Energy's
National Nuclear Security Administration under Contract DE-AC04-94AL85000.

Sandia National Laboratories

Issued by Sandia National Laboratories, operated for the United States Department of Energy by Sandia Corporation.

Available to DOE and DOE contractors from
U.S. Department of Energy
Office of Scientific and Technical Information
P.O. Box 62
Oak Ridge, TN 37831

Telephone: (865)576-8401
Facsimile: (865)576-5728
E-Mail: reports@adonis.osti.gov
Online ordering: http://www.osti.gov/bridge

Available to the public from
U.S. Department of Commerce
National Technical Information Service
5285 Port Royal Rd
Springfield, VA 22161

Telephone: (800)553-6847
Facsimile: (703)605-6900
E-Mail: orders@ntis.fedworld.gov
Online order: http://www.ntis.gov/help/ordermethods.asp?loc=7-4-0#online

SAND2004-1057
Unlimited Release
Printed May 2004

Analytical Investigation of $AlCl_3/SO_2Cl_2$ Catholyte Materials for Secondary Fuze Reserve Batteries

Timothy J. Boyle[a], Nicholas L. Andrews
Chemical Synthesis and Nanoparticles

Todd M. Alam, Judith M. Segall, and Brian R. Cherry
Organic Materials Aging and Reliability

David R. Tallant, Mark A. Rodriguez, Manuel Garcia, and Regina Simpson
Materials Characterization

Louis A Malizia, Jr.
Long Life Power Sources

David Ingersoll
Lithium Battery Research and Development

Nancy Clark and Paul Butler
Power Source Engineering

Sandia National Laboratories
P. O. Box 5800
Albuquerque, NM 87185-1349

1. Abstract.

Exploration of the fundamental chemical behavior of the $AlCl_3/SO_2Cl_2$ catholyte system for the ARDEC Self-Destruct Fuze Reserve Battery Project under accelerated aging conditions was completed using a variety of analytical tools. Four different molecular species were identified in this solution, three of which are major. The relative concentrations of the molecular species formed were found to depend on aging time, initial concentrations, and storage temperature, with each variable affecting the kinetics and thermodynamics of this complex reaction system. We also evaluated the effect of water on the system, and determined that it does not play a role in dictating the observed molecular species present in solution. The first Al-containing species formed was identified as the dimer $[Al(\mu\text{-}Cl)Cl_2]_2$, and was found to be in equilibrium with the monomer, $AlCl_3$. The second species formed in the reaction scheme was identified by single crystal X-ray diffraction studies as $[Cl_2Al(\mu\text{-}O_2SCl)]_2$ (**1**), a scrambled $AlCl_3 \bullet SO_2$ adduct. The $SO_2(g)$ present, as well as $Cl_2(g)$, was formed through decomposition of SO_2Cl_2. The $SO_2(g)$ generated was readily consumed by $AlCl_3$ to form the adduct **1** which was experimentally verified when **1** was also isolated from the reaction of $SO_2(g)$ and $AlCl_3$. The third species found was tentatively identified as a compound having the general formula $\{[Al(O)Cl_2][OSCl_2]\}_n$. This was based on ^{27}Al NMR data that revealed a species with tetrahedrally coordinated Al metal centers with increased oxygen coordination and the fact that the precipitate, or gel, that forms over time was shown by Raman spectroscopic studies to possess a component that is consistent with $SOCl_2$. The precursor to the precipitate should have similar constituents, thus the assignment of $\{[Al(O)Cl_2][OSCl_2]\}_n$. The precipitate was further identified by solid state ^{27}Al MAS

NMR data to possess predominantly octahedral Al metal center which implies $\{[Al(O)Cl_2][OSCl_2]\}_n$ must undergo some internal rearrangements. A reaction sequence has been proposed to account for the various molecular species identified in this complex reaction mixture during the aging process.

The metallurgical welds were of high quality. These results were all visually determined there was no mechanical testing performed. However, it is recommended that the end plate geometry and weld be changed. If the present weld strength, based on .003" - .005" penetration, is sufficient for unit performance, the end plate thickness can be reduced to .005" instead of the .020" thickness. This will enable the plug to be stamped so that it can form a cap rather than a plug and solve existing problems and increase the amount of catholyte which may be beneficial to battery performance.

2. Table of Contents

List of Figures

Section 1. Catholyte Analytical Investigation

3. Introduction

In order to increase the probability for mission success as well as to decrease the quantity of unexploded ordinance remaining on the battlefield. a new generation of weapons is necessary. These weapons must be safer, smarter, more robust, and more reliable than current munitions. Of particular interest is the timely detonation of submunitions that typically consist of explosive-filled items designed for both offensive and defensive saturation of large areas. Examples of these include cluster bombs and grenades, whose initiation is controlled by their impact. Submunitions have a reliability requirement of greater than 95 %; however, field tests have shown the actual detonation yield to be substantially less. Part of the reason for these so-called "duds" (un-exploded submunitions) is the variable nature of the battlefield and its effect on the impact primer used (e.g., soft impacts into mud, snow, water, or entanglement with species such as tree branches) that prevent the orientation necessary for primer actuation.

Figure 1. Test results from grenades fired without and with secondary delay fuze (SDF).

The use of a secondary delay fuze (SDF) is one means for ensuring improved detonation yield, as illustrated in the case of the M915 Cartridge. In a typical test of M915 Cartridges (4200 M80 grenades - 42 per cartridge) without a secondary fuze, there

were 126 duds; however, when a secondary fuze was employed, there were only 8 such duds. This is seen by the data contained in Figure 1.

A battery is used to power a timer-drive that is used as the secondary fuze which consists for this system of a reserve lithium/aluminum chloride sulfuryl chloride ($AlCl_3/SO_2Cl_2$) catholyte, shown in Figure 2a . A catholyte is a material that acts as both cathode and electrolyte. As can be observed in Figure 2b, the battery in this setup is activated by breaking a glass plate at the bottom of the sealed ampule containing the $AlCl_3/SO_2Cl_2$ catholyte. Once released, the liquid is wicked into the active electrode area.

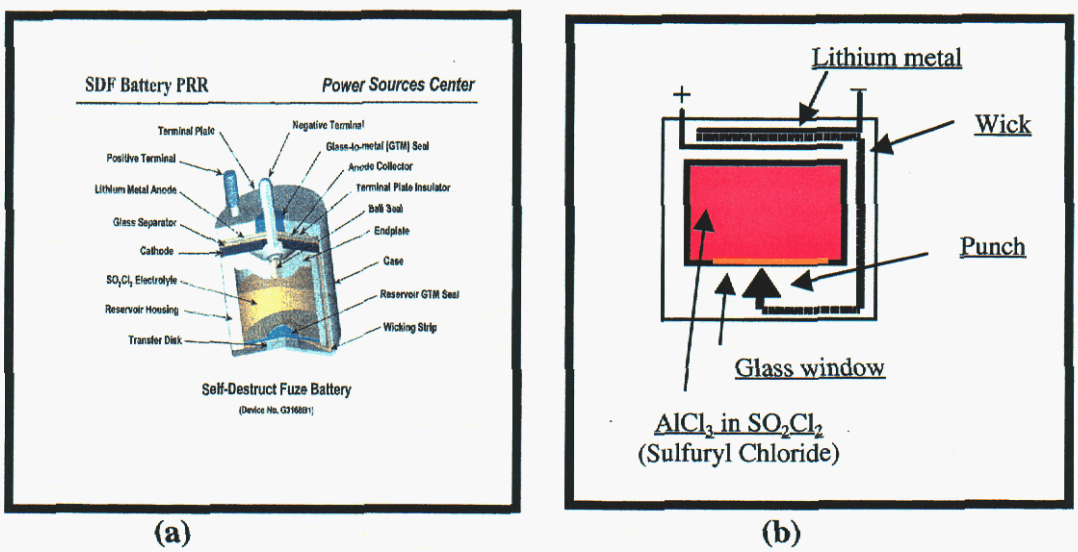

Figure 2. Schematic designs of the (a) KDI design and (b) simplistic diagram of component.

As a part of the constraints placed on this system, this battery must be able to function over a wide environmental temperature range, from temperatures as low as -50 °C to a high of +75 °C. In addition, there are severe long-term storage requirements of both time and temperature that must also be met. However, although the characteristics of $AlCl_3/SO_2Cl_2$ system and similar catholyte systems have been previously investigated[1-3] but the components of these systems have not been unequivocally identified nor have they been shown to be stable under the severe environmental constraints imposed here.

It is critical to understand the chemistry of this system since additional complicating factors concerning their long-term stability have arisen during fabrication. It was noticed that in large scale preparation several reservoirs of this catholyte formed precipitates or gels over time. Understanding the effect of this gel on the operation of the SDF battery is critical since their long-term life expectancy is 20 years. It is not possible to say *a priori* how the gel would affect battery performance, either in the activation stage or during operation when the diffusion coefficient of Li^+ may be drastically lowered. Therefore, it is necessary to understand the chemical changes that occur in this catholyte solution over time and temperature to understand the effect that these changes impart to catholyte. Since there were no literature studies available on the chemistry of this system, we undertook a series of analytical experiments to define the chemistry of this system. The following summarizes the information garnered concerning the catholyte system. Appendices A - H are monthly summaries detailing the advances made during the course of this investigation.

4. Experimental Section

All compounds described below were handled with rigorous exclusion of air and water using standard Schlenk line and glovebox techniques. The SO_2Cl_2 (MCB Reagents) and $AlCl_3$ (99.999 %, Aldrich) were handled under an argon atmosphere in a glovebox. Stock solutions of the standard catholyte were also received from KDI and handled under identical conditions. Solutions of $AlCl_3$ of varying concentrations were

prepared by both the dissolution of $AlCl_3$ in neat SO_2Cl_2 or by the addition of either $AlCl_3$ or SO_2Cl_2 to the KDI catholyte solution. Water was added via syringe to the appropriate samples.

4a. Instrumentation. All FT-IR, NMR, and Raman spectroscopic samples were prepared under argon atmospheres by loading glass ampules with the catholyte solution and flame sealing them under vacuum. A variety of ampules were used, including NMR tubes and gas tight IR containers.

The water content of SO_2Cl_2 and $SO_2Cl_2/AlCl_3$ solutions was determined using transmission infrared (IR) spectroscopy, with the solutions being contained in 10 mm pathlength quartz cells having a glass extension used for filling and that could be flame-sealing. The absorbance of the O-H stretching vibrations was used to determine the water concentration.

All solution ^{27}Al NMR spectra were obtained at room temperature using a Bruker DRX400 NMR spectrometer at 104.2 MHz having a 5 mm broadband probe. Typical acquisition conditions were 64 scan averages, 1 s recycle delay, 7.75 μs π/2 pulse length, with a 62 kHz spectral width. Samples were referenced to a secondary external standard $Al[H_2O]_6^+$ (δ = 0.0 ppm). The solid state magic angle spinning (MAS) NMR spectra were obtained on a Bruker Avance 600 spectrometer at 156.4 MHz using a 4 mm broadband MAS probe spinning between 10 and 15 kHz. Spectral deconvolutions were obtained using the XEDPLOT simulation software (Bruker Biospin)[4,5]. For the variable temperature spectra, samples were placed in a controlled temperature environment and allowed to come to equilibrium at various temperatures before measurement.

Raman spectra were obtained using the 458 or 514 nm laser line for excitation and a triple spectrograph and charge-coupled-device detector for dispersing and recording the Raman-scattered light. We used a 90° scattering configuration to obtain Raman spectra from the solutions sealed in NMR tubes. For solutions in battery reservoirs, we employed a microscope accessory and a 180° scattering configuration.

4b. X-ray Crystal Structure Information.[6] A colorless crystal was mounted on a thin glass fiber using Fluorolube. The crystal, which was mounted from a pool of Fluorolube, was then immediately placed under a liquid N_2 stream on a Bruker AXS diffractometer. The radiation used was graphite monochromatized Mo Kα radiation (λ=0.71073 Å). The lattice parameters were optimized from a least-squares calculation on approximately 500 centered reflections. Lattice determination and data collection were carried out using SMART Version 5.054 software. Data reduction was performed using SAINT+ 6.02 (7/13/99) software. Structure solution was performed using SHELXTL 5.1 (10/29/98) software. The structure refinement was performed using XSHELL 4.1 (11/08/2000) software. The data was corrected for absorption using the program SADABS within the SAINT+ package. Data collection parameters are given in Table 1. The structure was solved in the space group P-1 using Direct methods. This solution yielded the entire molecule with the Cl atoms properly identified. Subsequent refinements enabled proper identification of Al, S, and O atoms. The final refinement included anisotropic thermal parameters on all atoms, and converged to R1 = 2.94 % and R2w = 7.32 %. Full structure information is given in Appendix I.

5. Discussion.

Initial investigations of the catholyte system focused on the purification of the starting materials. The corrosive nature of the SO_2Cl_2 proved too great for the use of standard Schlenk methods. In fact, the level of impurities increased due to the introduction of organic matter resulting from decomposition of Tygon tubing and/or trapped pump oil vapors using these methodologies. In addition, samples of $AlCl_3$ were found to produce fluorescence in the Raman spectra that was reasoned to be due to transition metal impurities. Several attempts to purify this material by sublimation also proved fruitless. Therefore, the SO_2Cl_2 was used as received and the $AlCl_3$ was purchased in as high a purity level as possible and then used as received. (*Note*: even at 99.999% pure, a number of impurities were noted by Raman spectroscopic studies. However, they did not overlap with the area of interest for this study).

5a. Starting Materials. Our initial investigations focused on the properties of the starting materials in solution. It is widely reported that the coordination of Al metal centers are directly related to the chemical shifts of the ^{27}Al NMR resonance. For $AlCl_3$ in toluene-d_8, a broad singlet at $\delta = +101$ ppm was observed, consistent with a tetrahedral (T_d) coordination geometry. Combining this result with the observed width of the peak, an equilibrium between the monomer and dimer has been identified and reported, eq 1.[7]

$$2\ AlCl_3 \rightleftharpoons [Cl_2Al(\mu\text{-}Cl)]_2 \quad (1)$$

$$SO_2Cl_2 \rightleftharpoons SO_2\ (g) + Cl_2\ (g) \quad (2)$$

Due to the limited number of NMR handles available for SO_2Cl_2, Raman studies were also undertaken. From an aged sample of SO_2Cl_2 in a flame sealed NMR tube, the

ingrowth of a peak at 1142 cm^{-1} was noted which is consistent with SO_2 gas. The Raman spectra are shown in Figure 3. Also observed at 500 to 550 cm^{-1}, but not shown here, were bands associated with $Cl_2(g)$ that grew in a manner consistent with the amount of SO_2 (g). This implies that SO_2Cl_2 decomposes as shown in eq 2.

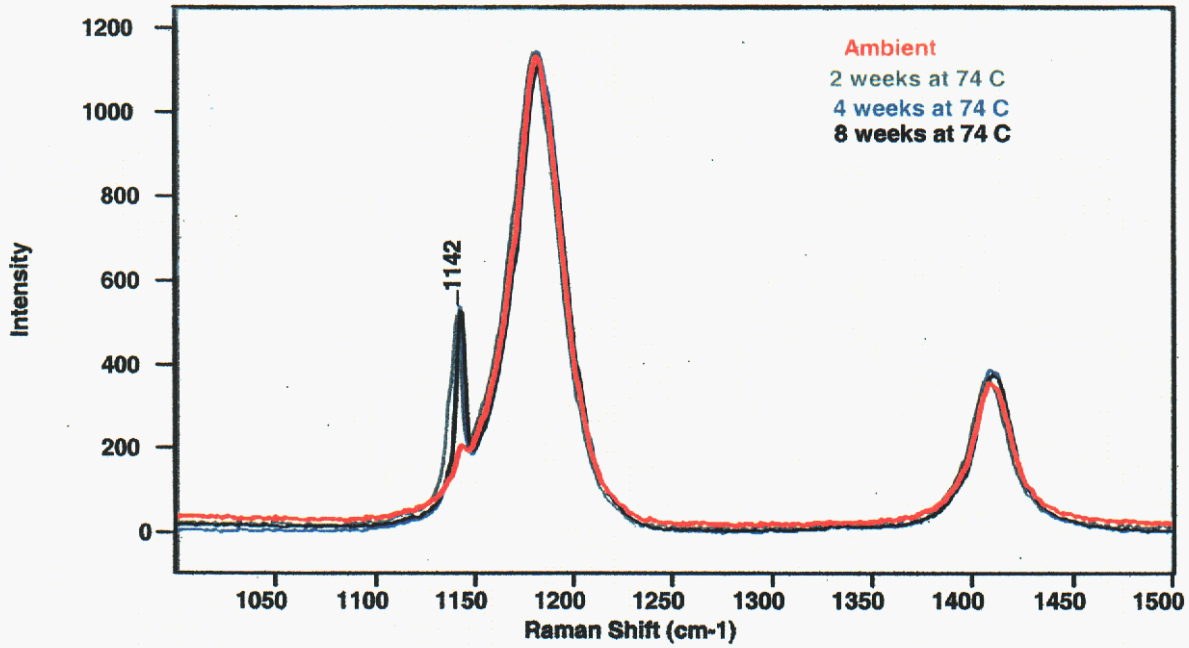

Figure 3. Raman spectrum of SO_2Cl_2 monitored over time

5b. Catholyte solution. Upon mixing $AlCl_3$ and SO_2Cl_2, the solution turns pale yellow. Several questions concerning the chemical behavior of the starting materials were investigated prior to determining the subsequent chemistry of the catholyte solution. Initially it was of interest to determine if H_2O had any effect on speciation. From the ^{27}Al NMR spectra in Figure 4, it is obvious that there is no change in the Al species present in the catholyte. This minimal variation in the Al speciation was expected since the

chemistry associated with SO_2Cl_2 (the major component) would dominate. Water addition to SO_2Cl_2 should follow the reactions shown in eq 3 and 4. These changes would have little effect on the Al species present. In addition, it was observed that the Al speciation during accelerated aging was not affected by the inclusion of varying amounts of H_2O added to solution (see below). Further, Raman and IR spectra showed no significant effect on the speciation of the SO_2Cl_2 and $SO_2Cl_2/AlCl_3$ species through the

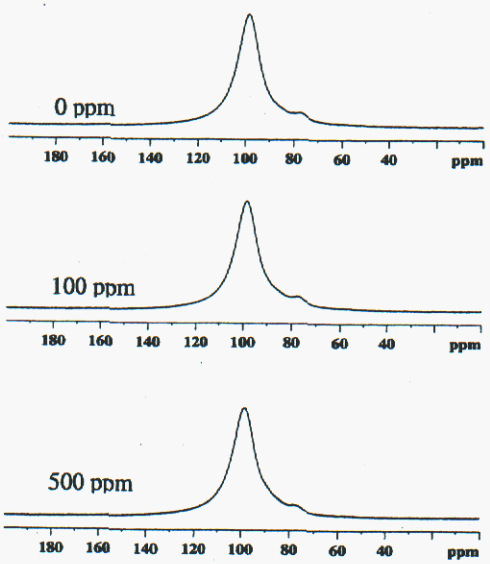

Figure 4. ^{27}Al NMR of $AlCl_3$ with various aliquots of water added.

addition of water at various concentrations (up to 500 ppm). Therefore water was removed as a potential part of any reactivity observed in this system.

$$SO_2Cl_2 + 2\,H_2O \rightleftharpoons H_2SO_4 + 2\,HCl \qquad (3)$$

$$SO_2Cl_2 + H_2SO_4 \rightleftharpoons 2\,ClSO_3H \qquad (4)$$

It was noted throughout the various samples prepared and analyzed (see Appendices A - G) that the same Al species were present in each sample, but at different relative concentrations, and that the relative ratios varied by mixing time, temperature of reaction, and concentration. However, the final composition of each sample given extended aging times was ultimately the same species mix in every case. Further, the nature of the Al metal centers for each sample was T_d and became more oxo in character as the solutions aged (see Figure 5). Deconvolution of these resonances shows the presence of 3 types of T_d bound Al compounds (see Figure 6) at $\delta = +101$, +85, and +80 ppm. Further investigations using 2-D NMR exchange (Figure 7) techniques reveal the presence of another species at ~ +90 ppm but that was present at only very small (> 1 %) amounts. Further, this data shows that the Al species producing the peaks at $\delta = +101$ and +80 ppm are in rapid exchange, on the order of 1 msec.

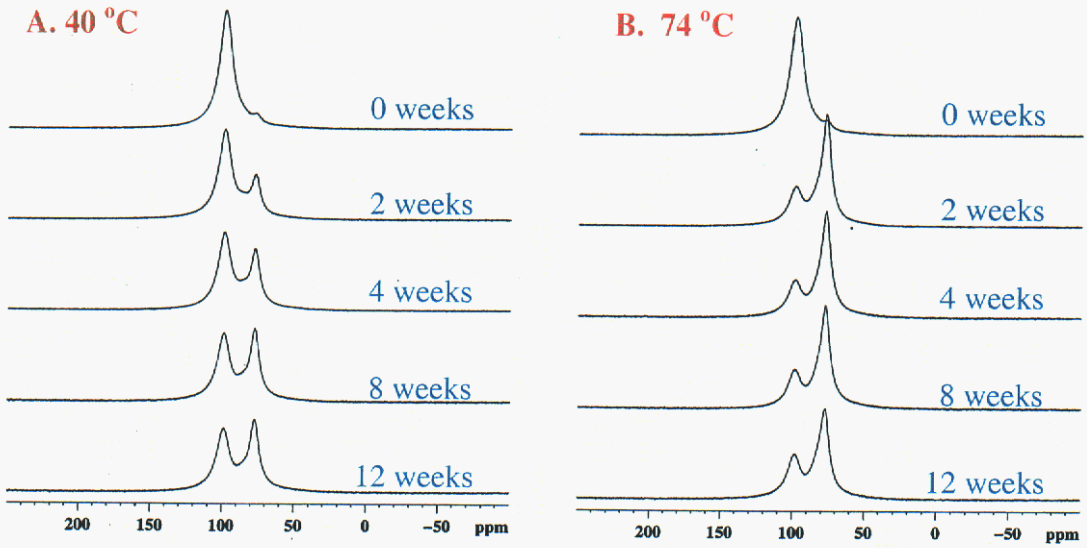

Figure 5. Solution ^{27}Al NMR data for aging of catholyte at (a) 40 °C and (b) 74 °C.

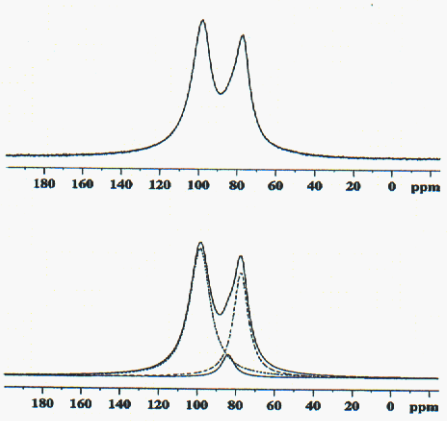

Figure 6. ^{27}Al NMR spectrum of catholyte catholyte solution (a) collected spectrum (b) deconvoluted.

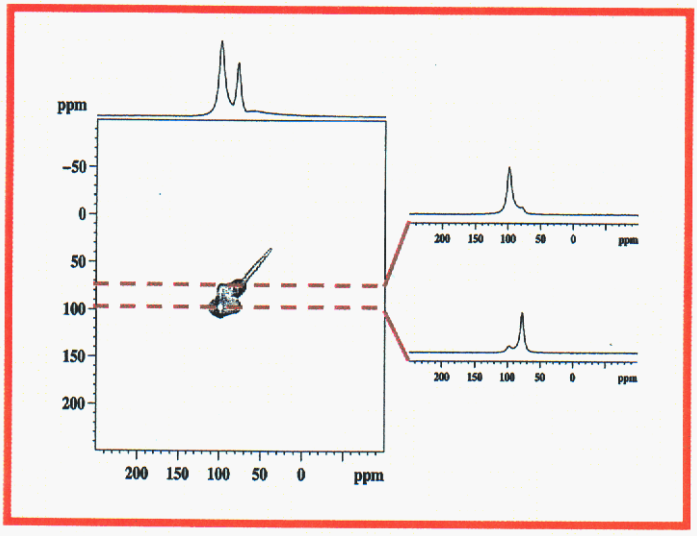

Figure 7. 2D ^{27}Al NMR exchange spectrum of catholyte solution.

In an effort to identify some of these species, we investigated the early-timed, low temperature behavior of $AlCl_3$ in SO_2Cl_2. This was undertaken by generating a sample of the catholyte, sealing it in a glass tube, and freezing it in liquid nitrogen. The sample was transferred to a cold NMR probe and ^{27}Al NMR spectra collected as the sample was

slowly warmed to room temperature (shown in Figure 8). For the frozen samples, the ^{27}Al NMR lines are extremely broad and could not be observed. A broad background signal originating from the probe, tubes and glass inserts is observed at $\delta \sim +68$ ppm. With heating only a single resonance is observed at $\delta = +101$ ppm, which is identical to what was recorded for $AlCl_3$ in toluene-d_8. Therefore, this resonance was assigned to $AlCl_3$. At higher temperatures an additional resonance grows in at $\delta \sim +92$ ppm, consistent with the $AlCl_3$ dinuclear complex.

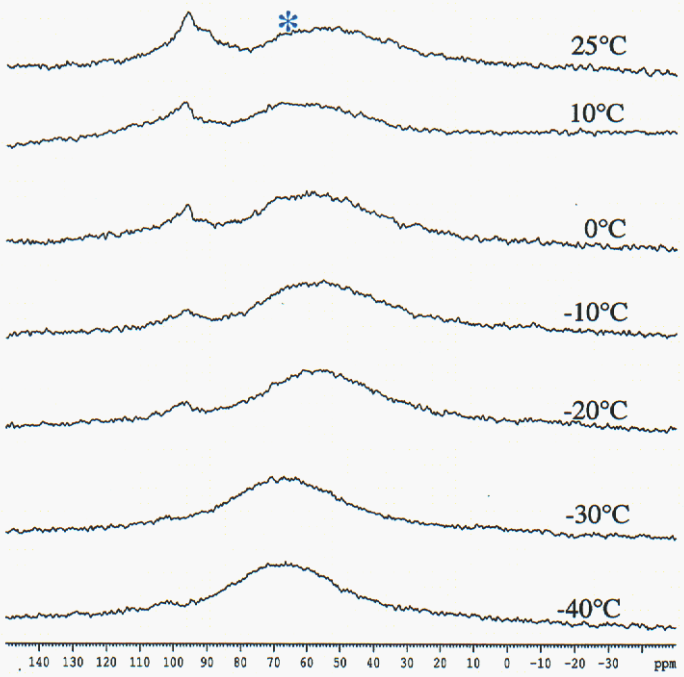

Figure 8. ^{27}Al NMR spectrum of slowly warmed catholyte solution (* probe background)

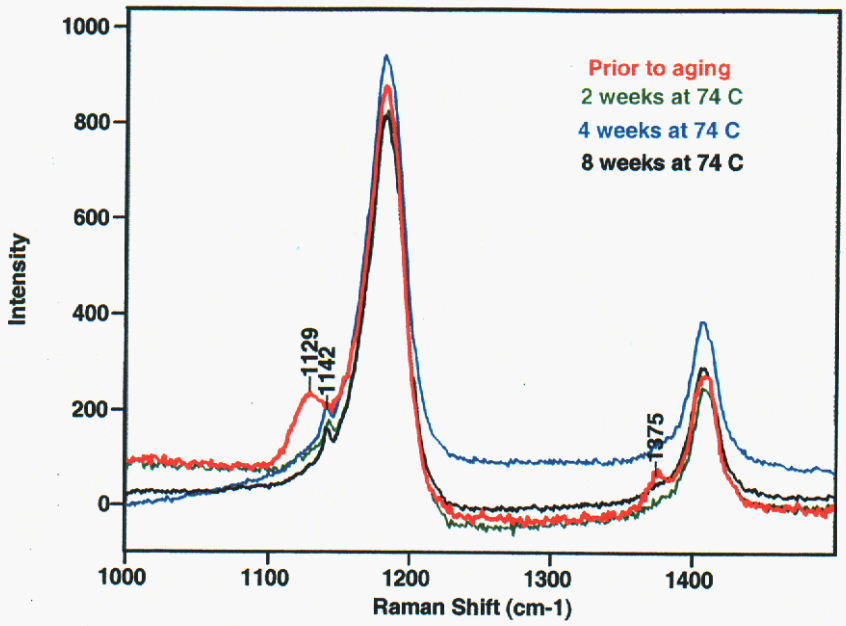

Figure 9. Raman spectrum of catholyte ($SO_2Cl_2/AlCl_3$) monitored over time.

After 8 weeks at 74°C the Raman spectrum of the catholyte shows relatively low intensity SO_2(g) bands (Figure 9) compared to the Raman spectrum of the solution with SO_2Cl_2 only (Figure 3). This implies that the $AlCl_3$ is consuming the SO_2 gas or the equilibrium is being forced back to the SO_2Cl_2 samples. Cooling a sample that had been aged yielded a crystalline material that was identified as $[Cl_2Al(\mu\text{-}O_2SCl)]_2$ (**1**) and whose structure is shown in Figure 10.

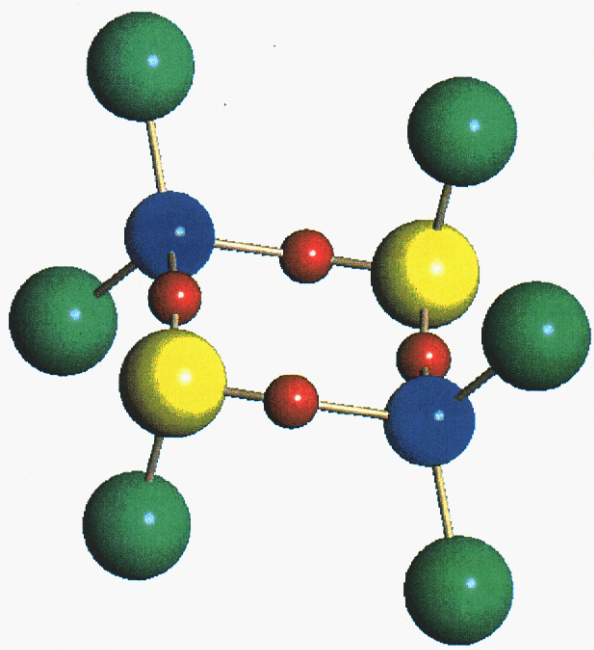

Figure 10. Single crystal X-ray structure of 1 where Al is shown in blue, Cl in green, O in red, S in yellow.

The transient bands at 1129 and 1375 cm^{-1} in the Raman spectrum of the $SO_2Cl_2/AlCl_3$ mixture (Figure 9) that are present prior to aging are believed to be related to **1**.

Compound **1** is unique and can either represent coordination of SO_2Cl_2 with loss of $Cl_2(g)$ or as an $SO_2(g)$ insertion into an Al-Cl bond. Due to the consumption of the $SO_2(g)$ observed by the Raman spectra, the latter explanation is favored. Compound **1** is not stable at high temperature and will convert to $AlCl_3$ (as confirmed by solid state ^{27}Al MAS NMR) upon washing with any solvent. This implies a reversible insertion of $SO_2(g)$. This leads to an unstable species, which is in an equilibrium shown in equation 5.

$$(xs)\ SO_2\ (g)\ +\ 2\ AlCl_3 \rightleftharpoons [Cl_2Al(\mu\text{-}O_2SCl)]_2 \qquad (5)$$

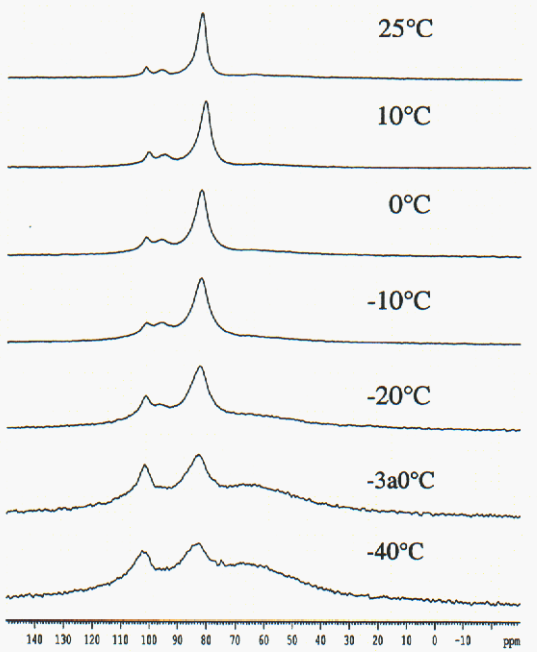

Figure 11. Variable temperature ^{27}Al NMR spectrum of a fresh $AlCl_3$ + SO_2 gas in toluene-d_8.

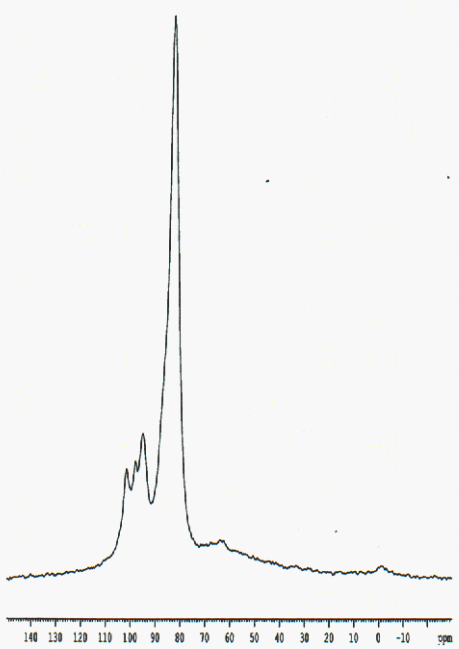

Figure 12. ^{27}Al NMR spectrum of aged $AlCl_3$ + SO_2 gas in toluene-d_8 solution

The solid state ^{27}Al MAS NMR spectrum of **1** showed two peaks at $\delta =$ +101 ppm and +96.5 ppm. Due to the rapidity of decomposition (gas evolution), the peak associated with $AlCl_3$ present in the samples are not expected to be seen. The other NMR peak may be the smaller transitory species noted earlier. Raman data also suggests that this compound is not present in a large amount nor is it present after two weeks. Therefore, either **1**, a compound similar to it, or a SO_2Cl_2 adduct may account for the ^{27}Al NMR peak around δ = +90 ppm.

Crystals isolated from a reaction mixture of $SO_2(g)$ bubbled through $AlCl_3$ in toluene yielded crystals identical to **1**. Again, studying the species present by freezing an NMR tube of $AlCl_3$ with $SO_2(g)$ and allowing it to slowly warm to room temperature allowed some insight into the reaction behavior of the $AlCl_3$. Initially the $AlCl_3$ was observed, however, an $SO_2(g)$ adduct was also observed around +80 ppm (see Figure 11). Over time, the reaction mixture favors the latter species (Figure 12). Similar species are observed in the $AlCl_3$-$SO_2(g)$ system but this mixture is not identical to the catholyte $AlCl_3$-SO_2Cl_2 system.

As shown in Figure 5, the catholyte reaction species become more oxygen coordinated as time progresses until a precipitate forms. The precipitate was analyzed by Raman spectroscopy and is shown in Figure 13. The difference spectra (after subtraction of SO_2Cl_2 bands) have bands similar to $SOCl_2$, which indicates that the precipitate material has $SOCl_2$ moieties associated with it. Therefore any precursor to the precipitate must also have a similar make up.

One possible representation of the formation of precipitate adduct is shown in Figure 14. NMR data indicates a great deal of exchange between the different

intermediate species is occurring (Figure 14). If, as shown in step i, an O-S bond is broken, then the Al can rearrange by bridging to the freed O atoms (step ii). Then a simple Cl transfer shown in step iii forms a small dinuclear species with more oxo character and the $SOCl_2$ moiety.

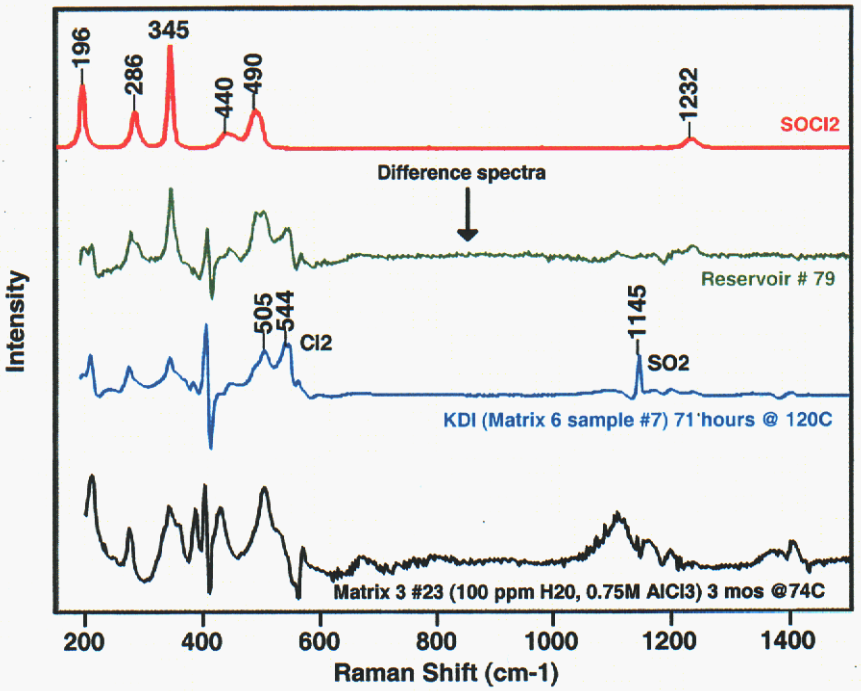

Figure 13. Raman spectra of (a) $SOCl_2$, and difference spectra of (b) reservoir #79 (gelled),(c) KDI sample, and (d sample prepared from commercial reagents.

Once formed, this precursor can also start to rearrange to form larger species as shown in Figure 15. For this process a slight rearrangement of Al-O bonds results in larger oligomers. The degree of oligomerization will determine the solubility. For this mechanism it should be noted that the Al atoms all remain T_d and adopt more oxo character with increasing oligomerization.

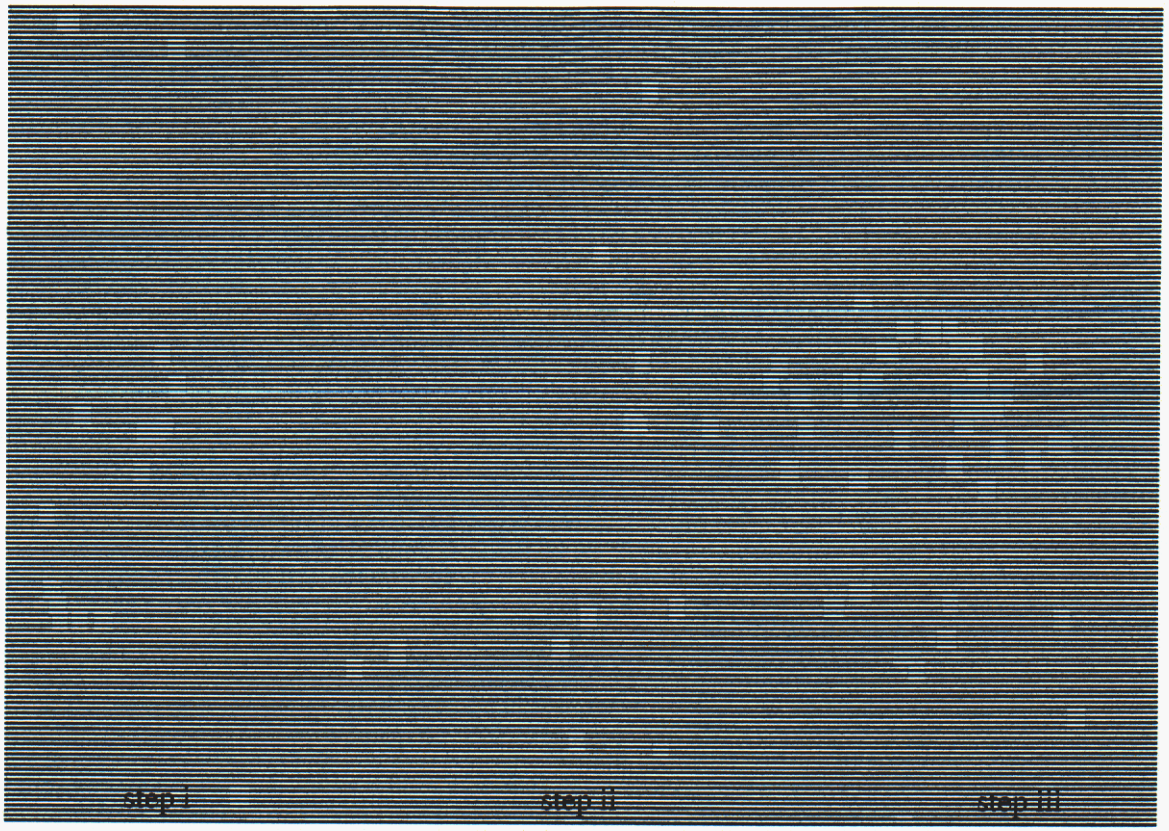

Figure 14. Schematic representation of potential rearrangement of SO_2 adduct to precipitate precursor.

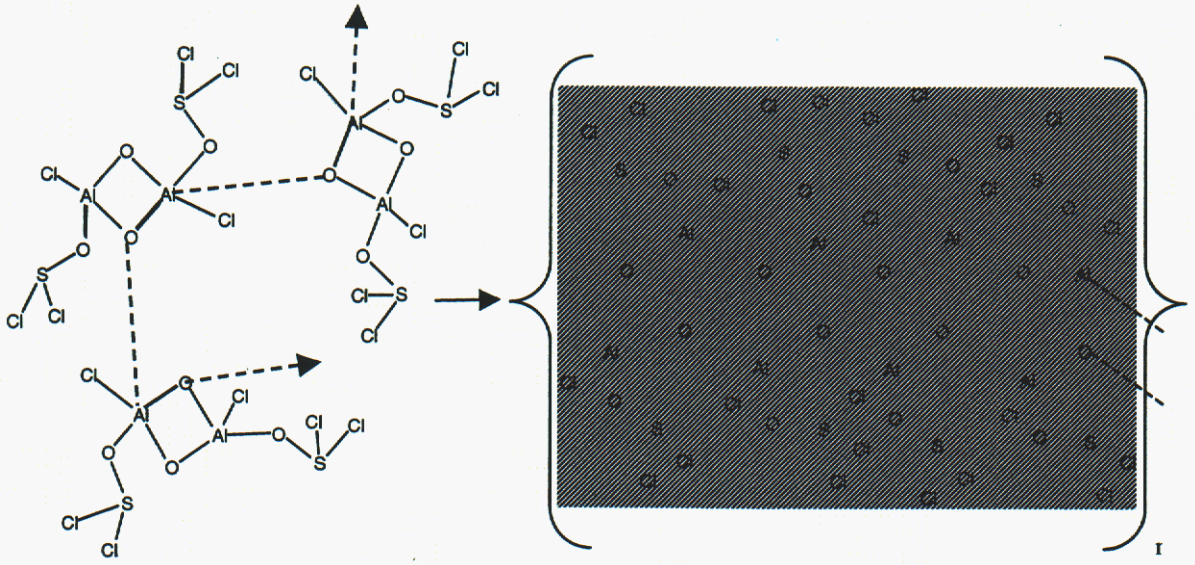

Figure 15. Schematic representation of potential intermolecular rearrangement to form long chain polymer precipitate.

5c. Precipitate. Investigation of the precipitate has also been undertaken. Shown in Figure 16 are the visual changes that occur upon high temperature treatment. The samples proved to be under a great deal of pressure, and in fact the reaction mixture was

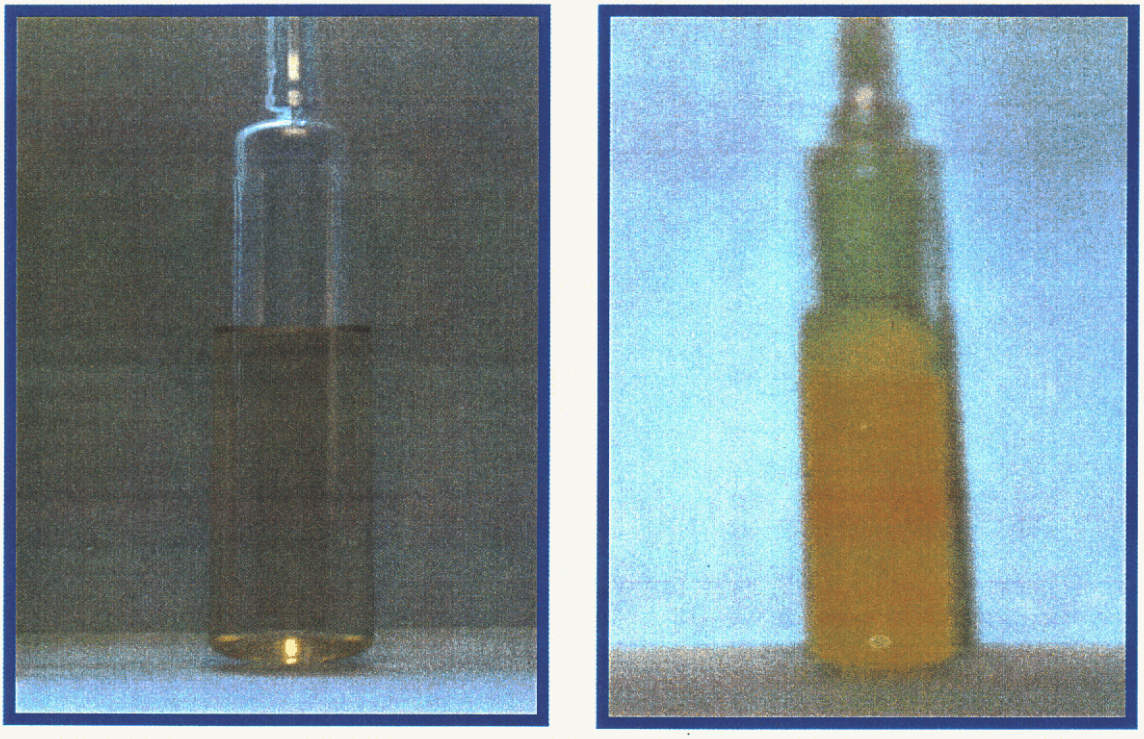

(a) (b)

Figure 16. Pictures of catholyte at 120°C at (a) O h. and (b) 168 h.

forcefully expelled from the ampule upon opening. Therefore, the samples were frozen in liquid nitrogen, transferred into a glovebox, opened, and allowed to slowly degas while warming to ambient temperature. The precipitate was collected and analyzed by solid state NMR and Raman spectroscopy.

Intense fluorescence obscured any Raman bands in the spectrum of the precipitate, so no meaningful information could be garnered using this technique. The

solid state NMR is shown in Figure 17, and from these data it is readily apparent that the T_d coordination is no longer the dominant feature. It appears that the major species present now have octahedral (O_h) and trigonal bipyramidal (tbp) geometries.

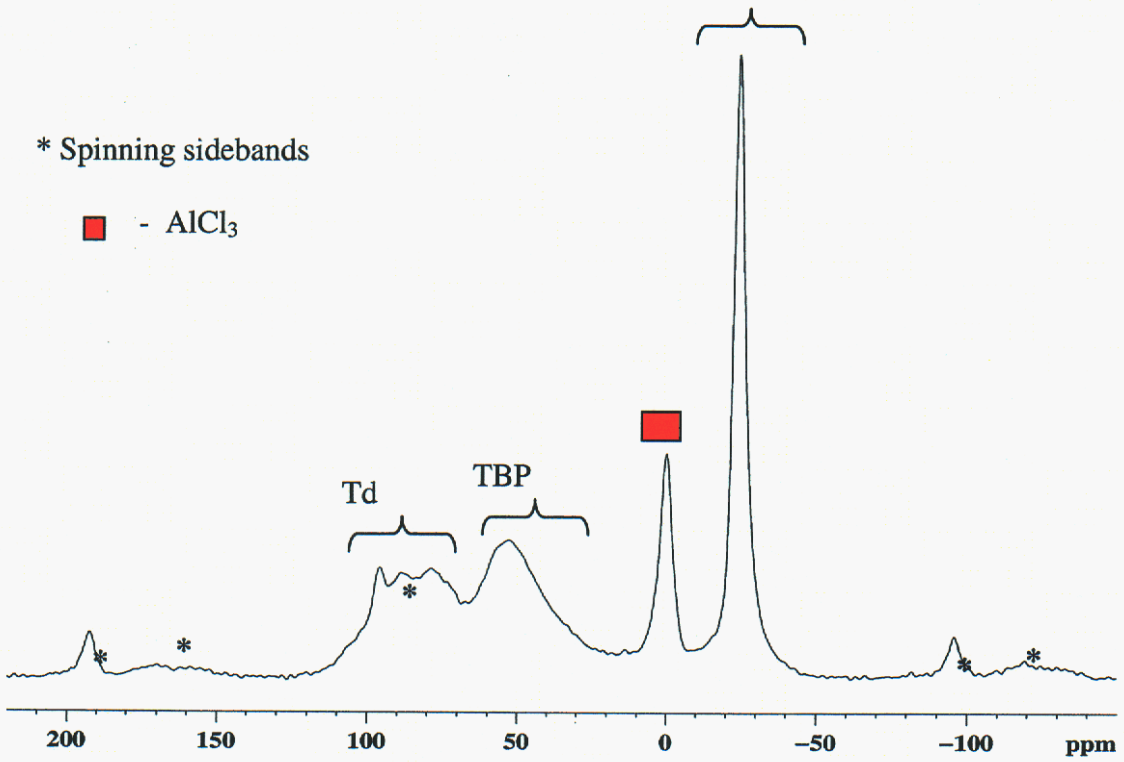

Figure 17. Solid state ^{27}Al MAS NMR spectrum of precipitate.

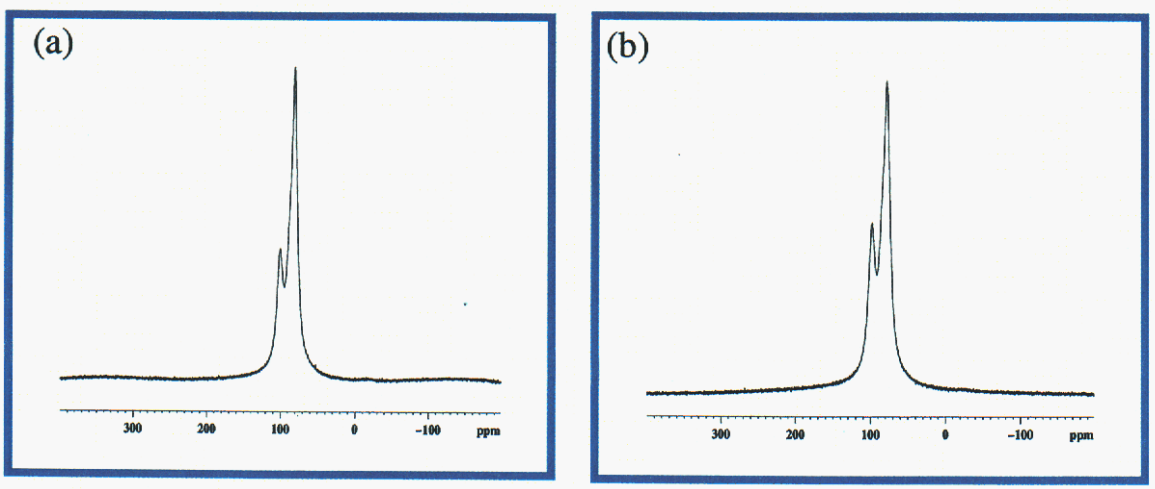

Figure 18. ^{27}Al NMR solution spectrum of the mother liquor of the catholyte precipitate (a) 0 h from thaw and (b) 2 h after thaw.

The cross-linking of the proposed polymers in Figure 15 is easily envisioned to generate these different Al-coordinated species. Further, this cross-linking between species leads to formation of larger oligomers and therefore yields precipitated materials.

Investigation of the mother liquor lends some insight into the behavior of this precipitate (Figure 18) and eq 6. For the 24 h mother liquor, NMR data collected at different times during the thaw reveal that there is no change in the speciation observed. Further, the mother-liquor solutions look very similar to the freshly prepared $AlCl_3/SOCl_2$ solutions previously discussed. However, when compared to the 168 h sample, $AlCl_3$ dominates the spectrum (Figure 19). This shift in the Al-speciation can only be accounted for if the precipitate is in equilibrium with the solution. That is, $AlCl_3$ cannot be the dominate species in solution if the equilibrium is being slowly shifted to the right (eq 6) to form a precipitate. However, if the precipitate re-dissolves, the equilibrium will be shift back to the left, favoring the formation of $AlCl_3$.

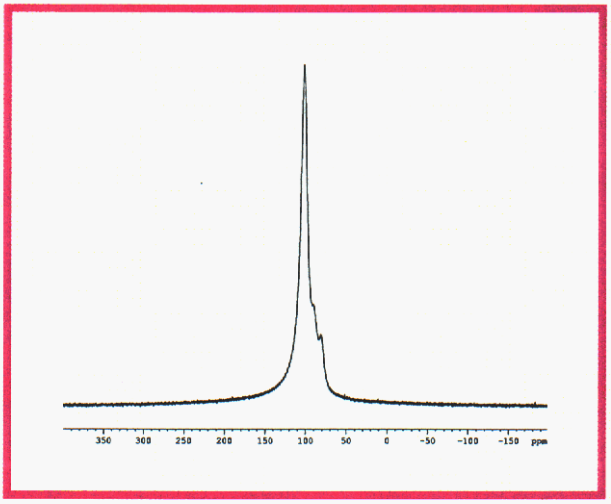

Figure 19. ^{27}Al NMR spectrum of mother liquor of sealed sample of precipitated catholyte.

$$(AlCl_3 + SO_2Cl_2) \rightleftharpoons [AlCl_3]_2 + SO_2 + Cl_2 \rightleftharpoons$$

$$[Cl_2Al(\mu\text{-}O_2SCl)]_2 \rightleftharpoons [AlCl(O)(SOCl_2)]_n \quad \text{PPT} \qquad (6)$$

6. Summary and Conclusion

The fundamental chemical behavior of the catholyte $AlCl_3/SO_2Cl_2$ system for the ARDEC Self-Destruct Fuze Reserve Battery Project was elucidated using a variety of analytical tools including infrared absorption (FTIR), Raman, and ^{27}Al NMR spectroscopy, and single crystal X-ray diffraction. From these investigations it was determined that all catholyte samples possessed the same chemical species in solution. However, there are differences in the relative concentrations of these species and that the distribution of species are associated with aging, concentration, and sample storage temperature, each of which controls the kinetics of this complex reaction system. FTIR studies revealed that very little water (<20 ppm) is present in as-received (or prepared) neat SO_2Cl_2 or the catholyte solution. Further studies reveal that water has little effect on the species present. Three major and one minor product are observed in solution.

The first species was found by ^{27}Al NMR experiments to be consistent with $[Al(\mu\text{-}Cl)Cl_2]_2$, an equilibrium product of $AlCl_3$ in solution. Raman spectroscopic studies showed that $SO_2(g)$ and $Cl_2(g)$ are present in quasi-equilibrium with SO_2Cl_2. However, in solutions containing $AlCl_3$, the amount of $SO_2(g)$ is much lower, apparently because of a reaction with $AlCl_3$. The single crystal X-ray diffraction studies identified an adduct formed at low temperatures as $[Cl_2Al(\mu\text{-}O_2SCl)]_2$ (**1**). Chemical investigations indicate that this adduct can reversibly eliminate/insert SO_2.

The third species was tentatively identified as a compound with the general formula $\{[Al(O)Cl_2][OSCl_2]\}_n$. This was based on ^{27}Al NMR data that reveal a species with tetrahedrally (T_d) coordinated Al metal centers with increased oxygen coordination.

Further, the precipitate or gel that forms from this solution over time was found by Raman spectroscopic studies to possess a component that is consistent with $SOCl_2$. This implies that **1** may be transformed to a polymeric species with Al-O-Al bonds coordinated by $SOCl_2$. In order to form a precipitate, it is necessary to have larger oligomers. The precipitate was further characterized by solid state ^{27}Al MAS NMR data to possess predominantly octahedral (O_h) Al metal center. This implies $\{[Al(O)Cl_2][OSCl_2]\}_n$ must undergo some internal rearrangements prior to precipitation. In summary, Figure 20 shows a representation of the chemical pathway elucidated from this investigation.

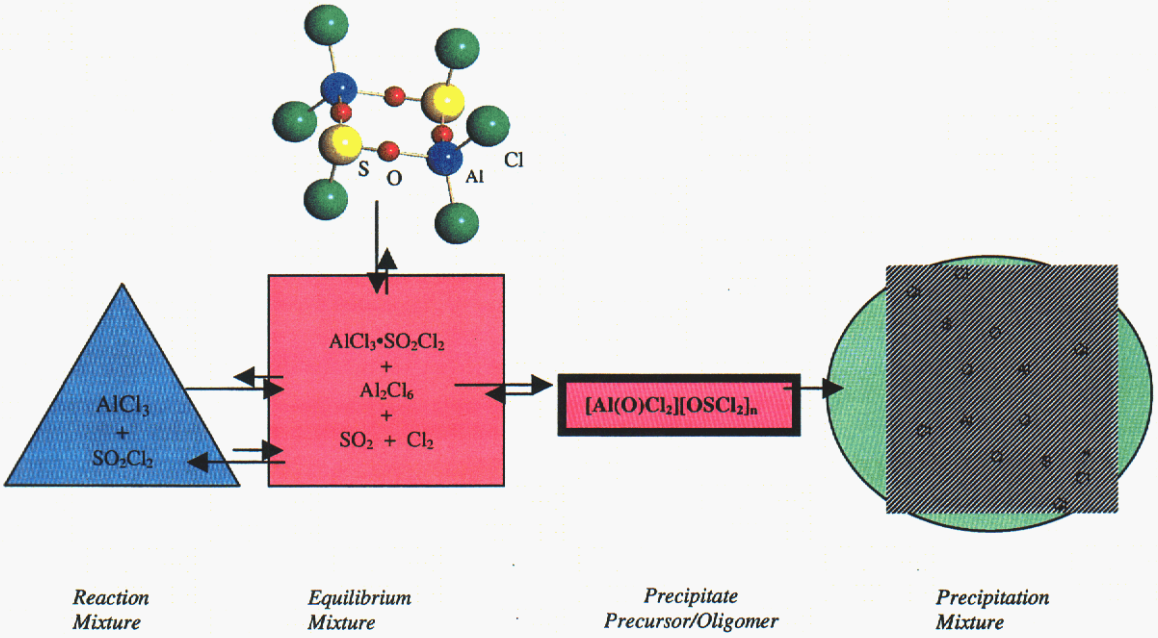

Figure 20. Schematic representation of various equilibriums determined in this study.

Some conclusions concerning battery performance may be extrapolated from the data collected in this study. It appears that while storing the catholyte at low temperature may result in a precipitate under some conditions, consistent with the species identified as **1**, this may be preferred since it will prevent the formation of the polymeric species

during additional aging. With warming above room temperature, the decomposition of this adduct occurs, reintroducing the $AlCl_3$ into solution, and therefore will not effect the overall capacity of the catholyte. At higher temperatures and extended aging periods, a gel or precipitant will form. However, preliminary studies indicate that the gel that forms may be in equilibrium with the solution. Therefore, precipitation that occurs due to long term storage or heating will not be a concern for battery operation, since a large excess of catholyte is initially used and there is not a continuous drain of Al from solution. However, since no electrochemical studies (either half-cell or full-cell) were conducted in this work, definitive statements regarding battery performance from long-term aging of the catholyte at elevated temperature cannot be made.

7. References.

(1) Glidewell, C. *Inorg. Chim. Acta* **1986**, *117*, L7.

(2) Geiko, V. I.; Stryfina, O. P.; Doda, S. A.; Borovikov, A. Y. *J. Appl. Chem. USSR* **1990**, *63*, 648.

(3) Pray, A. R.; McCrosky, C. R. *J. Am. Chem. Soc.* **1952**, *74*, 4719.

(4) Smith, M. E. *Bruker Report* **1990**, *1*, 33.

(5) Smith, M. E.; Taulelle, F.; Massiot, D. *Bruker Report*, *2*, 16.

(6) The listed versions of SAINT, SMART, XSHELL, and SADABS Software from Bruker Analytical X-Ray Systems Inc., 6300 Enterprise Lane, Madison, WI 53719 were used in analysis.

(7) Cerny, Z.; Machacek, J.; Fuzek, J.; Casensky, B.; Kriz, O.; Tuck, D. G. *Inorg. Chim. Acta* **2000**, *300-302*, 556.

Section 2. SDF Battery Reservoir Welding Study

8. Introduction

While the catholyte was being investigated, it was also necessary to understand how this effected the reservoir that held the catholyte solution (Figure 1). The following was the information garnered on the evaluation of laser welding of the end plate onto the reservoir.

9. Experimental Section

Thirty reservoirs filled with catholyte and sealed by pulse laser welding were received from KDI. Upon receipt, a visual inspection of all of the reservoirs was made. The Catholyte solution was then removed from the reservoirs by breaking the glass seal on the bottom of the reservoir in an inert environment. (The catholyte recovered was utilized for another aspect of the program.) Residual catholyte was removed from the reservoirs by flushing the reservoir with alcohol.

After removal of the catholyte, microscopic examination of all of the welds on each reservoir was completed, and Figure 21 shows photomicrographs of the typical closure welds observed. As can be seen, the weld beads are uniform in width, and there did not appear to be excessive concavity in the bead. However, the solidification lines resulting from the pulsed laser source did show somewhat excessive pulse-to-pulse overlap. These observations were the same in every case, demonstrating high reproducibility.

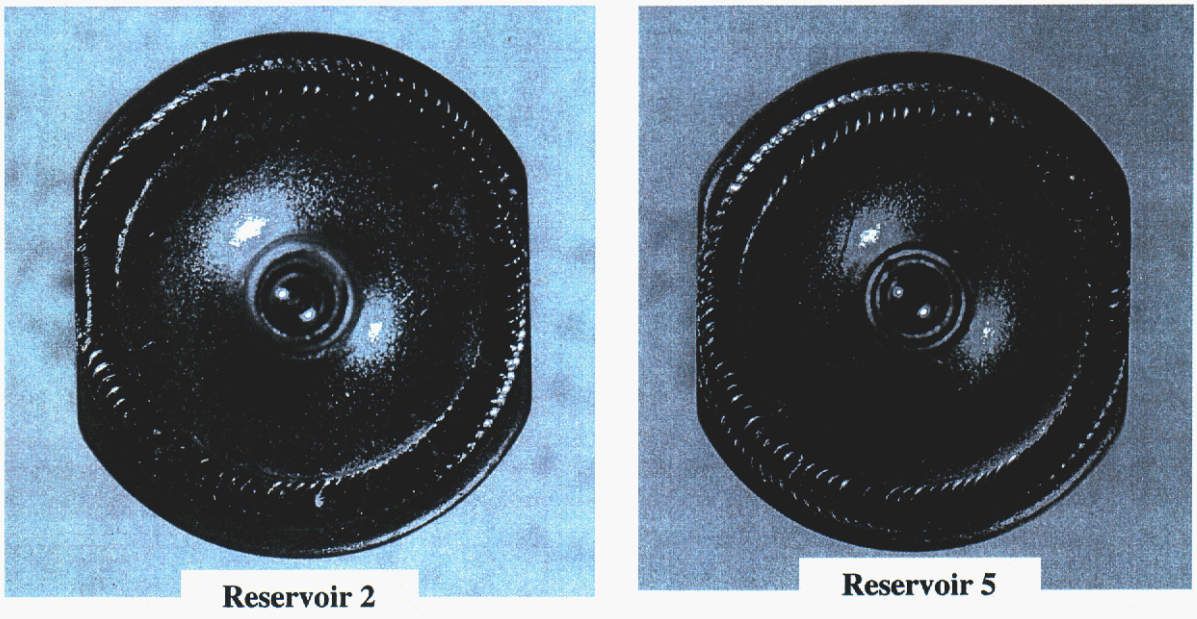

Figure 21. Photomicrographs of two different reservoirs showing typical laser weld.

The first twenty numerically sequenced reservoirs were selected for further metallurgical examination, and the remaining ten reservoirs were held in reserve. Metallurgical examination was done by microscopic examination of a cross-section through the weld. Sectioning of the reservoirs was done by first positioning the reservoir in a mount, and then grinding to the approximate middle of the reservoir. The ground samples were then polished and etched.

As seen in the photomicrographs of Figure 21, the welds themselves are circular in nature, and the outer circumference of the reservoir displays two flats diametrically opposed to one another along the perimeter. Since it is conceivable that the nature of the weld is different in these areas, two reservoirs were cross-sectioned through the flats and two reservoirs were cross-sectioned at 90-degrees to the flats. Figure 22 shows cross-sectional photomicrographs of these four reservoirs. As seen, these welds were found to

be essentially identical in every case, consequently the remaining 16 reservoirs were cross-sectioned through the welds at 90-degrees to the flats.

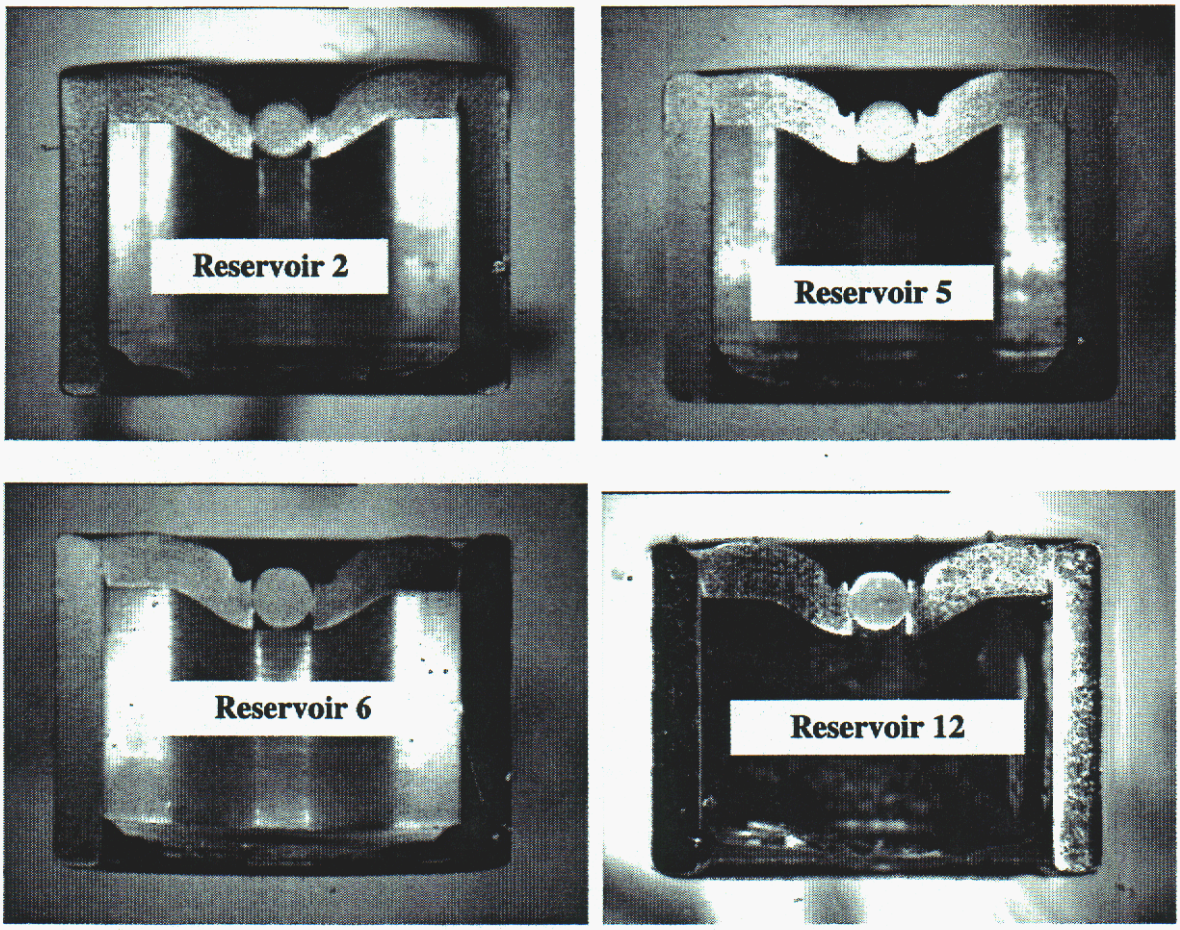

Figure 22. Cross sectional photomicrographs of the weld taken parallel and normal to the flat.

Figures 23 through 32 show photomicrographs of welds of various reservoirs. All of the photomicrographs were examined in detail, and several important weld measurements were made. These measurements including: 1) the weld depth, corresponding to the distance between the fusion lines on the surface; 2) the maximum weld depth, corresponding to the dimension of the deepest portion of the fusion zone; and 3) the effective weld depth corresponding to the minimum thickness of the weld at the joint

between the cap and case. A tabular compilation of these dimensions for each reservoir is given in Table 1.

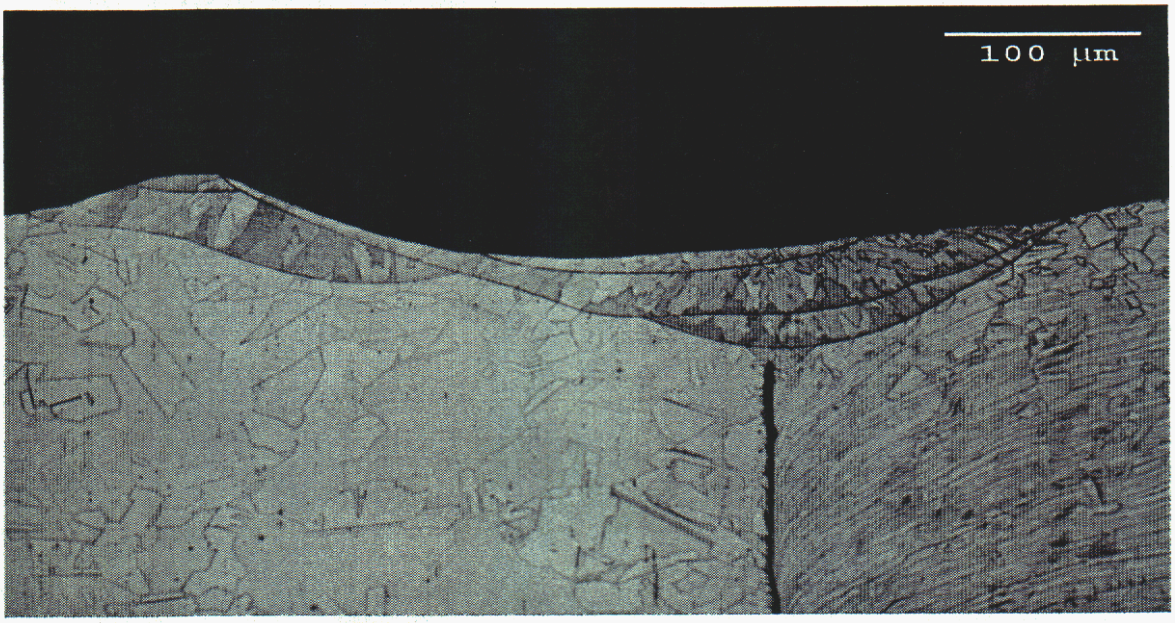

Figure 23. Side 1 of Reservoir 2 Laser Weld Width = .017"; Max. Depth - .0041"; Eff. Depth - .0036"; Fusion Lines – 6.

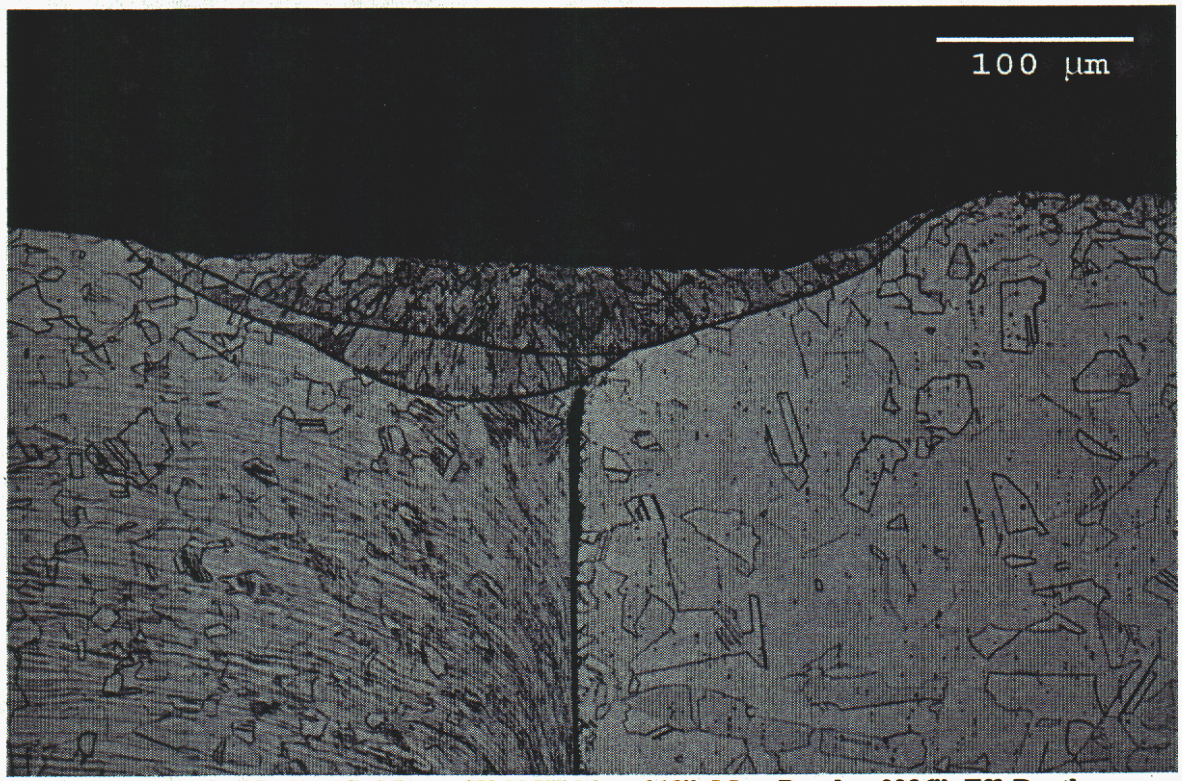

Figure 24 . Side 2 of Reservoir 2 Laser Weld Width = .018"; Max. Depth - .0036"; Eff. Depth - .003"; Fusion Lines – 3. The weld is a slight amount of a root void that reduced the leak path.

Figure 25. Side 1 of Reservoir 5 Laser Weld Width = .020"; Max. Depth - .0044"; Eff. Depth - .0044"; Fusion Lines – 4. The weld is slightly off-center of the weld joint.

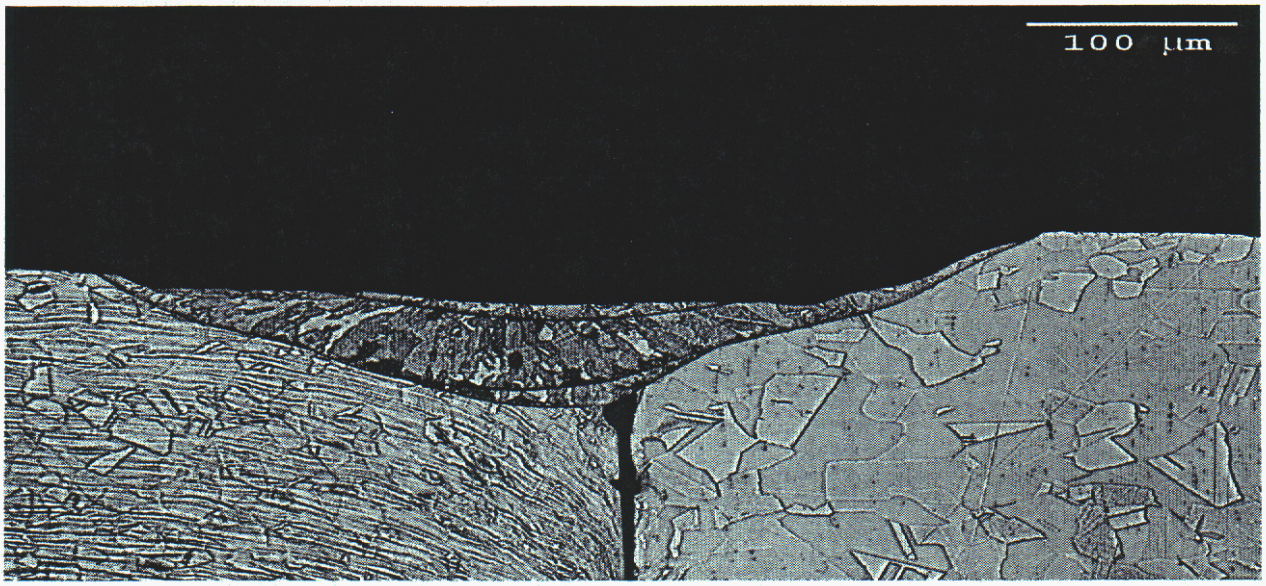

Figure 26. Side 2 of Reservoir 5 Laser Weld Width = .018"; Max. Depth - .0041"; Eff. Depth - .0028"; Fusion Lines – 3. A small amount of root porosity is shown here.

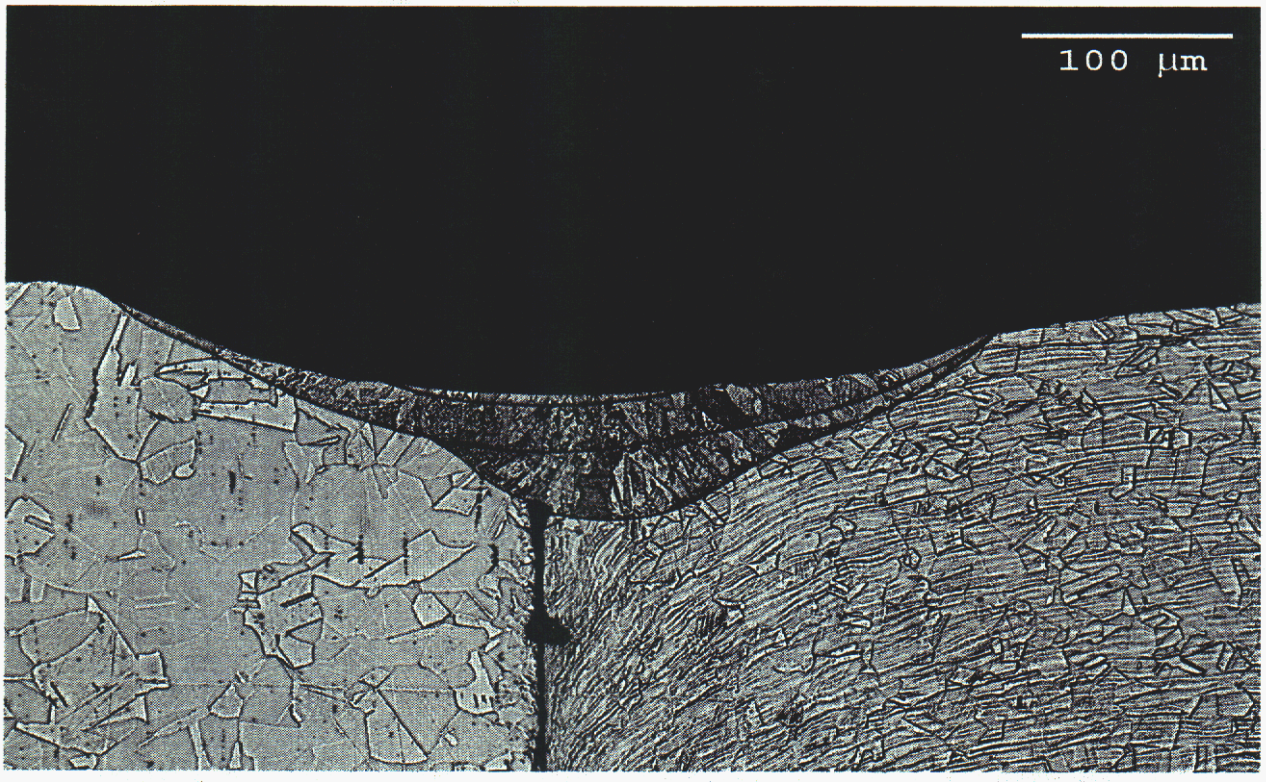

Figure 27. Side 1 of Reservoir 6 Laser Weld Width = .018"; Max. Depth - .0030"; Eff. Depth - .0025"; Fusion Lines – 3. The weld is slightly off-center of the weld joint.

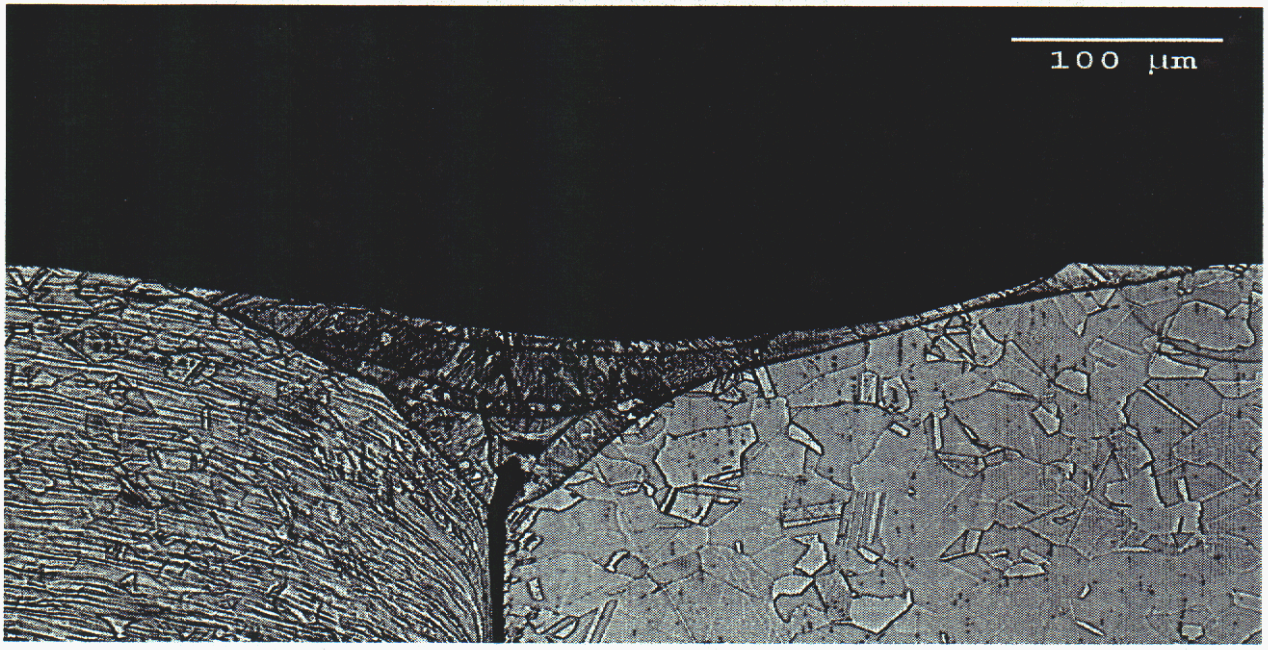

Figure 28. Side 2 of Reservoir 6 Laser Weld Width = .020"; Max. Depth - .0052"; Eff. Depth - .0033"; Fusion Lines – 4. A large amount of root void/porosity can be seen in this cross-section.

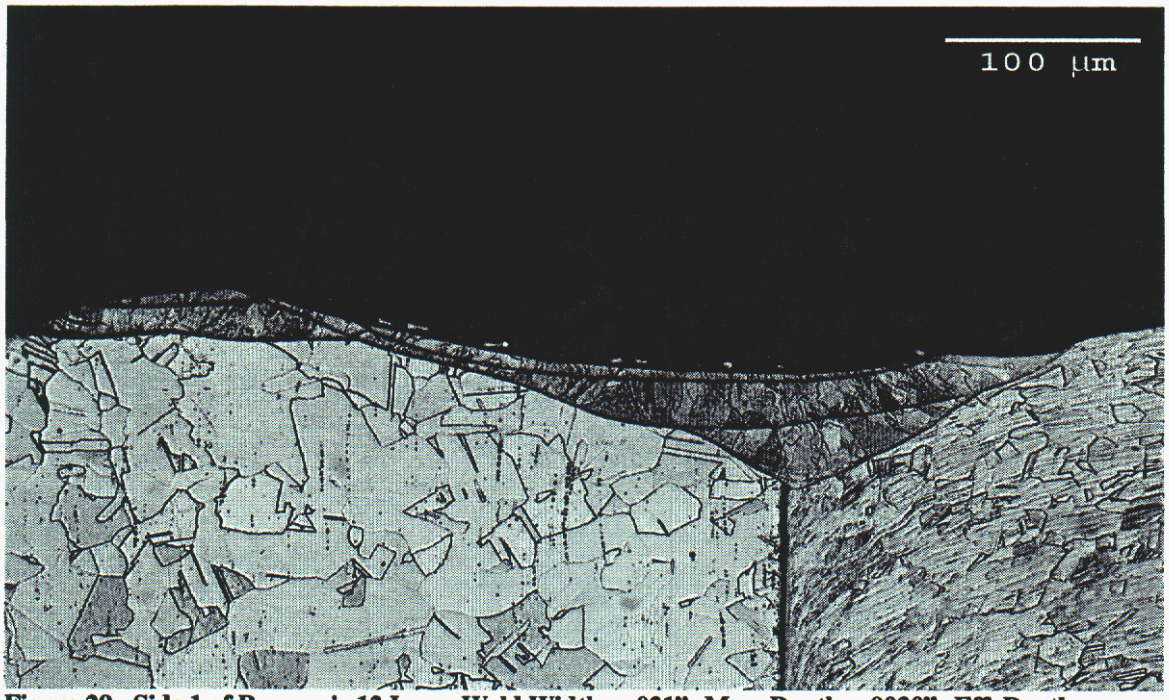

Figure 29. Side 1 of Reservoir 12 Laser Weld Width = .021"; Max. Depth - .0030"; Eff. Depth - .0030"; Fusion Lines – 3 – 5. The number of fusion lines reflects a power ramp down area.

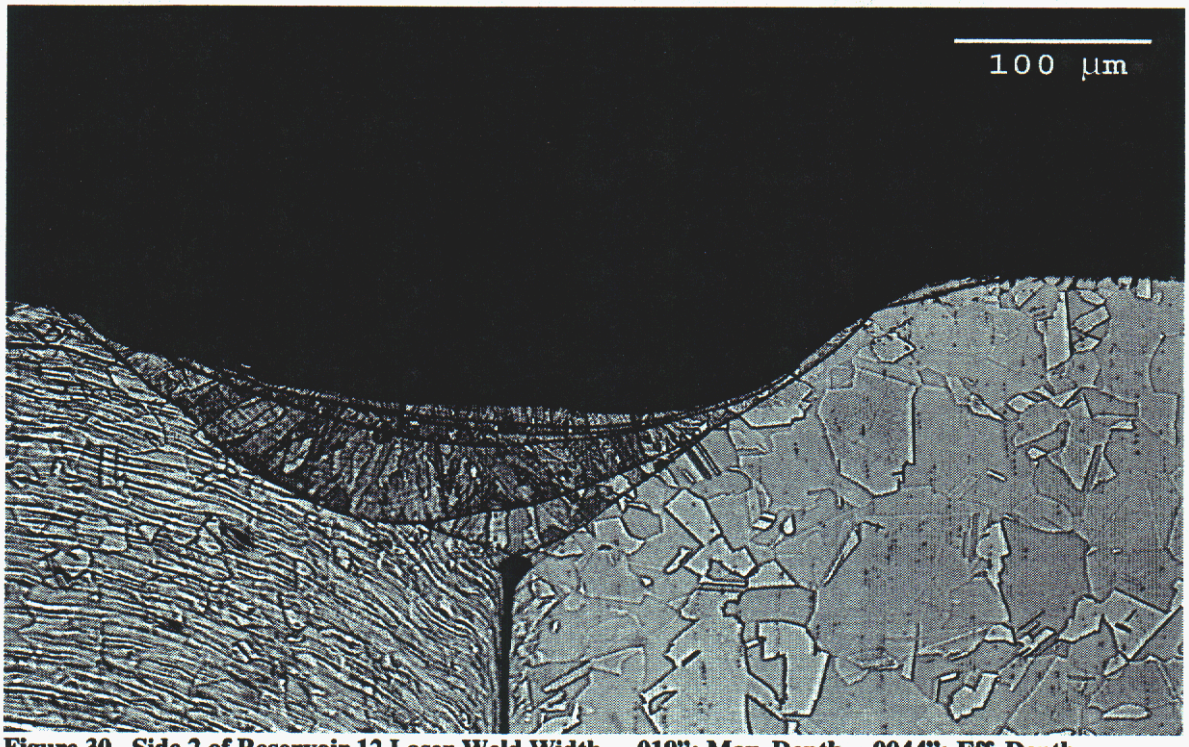

Figure 30. Side 2 of Reservoir 12 Laser Weld Width = .019"; Max. Depth - .0044"; Eff. Depth - .0036"; Fusion Lines – 6. The number of fusion lines reflects a power ramp down area. Some root void/porosity can also be seen in this cross-section.

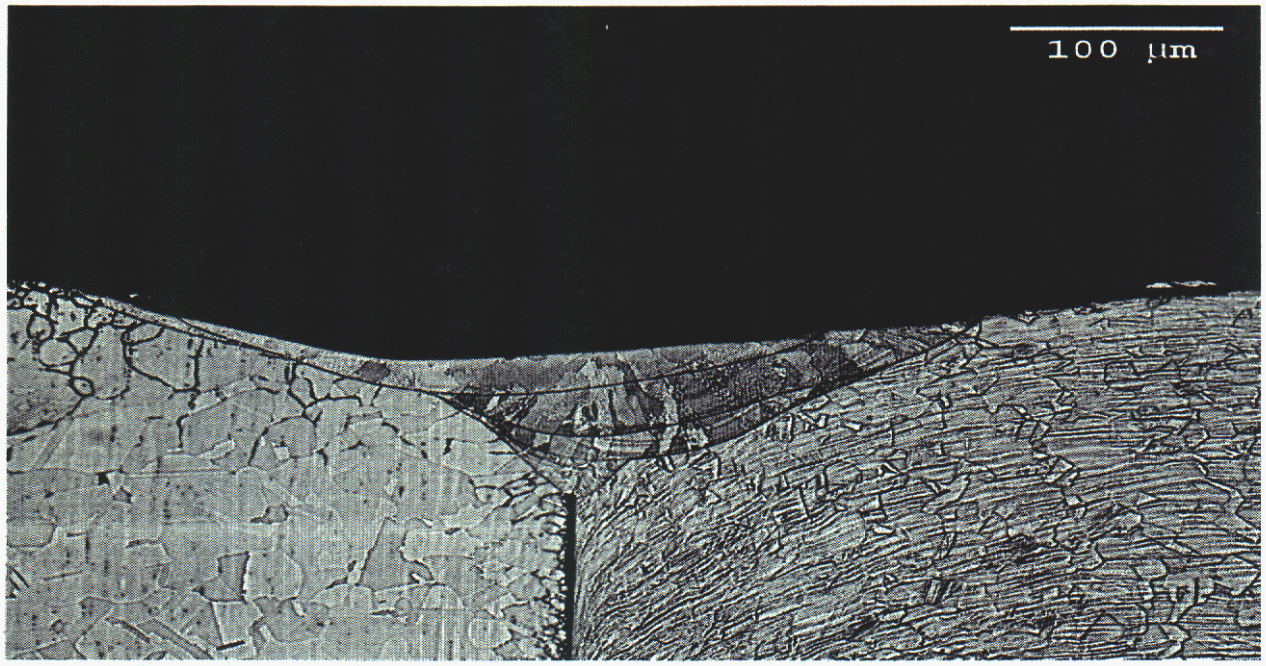

Figure 31 . Side 1 of Reservoir 14 Laser Weld Width = .018"; Max. Depth - .0038"; Eff. Depth - .0038"; Fusion Lines – 4. Areas of sensitization can be seen on the top & side of the case.

Figure 32. Side 2 of Reservoir 14 Laser Weld Width = .017"; Max. Depth - .0041"; Eff. Depth - .0036"; Fusion Lines – 5. Areas of sensitization can be seen on the top & side of the case.

Table 1. Compilation of critical weld characteristics for each reservoir.

Sample #	Weld X-Section	Width	Maximum Depth	Effective Depth	# Of Fusion Lines
1	1	0.017	0.0041	0.0036	3
	2	0.019	0.0041	0.0041	5
2	1	0.018	0.0036	0.0033	6
	2	0.018	0.0036	0.0030	3
3	1	0.020	0.0059	0.0050	3
	2	0.018	0.0038	0.0033	3
4	1	0.020	0.0059	0.0041	4
	2	0.018	0.0038	0.0033	4
5	1	0.020	0.0044	0.0044	4
	2	0.018	0.0041	0.0028	3
6	1	0.018	0.0030	0.0025	3
	2	0.020	0.0052	0.0033	4
7	1	0.019	0.0030	0.0027	3
	2	0.018	0.0038	0.0036	3
8	1	0.018	0.0041	0.0027	3
	2	0.020	0.0050	0.0044	4
9	1	0.020	0.0030	0.0030	3
	2	0.018	0.0036	0.0036	3
10	1	0.018	0.0044	0.0038	3
	2	0.018	0.0038	0.0038	4
11	1	0.019	0.0041	0.0041	4
	2	0.021	0.0056	0.0047	3
12	1	0.021	0.0030	0.0030	3-5
	2	0.019	0.0044	0.0036	6
13	1	0.018	0.0046	0.0044	5
	2	0.019	0.0059	0.0056	3
14	1	0.018	0.0038	0.0038	4
	2	0.019	0.0044	0.0041	5
15	1	0.017	0.0030	0.0027	4
	2	0.018	0.0047	0.0047	3
16	1	0.019	0.0053	0.0038	4
	2	0.019	0.0036	0.0036	5
17	1	0.017	0.0030	0.0022	3
	2	0.017	0.0044	0.0044	3
18	1	0.017	0.0031	0.0024	3
	2	0.020	0.0050	0.0050	4
19	1	0.020	0.0056	0.0056	4
	2	0.018	0.0038	0.0030	3
20	1	0.017	0.0030	0.0030	3
	2	0.020	0.0071	0.0059	4
	Average	***0.0186***	***0.0043***	***0.0037***	
	STD Dev.	***0.0012***	***0.0010***	***0.0009***	

10. Discussion

The condition of the welds from a metallurgical perspective showed no cracks, porosity or other anomalies found in the main portion of the weld bead in any of the cross-sections. Also, the grain structure was very good and similar to that of the base metal. However, there was a possible effect of a minor amount of catholyte (moisture) being present in the weld joint prior to welding. In the root (bottom of the weld) of reservoir 1 - welds 1 and 2, reservoir 3 - weld 1, reservoir 4 - weld 1, reservoir 5 - weld 2 and reservoir 6 - weld 2, to list several of the examples, there was a minor amount of root porosity. In all likelihood, this root porosity can be attributed to small amounts of moisture being vaporized. This vapor created a bubble-shaped void in the root weld metal. Alternatively this amount of root porosity could be attributed to weld metal shrinkage that can sometimes occur in these type welds. Regardless of the cause, the root porosity that was found is considered minor. Problems could arise if variations occur either in the fit of the end plate into the case or in the catholyte level that allows sufficient moisture to be present such that it creates a blowout.

The welding parameters (power, pulse length & rate, travel speed, etc.) used to make the welds also appears to be of high quality. The parameters used are producing a very consistent conductive (low depth to width ratio) weld. As shown in Table 1, the average width of the welds is .0186" with a standard deviation (STD) of .0012"; the average maximum penetration depth is .0043" with an STD of .001"; and the effective depth (leak path) average is .0037" with an STD of .0009". However, there is margin in the parameters to reduce the heat input by lowering the welding pulse rate or increasing the welding speed. The photomicrographs, Figures 23 and 27 for example, show 3 - 5

solidification lines in the cross-section of each weld. This number of solidification lines is an indication that there is too much overlap, by as much as 75%, of the individual pulses. Normal overlap is around 50% and results in 2-3 solidification lines. Too much overlap adds unnecessary heat input to the weld & reservoir.

There were no signs of sensitization as a result of welding in any of the cases investigated. However, for reservoir 14, sensitization is evident on the container itself and well removed from the weld areas (see Figures 21 and 22). Based on the location of the areas of sensitization, this undoubtedly occurred prior to welding. Since we do not have information regarding the production process up to this point, we cannot definitively say when the sensitization occurred. However, one likely production process to consider is the glassing step. Furthermore, an assessment of the effect that these areas have on corrosion processes should be considered. It should be reemphasized that the welding of this sensitized base metal is unaffected by the prior sensitization, and in fact this weld is as good as any of the other nineteen reservoirs.

However, two reservoirs, 2 and 12, have six fusion lines in one of the weld sections. This number of fusion lines indicates that the sectioning was in a ramping up or ramping down region of the weld. In a ramp up/down the power of the laser is raised or lowered in a series of incremental changes to or from the required weld power level. There were no anomalies found in these welds. In general, there were no signs of degradation of the welds due to the catholyte in the reservoir.

11. Summary and conclusions.

The metallurgical welds were of high quality. These results were all visually determined there was no mechanical testing performed. If the .003" - .005" penetration is acceptable

based on past performance of the units, no additional parameter development is needed to increase the weld strength via increased penetration. It is recommended that the weld parameters need to be adjusted to reduce the pulse-to-pulse overlap from ~75% to 50% to reduce the heat input. Reduction in the amount of overlap will not affect the penetration depth but will lower the excess heat input.

Based on these results, it is recommended that the end plate geometry and weld be changed. If the present weld strength, based on .003" - .005" penetration, is sufficient for unit performance, the end plate thickness can be reduced to .005" instead of the .020" thickness. By reducing the thickness to .005" the plug can be stamped such that it can form a cap rather than a plug. The cap outer diameter should be slightly smaller in diameter than the case as shown in Figure 33. The seal weld can then be made around the edge of the cap producing a meltdown type fillet weld which is easy and results in a low-stress joint, eliminate the 'coalescence' problem when there is a gap in the 'butt' weld (plug/case), and reduce the effect of catholyte in the root of the joint. There should not be any catholyte present as the weld is being made to the outer portion of the end of the case rather than the inner portion where the catholyte is present. This option provides the opportunity of being able to increase the amount of catholyte in the reservoir by ~15% when the end plate thickness is reduced. The increase can be seen in the calculations shown with Figure 33 which may be beneficial to battery performance.

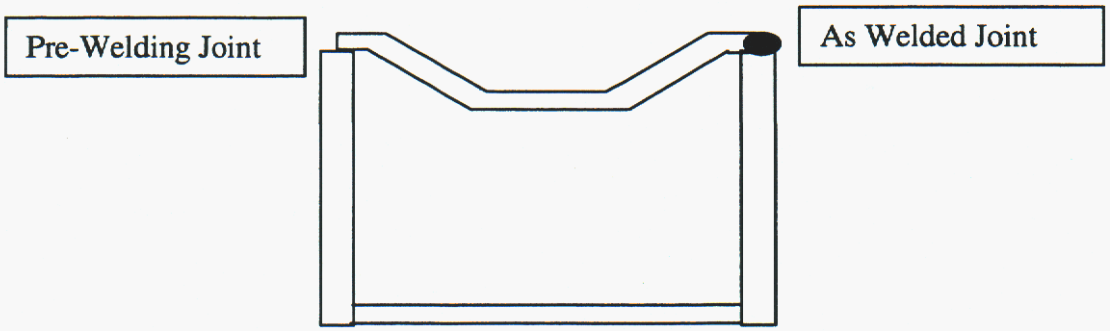

Figure 33. Proposed Endplate to Case Weld

By reducing the endplate thickness from .020" to .005" the interior volume of the reservoir can be increased by approximately 15%, according to the calculations below.

OD of Reservoir =	**.21"**
ID of Reservoir =	**.16"**
Case Wall Thickness =	**.023"**
Present Depth of catholyte =	**.083"**
(Based on bottom of endplate)	
Additional Electrolyte from Thinner Endplate	**.098"**

$$\text{Volume} = \pi r^2 h$$

$$\text{Present Volume} = (3.14)\,(.08")^2(.083") = .0017\ in^3$$

$$\text{New Volume} = (3.14)\,(.08")^2(.098") = .0020\ in^3$$

$$\text{Additional Volume} = .003/.017 = \sim 17\%$$

Allowing for a little less electrolyte, a 15% increase is possible.

12. Acknowledgements

Garry Bryant, Alice Kilgo and Robert Wright were responsible for the preparing and photographing the metallographic.

Section 3. Appendices List

13. Appendix A

Monthly Report
May 31, 2002

Sandia National Laboratories

Operated for the U.S. Department of Energy by Sandia Corporation

Albuquerque, New Mexico 87185-

date: May 31, 2002

to: Distribution

from: Nancy Clark, 2522 and David Ingersoll, 2521

subject: Activities on ARDEC Self-Destruct Fuze Reserve Battery Project during May, 2002

This memo summarizes the activity performed in May, 2002, on the Self-Destruct Fuze Reserve Battery Project. It also provides an update on the status of the Action Items from the February review meeting.

Project Status
Major activities completed in May include:

"Aged/Gelled" Reservoirs

Ten reservoirs containing "aged/gelled" electrolyte were received from ARL, thereby satisfying Items 2a and 3 of the February 2002 Action Item List. We have completed an incoming visual/microscopic inspection of these reservoirs, and have identified both brown (iron oxide perhaps) and white crystalline materials on the external surface of many of these reservoirs. While the brown material was found at both the ball seal end of the reservoir as well as on the glass-to-metal seal end, the white material was found predominately on the ball seal end of the reservoirs. Examples of the deposits observed are shown in Figures 1-5 below, and Table 1 summarizes the visual observations made on all of the reservoirs.

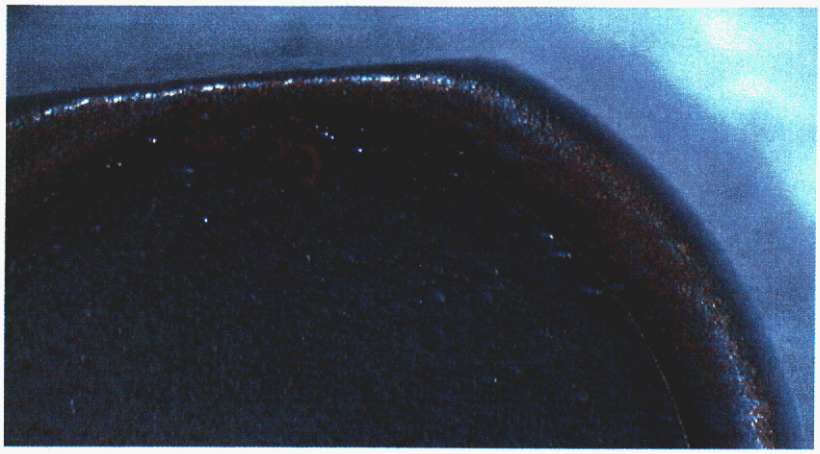

Figure 1. Photomicrograph of brown deposit at the glass-to-metal seal of Reservoir 94.
Army94A1.psd

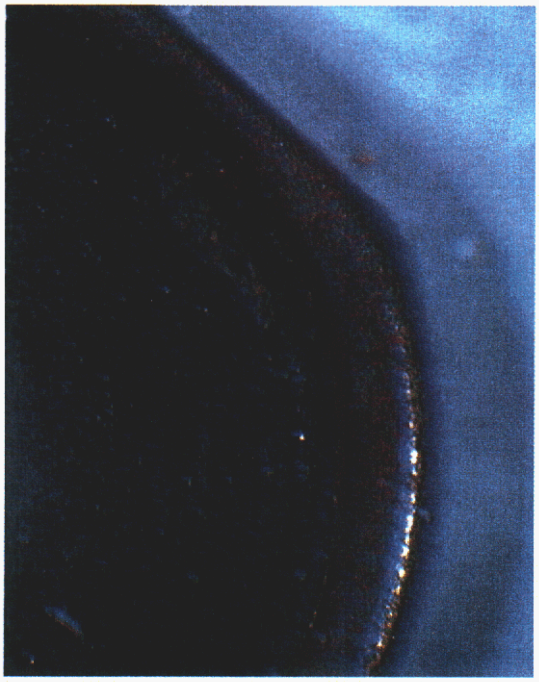

Figure 2. Photomicrograph of brown deposit on glass-to-metal seal of Reservoir 54.
ARMY54AC.psd

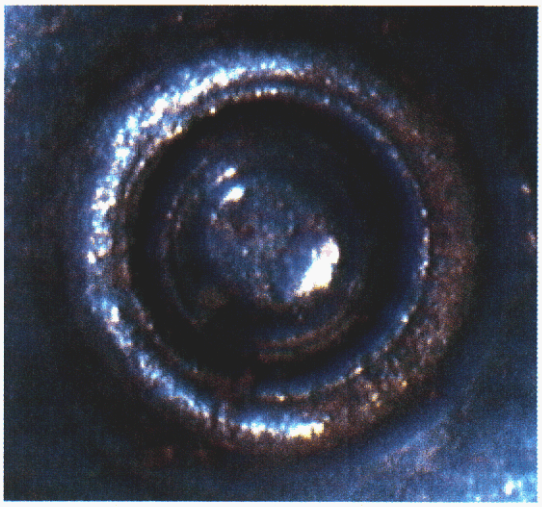

Figure 3. Photomicrograph of brown material at the ball seal end of Reservoir 73.
ARMY73B2.psd

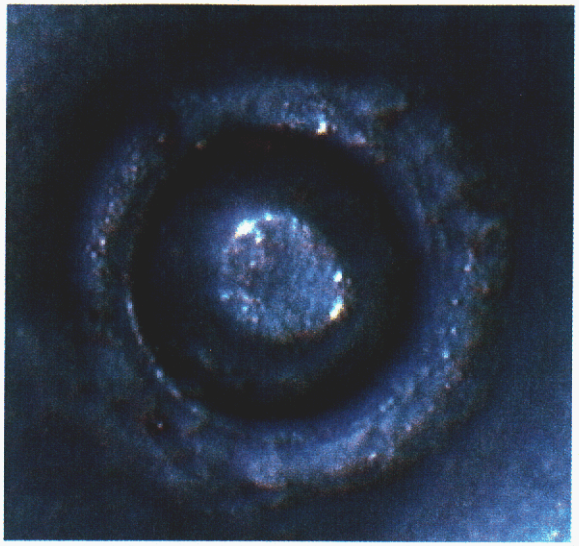

Figure 4. Photomicrograph of brown material at the ball seal end of Reservoir 81.
ARMY81b2.psd

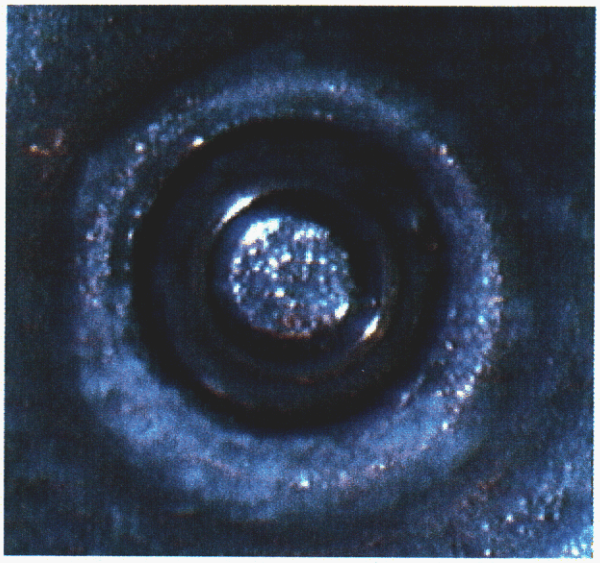

Figure 5. Photomicrograph of white material at the ball seal end of Reservoir 94.
ARMY94bd.psd

Table 1. Visual comments regarding incoming inspection of "aged/gelled" reservoirs.

ID NUMBER	GENERAL COMMENTS ON VISUAL	
	Ball Seal	Glass to Metal Seal
54	Significant brown deposit .	Small amount of brown and off-white deposit. Not at interface.
57	White particulates. Brown deposit on ball.	Brown deposit, but not at interface.
63	Brown deposit on ball as well as at interface of ball/cell.	Clean.
70	Brown deposit.	Clean.
73	Brown fiber. Small amount of white deposit.	Brown deposit.
78	White and brown deposit.	Small amount of white material.
79	White crystals in well. Brown crust on ball perimeter.	Glass is frosted. Brown deposit, powder as well as deliquescent appearing material
81	White salt. Brown deposit.	Brown deposit at interface.
89	White residue. Brown deposit.	Clean.
94	White salt in well. Brown deposit.	Brown deposit.

Note – The brown deposit looks like iron oxide in color.
Two forms of the brown deposit are apparent. One looks like a dry powder, and the other looks like a wet, deliquescent material.

We have also examined the reservoirs for evidence of the presence of the gel. The criteria used for making this assessment was provided to us by B. Poese at ARL. This assessment is made on the basis of how the gas bubble in the reservoir moves in the window of the reservoir, and specifically whether or not the gas bubble can be move freely over the entire face of the window upon rotating/tilting the reservoir. If the bubble's motion is impeded at any point during its transverse of the face of the window, then there is some obstruction in the reservoir and this has been defined as the presence of the gel. With this as the working definition, a microscopic examination of the reservoirs was completed and obstructions that prevent/inhibit bubble mobility were observed. However, it should be mentioned that in every case the gas bubble, when visible, does move quickly. The implication being that there does not appear to be a significant increase of the solution viscosity. Table 2 provides a summary listing of the observations made as well as the initial ARL assessment provided by B. Poese

Table 2. Summary assessment of gas bubble impediment of "aged/gelled" reservoirs.

ID NUMBER	GEL ASSESSMENT	
	Initial ARL Assessment	Current Status
54	Yes – erratic bubble movement on one side.	Impediment present
57	No – Unimpeded bubble movement.	Impediment present
63	No – Unimpeded bubble movement.	No impediment
70	Yes - Strange bubble movement	No impediment
73	No – Unimpeded bubble movement.	No impediment
78	Yes – Erratic bubble movement.	Impediment present
79	Yes – Static bubble.	Cannot tell. The glass is frosted to an extent that the bubble cannot be seen.
81	No – unimpeded bubble movement.	No impediment
89	Yes – erratic bubble movement.	Impediment present
94	Yes – Erratic bubble movement.	Impediment present

These reservoirs are now being examined using Raman spectroscopy in order to identify the brown and white deposits, as well as to examine the solution in each.

(We have requested information from B. Poese regarding the history of each of these reservoirs.)

Electrolyte Aging Matrices

Matrix 1 – Reservoirs.

This matrix, corresponding to Task IV in the Statement of Work, involves aging new reservoirs at temperatures of 40°C, 65°C and 74°C with periodic removal for optical examination and Raman spectroscopic analysis. Table 3 summarizes the various conditions to be employed.

Table 3. Task IV - KDI Electrolyte in Reservoirs Aging Matrix

SAMPLE NUMBER	TEMPERATURE/°C		
	40	65	74
1	X		
2		X	
3			X
Characterization at 0, 1, 3, 6 and 12 months			

Thirty reservoirs to be used for this activity were received from KDI, and Raman spectra of all of the samples have been collected. These spectra will be used as a baseline for the

aging studies. The Raman spectra were collected in a 180° backscatter configuration using a microscope objective to focus the excitation beam through the glass of the reservoir window. By comparing Raman spectra of the glass of the window, of the bubble in the reservoir and of the liquid of the reservoir, we determined that the background fluorescence is due to a component of the liquid in the reservoir (but probably not the SO_2Cl_2, at least not in its "as-received" form). We have arbitrarily numbered the reservoirs # 1 through # 30, and due to variability in the Raman response of each, this labeling scheme will be retained throughout the program. Twenty-three of the reservoirs provide a strong Raman signal due to SO_2Cl_2 with a relatively low fluorescence background. Seven reservoirs yielded a very low intensity SO_2Cl_2 Raman signal and/or high background fluorescence. In these cases, the glass does not seem to be more opaque. Three reservoirs exhibited high background fluorescence, but relatively intense Raman bands. Figure 6 shows examples of the Raman responses from reservoirs that show a strong and a weak Raman signal.

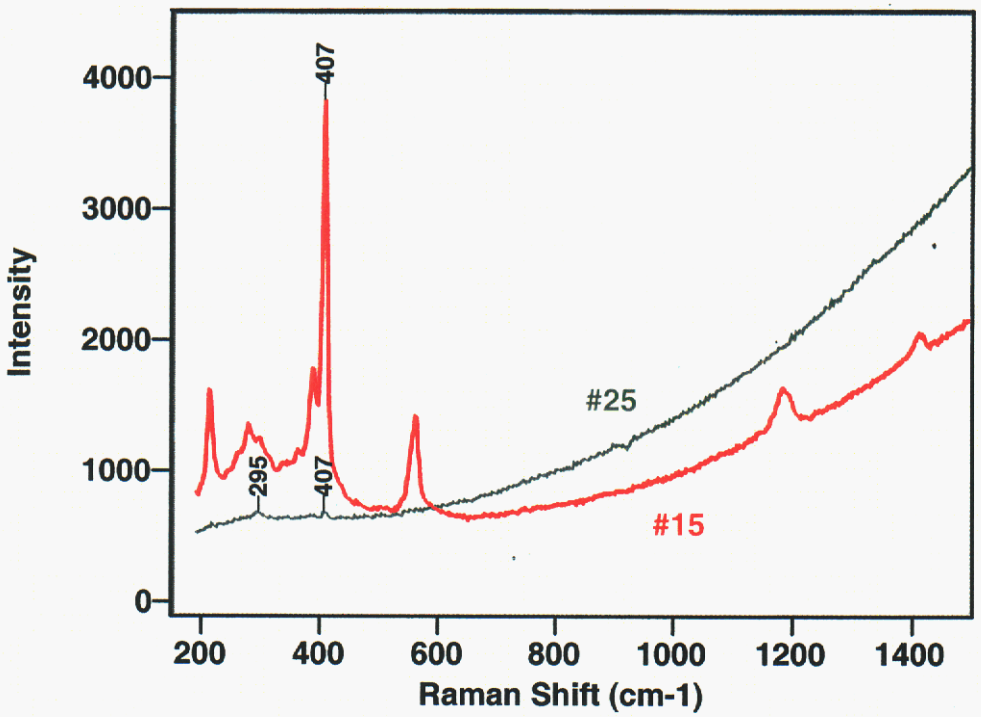

Figure 6. Raman spectra of the Army SDF battery reservoirs #15 and #25 as of 5/23/02. Raman spectra were obtained through the glass window using an 80X microscope objective and 458 nm excitation. Both reservoirs have liquid in them, and the glass in the reservoirs are similar in opacity. The spectrum of reservoir #15 exhibits a typical spectrum with the fundamental, Raman-active vibrational modes of SO_2Cl_2 (most intense peak at 407 cm-1). The spectrum of reservoir #25 exhibits only a low intensity 407 cm-1 band and a band (295 cm-1, plus a broad, underlying feature) due to the glass window. At this point it is not clear why we see such a difference in SO_2Cl_2 band intensity between

the two reservoirs. One possibility is that the glass window is much thicker in #25 so that the focal point of the excitation laser beam cannot be positioned through the glass into the solution.

Based on these results and the need to support the matrix, five reservoirs will be used to populate each temperature in the matrix and five will be set aside and stored at room temperature to serve as a basis for comparison. The reservoirs with the weak Raman signals will be held back in order to determine why they respond differently under Raman analysis. These samples will go into the ovens in mid-June, after microscopic examination of the gas bubble mobility for determination of the presence/absence of "gel".

Matrices 2 & 3 – Bulk electrolyte and purified electrolyte matrices.
Prior to implementation of these matrices several baseline studies were performed. Because it was expected that both Raman and NMR spectroscopy were to be used for characterization, it was hoped that the various samples could be placed into the ovens in flame-sealed NMR tubes. In this way the sample could be repeatedly placed into the oven and removed for characterization by both Raman and NMR. We have completed an evaluation of the feasibility of this approach by analyzing sealed samples using both NMR and Raman spectroscopy, as well as by placing samples into NMR tubes, flame sealing them, and then placing them into ovens regulated at 74°C (the highest temperature defined in the matrices) and at 85°C (the temperature used in some earlier-mentioned ARL studies). The samples used in the preliminary aging studies included: 1) SNL-purified SO_2Cl_2; 2) 1.5 **M** $AlCl_3$ in SO_2Cl_2 using commercial materials; and 3) 1.5 **M** $AlCl_3$ in SO_2Cl_2 electrolyte as received from KDI. One sample of each type at each condition was evaluated. These samples were allowed to age for one month at temperature, and have recently been removed from the oven. Three immediate observations can be made from these samples. First, this approach can be used for implementation of the full matrix. Second, the intensity of the color of the solution, presumably due to formation of Cl_2, increased in every case. Third, a precipitate formed in both samples containing $AlCl_3$ at the higher temperature, and some other material formed and adhered to the inside wall of the tube. All of the other samples remained clear. These samples are currently being characterized using both NMR and Raman.

In a separate experiment, a 1.5 **M** solution of $AlCl_3$ in SO_2Cl_2 was prepared using commercially available materials, allowed to stir for several days, and then placed at -25°C. After several days, some crystalline material formed (*note*: this sample had never been exposed to elevated temperatures). A single crystal X-ray diffraction pattern was obtained from these crystals, and its structure was determined and is shown in Figure 7 below.

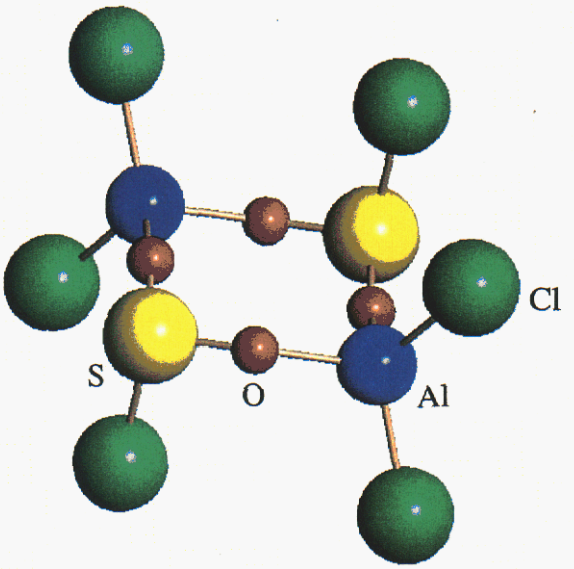

tjb116

$[AlCl_2SO_2Cl]_2$

$R_1 = 3.10\ \%$

Figure 7. Structure of crystallized material.

Final adjustments to the electrolyte aging matrices are in progress, and will be resolved by mid-June.

Modifications to the Statement of Work

- The ball seal corrosion study test matrix (Task III) was revised slightly based on ARDEC guidance. The revised matrix is presented below in Table 4. This study will begin in June.

Table 4. Task III Ball Seal Corrosion Study Test Matrix

SAMPLE NUMBER	METAL/COUPLES					WATER CONC/PPM			TEMPERATURE/°C		
	304	304 440C	304 316	304 Ni	304 WC	0	100	200-500	25	40	74
1	X					X			X		
2	X					X				X	
3	X					X					X
4	X						X		X		
5	X						X			X	
6	X						X				X
7	X							X	X		
8	X							X		X	
9	X							X			X
10		X	X	X	X	X			X		
11		X	X	X	X	X				X	
12		X	X	X	X	X					X
13		X	X	X	X		X		X		
14		X	X	X	X		X			X	
15		X	X	X	X		X				X
16		X	X	X	X			X	X		
17		X	X	X	X			X		X	
18		X	X	X	X			X			X
Perform optical & SEM inspections of balls after 12 months. All tests use 1.5 M $AlCl_3$											

- Two new tasks were finalized and a statement of work for both tasks was prepared and approved. Funding (MIPR) for these additional activities was received in late May. Work on this task will be initiated when the MIPR is processed by the DOE and Sandia financial organizations, presumably in early June.

Project Plan

Major activities planned for June include:

- Complete baseline analysis of KDI-electrolyte aging samples.
- Begin aging of KDI-electrolyte samples, both in NMR tubes and in reservoirs
- Start corrosion and welding studies.

Finally, Sandia will prepare to host a meeting with ARDEC and other project personnel in late June or early July.

February, 2002 Review Meeting Action Item Status Update

In the following list a brief description of each action item is given, followed by the identity of the person or organization having responsibility for completion of that activity. Those action items that have NOT been completed are shown in **Red** (bold), while those action items shown in *blue* (italics) have been completed. Note that Sandia is using the term "reservoir" to identify the specific electrolyte container used inside the battery. We use the term "ampoule" to identify any other sample holder (generic).

☺ 1. Specific documents dealing with electrolyte gelling in SDF batteries still need to be obtained by SNL. (Ben Lagasca will forward any e-mails on this subject by 2/22/02, Bruce Poese will check with Allan Goldberg, ARL and inform SNL by 2/22/02. All Picatinny Arsenal and ARL participants will check their records concerning information from a Battery Red Team Meeting at KDI and will forward that information to SNL by 2/22/02). *Documents have been received and reviewed.*

2. SNL will prepare a Wish List of items needed for further investigation. (Paul Nigrey will send the list to Joe Donini by 2/22/02). *Done. The Wish List and status for each is shown below.*

a) Provide one to three reservoirs or ampoules of aged/gelled electrolyte for Raman investigation. (KDI). *Done. Ten reservoirs have been received.*
b) Provide one to three reservoirs or ampoules of aged/un-gelled electrolyte for Raman investigation. (KDI). *Materials have been received.*
c) Provide one to three reservoirs or ampoules with "new" or fresh electrolyte for Raman investigation. *Completed - received 25 reservoirs.* (This is also Action Item 9.)
d) Provide process documents for cell fabrication. (KDI/Mike Steele). **We have not received these documents.**
e) Provide any additional Army and Alliant Tech Aging Reports. (KDI/Mike Steele). **We have not received these documents.**
f) Provide information regarding the glass composition in the ampoule. (KDI/Mike Steele). **We have not received this information.**
g) Provide a sample of the electrolyte used in the current production activities. (KDI/Mike Steele). *Done. Mike Steele has informed us that the material that was previously shipped to us and which is now on site is in fact a representative production sample.*

☺ 3. ARL will ship gelled electrolyte in reservoirs to SNL. (Bruce Poese will provide gelled and ungelled reservoirs by 3/8/02. The reservoirs will include some which had been stored for up to 2 years @165 F and some stored for shorter periods of time). *Materials have been received.*

☺ 4. Picatinny Arsenal will ship a reservoir containing ethylene glycol to SNL. (Paul Nigrey will send an e-mail Bill Vogt providing a SNL shipping address by 2/22/02, Bill Vogt will mail sample to SNL by 2/22/02). *It was sent, however it was damaged during shipment and arrived broken. (The glass was cracked and the reservoir was empty). The purpose of the sample has been met in other ways; this action item is now completed.*

☺ 5. Picatinny/KDI will provide another 200 endplates to SNL. (Joe Donini will mail samples by 2/22/02). *Completed.*

☺ 6. Picatinny will provide separator material composition and the methods that are used to dry them. (Joe Donini will provide information by 2/22/02). *Completed.*

☺ 7. Picatinny will provide guidance on the appropriate value of the highest aging temperature. Currently the approach is to use 85 C. For example, a possible new set of temperatures could be 40, 65, and 75 C, with 75 C as the highest temperature. (Joe Donini will inform SNL on this issue by 3/8/02). *Done. New guidance has been received identifying 74 C as the maximum temperature.*

☺ 8. Clarification on KDI's involvement with SNL is needed. (Bill Vogt will send e-mail by 2/15/02). *At this point formal completion of this item has not been done. However, we have initiated discussions with KDI directly. Joe D. has an agreement with KDI for their active participation in the project.*

☺ 9. Picatinny Arsenal will ship fresh reservoirs prepared at KDI to SNL (Dean Booker will speak with KDI and inform SNL by 2/15/02, KDI to ship items by 3/8/02). *This has been completed with the receipt of 25 filled reservoirs. This is also one of the wish list items.*

If questions arise concerning any of the above items, please contact Nancy Clark at (505) 845-8056 or David Ingersoll at 844-6099.

Distribution:
email Joe Donini, TACOM-ARDEC
email Ben Lagasca, TACOM-ARDEC
email Bill Vogt, OPM-CAS ARDEC
email Dean Booker OPM-CAS ARDEC
email Alan Goldberg, ARL
email Bruce Poese, ARL
email P. Butler, 2522
email N. Clark, 2522
email D. Doughty, 2521

email D. Ingersoll 2521
email C. Crafts, 2521
email D. Tallant, 1822
email B. Hammetter, 1843
email T. Boyle, 1846
email J. Braithwaite, 1832
email R. Sorensen, 1832
email T. Alam, 1811
email P. Nigrey, 1321
MS 0614 Day File, 2522

14. Appendix B

Monthly Report
July 31, 2002

Sandia National Laboratories

Operated for the U.S. Department of Energy by Sandia Corporation

Albuquerque, New Mexico 87185-

date: July 31, 2002

to: Distribution

from: Nancy Clark, 2522 and David Ingersoll, 2521

subject: Activities on ARDEC Self-Destruct Fuze Reserve Battery Project during June/July, 2002

This memo summarizes the activity performed in June/July, 2002, on the Self-Destruct Fuze Reserve Battery Project.

Project Status

Baseline Studies for Electrolyte Matrices.

Prior to implementation of the aging matrices, several baseline studies were completed. Because it was expected that both Raman and NMR spectroscopy were to be used for characterization, it was hoped that the various samples could be placed into the ovens in flame-sealed NMR tubes. In this way each sample could be repeatedly placed into the oven and removed at various time intervals for characterization by both Raman and NMR spectroscopy. We have completed an evaluation of the feasibility of this approach by analyzing sealed samples using both NMR and Raman spectroscopy, as well as by placing samples into NMR tubes, flame sealing them, and then placing them into ovens regulated at 74°C (the highest temperature defined in the statement of work) and at 85°C (the temperature used in some earlier-mentioned ARL studies). The samples used in these preliminary aging studies included: 1) Pure SO_2Cl_2; 2) 1.5 **M** $AlCl_3$ in SO_2Cl_2 using commercial materials; and 3) 1.5 **M** $AlCl_3$ in SO_2Cl_2 electrolyte as received from KDI (ARMY). One sample of each type at each condition was evaluated. These samples were allowed to age for one month at temperature, and were removed from the oven. The characterization of these samples is now complete. Samples were characterized using both NMR and Raman spectroscopy.

NMR Results

^{27}Al NMR analysis was done on all samples containing $AlCl_3$. Figure 1 shows a comparison between the data collected from the samples prior to aging and after having been aged for one month.

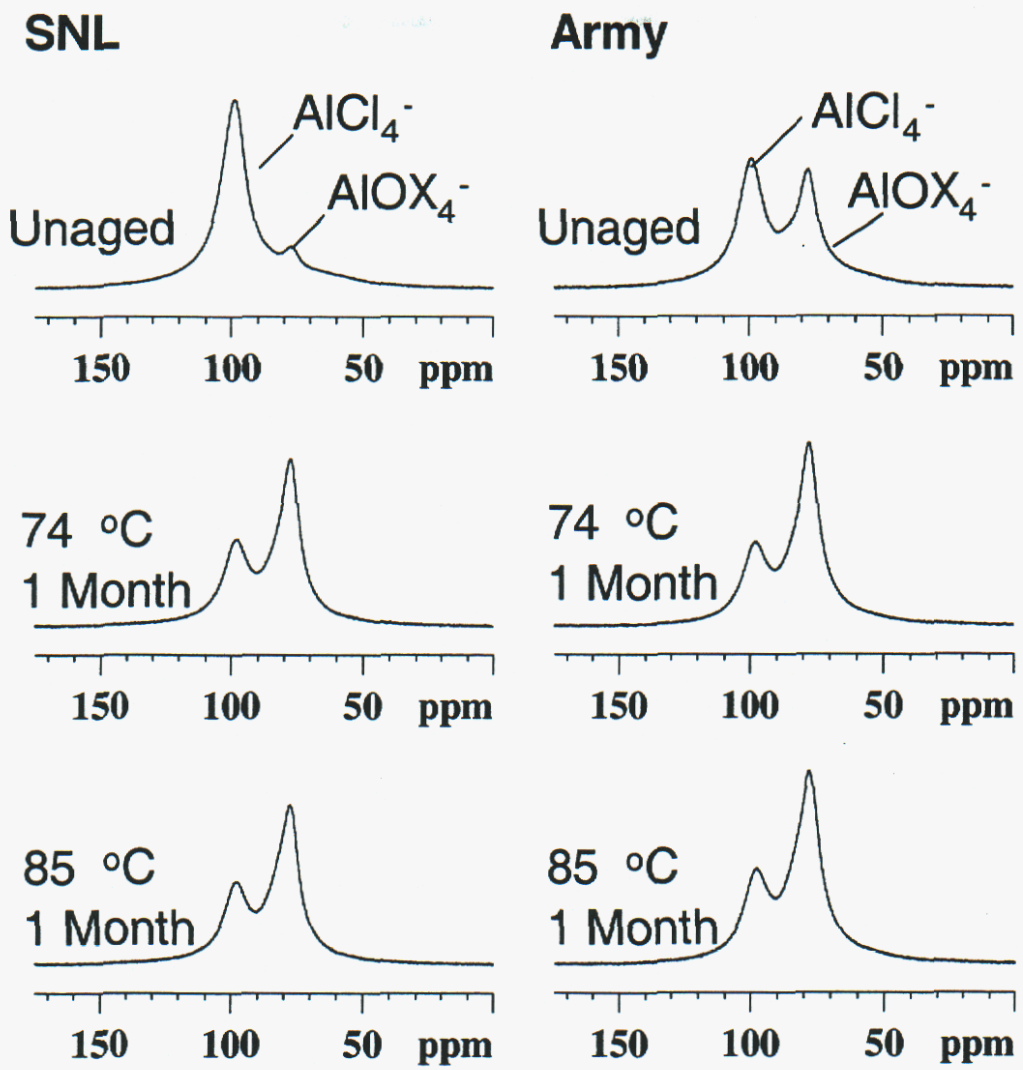

Figure 1. Effects of Thermal Aging on Al Coordination

As seen, these data provide at least two useful pieces of information. First, they support the earlier identification of formation of the Al complex with SO_2Cl_2. Second, regardless of the initial starting composition or the aging conditions employed, the NMR spectra for all of the samples are essentially the same after aging at one month. The implication of this later observation is that the initial sampling time interval employed for characterization of the matrix samples should be less than one month.

Raman Results

The unaged sulfuryl chloride/aluminum chloride/water solutions were analyzed by Raman spectroscopy in order to obtain baseline spectra. Other than absorption and some associated fluorescence, our analysis of the unaged sulfuryl chloride solutions yielded Raman spectra in which the dominant bands are exactly those associated with sulfuryl chloride. Aluminum chloride provides no features that can be explicitly associated with it, and the water, at a maximum concentration of 500 ppm, does not yield Raman features intense enough to be distinguished from the noise levels of the spectra. However, the presence of some low-intensity bands in these spectra is of interest.

In Figure 2 we show a portion of the spectra of unaged sulfuryl chloride solutions featuring the region where the S-O stretching vibrations occur. One spectrum is of unaged, neat, reagent grade sulfuryl chloride, and the other is from the Army formulation with added aluminum chloride. The spectrum of neat sulfuryl chloride is representative of such solutions, including a low-intensity band peaking near 1140 cm^{-1} due to SO_2. The spectrum of the Army formulation does not include the SO_2 band, but has two features that appear as low-frequency shoulders on the S-O stretch bands of sulfuryl chloride. These shoulders appear to be related to S-O stretches in an environment different from that of sulfuryl chloride. One possible explanation for these bands is that they are due to an adduct of SO_2 with aluminum chloride ($SO_2 + AlCl_3 \Rightarrow SO_2{:}AlCl_3$), having a structure such that both S-O stretching modes are Raman-active. In this explanation aluminum chloride would abstract the SO_2 that appears to be intrinsic to neat sulfuryl chloride. It is conceivable that the aluminum chloride-sulfur dioxide adduct might also be a precursor to the precipitate observed in certain aged sulfuryl chloride/aluminum chloride electrolytes.

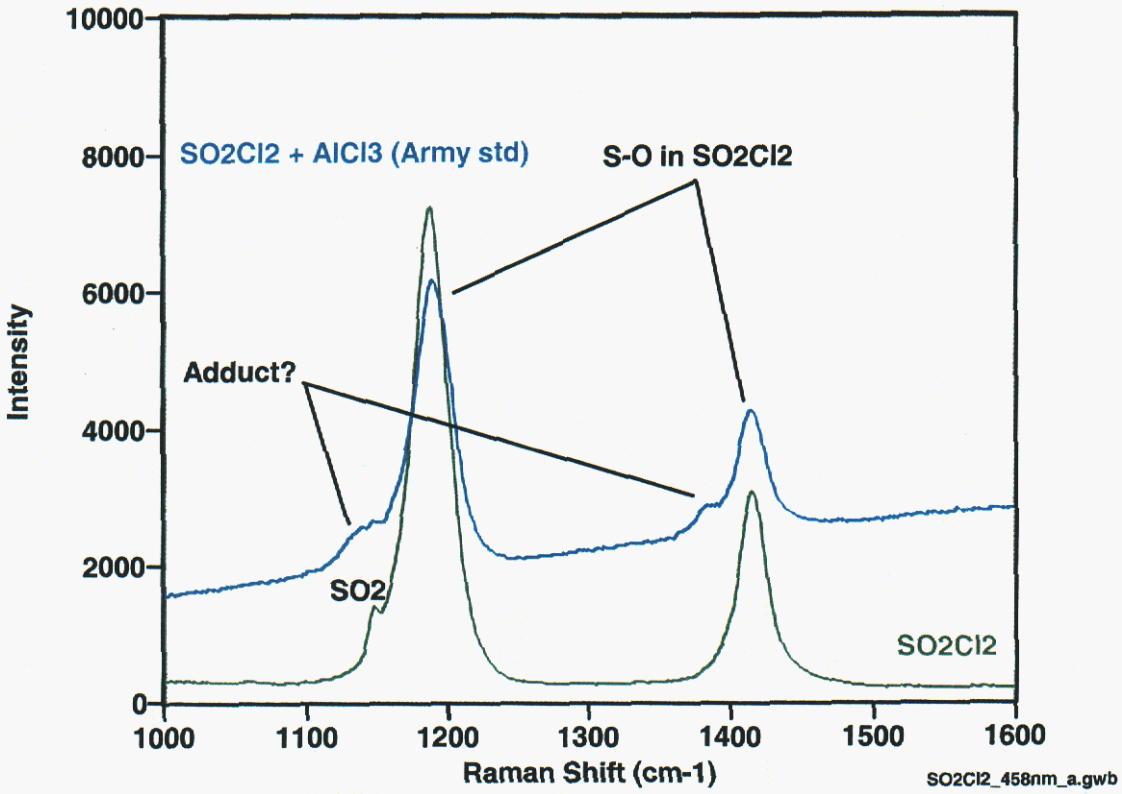

Figure 2. S-O stretch region of Raman spectra of unaged sulfuryl chloride solutions

We have also analyzed neat sulfuryl chloride and sulfuryl chloride with added aluminum chloride (but no added water) that had been aged at 85°C for a month. Spectra featuring the S-O stretch frequency region of unaged and aged sulfuryl chloride solutions are shown in Figure 3. In these Raman spectra we see a distinct increase in the intensity of the SO_2 Raman band in neat sulfuryl chloride with a month of aging. Neat sulfuryl chloride is apparently decomposed resulting in formation of SO_2. However, the spectrum of aged sulfuryl chloride/aluminum chloride does not include a band due to SO_2. These spectra suggest, as do those in Figure 2, that aluminum chloride is abstracting SO_2 released by sulfuryl chloride decomposition. The alternative is to propose that aluminum chloride is suppressing the decomposition of sulfuryl chloride. We cannot determine whether adduct bands (Figure 2) are present in the last spectrum shown in Figure 3 due to the fact that the noise in this spectrum is relatively high. We should be able to reduce this noise by appropriate filtering.

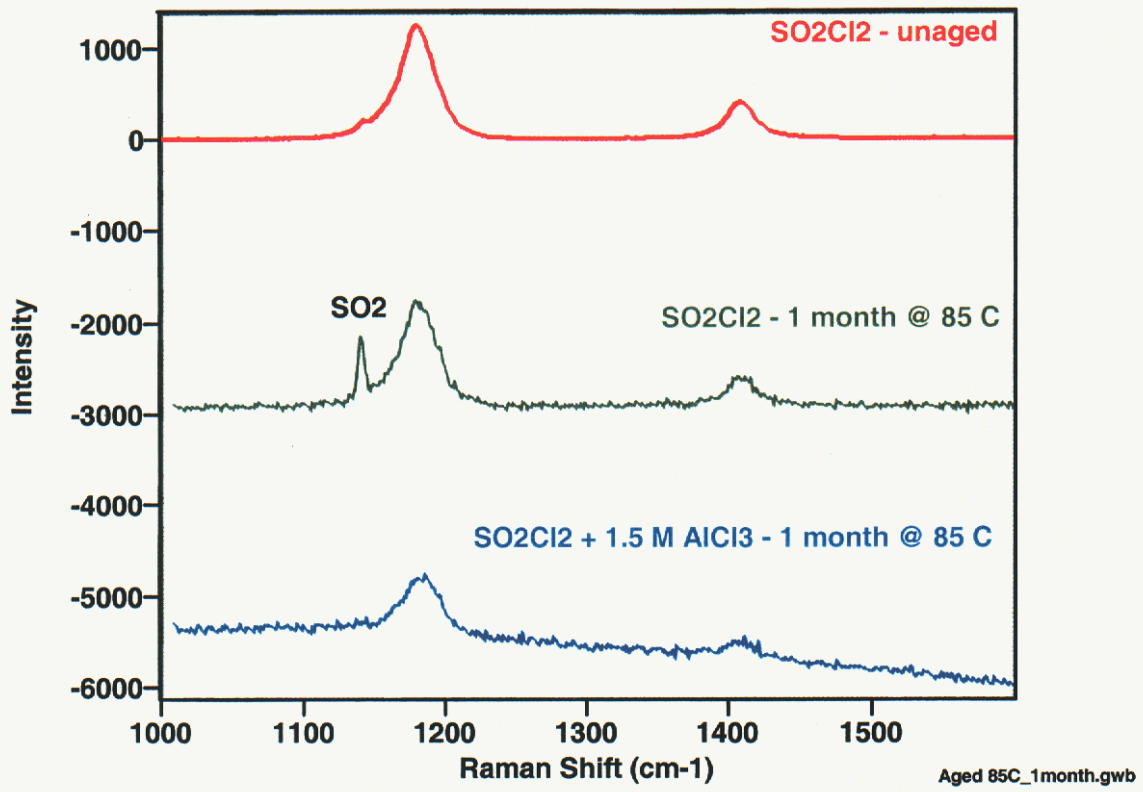

Figure 3. S-O stretch region of Raman spectra of unaged and aged sulfuryl chloride solutions

Increased turbidity has been noted in some of the aged solutions, and this is apparently due to formation of a precipitate. If enough of this precipitate accumulates after further aging, we should be able to obtain a Raman spectrum of this material with the hope of identifying its composition and structure.

Electrolyte Aging Matrices

On the basis of this preliminary work, we have initiated three of the aging matrices, and this work is briefly summarized below.

Matrix 1 – Reservoirs.

This matrix, corresponding to Task IV in the Statement of Work, involves aging new reservoirs at temperatures of 40°C, 65°C and 74°C with periodic removal for optical

examination and Raman spectroscopic analysis. Thirty reservoirs to be used for this activity were received from KDI, and Raman spectra from each were collected. These spectra will be used as a baseline for the aging studies, hence each reservoir was provided with a unique identification label. The spectra were collected in a 180° backscatter configuration using a microscope objective to focus the excitation beam through the glass of the reservoir window. (This was described more fully in the previous monthly progress report.)

The matrix was populated with five reservoirs at each temperature, and Table 1 summarizes the matrix details. One of the considerations in the implementation of this matrix is the relative orientation of the reservoir during the aging process. Consequently, the relative orientation of the reservoir during the aging process was documented, and this information is also shown in the table. (It is not clear at this point if this will in fact have a significant impact on the experimental results. However, in the event that we want to further evaluate this factor, we have held some reservoirs in reserve to further evaluate this possibility.)

Samples were placed into ovens on June 28, 2002. On July 26, 2002 the samples were removed from the ovens for characterization by Raman spectroscopy. These spectra are not yet available. (Recall that the preliminary data obtained using NMR suggested use of a shorter initial sampling interval. However, in this matrix only Raman spectroscopy will be employed due to the fact that the sample containers are reservoirs. The nondestructive use of reservoirs precludes characterization by NMR. Consequently, the initial sample interval was left at 30 days.)

Table 1.
Matrix 2 – Commercial Materials

Reservoir Id Number	Temperature °C	Orientation of glass during aging
1	40	Glass to the side
2	40	Glass to the side
3	40	45 with glass up
4	40	Glass to the side
5	40	Glass up
6	65	Glass up
7	65	45 with glass up
8	65	Glass to the side
9	65	Glass at approximately 20 and uphill side
10	65	Glass on the side
11	74	45 with the glass down
12	74	Glass up
13	74	Glass to the side
15	74	Glass at approximately 20 and uphill side
16	74	Glass up

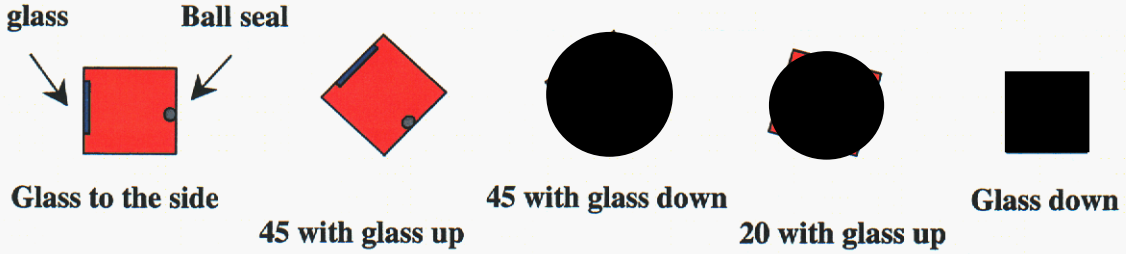

Note - Pictorial representation of orientation descriptions found in the table.

Electrolyte Matrices - Commercial Materials

Two matrices using commercially available materials were developed. The first of these, called Matrix 2, is shown in Table 2. This matrix is a Full Factorial design and employs a fixed concentration of $AlCl_3$ of 1.5 **M**. The factors that are being evaluated in this study include water content, temperature and time at temperature. The samples were prepared by placing the requisite materials into glass NMR tubes that were then flame-sealed. After sealing and before aging, the samples were characterized using both NMR and Raman spectroscopy. The samples were placed into ovens on July 19, 2002. The initial sampling protocol called for the first characterization to be completed at the end of 30 days, however preliminary data collected during our initial screening work indicated that the first sampling interval should be done at a shorter time interval, in this case two weeks (as described above). The first withdrawal of these samples is scheduled for August 1, 2002.

Table 2

Matrix 2 Full Factorial Design		
Sample ID	Water Content ppm	Temperature °C
1	100	65
2	500	40
3	0	74
4	500	74
5	0	74
6	100	65
7	0	40
8	500	40
9	0	40
10	500	74
11	100	65

The third matrix implemented is that described in the Statement of Work, and the sample compositions and aging conditions are summarized in Table 3. These samples were prepared and handled in a manner similar to that just described for Matrix 2. Aging was initiated on June 27, 2002, and their first withdrawal from the oven occurred on July 11, 2002, for a total aging time interval of 14 days. (The first sample withdrawal was changed to 14 days from 30 days on the basis of the preliminary data described above.)

Table 3.
Matrix 3 – Commercial materials

Spl #	Temperature/C			Water Conc/ppm			$AlCl_3$ Conc/M		
	40	65	74	0	100	500	0	0.75	1.5
1	X			X			X		
2	X			X				X	
3	X			X					X
4	X				X		X		
5	X				X			X	
6	X				X				X
7	X					X	X		
8	X					X		X	
9	X					X			X
10		X		X			X		
11		X		X				X	
12		X		X					X
13		X			X		X		
14a		X			X			X	
14b		X			X			X	
14c		X			X			X	
15		X			X				X
16		X				X	X		
17		X				X		X	
18		X				X			X
19			X	X			X		
20			X	X				X	
21			X	X					X
22			X		X		X		
23			X		X			X	
24			X		X				X
25			X			X	X		
26			X			X		X	
27			X			X			X
Characterization of samples at 0, 0.5, 1, 3, 6 and 12 months									

After withdrawal the samples were analyzed by solution ^{27}Al NMR. (Characterization by Raman of these samples has not yet been completed.) At least two different Al species are observed in the solutions containing $AlCl_3$. The relative concentrations of these species were determined and tabulated as a function of nominal H_2O content and aging temperature. Figures 4 and 5 show the decrease in the "unaged" $AlCl_3$ species as a function of aging conditions.

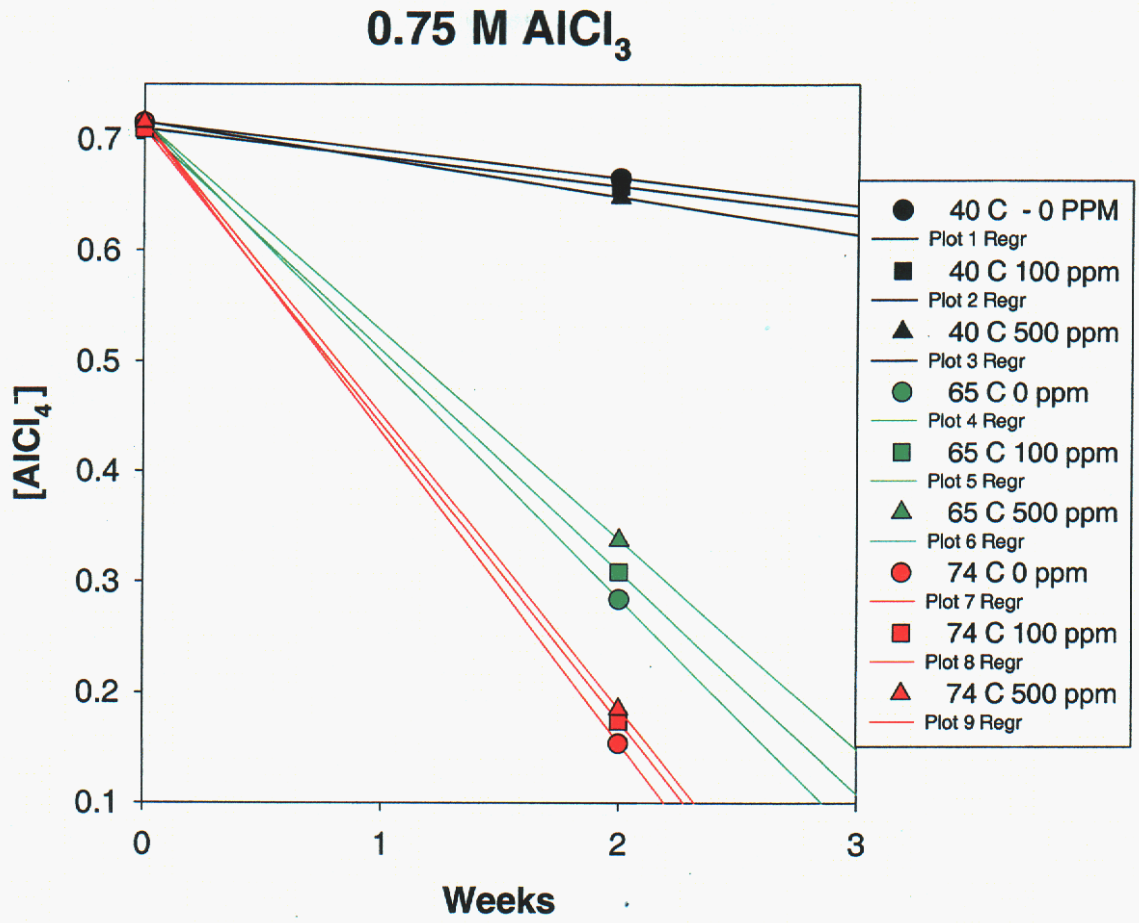

Figure 4. $AlCl_3^-$ species as a function of aging conditions

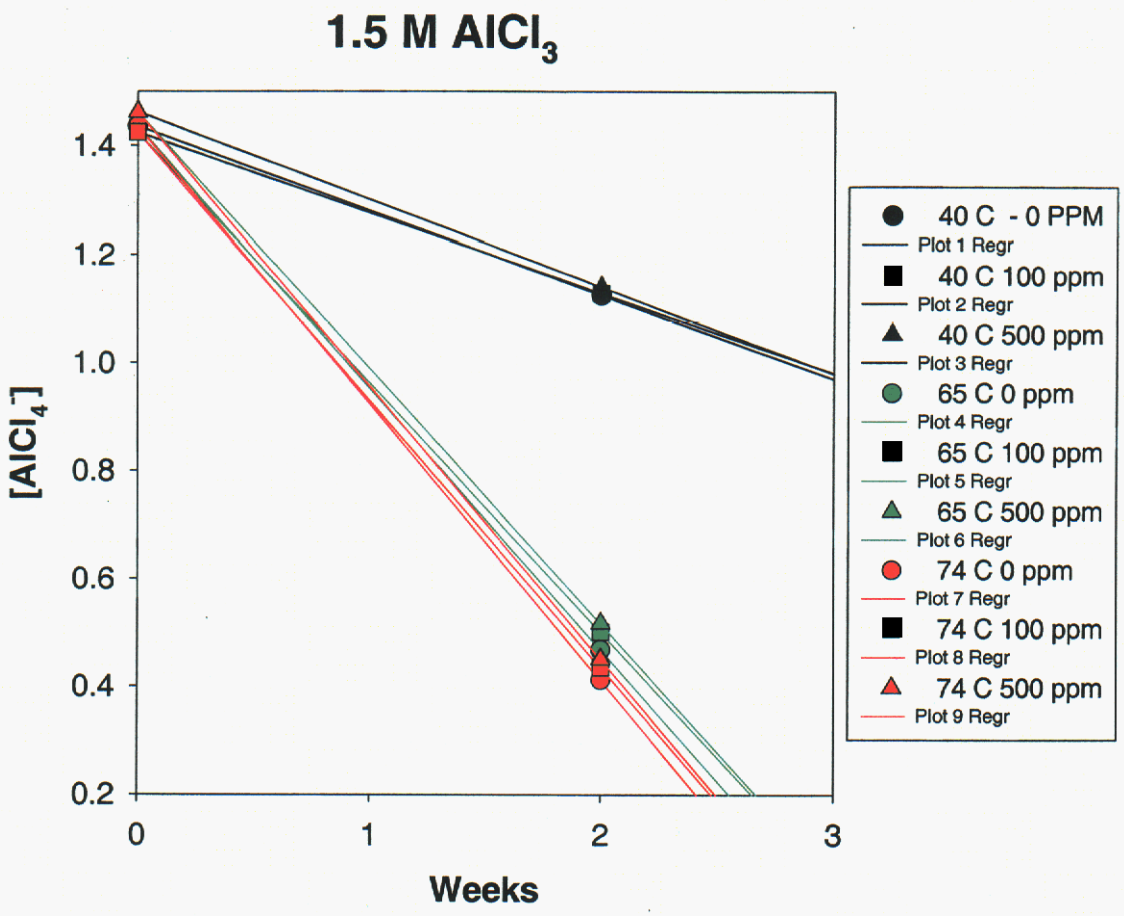

Figure 5. $AlCl_3^-$ species as a function of aging conditions

At this point a single aging time interval has been analyzed. However, in spite of the preliminary status of the aging data, several observations can be made. These are:

1) There is an increased rate of $AlCl_3$ species disappearance with increasing temperature.
2) These rate of loss is independent of the initial H_2O concentration. (The caveat here however, is that we are using the nominal "as prepared" concentrations assigned during preparation.)
3) There is a difference in the temperature behavior observed between 1.5 M and 0.75 M $AlCl_3$ (note the differences in the 65 °C versus 74 °C set of samples).

Modifications to the Statement of Work

Effect of water contamination on the corrosion of ball and endplate materials

After the review meeting a revised SOW was developed based on the concern and objectives described below.

Concern:
Previous work has shown that most of the typical corrosion-resistant engineering materials are very stable in the SO_xCl_2-type electrolytes if the water-content is very low. Unfortunately, a quantitative definition of "very low" is not known. Also, we expect that the candidate metals to only be susceptible to localized forms of corrosion (e.g., pitting, crevice, intergranular and possibly focused near the fill line) with crevice corrosion under the ball seal being the most likely mode of attack. Other work has also shown that the majority of the corrosion products will not be soluble in the electrolyte.

Objective:
Assess the effect of the level of water contamination in the electrolyte on the corrosion characteristics of the endplate/ball seal materials.

Scope of Work: the test matrix to be followed is listed in Table 4 shown below and described as follows:

Electrolyte: As a baseline, only the 1.5 M $AlCl_3$ electrolyte supplied directly from ARDEC will be used. We expect that all the candidate $AlCl_3$ levels in combination with the solvent will have [Cl^-] clearly above the critical levels to initiate the possible localized forms of corrosion (for aqueous solutions, typically in the 100-1000 ppm range).
Duration: All the exposures will be performed for 12 months because we do not expect significant corrosion and therefore we can minimize analysis costs by assessing corrosion. Clearly, the initiation and propagation stages of corrosion will have had ample opportunity to proceed during this extended period.
Water content: 3 total - as received baseline, baseline + 100 ppm, and baseline +500 ppm (the upper level of 500 ppm may change based on the water analysis to be performed by Dave Tallant on the electrolyte contained in a supplied KDI reservoir.
Temperature: 3 total – 25, 40 and 74°C, so that we can determine if the water sensitivity is influenced by temperature.
Metals: baseline 304L stainless + 304L stainless galvanically coupled with 4 prime ball materials – 440C, 316L, Ni 201, tungsten carbide (WC). We will age 1 cm^2 metal coupons either alone (304L stainless steel) or in a galvanic-coupled configuration (ball material coupon laser welded along one side to base 304L stainless plate to produce a crevice and a heat affected zone).
Configuration: 18 sealed glass ampoules (3 water levels x 3 temperatures x 2 metal combinations). The samples will be contained in one-inch diameter glass ampoules. To isolate the galvanic coupled samples, a glass spacer will be used between each set. Each sample be replicated in the same ampoule (for a total of 90 samples).
Post Exposure Analysis: The extent of corrosion will be characterized primarily through optical and scanning electron microscopy. If corrosion does occur under these conditions, every effort will be made to quantify its extent to permit so form of predictive equation

(e.g., Arrhenius) to be postulated.

Table 4. Task III – Test Matrix for Water Contamination Corrosion Studies

EXP NUM	METAL COUPLES					WATER CONC(PPM)			TEMPERATURE (°C)		
	304	304 440C	304 316	304 Ni	304 WC	0	100	200-500	25	40	74
1	X					X			X		
2	X					X				X	
3	X					X					X
4	X						X		X		
5	X						X			X	
6	X						X				X
7	X							X	X		
8	X							X		X	
9	X							X			X
10		X	X	X	X	X			X		
11		X	X	X	X	X				X	
12		X	X	X	X	X					X
13		X	X	X	X		X		X		
14		X	X	X	X		X			X	
15		X	X	X	X		X				X
16		X	X	X	X			X	X		
17		X	X	X	X			X		X	
18		X	X	X	X			X			X

When agreement is received from the Army, this task will proceed.

Effect of external electrolyte contamination on the corrosion of reservoir endplate materials

After the review meeting a revised SOW was developed based on the corncern and objectives and important considerations below.

Concern:
The 304L stainless steel used in the fabrication of the reservoir endplate is susceptible to pitting, crevice, and intergranular corrosion in chloride-containing, aqueous environments. If, during reservoir filling, some electrolyte is spilled on the external surface of the reservoir endplate and not thoroughly cleaned, absorption of water may occur during the short time period the endplate is exposed to the dry-room and later cleaning-room atmospheres. An acidic, adsorbed, aqueous layer may result that can lead to serious pitting and, to intergranular attack if the stainless steel did become locally sensitized during the subsequent welding operation (not expected).

Objective:
Determine the vulnerability of the stainless steel to localized attack and estimate the possible significance of such attack under realistic, but bounded conditions.

Important considerations:
The possible types of localized corrosion on stainless steel typically takes a finite time to initiate (hours to days to weeks) depending on the environment and the specific metallurgy of the material. Under conditions that sustain the attack (adequate supply of reactants and water), propagation rates are relatively quite fast. However, under many conditions (e.g., atmospheric exposure such as this one), the corrosion that is initiated is often metastable and repassivation of the surface can occur. In this case the actual extent of damage could simply be "cosmetic", with no structural penetration and associated loss of hermeticity. Also, the subsequent final-closure welding operation is a factor that we may need to explicitly consider for at least three reasons: (1) as noted above, welding could locally sensitize the stainless (especially if it is not 304L) and make it susceptible to intergranular attack, (2) due to even small amounts of heating, a significant change could be produced in the composition of the adsorbed water/electrolyte decomposition layer, and (3) the heating could clearly accelerate all the corrosion processes.

Scope of work:
Characterize the types and extent of corrosion on actual endplates under realistic and "worst-case" bounding conditions by executing the experimental matrix presented in the table below and described in a narrative manner as follows:

Overview of specific steps: To simulate the possible types of exposures during the reservoir fabrication process, each endplate sample will be prepared (Step 1), contaminated (Step 2), exposed to the Sandia dry room environment (Step 3), and then either (a) immediately sealed in a hermetic enclosure (Step 6), or (b) exposed to a normal Sandia laboratory environment (Step 4) and immediately sealed in the hermetic enclosure (Step 6), or (c) exposed to the laboratory environment and then cleaned (Step 5), prior to sealing in the hermetic enclosure (Step 6). Following sealing, each sample will be aged primarily at a slightly elevated temperature (~40°C), but with selected samples at two other temperatures (Step 7). Three welded reservoirs (recovered from electrolyte studies) will also be tested to allow possible sensitization effects of the localized heating from laser welding to be assessed. We will not perform a full test matrix around each of these variables (see the table). Instead, variables will be characterized around a baseline that consists of dipping, a 15-minute dry room exposure and aging at 40°C for six months. Because of the stochastic nature of corrosion, each of these aging experiments will be replicated in the same packaging enclosure. The aging time for the replicates from the welded samples might be extended depending on the associated results from the one-month exposures.

Experimental Steps:

1. Material: ARDEC supplied endplates containing 440C ball seals will be endplate configuration used. The as-received (passivated) samples will all first be degreased and then vacuum baked at 150°F for 24 hours.
2. Contamination of endplates: quantity of SO_2Cl_2 electrolyte: 2 levels: minor (~ micro-sized drop), and horizontally dipped. Only the electrolyte as-received from the Army will be used.
3. Immediate exposure in dry-room environment for three selected times: 15, 30, and 120 minutes (to allows electrolyte evaporation, water adsorption, & electrolyte hydrolysis to occur). The Sandia dry room will be at about 1% relative humidity during these activities.
4. Selected samples, following the dry-room exposure, will be further exposed in a laboratory hood to simulate the time in which a loaded tray of reservoirs could be exposed prior to cleaning. Exposure times will again be 15, 30, and 120 minutes.
5. A few samples exiting from Step 4 will then be thoroughly cleaned following the KDI procedure (ultrasonic-bath immersion for 2 minutes each: 20% $NaHCO_3$ followed by DI water rinse). Most samples from Step 4 will not be cleaned because our expectation is that the cleaning will be adequate to remove the undesirable contamination and thus completely stop corrosion.
6. Immediately following the appropriate step (either 4, 5, or 6), the samples will be packaging within the dry room in a hermetic enclosure. For this small-volume enclosure, we will use standard ¼" stainless steel Swagelok fittings consisting of an end plug and an end cap and strictly follow torqueing instructions.
7. Each packaged sample will be aged at 25°C, 40°C or 74°C in the hermetic enclosure for time periods of 1 month, 6 months, or 1 year.
8. The extent of corrosion damage will be determined using a combination of optical and electron microscopy on plan-view and cross-sectioned samples. Visual observations will also be made just prior to packaging for an initial assessment of any immediate damage.

Table 5. Task N1. Test matrix for the external electrolyte contamination corrosion studies (Experiment #1-#3 are baseline test configuration)

Aging Expt #	*Material*	*Electrolyte Contamination*		*Dry room Exposure Time*	*Lab Exposure Time*	*Cleaned*	*Temp*	*Aging Time*
		Drop	*Dipped*	*Minutes*	*Minutes*		*°C*	*Months*
Baseline conditions								
1	Endplate		X	15	--	--	40	6
2	Endplate		X	15	15	--	40	6
3	Endplate		X	15	15	yes	40	6
Alternate Contamination								
4	Endplate	X		15	--	--	40	6
5	Endplate	X		15	15	--	40	6
6	Endplate	X		15	15	yes	40	6
Dry Room Exposure Time								
7	Endplate		X	30	--	--	40	6
8	Endplate		X	120	--	--	40	6
Standard Laboratory Exposure Time								
9	Endplate		X	15	30	--	40	6
10	Endplate		X	15	120	--	40	6
Aging Time								
11	Endplate		X	15	--	--	40	1
12	Endplate		X	15	--	--	40	12
Welded Reservoir								
13	Reservoir		X	15	--	--	40	6
14	Reservoir		X	15	15	--	40	6
15	Reservoir		X	15	15	yes	40	6
Low Temperature								
16	Endplate		X	15	--	--	25	6
17	Endplate		X	15	15	--	25	6
18	Endplate		X	15	15	yes	25	6
High Temperature								
19	Endplate		X	15	--	--	74	6
20	Endplate		X	15	15	--	74	6
21	Endplate		X	15	15	yes	74	6

When agreement is received from the Army, this task will proceed.

Welding Study

Parts have not been received for this study. When they are received this task will begin.

Proposed New Tasks

Characterization of Solid in Electrolyte

We will investigate the nature of the product formed in the reaction mixture between $AlCl_3$ and SO_2Cl_2. The material isolated from the reaction mixture will be analyzed by single crystal x-ray diffraction, powder XRD, multi-nuclear NMR spectroscopy, Raman spectroscopy, elemental analysis, and/or FT-infra red spectroscopy. The dried powder will be analyzed after mixing in order to attempt to determine the degree of reactivity maintained upon mixing. Attempts to generate crystals and characterize them will also be undertaken.

Additional experiments investigating the addition of water by NMR, XRD, and/or single crystal investigations will also be undertaken.

Electrolyte Performance at Temperature Extremes and in Thermal Cycling

In the predictive surveillance testing being completed by the Army, a maximum temperature of 250°F is employed. However, it is not clear if this high temperature will result in the formation of new and/or different reactions and reaction products. The implication of this situation is the question of the utility of data collected at these elevated temperatures in being able to make predictive statements on long term stability, especially in the event that there is a change in the reaction mechanisms at higher temperatures. Hence, this additional task is intended to evaluate this possibility.

The lower storage temperature for the fuze is –60°F. Furthermore, during the preliminary stages of work on this program, formation of a precipitate was observed in samples that had been stored at low temperature. A question invariably arises concerning this process, as well as the implications on battery performance.

Other unresolved issues concerning the precipitate /gel formation at low temperature relate to the reversibility of the process. That is, does the precipitate redissolve upon an increase in the temperature. The matrix shown below in Table 6 summarizes the additional testing to be performed in order to explore these temperature extremes. .

Table 6. Supplemental Matrix at Temperature Extremes

Sample Number	Temperature			Water Content/ppm			$AlCl_3$ Concentration/M		
	250°F	-60°F	Thermal cycle	0	100	500	0	0.75	1.5
1		X		X			X		
2		X		X				X	
3		X		X					X
4		X			X		X		
5		X			X			X	
6		X			X			X	
7		X			X			X	
8		X			X				X
9		X				X	X		
10		X				X		X	
11		X				X			X
12	X			X			X		
13	X			X				X	
14	X			X					X
15	X				X		X		
16	X				X			X	
17	X				X			X	
18	X				X			X	
19	X				X				X
20	X					X	X		
21	X					X		X	
22	X					X			X
23			X	X			X		
24			X	X				X	
25			X	X					X
26			X		X		X		
27			X		X			X	
28			X		X			X	
29			X		X			X	
30			X		X				X
31			X			X	X		
32			X			X		X	
33			X			X			X

Characterization at 0, 0.5, 1, 3, 6 and 12 months

Work on these tasks will be initiated when the MIPR is processed by the DOE and Sandia financial organizations, presumably in early August.

February, 2002 Review Meeting Action Item Status Update

This list is essentially complete so we will no longer report on it.

If questions arise concerning any of the above items, please contact Nancy Clark at (505) 845-8056 or David Ingersoll at (505) 844-6099.

Distribution:
email Joe Donini, TACOM-ARDEC
email Ben Lagasca, TACOM-ARDEC
email Bill Vogt, OPM-CAS ARDEC
email Dean Booker OPM-CAS ARDEC
email Alan Goldberg, ARL
email Bruce Poese, ARL
email P. Butler, 2522
email N. Clark, 2522
email D. Doughty, 2521
email D. Ingersoll 2521
email D. Tallant, 1822
email B. Hammetter, 1843
email T. Boyle, 1846
email J. Braithwaite, 1832
email R. Sorensen, 1832
email T. Alam, 1811
MS 0614 Day File, 2522

15. Appendix C

Monthly Report
August 29, 2002

Sandia National Laboratories
Operated for the U.S. Department of Energy by Sandia Corporation
Albuquerque, New Mexico 87185-0613

date: August 29, 2002

to: Distribution

from: Nancy Clark, 2522 and David Ingersoll, 2521

subject: Activities on ARDEC Self-Destruct Fuze Reserve Battery Project during August, 2002

This memo summarizes the activity performed in August, 2002, on the Self-Destruct Fuze Reserve Battery Project.

Project Status

Electrolyte Aging Matrices

On the basis of the preliminary work reported last month, we have initiated three of the aging matrices, and this work is briefly summarized below.

Matrix 1 – Reservoirs

This matrix, corresponding to Task IV in the Statement of Work, involves aging new reservoirs at temperatures of 40 °C, 65 °C and 74 °C with periodic removal for optical examination and Raman spectroscopic analysis.

Samples were placed into ovens on June 28, 2002. On July 26, 2002 the samples were removed from the ovens for characterization by Raman spectroscopy. These spectra are not yet available. The Raman lab has been delayed and this data is expected to be available for the September report. The samples wll be returned to the ovens as soon as the spectra are taken.

Matrix 2 – Electrolyte Matrix: Commercial Materials - Full Factorial

Two matrices using commercially available materials were developed. The first of these, called Matrix 2, is shown in Table 1. This matrix is a Full Factorial design and employs a fixed concentration of $AlCl_3$ of 1.5 M. The factors that are being evaluated in this study include water content, temperature and time at temperature. These samples were placed into ovens on July 19th, and were then removed at the end of two weeks. (The first sample withdrawal was changed to 14 days from 30 days on the basis of the preliminary data). Both Raman and NMR spectra were collected on all of the samples, however the data has not yet been processed. The samples were placed back into ovens on August 28th for continuation of the aging.

Table 1. Matrix 2- Full Factorial

Matrix 2 Full Factorial Design		
Sample ID	Water Content Ppm	Temperature °C
1	100	65
2	500	40
3	0	74
4	500	74
5	0	74
6	100	65
7	0	40
8	500	40
9	0	40
10	500	74
11	100	65

Matrix 3 – Electrolyte Matrix: Commercial Materials - Original Plan

The third matrix, Matrix 3, is that described in the Statement of Work. The sample compositions and aging conditions are summarized in Table 2. Aging was initiated on June 27, 2002, and their first withdrawal from the ovens occurred on July 11, 2002, for a total aging time interval of 14 days. (The first sample withdrawal was changed to 14 days from 30 days on the basis of the preliminary data). The second withdrawal was on August 19th after an additional two weeks of aging. These samples will be placed back in the aging ovens on August 30.

Table 2
Matrix 3 – Commercial materials - Original Plan

Spl #	Temperature/C			Water Conc/ppm			$AlCl_3$ Conc/M		
	40	65	74	0	100	500	0	0.75	1.5
1	X			X			X		
2	X			X				X	
3	X			X					X
4	X				X		X		
5	X				X			X	
6	X				X				X
7	X					X	X		
8	X					X		X	
9	X					X			X
10		X		X			X		
11		X		X				X	
12		X		X					X
13		X			X		X		
14a		X			X			X	
14b		X			X			X	
14c		X			X			X	
15		X			X				X
16		X				X	X		
17		X				X		X	
18		X				X			X
19			X	X			X		
20			X	X				X	
21			X	X					X
22			X		X		X		
23			X		X			X	
24			X		X				X
25			X			X	X		
26			X			X		X	
27			X			X			X
Characterization of samples at 0, 0.5, 1, 3, 6 and 12 months									

These samples have been analyzed by both solution ^{27}Al NMR and Raman spectroscopy and the results are summarized below.

^{27}Al NMR Results on Matrix 3 (Commercial Materials-Original Plan)

^{27}Al NMR was performed at time intervals of 0, 2 and 4 weeks of aging. At least two different Al species are observed in the solutions containing $AlCl_3$. The relative concentrations of these species were determined and tabulated as a function of nominal H_2O content and aging temperature. Figures 1 and 2 show the decrease in the $AlCl_3$ species concentrations as a function of aging conditions.

The following observations were noted:

1) The reduction of the $AlCl_4^-$ species concentrations at 40 °C continues in an approximately linear fashion for both the 0.75 M and the 1.5 M $AlCl_3$ initial concentration samples.
2) A very ***non-linear*** loss of $AlCl_4^-$ is noted for the samples aged at 65 °C and 74 °C. In particular there is a plateau of the $AlCl_4^-$ concentration between 2 and 4 weeks. This is most notable for the samples aged at 65 °C and 74 °C with 1.5 M $AlCl_3$ initial concentration, where almost **NO** change in the $AlCl_4^-$ concentration is noted (Fig. 2). For the 0.75 M initial concentration samples aged at 65 °C, there is a slight decrease in the $AlCl_4^-$ species, while the samples aged at 74 °C show almost no variation between 2 and 4 weeks.

In summary, it appears that at higher temperatures an equilibrium has been reached between the $AlCl_4^-$ species and the other aged Al species in solution. For the samples aged at 40 °C this equilibrium has not yet been reached.

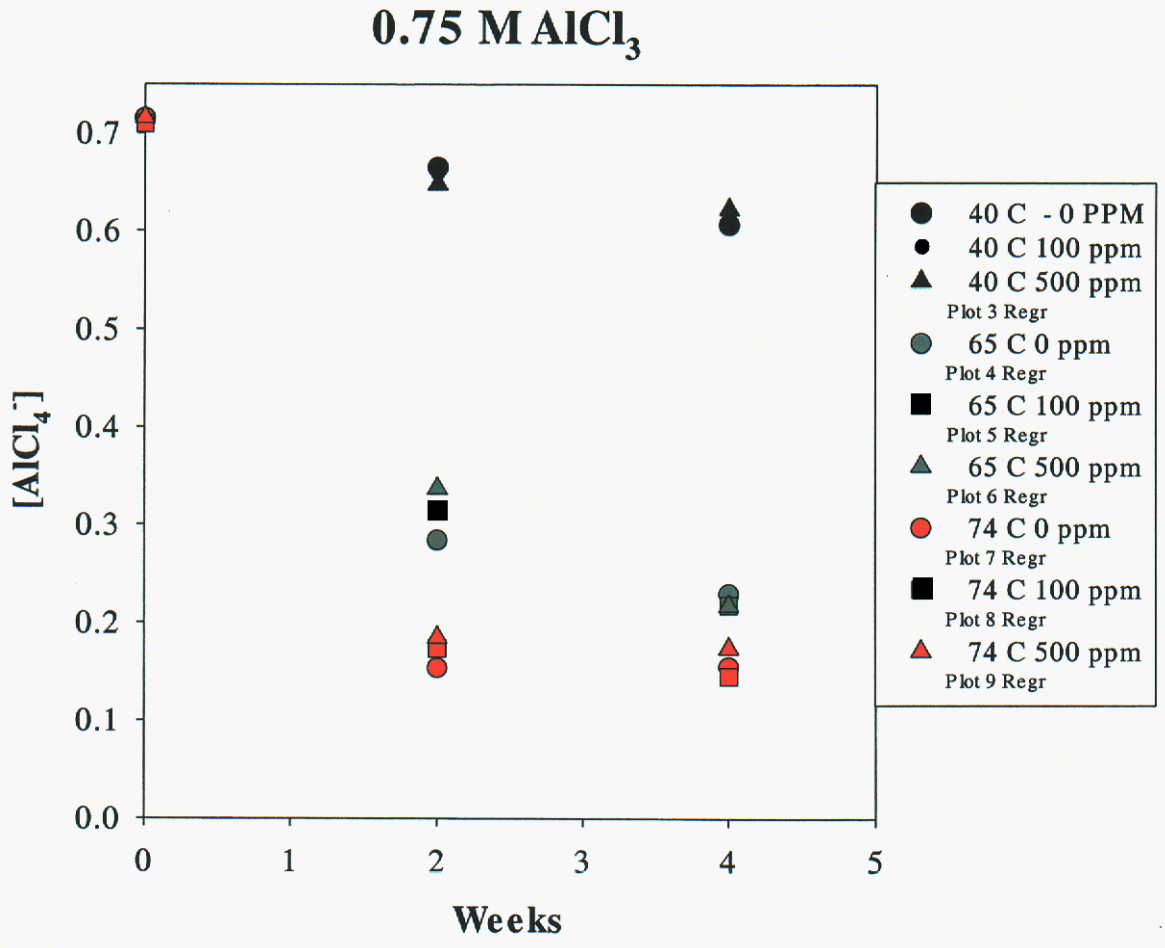

Figure 1. $AlCl_4^-$ species in M as a function of aging conditions for initial 0.75 M $AlCl_3$ concentration

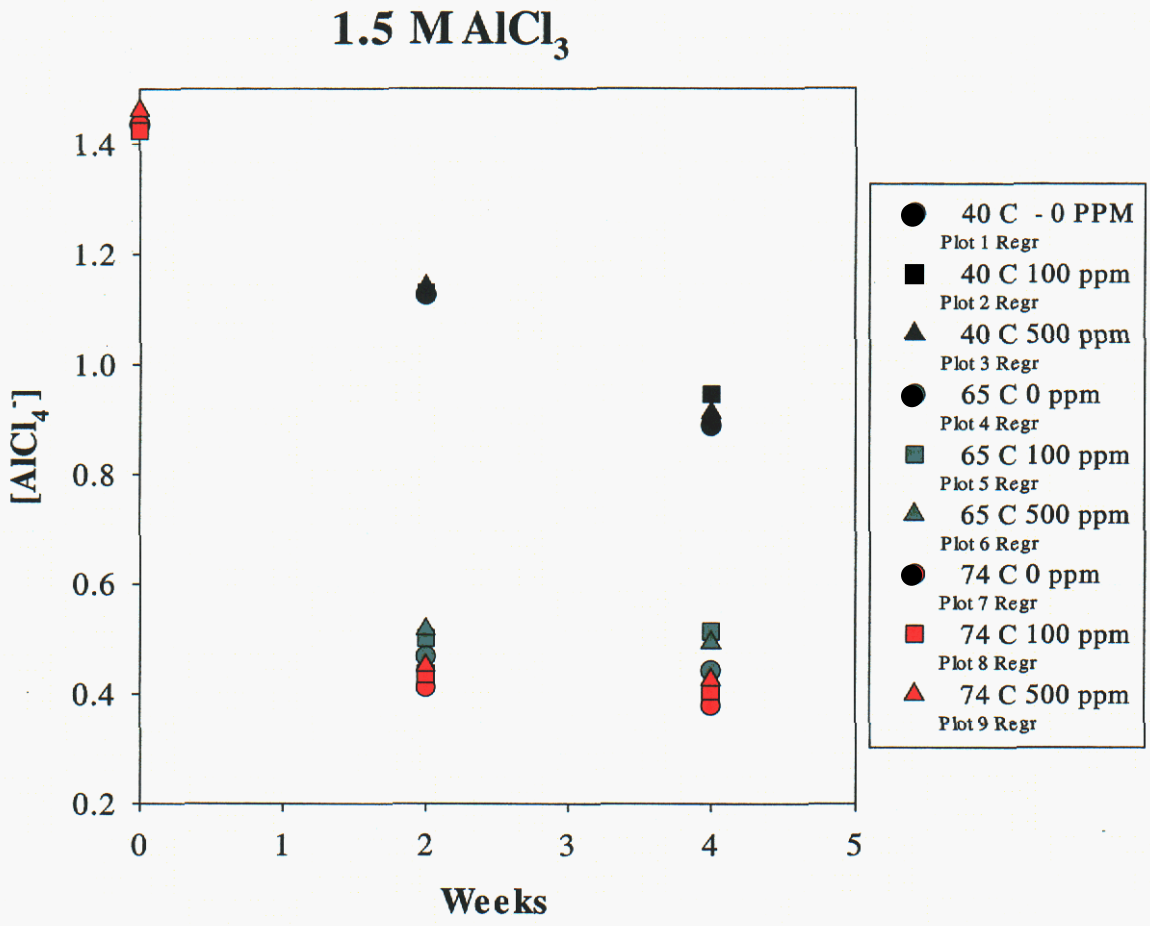

Figure 2. $AlCl_4^-$ species in M as a function of aging conditions for initial 1.5 M $AlCl_3$ concentration

Raman Characterization of Matrix 3 Samples (Commercial Materials- Original Plan)

Raman spectra of selected two-week-aged samples are shown in Figures 3 through 8. These spectra were obtained using a 785 nm laser for excitation. Self-absorption by the more colored samples and uncertainty in positioning the NMR tubes holding the electrolyte solutions results in about a 10% variation in the overall intensities of the Raman spectra. Some spectra have been scaled in intensity for ease of comparison.

Figures 3 and 4 show different portions of the Raman spectra from sulfuryl chloride (SO_2Cl_2) solutions with 0 ppm (added) H_2O and 0 M $AlCl_3$. The figures include spectra of ambient-temperature aged sulfuryl chloride and sulfuryl chloride aged at 40°C, 65°C

and 74°C for two weeks. Except for the features labeled with their peak frequencies, all the bands in the spectra are due to fundamental vibrations of sulfuryl chloride. The feature peaking at 1142 cm^{-1} (bottom set of spectra) is due to dissolved sulfur dioxide (SO_2). The feature at 538 cm^{-1} (top set of spectra) is not intense enough to be well defined, but we believe that it is due to dissolved chlorine (Cl_2). Sulfur dioxide and chlorine are apparently decomposition products of sulfuryl chloride, and the intensities of their Raman bands (likewise, their concentrations) increase with increasing aging temperature. For solutions of containing only sulfuryl chloride, the aging so far appears to involve decomposition into sulfur dioxide and chlorine.

Figures 5 and 6 show different portions of the Raman spectra from sulfuryl chloride (SO_2Cl_2) solutions with 0 M $AlCl_3$ and 0 ppm, 100 ppm and 500 ppm (added) H_2O. These solutions were aged two weeks at 74°C. The only features not due to sulfuryl chloride are those bands at 1142 cm^{-1} (sulfur dioxide) and 538 cm^{-1} (chlorine). The intensity of the sulfur dioxide and chlorine bands decreases with increasing water content. The presence of water either suppresses the decomposition of sulfuryl chloride or causes its decomposition products to react to products with less distinguishable Raman features. Further aging should help to better understand the how water is interacting with sulfuryl chloride and its decomposition products.

Figures 7 and 8 show different portions of the Raman spectra from sulfuryl chloride (SO_2Cl_2) solutions containing 1.5 M $AlCl_3$ and 0 ppm (added) H_2O. One of these solutions was not exposed to elevated temperatures, while the others were aged for two weeks at 40°C, 65°C and 74°C. Sulfuryl chloride bands dominate all these spectra, but features at 254 cm^{-1} and 429 cm^{-1} (top spectra) and 1128 cm^{-1} and 1375 cm^{-1} (bottom spectra) are also present in the spectra of the ambient-temperature and 40°C-aged solutions. These features are associated with the addition of aluminum chloride. We have proposed that they are some type of adduct of sulfur dioxide with aluminum chloride, since the sulfur dioxide band (1142 cm^{-1}) present in ambient-temperature, neat sulfuryl chloride is not discernable in ambient-temperature sulfuryl chloride containing 1.5 M $AlCl_3$. Interestingly enough, these "adduct" bands are less intense in the sulfuryl chloride/1.5 M $AlCl_3$ solutions aged at 65°C and 74°C, where bands due to sulfur dioxide (1142 cm^{-1}) and chlorine (538 cm^{-1}) become apparent. Apparently this adduct, or whatever type of intermediate it is, decomposes at these higher temperatures. Addition of up to 500 ppm of water had no discernable effect on the Raman spectra of the sulfuryl chloride/1.5 M $AlCl_3$ solutions at any of the aging temperatures. Again, further aging should help us understand the reactions that are occurring.

IR Analysis of Water Content of Electrolyte in Reservoirs

Samples have been prepared in sealed IR tubes for the water content analysis of electrolyte in reservoirs. Samples of the electrolyte from reservoirs to be used in the welding are also being gathered. It is expected that the analysis of the water content samples will be completed in late September.

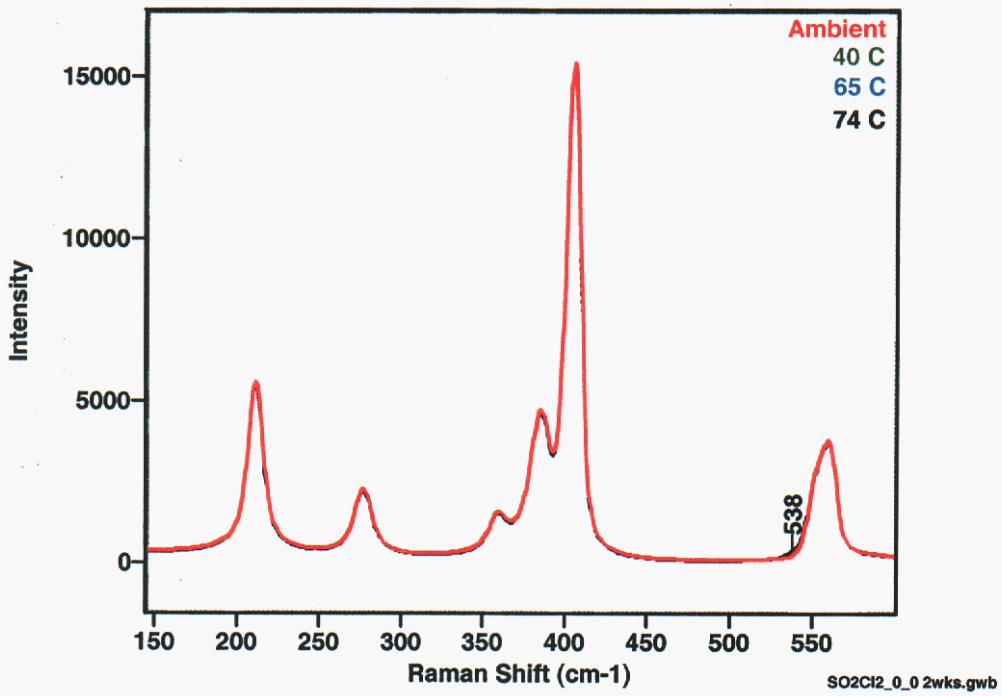

Figures 3 and 4. Raman spectra of SO_2Cl_2 with 0 ppm H_2O and 0 M $AlCl_3$, after two weeks of aging at four temperatures over two ranges of Raman Shift

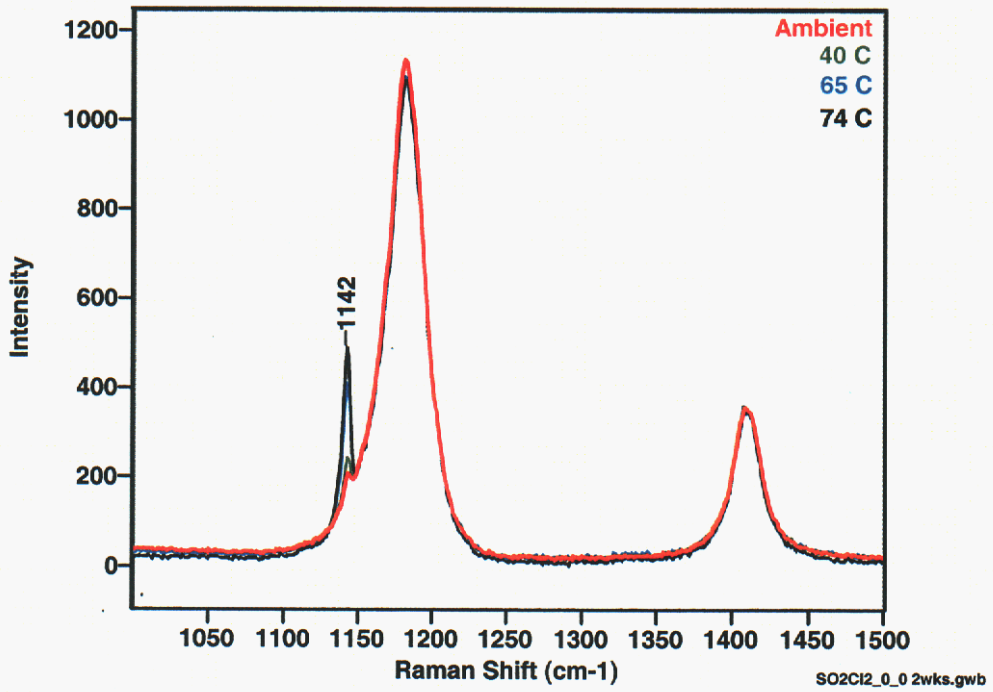

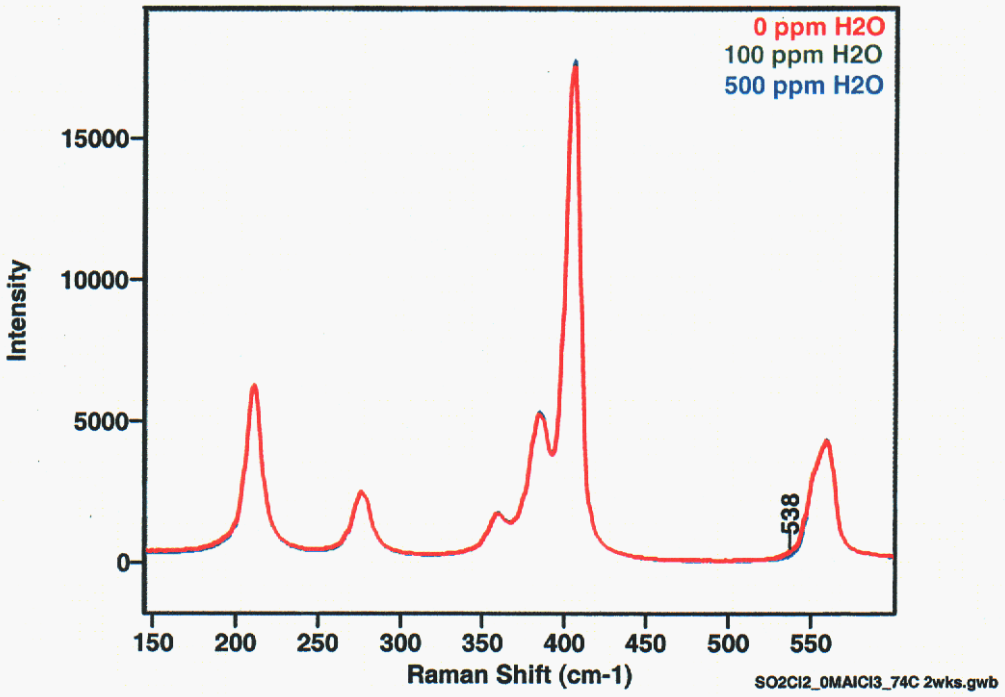

Figures 5 and 6. Raman spectra of SO_2Cl_2 with 0 M $AlCl_3$, after two weeks of aging at 74°C for three concentrations of water over two ranges of Raman Shift

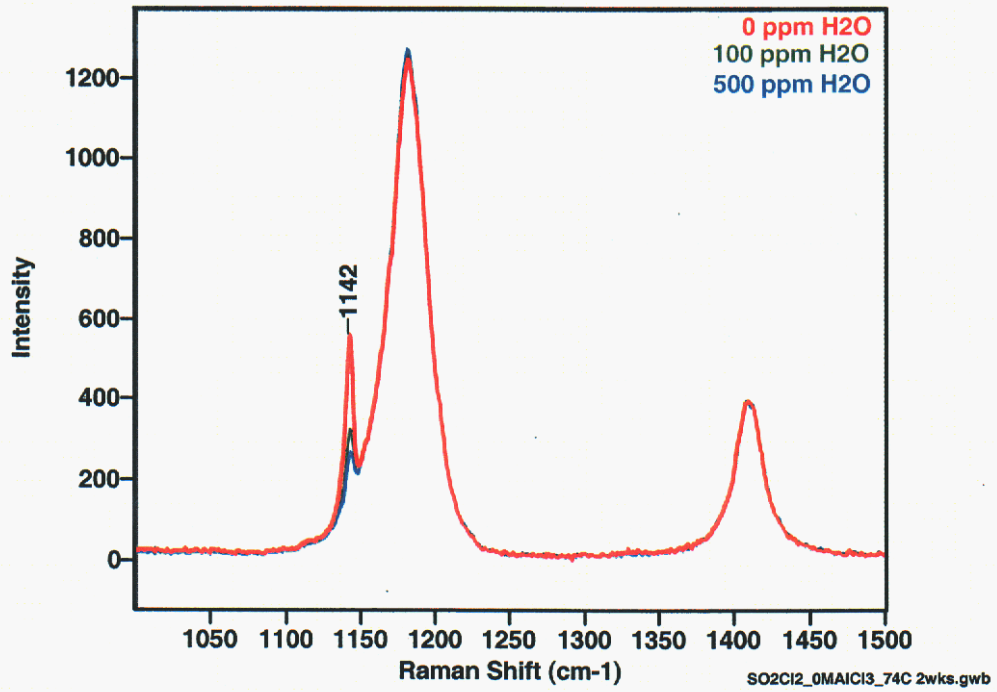

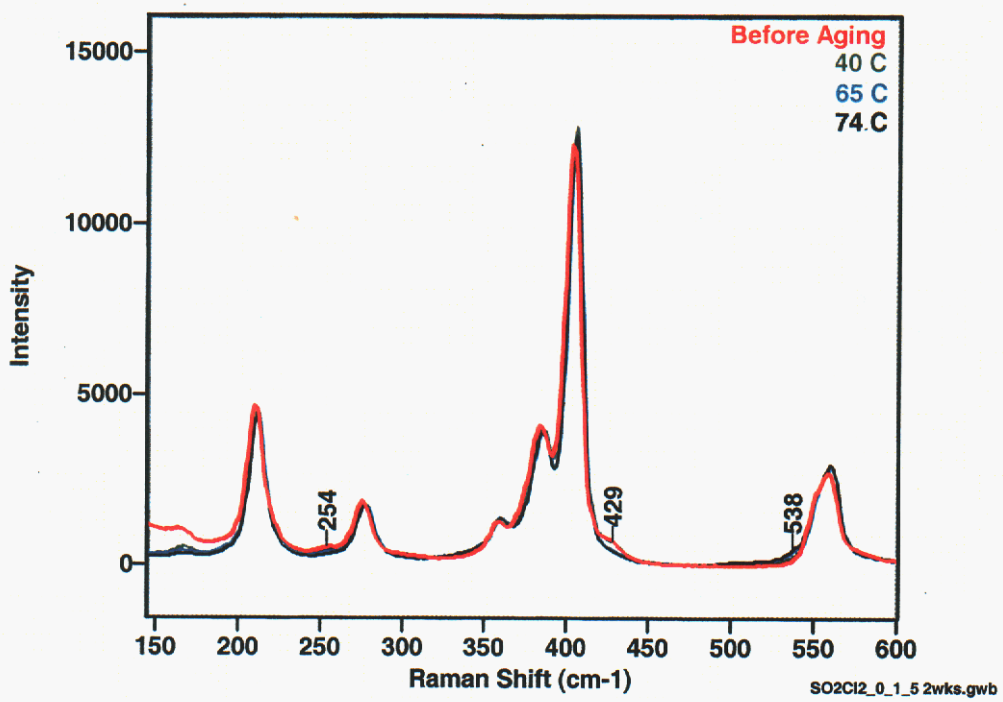

Figures 7 and 8. Raman spectra of SO_2Cl_2 with 0 ppm H_2O and 1.5M $AlCl_3$, for an ambient- temperature baseline sample and after two weeks of aging at three temperatures over two ranges of Raman Shift

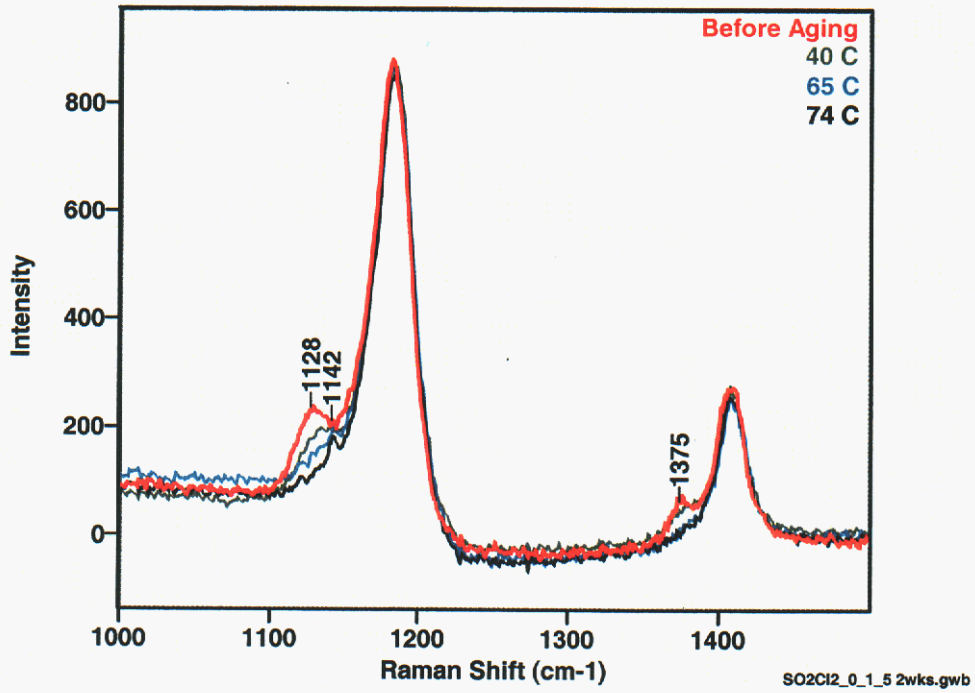

Effect of water contamination on the corrosion of ball and endplate materials
During the past month, activity focused on preparing samples and exposure vessels for characterizing the effect of moisture on the corrosion behavior of candidate end-plate and ball seal materials. Needed progress is being made and our expectation is that all corrosion tests will be underway by the middle of September. The primary obstacles that were eliminated included (1) the identification of a method to contain the moisture-contaminated electrolyte and yet electrically isolate the various metal specimens (see Figure 9), and (2) establishing a baseline moisture content of the KDI electrolyte (in progress). The needed 1-cm^2 metal samples (304L, 316L, 440C, Ni-200, and tungsten carbide) have been procured and prepared and will be laser-welded along one side to create a realistic heat-affected zone and a tight crevice. A local glassblower will fabricate the vials and load the metal samples prior to filling with three levels of contaminated electrolyte. An appointment has been made with the glassblower to perform these activities during the first week in September. The specific moisture levels to be used will be selected in conjunction with ARDEC after the analysis of the electrolyte extracted from the KDI reservoirs has been completed. Also, several empty and cleaned KDI reservoirs will be made available for the second corrosion task that is addressing any impact of spilling electrolyte on the external surface of the reservoirs.

The primary remaining obstacle is the lack of KDI electrolyte.

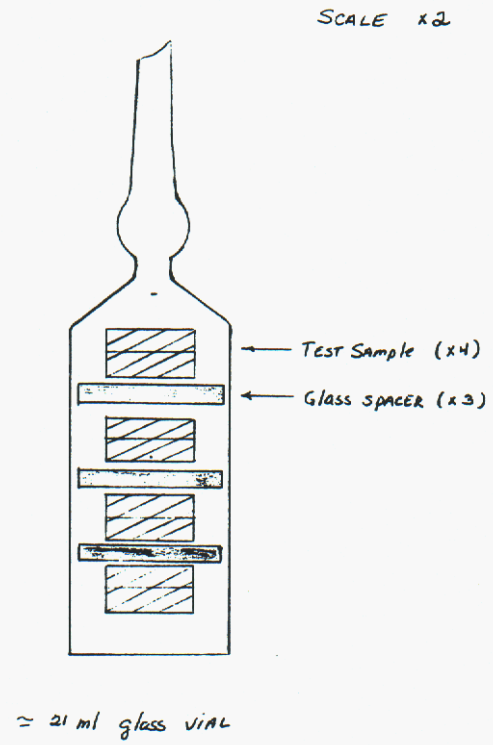

Figure 9. Schematic diagram of the vial and sample configuration to be used in the moisture-induced corrosion sensitivity studies

Effect of external electrolyte contamination on the corrosion of reservoir endplate materials

ARDEC supplied endplates containing 440C ball seals have been received. The reservoirs that will provide the as built weld joint have been received and are in the process of being cleaned for use in this study. This study will be started as soon as the KDI electrolyte is received and the cleaned reservoirs are available. Table 3 shows the test matrix to be used.

Table 3. Matrix for the external electrolyte contamination corrosion studies (Experiments #1-#3 are the baseline test configuration)

Aging Expt #	*Material*	*Electrolyte Contamination*		*Dry room Exposure Time*	*Lab Exposure Time*	*Cleaned*	*Temp*	*Aging Time*
		Drop	*Dipped*	*Minutes*	*Minutes*		*°C*	*Months*
Baseline conditions								
1	Endplate		X	15	--	--	40	6
2	Endplate		X	15	15	--	40	6
3	Endplate		X	15	15	yes	40	6
Alternate Contamination								
4	Endplate	X		15	--	--	40	6
5	Endplate	X		15	15	--	40	6
6	Endplate	X		15	15	yes	40	6
Dry Room Exposure Time								
7	Endplate		X	30	--	--	40	6
8	Endplate		X	120	--	--	40	6
Standard Laboratory Exposure Time								
9	Endplate		X	15	30	--	40	6
10	Endplate		X	15	120	--	40	6
Aging Time								
11	Endplate		X	15	--	--	40	1
12	Endplate		X	15	--	--	40	12
Welded Reservoir								
13	Reservoir		X	15	--	--	40	6
14	Reservoir		X	15	15	--	40	6
15	Reservoir		X	15	15	yes	40	6
Low Temperature								
16	Endplate		X	15	--	--	25	6
17	Endplate		X	15	15	--	25	6
18	Endplate		X	15	15	yes	25	6
High Temperature								
19	Endplate		X	15	--	--	74	6
20	Endplate		X	15	15	--	74	6
21	Endplate		X	15	15	yes	74	6

Welding Study
Parts have been received for this study. Currently the electrolyte is being removed from the reservoirs. The weld analysis study is expected to be completed in about four weeks.

New Tasks

Characterization of Solid in Electrolyte and Electrolyte Performance at Temperature Extremes and in Thermal Cycling

Work on these tasks will be initiated when the DOE and Sandia financial organizations, presumably in early September, complete all required processing of the recent MIPR.

Needed Material from Sponsor

Additional KDI electrolyte is still needed before several of the tasks can be fully initiated.

If questions arise concerning any of the above items, please contact Nancy Clark at (505) 845-8056 or David Ingersoll at (505) 844-6099.

Distribution:
email Joe Donini, TACOM-ARDEC
email Ben Lagasca, TACOM-ARDEC
email Bill Vogt, OPM-CAS ARDEC
email Dean Booker OPM-CAS ARDEC
email Alan Goldberg, ARL
email Bruce Poese, ARL
email P. Butler, 2522
email N. Clark, 2522
email D. Doughty, 2521
email D. Ingersoll 2521
email L. Malizia 2525
email D. Tallant, 1822
email T. Boyle, 1846
email J. Braithwaite, 1832
email R. Sorensen, 1832
email T. Alam, 1811
MS 0614 Day File, 2522

16. Appendix D

Monthly Report
September 30, 2002

Sandia National Laboratories

Operated for the U.S. Department of Energy by Sandia Corporation

Albuquerque, New Mexico 87185-0613

date: September 30, 2002

to: Distribution

from: Nancy Clark, 2522 and David Ingersoll, 2521

subject: Activities on ARDEC Self-Destruct Fuze Reserve Battery Project during September, 2002

This memo summarizes the activity performed in September, 2002, on the Self-Destruct Fuze Reserve Battery Project.

Project Status

Electrolyte Aging Matrices

We have three of the aging matrices currently in progress, and this work is briefly summarized below.

Matrix 1 – Reservoirs

This matrix, corresponding to Task IV in the Statement of Work, involves aging new reservoirs at temperatures of 40 °C, 65 °C and 74 °C with periodic removal for visual examination and Raman spectroscopic analysis.

Samples were placed into ovens on June 28, 2002. On July 26, 2002 the samples were removed from the ovens for characterization by Raman spectroscopy. The matrices were returned to the ovens on September 23..

The Reservoir Matrix (#1) samples includes 15 reservoirs which were divided into three groups for aging at 40°C, 65°C and 75°C. The reservoirs have been analyzed by Raman spectroscopy prior to aging and after one month of aging. The small size and geometry of the reservoirs require that we perform the Raman analysis by focusing the excitation beam and collecting the Raman (180° back-) scattered light using the objective of a microscope. Since we have not yet worked out the procedures for using near infrared excitation with the microscope, we used a 458 nm laser line to obtain the Raman spectra. The excitation beam passes through the window of the reservoir and is focused into the solution. Some Raman spectra show bands due to the glass of the reservoir window. When present, these bands are removed by subtracting a spectrum obtained while focusing the laser beam on the glass of a reservoir window. These micro-Raman spectra have lower signal levels and higher background fluorescence (from using a visible versus a near infrared excitation wavelength) than those obtained from the sulfuryl chloride

solutions in NMR tubes (Matrices #2 and #3). However, the quality of the micro-Raman spectra is sufficient that changes equivalent to reaction of more than a few percent of the sulfuryl chloride should be detectable.

Figure 1 shows micro-Raman spectra of reservoir #11, prior to aging and after aging for one month at 75°C. Aging does not appear to have produced detectable levels of SO_2 in this reservoir, nor have there been any significant changes in most of the sulfuryl chloride bands. The only apparent change in the spectra on aging is a narrowing of the sulfuryl chloride band that peaks at 280 cm^{-1}. The narrower band present after aging is more like the corresponding band in Raman spectra of sulfuryl chloride in NMR tubes than the broader band present prior to aging. The spectra in Figure 1 are representative of those from all the other reservoirs at the different aging temperatures. The broadened region in the unaged sample spectra of the 280 cm^{-1} sulfuryl chloride band is near the peak (≈310 cm^{-1}) of the Raman band from solid aluminum chloride. It is possible that aluminum chloride species are responsible for the apparent broadening of the 280 cm^{-1} band.

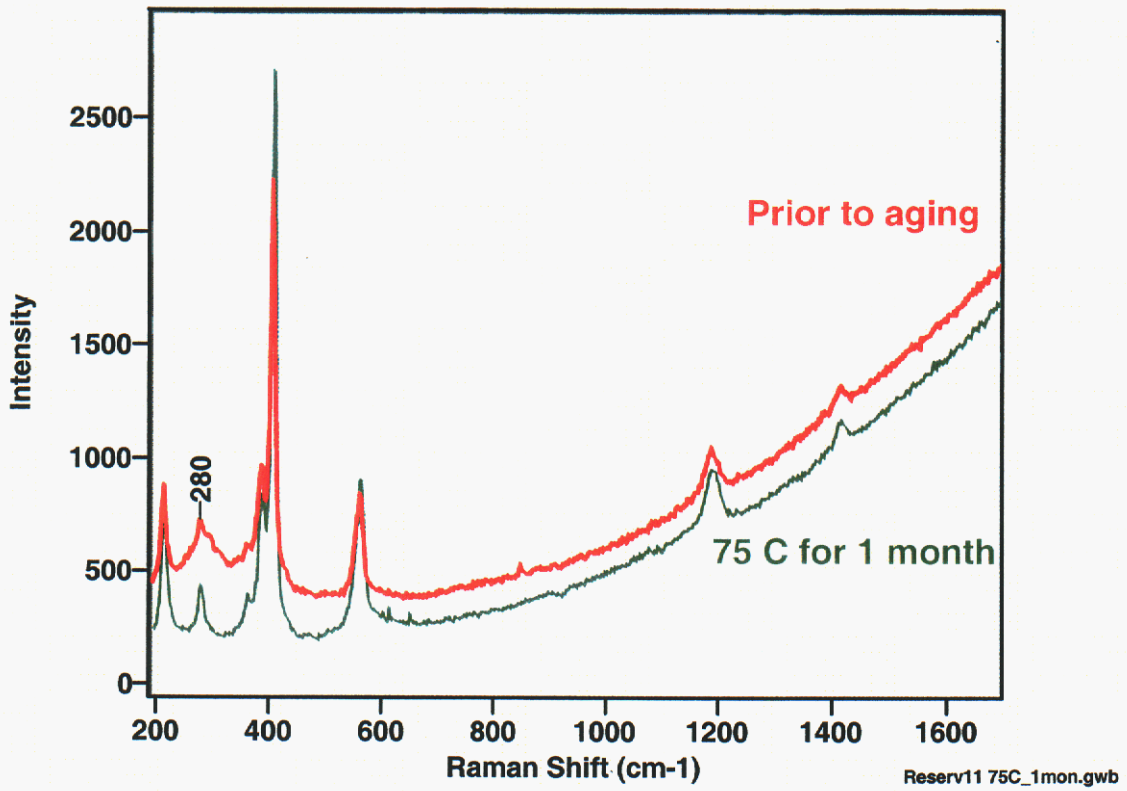

Figure 1. Raman spectra of reservoir #11 – prior to aging and aged at 75 C

Matrix 2 – Electrolyte Matrix: Commercial Materials - Full Factorial

Two matrices using commercially available materials were developed. The first of these, called Matrix 2, is shown in Table 1. This matrix is a Full Factorial design and employs a

fixed concentration of $AlCl_3$ of 1.5 M. The factors that are being evaluated in this study include water content, temperature and time at temperature. These samples were placed into ovens on July 19th, and were then removed at the end of two weeks. (The first sample withdrawal was changed to 14 days from 30 days on the basis of the preliminary data). Both Raman and NMR spectra were collected on all of the samples. The samples were placed back into ovens on August 28th for continuation of the aging. They were removed on September 12 and returned on September 23.. NMR and IR spectra were then taken. Analysis of the data will be done next month.

Table 1. Matrix 2- Full Factorial - Commercial Electrolyte

Matrix 2 Full Factorial Design		
Sample ID	Water Content Ppm	Temperature °C
1	100	65
2	500	40
3	0	74
4	500	74
5	0	74
6	100	65
7	0	40
8	500	40
9	0	40
10	500	74
11	100	65

Matrix 3 – Electrolyte Matrix: Commercial Materials - Original Plan

The third electrolyte matrix, Matrix 3, is that described in the Statement of Work. The sample compositions and aging conditions are summarized in Table 2. Aging was initiated on June 27, 2002, and the first withdrawal from the ovens occurred on July 11, 2002, for a total aging time interval of 14 days. (The first sample withdrawal was changed to 14 days from 30 days on the basis of the preliminary data). The second withdrawal was on August 19th after an additional two weeks of aging. These samples were aged from August 30 to September 30.

Table 2
Matrix 3 – Commercial Electrolyte - Original Plan

Spl #	Temperature/C			Water Conc/ppm			$AlCl_3$ Conc/M		
	40	65	74	0	100	500	0	0.75	1.5
1	X			X			X		
2	X			X				X	
3	X			X					X
4	X				X		X		
5	X				X			X	
6	X				X				X
7	X					X	X		
8	X					X		X	
9	X					X			X
10		X		X			X		
11		X		X				X	
12		X		X					X
13		X			X		X		
14a		X			X			X	
14b		X			X			X	
14c		X			X			X	
15		X			X				X
16		X				X	X		
17		X				X		X	
18		X				X			X
19			X	X			X		
20			X	X				X	
21			X	X					X
22			X		X		X		
23			X		X			X	
24			X		X				X
25			X			X	X		
26			X			X		X	
27			X			X			X
Characterization of samples at 0, 0.5, 1, 3, 6 and 12 months									

These samples have been analyzed by both solution ^{27}Al NMR and Raman spectroscopy and the results are summarized below. The Al NMR 2-month results will be reported next month. The Raman analysis for two and four weeks is reported below.

The Matrix 3 samples have permutations of sulfuryl chloride plus three concentrations (0, 0.75 and 1.5M) of aluminum chloride and three concentrations of added water (0, 100 and 500 ppm), aged at three temperatures (40°C, 65°C and 74°C). The samples are in NMR tubes. We used a 785 nm laser for excitation (near-infrared excitation wavelengths tend to reduce background photoluminescence). We focused the laser beam into the solution in a horizontally mounted tube and collected Raman scatter at 90° to the

propagation direction of the laser beam. A triple spectrograph and charge-coupled-device (CCD) detector analyzed and recorded the scattered light. We show selected spectra from the Matrix #3 samples that are representative of the aging behavior for up to four weeks of aging.

Figure 2 shows a portion of the Raman spectra of sulfuryl chloride solutions, with no aluminum chloride or added water, which have been stored at ambient conditions or aged for two and four weeks at 74°C (Spl# 19). The (marked) peak at 1142 cm^{-1} is due to dissolved SO_2, a probable decomposition product of sulfuryl chloride. The other two features are from fundamental vibrations of sulfuryl chloride. Two weeks of aging caused the band due to SO_2 to increase significantly from its intensity in unaged (or ambient) sulfuryl chloride, but an additional two weeks of aging at 74°C did not result in any significant change in the SO_2 band intensity. Likewise, for other frequency regions of the sulfuryl chloride spectra and for aging at 40°C and 65°C, there are no significant differences between the spectra obtained after 2 weeks and 4 weeks of aging.

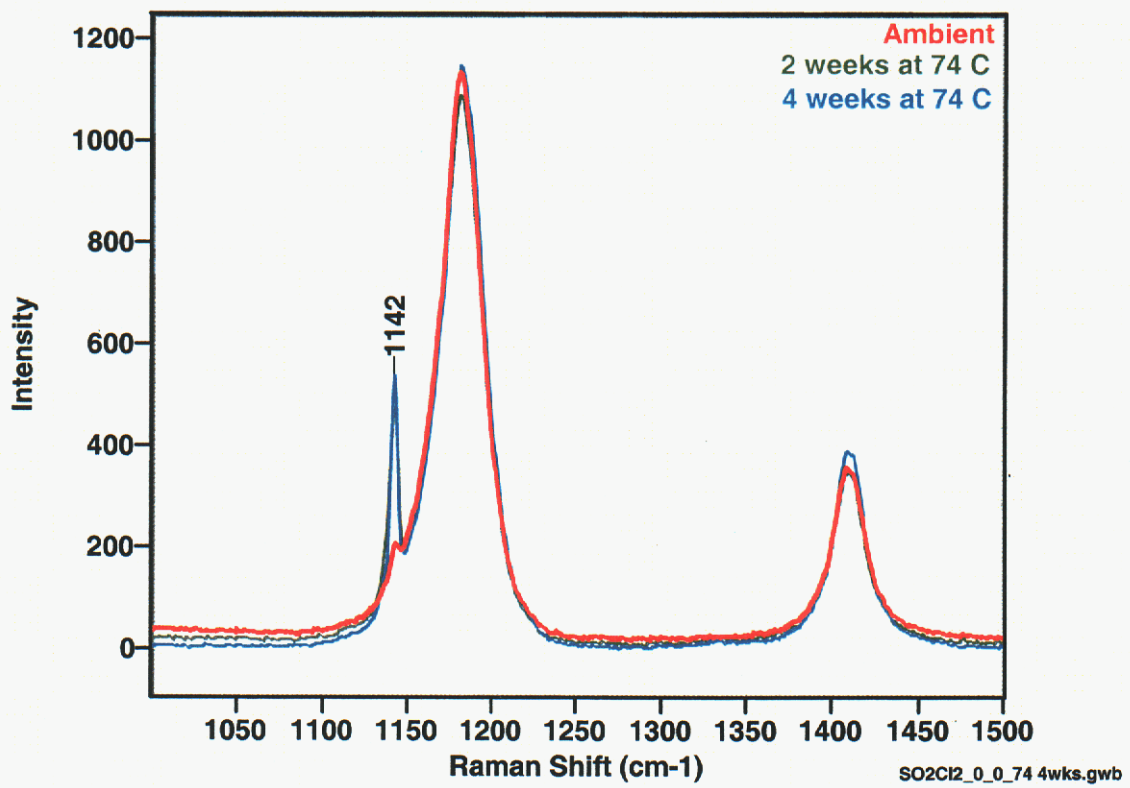

Figure 2. Raman spectra of SO_2Cl_2 (0 ppm H_2O, 0 M $AlCl_3$, Spl# 19), aged at ambient and 74°C, for up to four weeks.

Figure 3 shows a portion of the Raman spectra of sulfuryl chloride solutions with 1.5M aluminum chloride but no added water, prior to aging and aged for two and four weeks at 74°C (Spl# 21). The unmarked peaks are, as noted earlier, due to fundamental vibrations

of sulfuryl chloride. As we suggested in a previous report, the 1129 cm^{-1} and 1375 cm^{-1} features in the unaged sample may be from an adduct of the sulfuryl chloride and aluminum chloride. These features are not present in the two-week-aged sample, but a low-intensity peak (1142 cm^{-1}) due to SO_2 is. The Raman spectrum of the sample aged for four weeks does not show any significant differences compared to the spectrum of the two-week-aged sample, except for the broad background signal underlying the Raman peaks. This background is believed to be due to photoluminescence from small concentrations of impurities. Likewise, for other frequency regions of the sulfuryl chloride (plus 1.5 M aluminum chloride) spectra and for aging at 40°C and 65°C, there are no significant differences between the spectra obtained after 2 weeks and 4 weeks of aging.

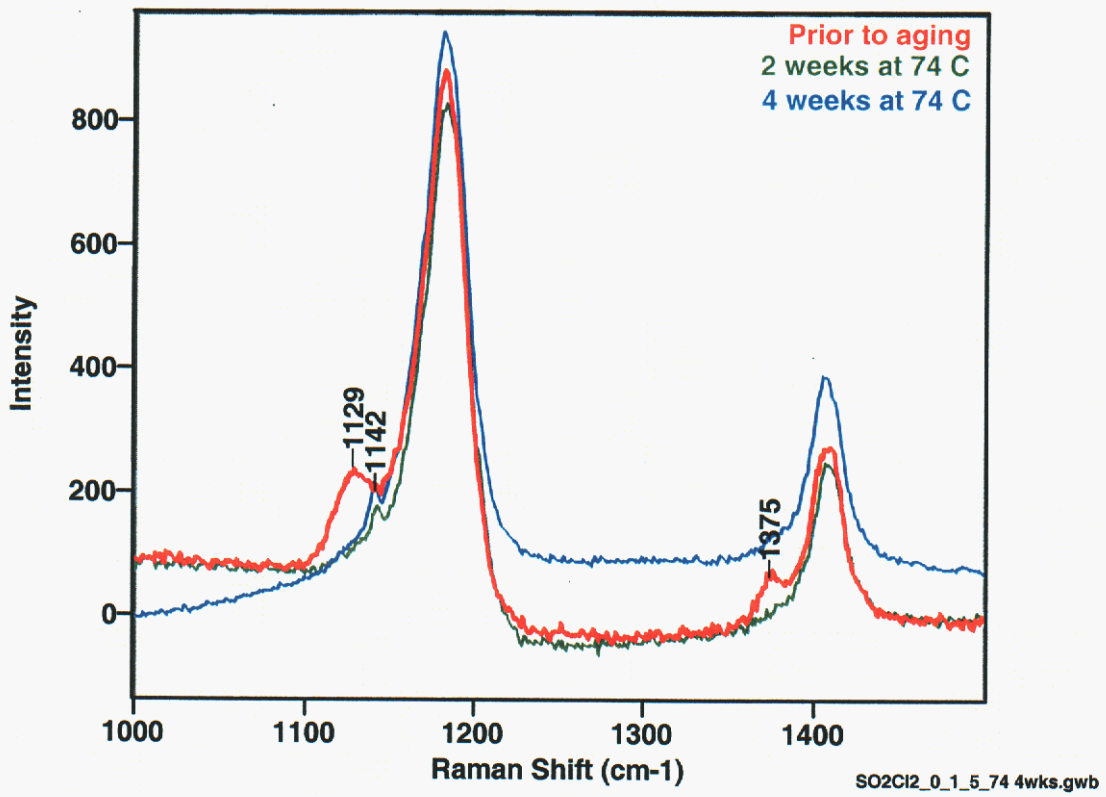

Figure 3. Raman spectra of SO2Cl2 (0 ppm H_2O, 1.5M $AlCl_3$, Spl# 21), with up to four weeks aging at 74°C

The spectra of solution compositions not represented in Figures 2 and 3 (0.75 M aluminum chloride and 100 ppm and 500 ppm added water) also show no significant changes between those aged for two weeks and those aged for 4 weeks. It appears that sulfuryl chloride solutions not exposed to elevated temperature have chemical species that, when exposed to elevated temperature, relatively quickly react with and achieve an

equilibrium with the other components of the solution. Other changes may appear as the aging experiments continue.

IR Analysis of Water Content of Electrolyte in Reservoirs

Samples have been prepared in sealed IR tubes for the water content analysis of electrolyte in reservoirs. Samples of electrolyte from reservoirs to be used in the welding study are also being gathered. It is expected that the analysis of the water content samples from these reservoirs will be evaluated in October if enough sample is obtained. The results for the previously-prepared IR tubes are reported below.

We have performed an infrared (IR) analysis of the 10-mm-pathlength, sealable quartz IR cells recently filled by Tim Boyle with undistilled sulfuryl chloride. Delays in transporting the cells (by SNL hazardous materials personnel) resulted in approximately a week's delay between filling/sealing of the cells and the IR analysis. It turns out that this delay is fortuitous, since it takes a few days for the hydroxyl absorption features in the IR spectra to stabilize after water addition (Fleischer et al., 1987).

We used the standard addition method of analysis, in which known amounts of the species to be analyzed (in this case, water) are added to the sample (sulfuryl chloride) containing an unknown amount of the water. The progressive increase in a parameter (intensity of hydroxyl IR bands) related to the amount of added water allows the analyst to extrapolate back to the amount of water in the original sample. IR spectra of the hydroxyl region from the sulfuryl chloride samples are shown in Figure 4. Other portions of the IR spectrum are largely saturated in absorption by fundamental vibrations of sulfuryl chloride and the silica of the IR cell.

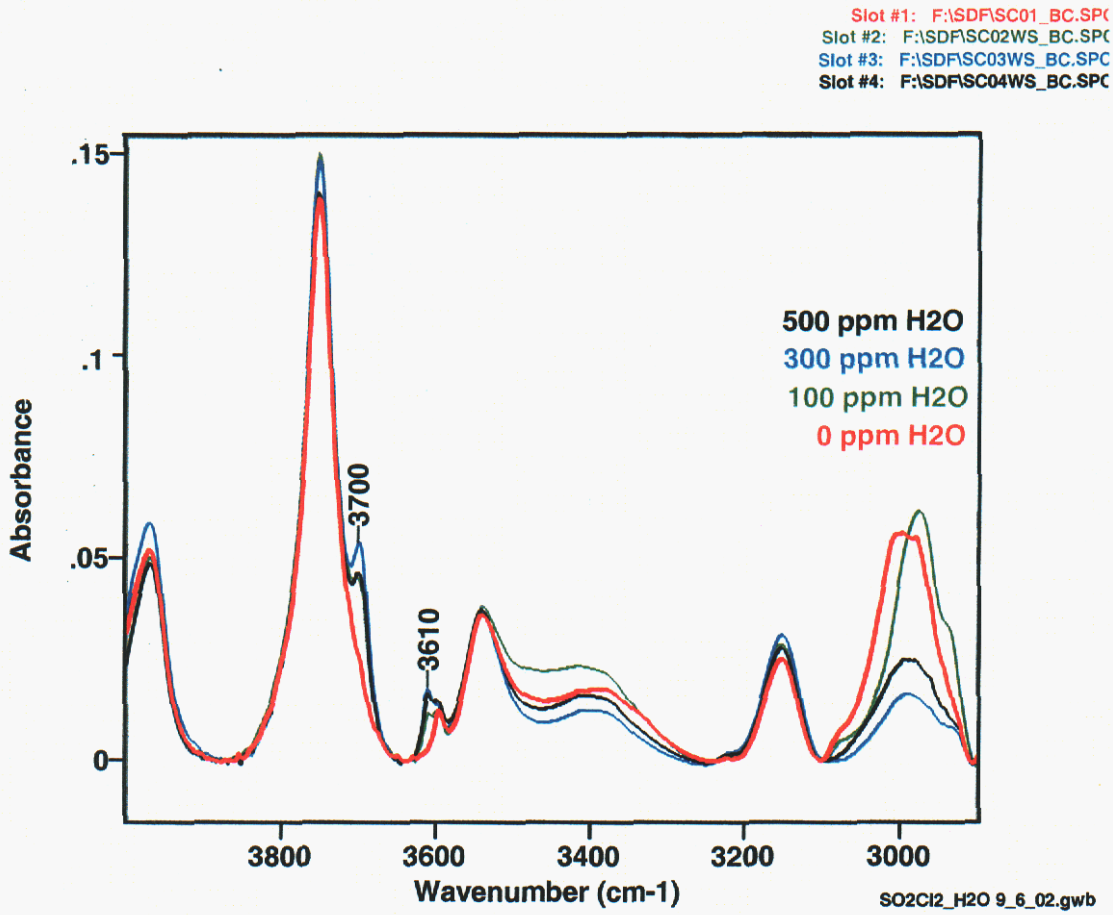

Figure 4. IR spectra of sulfuryl chloride with 0 - 500 ppm of added H_2O in 10 mm silica cells

Most of the features in Figure 4 are believed to be due to overtone and combination bands of the sulfuryl chloride, which are low in intensity in IR spectra taken through the normal sample thickness (a few to tens of micrometers) used in IR spectroscopy. We used a thick (10 mm) sample of sulfuryl chloride in this experiment to get detectable intensities in the hydroxyl bands related to added water. These bands occur at 3700 and 3610 cm^{-1} (see Figure 4 and Fleischer et al., 1987).

We integrated the intensities of the 3700 and 3610 cm^{-1} bands and plotted their intensities versus the concentration of water added to each sample (see Figure 5). The IR intensities of the 3700 and 3610 cm^{-1} bands peak at a concentration of added water of 300 ppm. Presumably this concentration represents equilibrium of the added water with sulfuryl chloride. Water present above this concentration reacts with sulfuryl chloride to form H_2SO_4 + HCl or chlorosulfonic acid (HSO_3Cl). Fleischer et al. (1987) obtained a plot similar to Figure 5. Since there is not a linear increase in IR intensity for the 3700 and 3610 cm^{-1} bands with added water concentration for the data points shown in Figure 5, we cannot do a linear extrapolation of <u>all</u> the data points to obtain the water content originally present in the sulfuryl chloride. However, we note that the absorption intensities of the 3700 and 3610 cm^{-1} bands in the sulfuryl chloride with no added water

are 10 – 20% of those in the sulfuryl chloride with 100 ppm added water, indicating that the equivalent water content of the original sulfuryl chloride is, roughly, 10 – 20 ppm.

SO2Cl2_H2O 9_6_02.xls

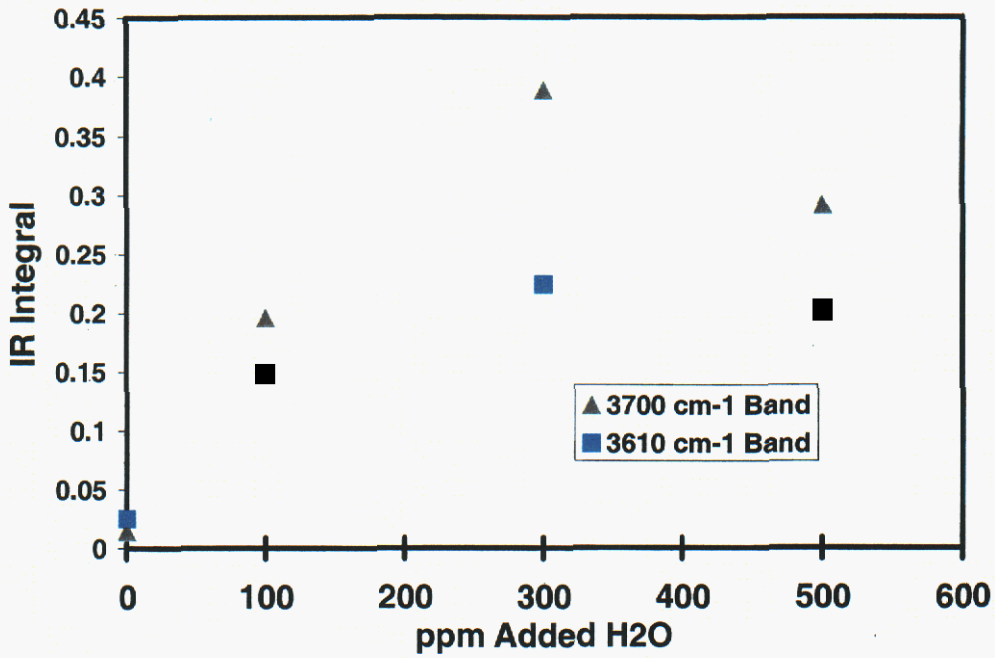

Figure 5. Integrated IR intensities of hydroxyl bands due to added water versus concentration of water added to sulfuryl chloride

We attempted to do a similar IR analysis with aluminum chloride added to the sulfuryl chloride, but the sealing tube broke off one cell, and another cell leaked through a (cracked?) seal. We have an unused IR cell, and the cell with the cracked seal should be reusable. Tim Boyle has agreed to fill these two cells, and then we will perform the IR analyses on their sulfuryl chloride/aluminum chloride plus water solutions.

Reference:

N. A. Fleischer, M. Pallivathikal and M. Babai, "Analysis of Traces of Water in Sulfuryl Chloride Electrolytes by Infrared Spectroscopy," *J. Electrochem. Soc.* **134 (3),** (1987), 513 – 516.

Corrosion Tasks

Effect of water contamination on the corrosion of ball and endplate materials and Effect of external electrolyte contamination on the corrosion of reservoir endplate materials

All of the metal samples for the inundated exposures were fabricated during the past month and are currently being welded. Primarily because the funding on this task is

limited and we decided to include such a large number of samples, we changed the approach from laser welding one edge to laser spot welding near two opposite sides. The advantage of this approach, besides speed, is that it will produce a better crevice environment and also permit much easier inspection and analysis at the conclusion of the aging experiments. The prime motivation for initially specifying laser welding was to better duplicate the heat input to the metal and thus permit the identification of any corrosion vulnerabilities to sensitization-related effects. However, based on the recent studies of the welded reservoirs performed for Lou Malazia and his years of experience, we no longer expect any such effects. As a final check on this conclusion, we will be studying the corrosion characteristics of actual welded reservoirs in the contamination task.

With the arrival of the KDI electrolyte last week (Sept. 24th) and the expected completion of the welded samples, we will proceed with the fabrication, loading, and sealing of our custom designed ampoules. As such, we expect to have all aspects of the two corrosion tasks started within a few weeks.

Welding Study

Parts have been received for this study. Eelectrolyte was removed from the reservoirs and they were then cleaned. All samples have been cross-sectioned and photographed. Figures 6, 7, and 8 show the first set of cross-sections from three of the reservoirs.

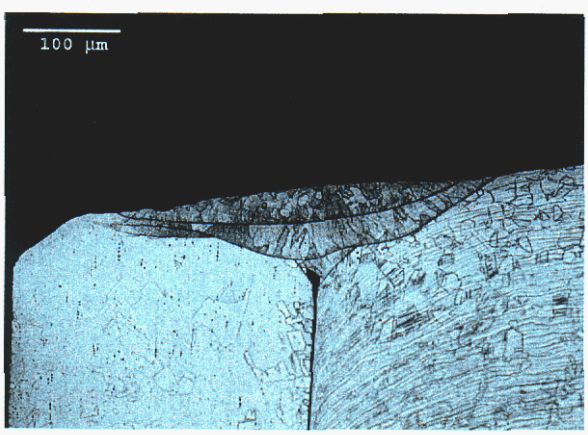

Weld 1

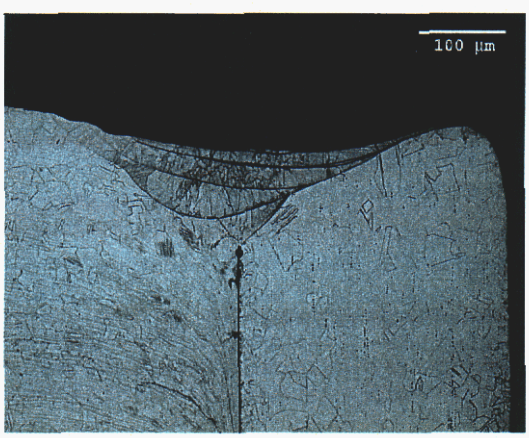

Weld 2

Figure 6: Cross-Sections of Reservoir 1

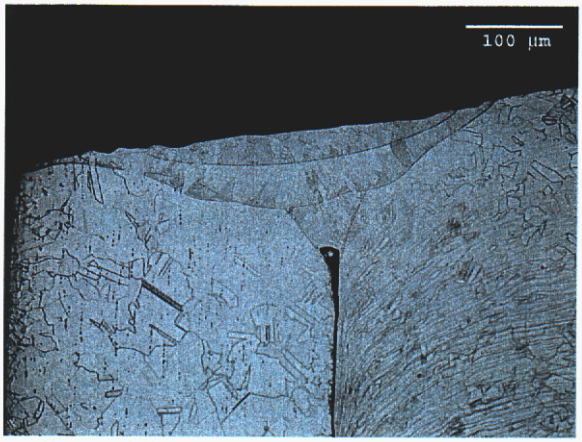

Figure 7: Cross-Section of Reservoir 3

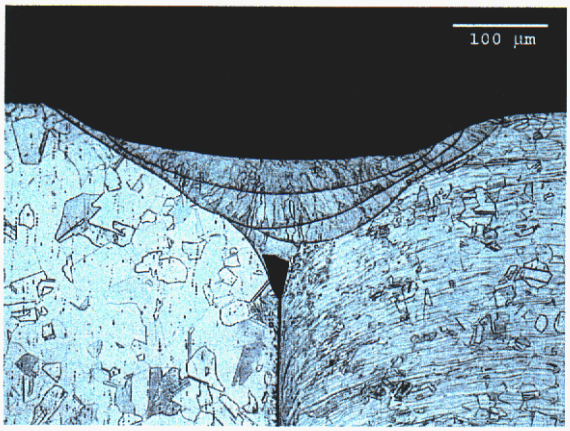

Figure 8: Cross-Section of Reservoir 4

Preliminary conclusions for the welding study are summarized below. They are based on looking at pictures of all the welds and comparing them with the ones shown in Figures 6-8. The pictures in Figures 6-8 were found to be typical.

1. The penetration is on the order of .003" to .004".

2. There are no signs of any sensitization.

3. There are no signs of degradation (cracking) of the welds due to the electrolyte in the cell.

4. However, there is a possible effect of a minor amount of liquid being present in the weld area. In the root area of reservoir 1, welds 1 & 2, reservoir 3, weld 1, and reservoir 4 weld 1, there is a minor amount of root porosity that could be attributable to moisture being turned into vapor. But this amount of root porosity can also be attributable to normal root shrinkage.

5. There is margin to reduce the heat input by reducing the welding pulse rate or increasing the welding speed. The cross-sections show 3-5 solidification lines in the weld. This is an indication that there is too much overlap of the pulses. Normal overlap is around 50% & this overlap results in two solidification lines. The additional re-melting is not good for the metallurgy of the stainless steel & adds to unnecessary heat input.

6. If the 3-4 mils penetration is acceptable from a strength viewpoint, then the entire plug need only be .005" thick instead of the .020" thickness. Reducing the thickness to .005" will enable the plug to be stamped so that it can form a cap rather than a plug. The cap can be slightly smaller in diameter than the case.

7. The seal weld then can be made around the edge of the cap producing a melt-down type fillet weld. This type of weld is easy & results in a low-stress joint. This type of weld will eliminate the 'coalescence' problem when there is a gap in the 'butt' weld (plug/case).

New Tasks

Characterization of Solid in Electrolyte and
Electrolyte Performance at Temperature Extremes and in Thermal Cycling

Work on these tasks will be initiated in October. The MIPR was released into the Sandia system during the week of September 23rd.

Needed Material from Sponsor

KDI electrolyte was received on September 24th. All materials are now at Sandia.

If questions arise concerning any of the above items, please contact Nancy Clark at (505) 845-8056 or David Ingersoll at (505) 844-6099.

Distribution:
email Joe Donini, TACOM-ARDEC
email Ben Lagasca, TACOM-ARDEC
email Bill Vogt, OPM-CAS ARDEC
email Dean Booker OPM-CAS ARDEC
email Alan Goldberg, ARL
email Bruce Poese, ARL
email P. Butler, 2522
email N. Clark, 2522
email D. Doughty, 2521
email D. Ingersoll 2521
email L. Malizia 2525
email D. Tallant, 1822
email T. Boyle, 1846
email J. Braithwaite, 1832
email R. Sorensen, 1832
email T. Alam, 1811
MS 0614 Day File, 2522

17. Appendix E

Monthly Report
October 31, 2002

Sandia National Laboratories

Operated for the U.S. Department of Energy by Sandia Corporation

Albuquerque, New Mexico 87185-0613

date: October 31, 2002

to: Distribution

from: Nancy Clark, 2522 and David Ingersoll, 2521

subject: Activities on ARDEC Self-Destruct Fuze Reserve Battery Project during October, 2002

This memo summarizes the activity performed in October 2002, on the Self-Destruct Fuze Reserve Battery Project for ARDEC.

Project Status

Electrolyte Aging Matrices – general comments

Three aging matrices are currently ongoing, and Table 1 attempts to summarize the current status of these samples based on the number of characterization intervals during the aging process. As seen, three data sets are being collected on the samples in Matrix 1, while four sets of data are being collected for the samples comprising Matrices 2 and 3.

Table 1. Time duration for each aging interval for each matrix currently under test.

Aging Duration/Days

	Matrix 1 Reservoirs		Matrix 2 Full Factorial		Matrix 3 Large Matrix	
Characterization Completed	Time in Oven During This Interval	Cumulative Total Time in Oven	Time in Oven During This Interval	Cumulative Total Time in Oven	Time in Oven During This Interval	Cumulative Total Time in Oven
Baseline Analysis	0	0	0	0	0	0
First Interval	28	28	13	13	14	14
Second Interval	28	56	14	27	14	28
Third Interval			28	55	30	58
Fourth Interval						
Fifth Interval						
Sixth Interval						
Seventh Interval						

In addition to the characterization of the samples using Raman and NMR spectroscopy, gross physical characterization of the samples at various intervals has also been done. Furthermore, in the case of the filled reservoirs (Matrix 1), a record of the sample orientation of the reservoir during aging has also been maintained. In this later case the

mobility of the gas bubble was assessed at each interval. The results of these gross physical observations are briefly summarized below.

At the end of the first interval corresponding to 28 days at temperature, there were no apparent gross physical changes in the samples of Matrix 1, the filled reservoirs. In every case the entrained gas bubble was freely mobile. At the end of the second aging period corresponding to 56 days of aging, the gross examination has not yet been completed (the samples are currently being examined using Raman spectroscopy).

In the case of the samples of Matrix 2 and 3, at the end of the first aging period all of the samples appeared yellow in color. However, some of the samples had appeared yellow in color prior to beginning the first aging period. During the sample analysis after the first aging period, differences in intensity of the color were subjectively categorized as light yellow, dark yellow, and intermediate yellow. The photograph in Figure 1 illustrates the differences in color between these three levels. (The color was not quantified by UV/VIS spectroscopy even though it is thought to result from free chlorine.) The dark yellow occurs, but not consistently, in those solution containing aluminum chloride.

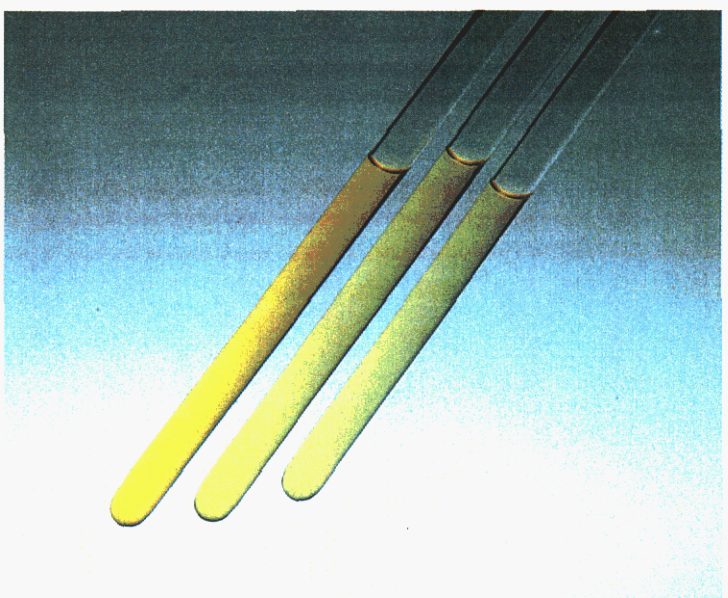

Figure 1. Picture showing relative differences in sample colors.

Observations of sample clarity, that is the presence/absence of a precipitate, were also made, and all of the samples remained clear through the second interval. Only recently, at the end of the third interval in the case of the Matrix 2 samples or partway into the fourth interval in the case of the Matrix 3 samples, did any of the samples begin to exhibit signs of turbidity. In these cases upon removal from the oven a fine, light colored precipitate was observed to have accumulated at the bottom of the tube. When these samples were agitated, the precipitate was resuspended in solution, with little or no

evidence of turbidity. This is seen in Figure 2, which show photographs of a single sample after removal from the oven and again after agitation of the sample. As seen, in the former case the deposit is clearly present, while in the later case there is little/no evidence of the deposit.

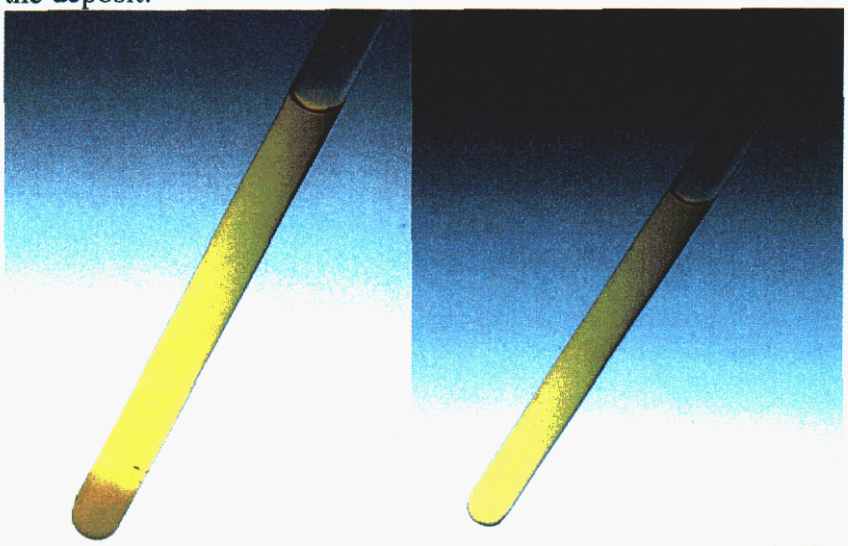

Figure 2. Photograph of a single sample before mixing, showing the presence of the deposit (on the left), and after mixing (on the right).

Electrolyte Aging Matrices – analytical characterization

During October, Raman spectra were obtained for eight-week-aged samples from Matrix 3, and we have completed preliminary analysis of the Raman spectra from the eight-week-aged Matrix 3 and the four-week-aged Full Factorial Matrix 2. *Preliminary* analysis of the ^{27}Al NMR analysis of the aging Matrix 3 at approximately eight weeks thermal exposure has also been completed.

Raman Analysis of Matrix 2 and Matrix 3 Samples

The Matrix 3 samples have permutations of sulfuryl chloride plus three concentrations (0, 0.75 and 1.5M) of aluminum chloride and three concentrations of added water (0, 100 and 500 ppm), aged at three temperatures (40°C, 65°C and 74°C). Matrix 2 samples are a subset of Matrix 3, selected by factorial design, including the same range of added water and aging temperatures but all with 1.5M aluminum chloride. The samples are being aged in sealed NMR tubes. We used a 785 nm laser for excitation (near-infrared excitation wavelengths tend to reduce background photoluminescence). We focused the laser beam into the solution in a horizontally mounted tube and collected Raman scatter at 90° to the propagation direction of the laser beam. A triple spectrograph and charge-coupled-device (CCD) detector analyzed and recorded the scattered light.

We now have Raman spectra of Matrix 2 samples aged out to about four weeks (27 days) and Matrix 3 samples aged out to about eight weeks (58 days). Selected spectra from Matrix 3 are shown to illustrate aging related changes in the solutions.

Figure 3 shows a portion of the Raman spectra of sulfuryl chloride solutions from Matrix 3, with no aluminum chloride or added water, which have been stored at ambient conditions or aged up to eight weeks at 74°C. The (marked) peak at 1142 cm^{-1} is due to dissolved SO_2, a probable decomposition product of sulfuryl chloride. The other two features are from fundamental vibrations of sulfuryl chloride. As we noted in the September report, two weeks of aging caused the band due to SO_2 to increase significantly from its intensity in unaged (or ambient) sulfuryl chloride, but an additional six weeks of aging at 74°C does not result in any further significant change in the SO_2 band intensity. Likewise, for other frequency regions of the sulfuryl chloride spectra and for aging at 40°C and 65°C, there are no significant differences between the spectra obtained on solutions aged two to eight weeks.

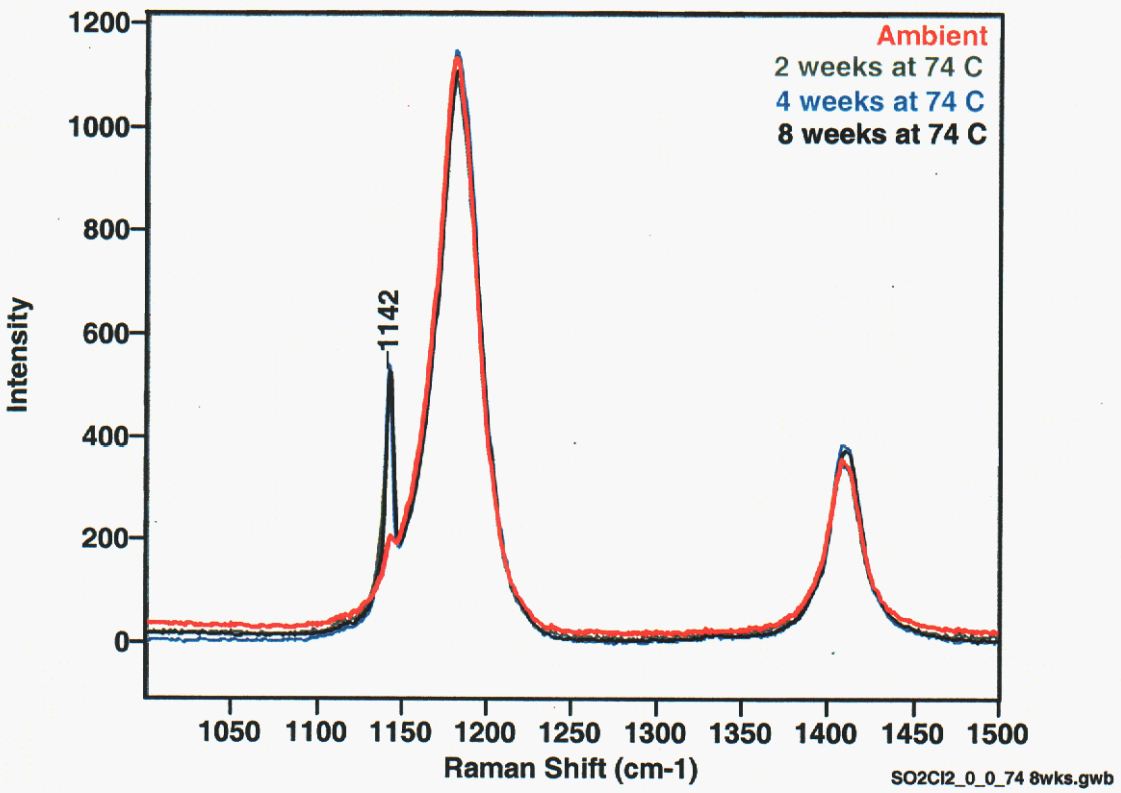

Figure 3. Raman spectra of SO_2Cl_2 (0 ppm H_2O, 0 M $AlCl_3$), aged at ambient and 74°C, for up to eight weeks.

Figure 4 shows a portion of the Raman spectra of sulfuryl chloride solutions with 1.5M aluminum chloride but no added water, prior to aging and aged up to eight weeks at 74°C. The unmarked peaks are, as noted earlier, due to fundamental vibrations of sulfuryl chloride. Features at 1129 cm^{-1} and 1375 cm^{-1} (possibly due to an adduct of the sulfuryl chloride and aluminum chloride) are present in the solution prior to aging but not in any of the aged samples. A low-intensity peak (1142 cm^{-1}) due to SO_2 is present in the aged samples, but it does not change significantly in intensity from two to eight

weeks of aging. For other frequency regions of the sulfuryl chloride (plus 1.5 M aluminum chloride) spectra and for aging at 40°C and 65°C, there are no significant differences between the spectra obtained after 2 weeks and 8 weeks of aging. The spectra of solution compositions not represented in Figures 3 and 4 (0.75 M aluminum chloride and 100 ppm and 500 ppm added water) also show no significant changes between those aged for two weeks and those aged for eight weeks.

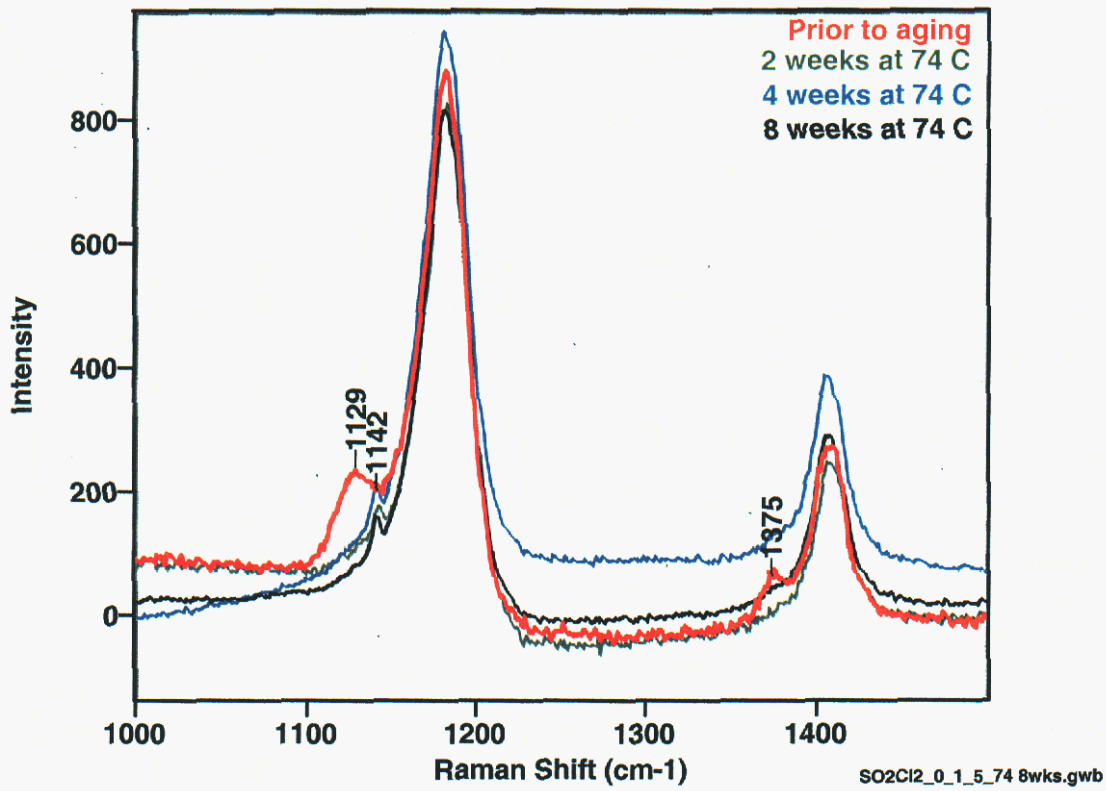

Figure 4. Raman spectra of SO_2Cl_2 (0 ppm H_2O, 1.5M $AlCl_3$), with up to eight weeks aging at 74°C

Raman spectra from Matrix 2 (data out to four weeks of aging) show changes similar to those in Figure 4. After some sort of equilibration reactions in the first two weeks of aging, the sulfuryl chloride solutions have no significant changes in their Raman spectra out to eight weeks of aging.

We will be analyzing eight-week-aged reservoirs (Matrix #1) and sulfuryl chloride solutions in NMR tubes (Matrix #2) over the next week or two.

NMR Results

Figures 5 and 6 show the decrease in the "unaged" $AlCl_4^-$ species as a function of aging conditions.

The following observations were noted:

1) The disappearance of the $AlCl_4^-$ species now shows *non-linear* behavior for all temperatures and concentrations beyond 4 weeks aging. This loss of the $AlCl_4^-$ resonance is accompanied by the formation of at least 2 different complexation species.
2) A plateau is observed in the loss of $AlCl_4^-$ for 65 °C and 74 °C at both starting concentrations. This plateau is ~30% of the original concentration. The 40°C samples are still evolving.
3) Precipitation on the glass walls has been noted for some of the 500 ppm H_2O samples at 74 °C. The loss of total Al signal by NMR is ~2%, but this is on the same order as the error in the integration. This precipitation has been noted (and pointed out to Tallant) and will be monitored for extended aging experiments.

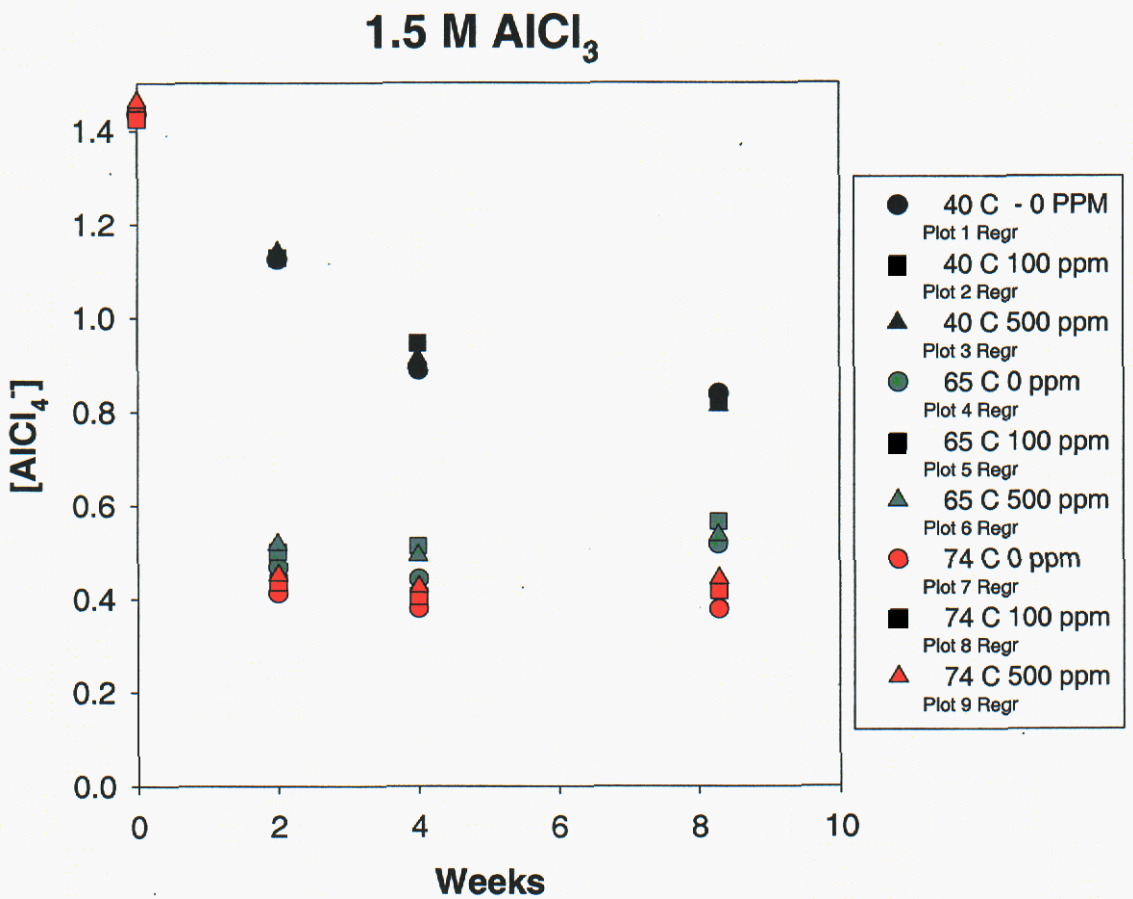

Figure 5. $AlCl_4^-$ concentration as a function of time, temperature, and water concentration for 1.5 M $AlCl_3$ (initial concentration) samples.

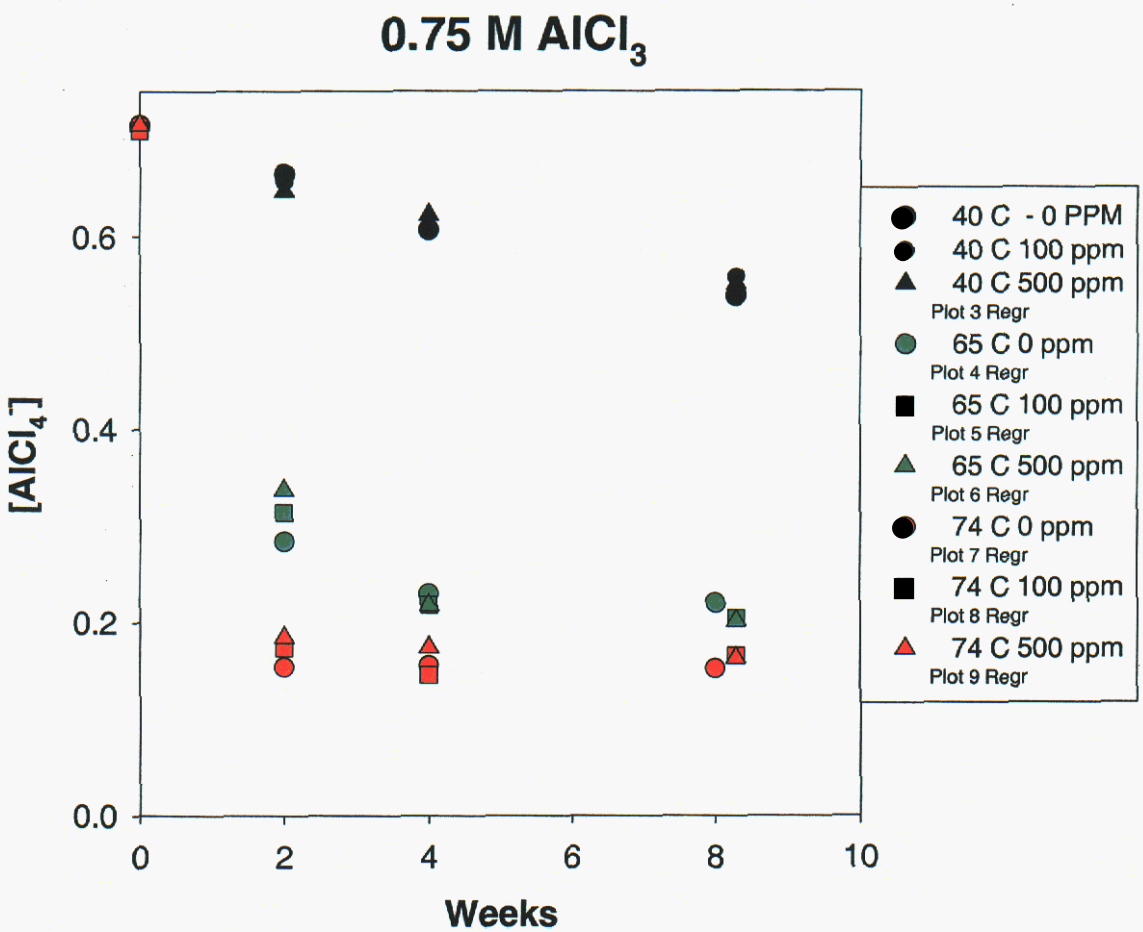

Figure 6. $AlCl_4^-$ concentration as a function of time, temperature, and water concentration for 0.75 M $AlCl_3$ (initial concentration) samples.

Incoming Inspections of Filled Reservoirs.
Micro-Raman Analysis of Corroded Reservoirs

Several months ago, near the outset of the program, we received several filled reservoirs from ARL that exhibited an impediment to fluid mobility as evidenced by the erratic movement of the gas bubble inside of the reservoir. On incoming visual inspection of these reservoirs we observed brown deposits on several of the reservoirs, as seen in the photomicrographs of Figure 7. Because these deposits have a striking resemblance to iron oxide (rust), we continued efforts to characterize them. This was done using micro-Raman spectroscopy as described below.

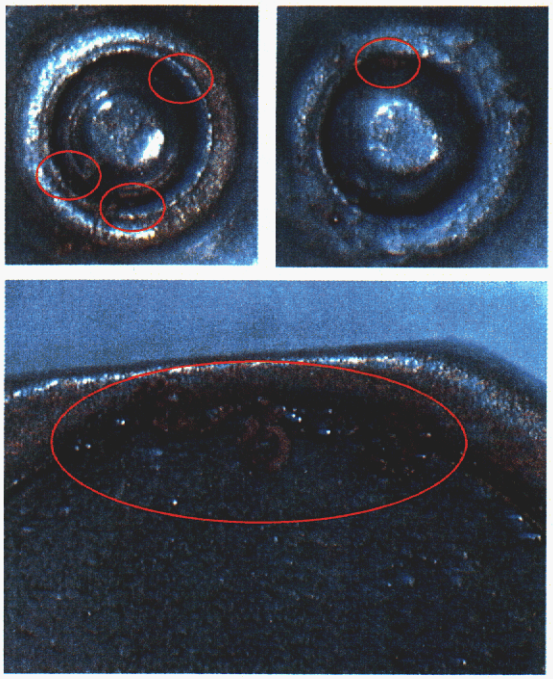

Figure 7. Photomicrographs of reservoir numbers 73 (top left), 81 (top right), and 94 (bottom) showing brown deposits.

Using micro-Raman spectroscopy we analyzed microscopic areas of five of the 15 reservoirs that have deposits and discolorations on their surfaces in the vicinity of the ball seal. (reservoir numbers 54, 57, 63, 70 and 73 were used for this work.) In micro-Raman spectroscopy the laser excitation beam is focused onto the sample using a microscope objective, which also collects light scattered from the sample. The collected light is transferred to instrumentation for dispersion and detection. Typically, a spatial resolution of about a micrometer is achieved with this technique. We visually identified five areas with deposits or discoloration on each reservoir from the magnified image provided by the microscope. Raman analysis of these areas found that the deposits and discolorations are largely composed of iron oxides (rust), sometimes mixed with charcoal-like inorganic carbon (residues of decomposed organic materials) and other transition metal oxides (perhaps of chromium). The deposits on the ten or so reservoirs not analyzed by micro-Raman do not visually appear different from those that were analyzed, hence we believe that these deposits are also composed primarily of iron oxides. Furthermore, the iron oxides are assumed to be corrosion products of the reservoir case.

Welding Study

Twenty (20) reservoirs have been cross-sectioned, examined, measured and photographed on both sides of the cross-sectioned sample. Based on the observations of these samples, the following preliminary conclusions can be made:

1. The average weld penetration depth is .0043" with a standard deviation of .001"; while the effective depth (leak path) average is .0037" with a standard deviation of .0009".

2. There are no signs of sensitization as a result of welding; however, one sample exhibited sensitization on the welded end and ID. The subsequent weld was unaffected by the sensitization but the surrounding base metal of the reservoir remained in a sensitized condition.

3. One reservoir appeared to have been reworked/rewelded by the addition of a second weld cycle. There were no deleterious effects of this apparent second weld cycle noted.

The remaining observations from the previous September report are still valid. These are:

1. There were no signs of degradation (cracking) of the welds due to the electrolyte in the reservoir.

2. However, there is a possible effect of a minor amount of liquid being present in the weld area. In the root area of reservoir 1, welds 1 & 2, reservoir 3, weld 1, and reservoir 4 weld 1, there is a minor amount of root porosity that could be attributable to moisture being turned into vapor. But this amount of root porosity can also be attributable to normal root shrinkage.

3. There is margin to reduce the heat input by reducing the welding pulse rate or increasing the welding speed. The cross-sections show 3-5 solidification lines in the weld. This is an indication that there is too much overlap of the pulses. Normal overlap is around 50% and this overlap results in two solidification lines. The additional re-melting is not good for the metallurgy of the stainless steel and adds unnecessary heat input.

4. If the 3-4 mils penetration is acceptable from a strength viewpoint, then the entire plug need only be .005" thick instead of the .020" thickness. Reducing the thickness to .005" will enable the plug to be stamped so that it can form a cap rather than a plug. The cap can be slightly smaller in diameter than the case.

5. The seal weld then can be made around the edge of the cap producing a meltdown type fillet weld. This type of weld is easily done and results in a low-stress joint. This type of weld will eliminate the 'coalescence' problem when there is a gap in the 'butt' weld (plug/case).

Corrosion Tasks

Activity during October focused on completing the welding of the stainless steel and stainless steel-ball material couples and then encapsulating the appropriate samples in the specially designed glass vessels. The welding process did not proceed as smoothly nor as easily as expected. Nevertheless, adequate weld procedures were developed and effectively implemented. However, success was not attained (in this case not surprising) for the tungsten carbide-stainless steel couple. In this case, the intimate electrical contact

and crevice was produced by tightly banding the two metal samples together. The 45 metal couples were distributed into 18 separate vessels (as defined in the test plan). These vessels will be filled with baseline KDI and water-contaminated electrolyte as soon as it becomes available. The KDI electrolyte was received at Sandia and currently is in transit between Sandia facilities where it will be processed and packaged. The plan is to have the electrolyte analyzed for water content and then decide on reasonable contamination levels (e.g., doubling and possibly quadrupling the baseline content). Once this decision is made, the vessels will be filled, sealed and transferred to the appropriate aging oven. Also at this same time, packaged KDI electrolyte will be delivered to the battery lab facilities and the atmospheric electrolyte-contamination task will be initiated. This is scheduled to occur in early November.

If questions arise concerning any of the above items, please contact Nancy Clark at (505) 845-8056 or David Ingersoll at (505) 844-6099.

Distribution:
email Joe Donini, TACOM-ARDEC
email Ben Lagasca, TACOM-ARDEC
email Bill Vogt, OPM-CAS ARDEC
email Dean Booker OPM-CAS ARDEC
email Alan Goldberg, ARL
email Bruce Poese, ARL
email P. Butler, 2522
email N. Clark, 2522
email D. Doughty, 2521
email D. Ingersoll 2521
email L. Malizia 2525
email D. Tallant, 1822
email T. Boyle, 1846
email J. Braithwaite, 1832
email R. Sorensen, 1832
email T. Alam, 1811
MS 0614 Day File, 2522

18. Appendix F

Monthly Report
December 20, 2002

Sandia National Laboratories

Operated for the U.S. Department of Energy by Sandia Corporation

Albuquerque, New Mexico 87185-0613

date: December 20, 2002

to: Distribution

from: Nancy Clark, 2522 and David Ingersoll, 2521

subject: Activities on ARDEC Self-Destruct Fuze Reserve Battery Project during November-December, 2002

This memo summarizes the activity performed in November-December 2002, on the Self-Destruct Fuze Reserve Battery Project for ARDEC.

Project Status

Electrolyte Aging Matrices – general comments

Three aging matrices are currently ongoing, and Table 1 summarizes the current status of these samples based on the number of characterization intervals during the aging process. As seen, three data sets have been collected on the samples in Matrix 1, while four sets of data have been collected for the samples comprising Matrices 2 and 3. The next set of data will be collected after 4 months aging for all matrices.

Table 1. Time duration for each aging interval for each matrix currently under test.

Aging Duration/Days

	Matrix 1 Reservoirs		Matrix 2 Full Factorial		Matrix 3 Large Matrix	
Characterization Completed	Time in Oven During This Interval	Cumulative Total Time in Oven	Time in Oven During This Interval	Cumulative Total Time in Oven	Time in Oven During This Interval	Cumulative Total Time in Oven
Baseline Analysis	0	0	0	0	0	0
First Interval	28	28	13	13	14	14
Second Interval	28	56	14	27	14	28
Third Interval			28	55	30	58
Fourth Interval					30	88
Fifth Interval						
Sixth Interval						
Seventh Interval						

In addition to the characterization of the samples using Raman and NMR spectroscopy, gross physical characterization of the samples at various intervals has also been done. Furthermore, in the case of the filled reservoirs (Matrix 1), a record of the sample orientation of the reservoir during aging has also been maintained. In this later case the

mobility of the gas bubble was assessed at each interval. The results of these gross physical observations are briefly summarized below.

At the end of the first and second intervals corresponding to 28 and 56 days at temperature, there were no apparent gross physical changes in the samples of Matrix 1, the filled reservoirs. In every case the entrained gas bubble was freely mobile.

In the case of the samples of Matrices 2 and 3, at the end of the first aging period all of the samples appeared yellow in color. Observations of sample clarity, that is the presence/absence of a precipitate, were also made, and all of the samples remained clear through the second interval. At the end of the third interval in the case of the Matrix 2 samples and part way through interval four in the case of the Matrix 3 samples, we observed the samples exhibiting signs of turbidity. In these cases upon removal from the oven a fine, light colored precipitate was observed to have accumulated at the bottom of the tube. When these samples were agitated, the precipitate was resuspended in solution, with little or no evidence of turbidity.

After completing the Fourth Interval of aging, there is clear visual evidence of formation of a deposit. This deposit is observed on the glass wall of the NMR sample tube in direct contact with solution, as well as a large amount of deposit at the bottom of the tube in some cases. The appearance of the deposit is found on those tubes held at the highest temperature. These observations are summarized in Table 2. In the previous sample interval at 58 days, there appeared to be deposits on wall of sample tubes 26, and 27, and in the case of sample 24 it appears as if there may be some deposit present.

Table 2. Summary of Visual Observations after 12 Weeks of Aging

Matrix 3 Visual Appearance at Month 3.			
Matrix Element Number	Tim's Label	Aging Temp °C	Comments
1	0 H_2O/0 $AlCl_3$ 1	40	No Deposit
2	0 H_2O/0.75 $AlCl_3$ 1	40	No Deposit
3	0 H_2O/1.5 $AlCl_3$ 1	40	No Deposit
4	100 H_2O/0 $AlCl_3$ 1	40	No Deposit
5	100 H_2O/0.75 $AlCl_3$ 1	40	No Deposit
6	100 H_2O/1.5 $AlCl_3$ 1	40	No Deposit
7	500 H_2O/0 $AlCl_3$ 1	40	No Deposit
8	500 H_2O/0.75 $AlCl_3$ 1	40	No Deposit
9	500 H_2O/1.5 $AlCl_3$ 3	40	No Deposit
10	0 H_2O/0 $AlCl_3$ 2	65	No Deposit
11	0 H_2O/0.75 $AlCl_3$ 2	65	No Deposit
12	0 H_2O/1.5 $AlCl_3$ 2	65	No Deposit
13	100 H_2O/0 $AlCl_3$ 2	65	No Deposit
14a	100 H_2O/0.75 $AlCl_3$ 2	65	No Deposit
14b	100 H_2O/0.75 $AlCl_3$ 1PB	65	May be some crystals on wall
14c	100 H_2O/0.75 $AlCl_3$ 2PB	65	May be some crystals on wall
14d	100 H_2O/0.75 $AlCl_3$ 3PB	65	May be some crystals on wall
15	100 H_2O/1.5 $AlCl_3$ 2	65	No Deposit
16	500 H_2O/0 $AlCl_3$ 2	65	No Deposit
17	500 H_2O/0.75 $AlCl_3$ 2	65	Looks like some crystals on wall
18	500 H_2O/1.5 $AlCl_3$ 2	65	No Deposit
19	0 H_2O/0 $AlCl_3$ 3	74	No Deposit
20	0 H_2O/0.75 $AlCl_3$ 3	74	No Deposit
21	0 H_2O/1.5 $AlCl_3$ 3	74	Deposit
22	100 H_2O/0 $AlCl_3$ 3	74	No Deposit
23	100 H_2O/0.75 $AlCl_3$ 3	74	Slight ppt., crystals on wall
24	100 H_2O/1.5 $AlCl_3$ 3	74	Deposit
25	500 H_2O/0 $AlCl_3$ 3	74	No Deposit
26	500 H_2O/0.75 $AlCl_3$ 3	74	Deposit
27	500 H_2O/1.5 $AlCl_3$ 1	74	Deposit

Attempts were made to characterize these deposits, and this work is discussed in each section describing the analytical reports.

Electrolyte Aging Matrices – analytical characterization
During November-December we performed Raman analyses and ^{27}Al NMR analysis of the aging Matrices 3 at approximately twelve weeks thermal exposure has also been completed.

Raman
During November we performed Raman analyses of Matrix #1 reservoir samples (2-month-aged), Matrix #2 "full factorial" samples (2-month-aged) and Matrix #3 "standard" samples (3-month-aged). Preliminary analyses of the Raman spectra from these samples follow. Solids were observed in some of the 3-month-aged Matrix #3 samples. Using our micro-Raman capability, we obtained Raman spectra of the solids.

Raman Analysis of Matrix 1 Reservoir Samples

The reservoir samples are analyzed through their glass windows in 180° backscatter configuration using the micro-Raman accessory and the 458 nm line from an argon ion laser. The Raman spectra of the solutions in the reservoir samples aged for two months show no significant change from those obtained after one month aging. Recall that the only change in the Raman spectra from prior to aging to one month of aging was the loss of low-frequency bands possibly due to aluminum chloride species. After two months of aging, the only readily apparent bands in the Raman spectra of the matrix #1 samples are due to sulfuryl chloride.

However, some physical changes are occurring in the reservoirs, as we have noted increased Rayleigh scatter from the glass of the reservoir windows. The increased scatter may be due to crazing at the glass/solution interface. The resulting Raman spectra show higher levels of Rayleigh background and more intense glass Raman bands, both of which we are able to process out of the spectra.

Raman Analysis of Matrix 2 and Matrix 3 Samples

The Matrix 3 samples have permutations of sulfuryl chloride plus three concentrations (0, 0.75 and 1.5M) of aluminum chloride and three concentrations of added water (0, 100 and 500 ppm), aged at three temperatures (40°C, 65°C and 74°C). Matrix 2 samples are a subset of matrix 3, selected by factorial design, including the same range of added water and aging temperatures but all with 1.5M aluminum chloride. The samples are in NMR tubes. We use a 785 nm laser for excitation (near-infrared excitation wavelengths tend to reduce background photoluminescence). We focus the laser beam into the solution in a horizontally mounted tube and collect Raman scatter at 90° to the propagation direction of the laser beam. A triple spectrograph and charge-coupled-device (CCD) detector analyze and record the scattered light.

As we noted in earlier reports, between initiation of aging and aging of two weeks duration, the Raman spectra from the NMR tubes showed an increase in the intensity of the band due to sulfur dioxide in those solutions without aluminum chloride. However, since the first two weeks of aging, there has been no apparent change in the Raman

spectra of the solutions in the NMR tubes for up to two months - Matrix #2 - and three months – Matrix #3 – of aging.

Raman Analysis of Solids in Matrix 3 Samples

After three months of aging, certain samples from Matrix #3 have solids visually apparent in the NMR tubes. The samples are listed below.

Sample #	ppm H_2O	M $AlCl_3$	Aging Temp, °C
13	100	0	65
17	500	0.75	65
21	0	1.5	74
23	100	0.75	74
24	100	1.5	74
26	500	0.75	74
27	500	1.5	74

We tilted the tube gently to flow the solution to one end while leaving the precipitate in the other and obtained micro-Raman spectra of the solid and the solution separately. The spectrum of the solution was subtracted from the spectrum of the solid to remove bands due to residual solution on the solid.

The solid in sample #13 is a single, relatively large, clear, glassy-appearing particle. The Raman spectrum of this solid is not significantly different from that of the glass composing the NMR tube. This particle is a shard of glass. The Raman spectrum from the solid in sample #17 also appears to be that of a glassy particle.

In the other samples the solid has the appearance of a fine, light-colored powder. Before they were subtracted, Raman bands due to residual solution dominated the spectra from the solids. Figure 1 shows a Raman spectrum from the solid in sample #23 after subtraction of the bands due to the solution (plus, for comparison, Raman spectra of sulfuryl chloride and aluminum chloride). This Raman spectrum is generally representative of the solids in samples #21, 23, 24, 26 and 27. Note that the solutions that produced these solids at three months of aging have two things in common: they contain aluminum chloride; and they were aged at 74°C.

The bands marked with peak frequencies in Figure 1 are those that can definitely be associated with the solid. Other features are probably residues from the subtraction procedure that (largely) removed the Raman bands due to the solution. Of the bands due to the solid, those at 1110 and 1370 cm^{-1} are due to stretching motions of O=S=O species, but they are shifted in frequency from those in sulfuryl chloride, indicating a different chemical environment. The lower frequency bands in the spectrum of the solid are probably also due to an SO_2 component and, possibly, to an aluminum chloride species (feature at 345 cm^{-1}). The solid is most likely a combination of SO_2 and $AlCl_x$ species. It may be similar to the $SO_2/AlCl_3$ adduct we proposed (September report) to explain Raman bands in the pre-aged Matrix 3 solutions containing aluminum chloride. However, the Raman bands due to this adduct do not all correspond to those from the solid in the aged solutions, suggesting that the two materials have a somewhat different structure.

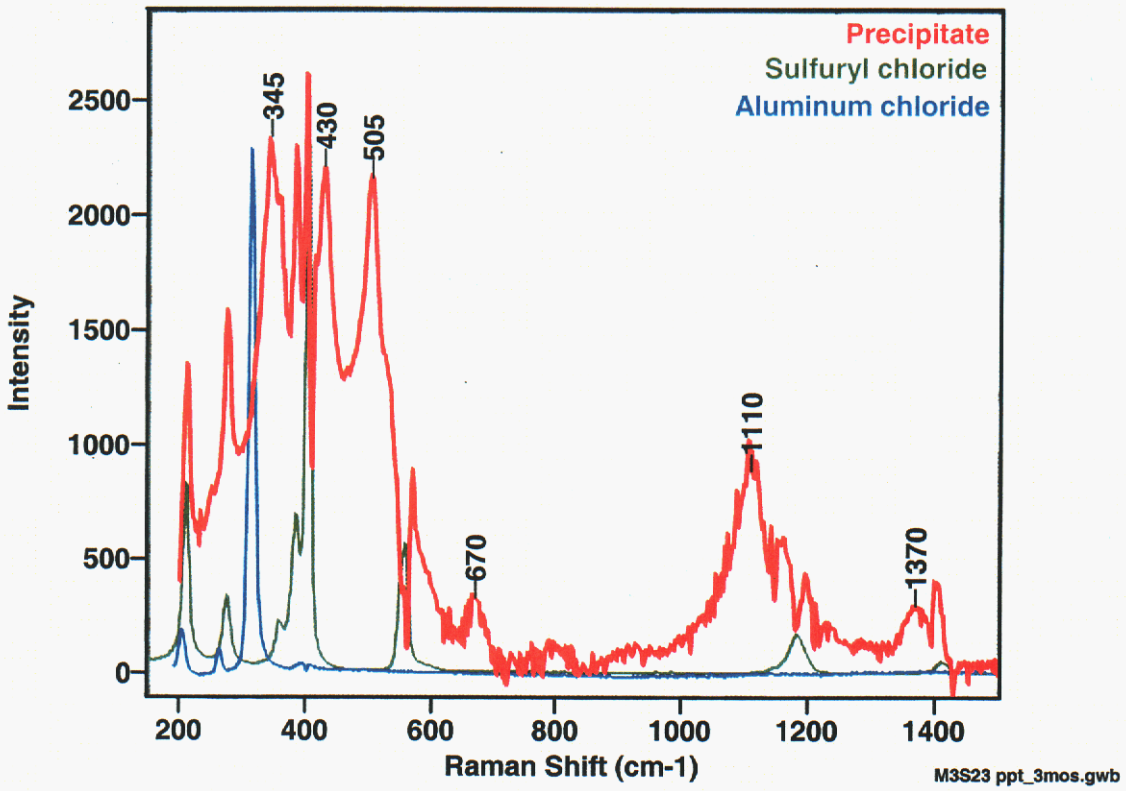

Figure 1. Raman spectrum (after removal of solution bands) of the solid in sample #23 after three months of aging at 74C.

We will be analyzing eight-week-aged reservoirs (Matrix #1) and sulfuryl chloride solutions in NMR tubes (Matrix #2) over the next week or two.

IR Analysis of KDI Electrolyte

We have performed an infrared (IR) analysis of the 10-mm-pathlength, sealable quartz IR cells recently filled by Tim Boyle and Nick Andrews with KDI ($SO_2Cl_2/AlCl_3$), electrolyte. We are using the standard addition method of analysis, in which known amounts of the species to be analyzed (in this case, water) are added to the sample (sulfuryl chloride) containing an unknown amount of the water analyte. The progressive increase in a parameter (intensity of hydroxyl IR bands) related to the amount of added analyte should allow the analyst to extrapolate back to the amount of analyte in the original sample. Some of the IR cells were under filled, but we adjusted their position in the IR beam so that the entire beam passed through the solution. Background fitting resolved any issues with respect to background levels in the spectra associated with moving the cells in the IR beam.

IR spectra of the hydroxyl region from the KDI solutions are shown in Figure 2. Other portions of the IR spectrum are largely saturated in absorption by fundamental, overtone

and combination vibrations of sulfuryl chloride and the silica of the IR cell. The band at 3375 cm^{-1} is assigned to the hydroxyl vibration in $Al(OH)Cl_2$ and was shown to be stable for weeks at typical ambient temperatures (N. A. Fleischer, M. Pallivathikal and M. Babai, "Analysis of Traces of Water in Sulfuryl Chloride Electrolytes by Infrared Spectroscopy," *J. Electrochem. Soc.* **134 (3),** (1987), 513 – 516.). These IR spectra were obtained on 12/12/02, and the cells, we believe, were filled during the first week in December.

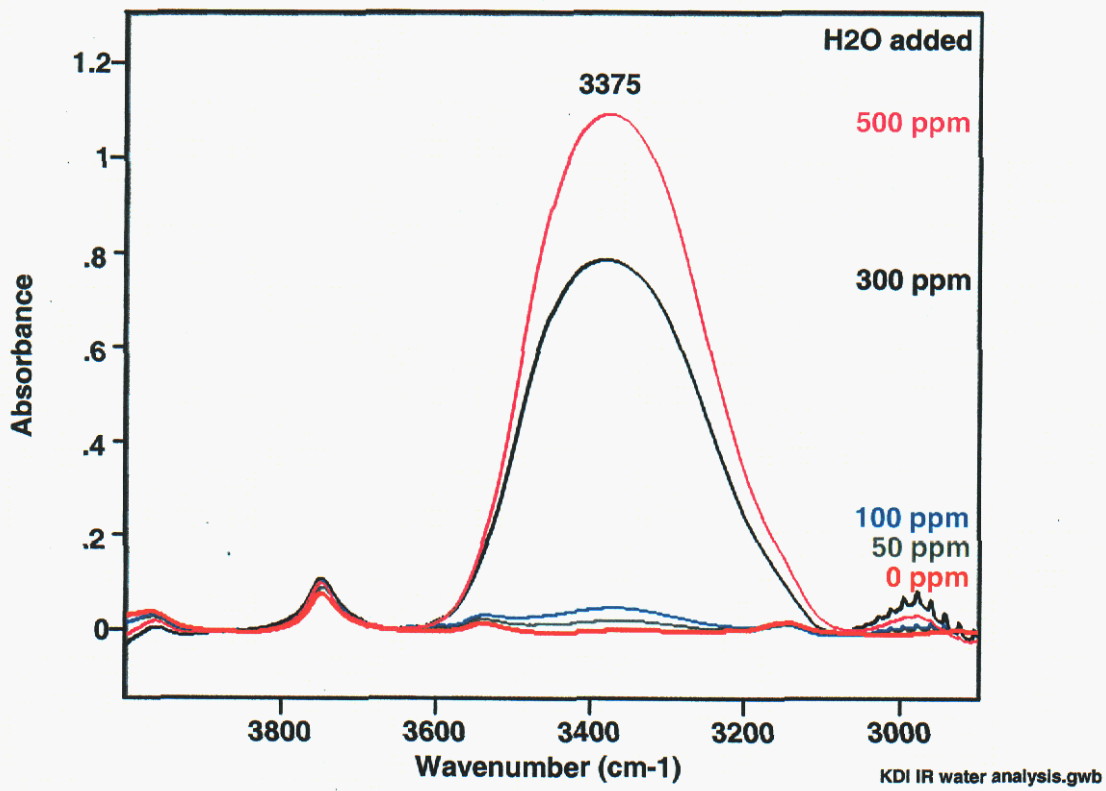

Figure 2. IR spectra of KDI electrolyte plus 0 - 500 ppm H2O in 10 mm silica cells

The intensity of the 3375 cm^{-1} hydroxyl band progressively increases with added water content, but it is obviously not a linear increase. The hydroxyl bands from the two largest added water contents, 300 ppm and 500 ppm, are proportionately much more intense than those from the 50 ppm and 100 ppm water additions. The hydroxyl band of the KDI solution with no added water has the lowest intensity of the five solutions. What I think is happening with respect to the nonlinearity of the hydroxyl band intensities relative to the added water goes back to the chemists' traditional rule – "add acid to water, not water to acid," because the heat generated by the solvation reaction can vaporize small quantities of water (with safety implications, in addition to loss of water that otherwise would be in the resulting solution). In the work described in the Fleischer reference, they added water to the $SO_2Cl_2/AlCl_3$ solutions by adding a weighed amount of $AlCl_3 \bullet 6H_2O$ to $SO_2Cl_2/AlCl_3$ and then adding aliquots of this solution to the $SO_2Cl_2/AlCl_3$ to be analyzed

by IR. Perhaps this approach would give us more linear IR results, but it is probably not necessary.

The bottom line is that, if we are losing, a certain amount (say, equivalent to tens of ppm) of water during its addition to the KDI electrolyte, the actual water concentration in the solutions with, nominally, 300 ppm and 500 ppm added water will be somewhat lower than expected, but the actual water concentration in the solutions with, nominally, 50 ppm and 100 ppm added water will be much lower than expected. The water content of the KDI electrolyte determined by using the nominal added water concentrations will be higher than it actually is, i.e., an upper limit.

Based on ratios of the integral of the IR hydroxyl band from the solution with 0 ppm added water to the solutions with 50 ppm to 500 ppm added water, the equivalent water concentration in the KDI electrolyte is 1 ppm to 5 ppm. Therefore, we can put an upper limit on the water content of the KDI electrolyte of about 5 ppm. For our purposes, it is probably not necessary to know the KDI water content more accurately.

NMR Results

Figure 3 and Figure 4 show the decrease in the concentration of the "unaged" $AlCl_4^-$ species as a function of aging conditions. This is different from the trends reported previously, but consistent with the Raman and Visual Observations.

The following observations were noted:

1) Precipitate was noted for all the 74 °C aged samples.
2) The precipitation process results in a portion of the Al being "invisible" to solution ^{27}Al NMR. In addition the precipitate falls to the bottom of the tube, which is outside the detection coil of the NMR. Approximately 6-7% of the Al in these samples has become non-detectable. The precipitation process is causing a problem with quantification of the Al concentration for the 74 °C samples. I will continue to report results for this temperature, but the error bars for these determined concentrations have gotten much larger. This error is probably responsible for the "increase" in the $AlCl_4^-$ species with longer aging periods.
3) The relative ratio between the $AlCl_4^-$ and the other Al-containing species has changed dramatically for the 74 °C samples following precipitation. Prior to precipitation ~ 22-25% of the Al was in $AlCl_4^-$, while presently in the samples that have precipitated the ratio has increased back to 30-35%. This observation suggests a change in the Al equilibrium following precipitation.

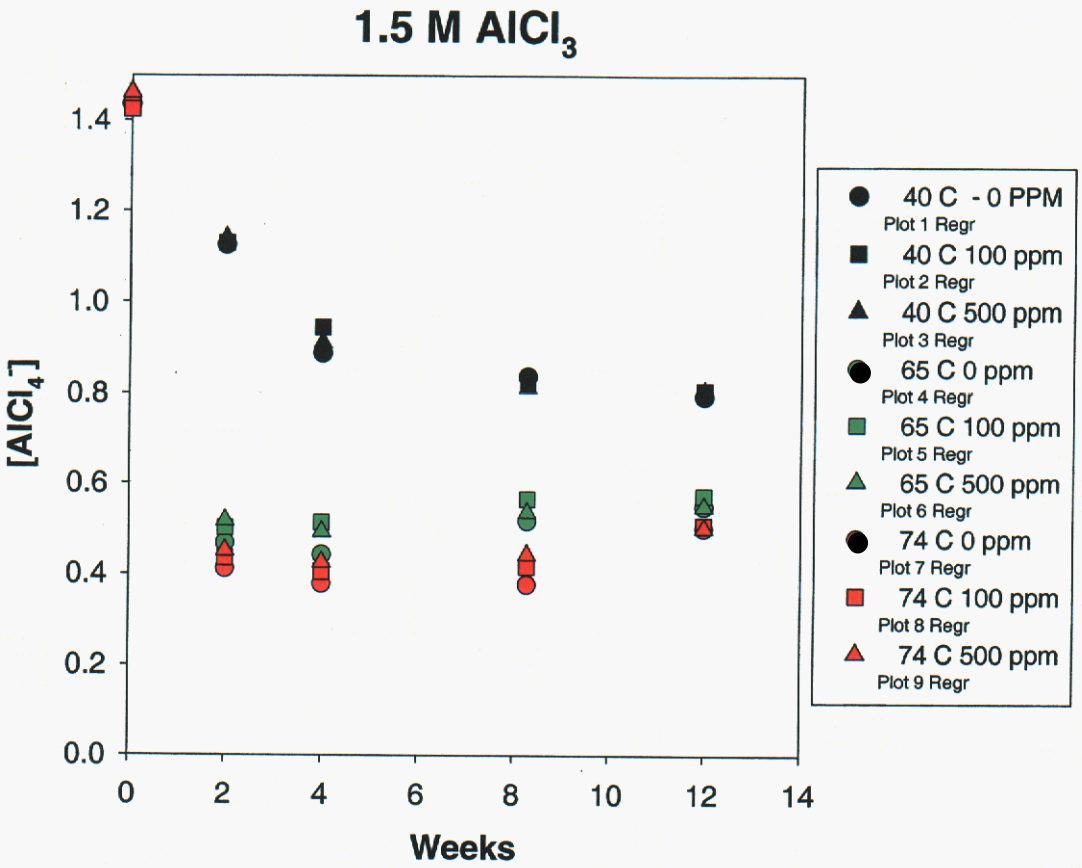

Figure 3. Concentration of $AlCl_4^-$ as a Function of Aging Time with Initial Concentration of 1.5M $AlCl_3$

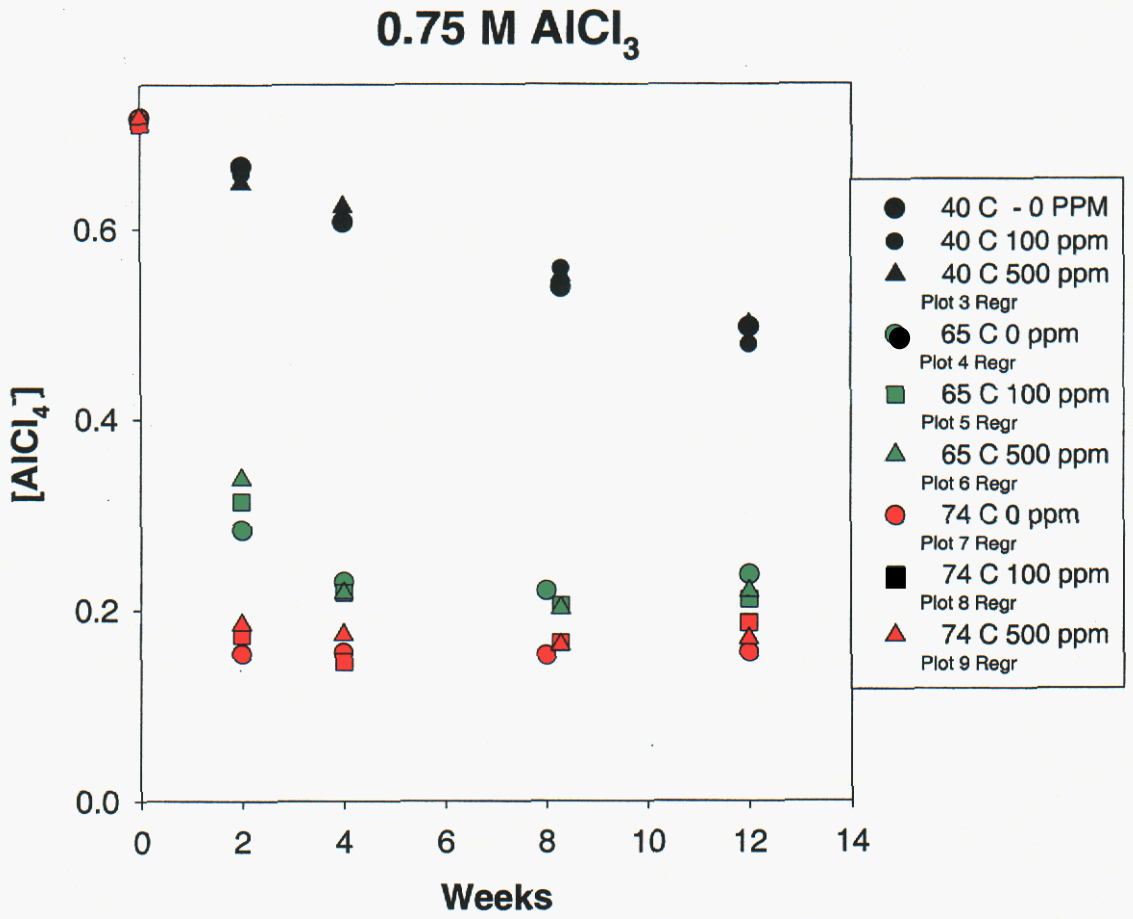

Figure 4. Concentration of as a Function of Aging Time with an Initial Concentration of O.75M $AlCl_3$

Welding Study

The weld study has been completed. This study contains numerous pictures and thus the file is very large. It will be sent as a separate report Titled "Welding Study Final Report"

Corrosion Tasks

During the reporting period, needed activity to initiate all the corrosion-aging experiments was completed. The key factors included the availability of the KDI electrolyte and an associated analysis of its baseline water content (performed by David Tallent). Because the water content of the baseline electrolyte is very low (estimated at < 5ppm), the original decision to use three formulations in the water-sensitivity studies is sound: as-received, + 100 ppm, and + 500 ppm. As such, the +100 level represents an overtest condition, but one that may be possible if electrolyte becomes contaminated during the fabrication process. The +500 level should be very stressful and will thus allow us to determine if corrosion is even viable under extreme conditions. The firm plan now is to fill the existing 45 metal couples contained in the 18 special glass vials during the third week in December and place each in the appropriate ovens for long-term aging.

The majority of the work that was performed involved starting the entire matrix of corrosion experiments designed to determine if electrolyte contamination on the outside of the reservoir would cause significant corrosion. This activity consisted of implementing the test matrix shown below in Table 3 (modified during the ARDEC/KDI visit last summer). In addition to this matrix, several other endplates were exposed and analyzed during the initiation of this matrix to determine if corrosion actually occurred during the short time associated with sample preparation.

A few photographs of the endplates taken during the setup of this matrix are shown in Figures 5-7: as-received endplates (Figure 5), endplates after being dipped, exposed to dryroom/lab for 15 minutes and cleaned (Figure 6), and endplates after being dipped or contaminated with a drop, and dried in dryroom – no cleaning (Figure 7). As shown by comparing Figures 5 and 6, but better seen in the microscope itself, no corrosion was observed by inundating the endplates either horizontally or vertically in electrolyte, letting them dry in the dryroom environment for 15 minutes, and then letting them sit in a more humid lab environment for another 15 minutes prior to cleaning. Finally, the photographs in Figure 8 demonstrate the relatively substantial amount of salt coverage that is left following solvent evaporation on the endplates and how its distribution is affected by the contamination method (dipping or drop). Overall based on what we observed during this initial phase, we feel that the matrix we have implemented will provide ARDEC with the information they need.

Table 3. Test matrix for the external electrolyte contamination corrosion studies (Experiment #1to #3 represent the baseline test configuration)Test matrix for the external electrolyte contamination corrosion studies (Experiment #1to #3 represent the baseline test configuration)

Aging Expt #	*Material*	*Electrolyte Contamination*		*Dry room Exposure Time*	*Lab Exposure Time*	*Cleaned*	*Temp*	*Aging Time*
		Drop	*Dipped*	*Minutes*	*Minutes*		*°C*	*Months*
Baseline conditions								
1	Endplate		X	15	--	--	40	6
2	Endplate		X	15	15	--	40	6
3	Endplate		X	15	15	yes	40	6
Alternate Contamination								
4	Endplate	X		15	--	--	40	6
5	Endplate	X		15	15	--	40	6
6	Endplate	X		15	15	yes	40	6
Dry Room Exposure Time								
7	Endplate		X	30	--	--	40	6
8	Endplate		X	120	--	--	40	6
Standard Laboratory Exposure Time								
9	Endplate		X	15	30	--	40	6
10	Endplate		X	15	120	--	40	6
Aging Time								
11	Endplate		X	15	--	--	40	1
12	Endplate		X	15	--	--	40	12
Welded Reservoir								
13	Reservoir		X	15	--	--	40	6
14	Reservoir		X	15	15	--	40	6
15	Reservoir		X	15	15	yes	40	6
Low Temperature								
16	Endplate		X	15	--	--	25	6
17	Endplate		X	15	15	--	25	6
18	Endplate		X	15	15	yes	25	6
High Temperature								
19	Endplate		X	15	--	--	74	6
20	Endplate		X	15	15	--	74	6
21	Endplate		X	15	15	yes	74	6

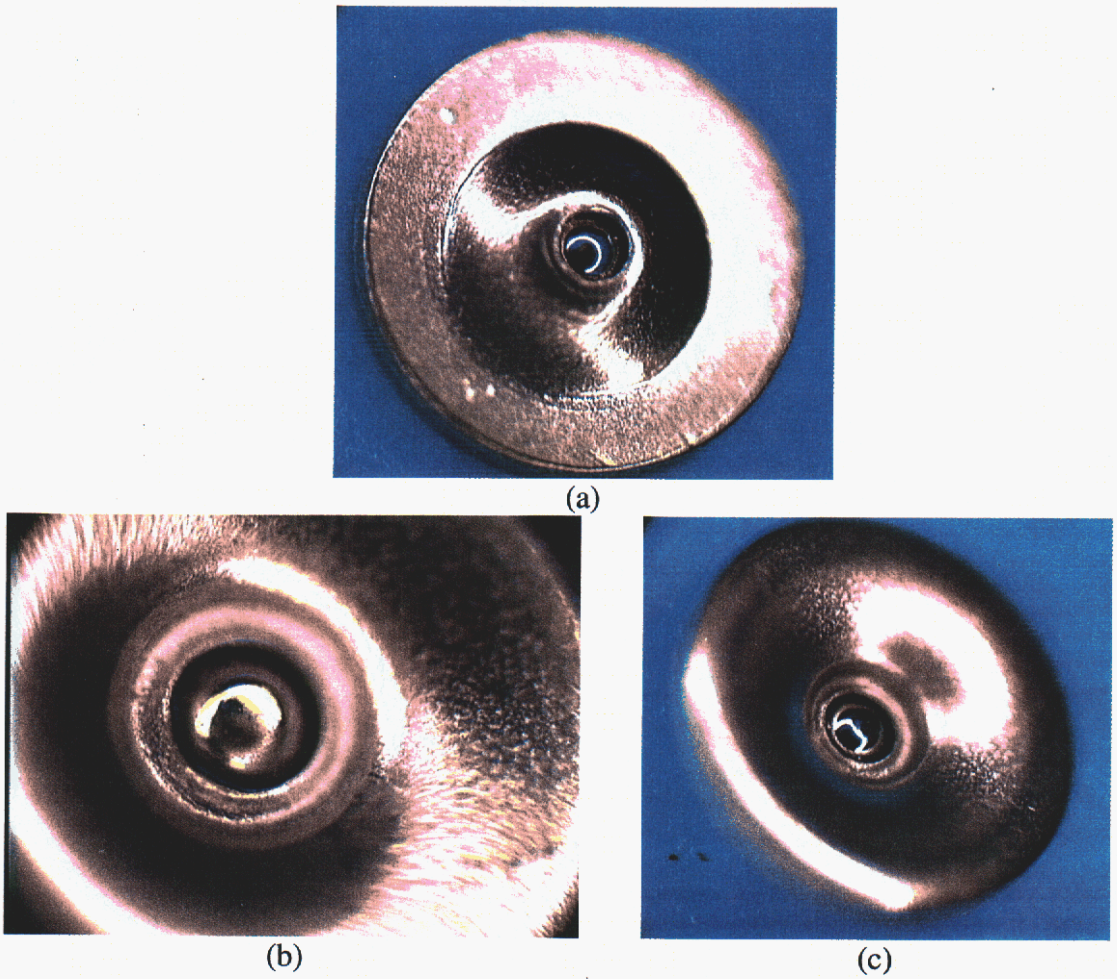

Figure 5. Photographs of as-received endplates (a) bottom, (b) top showing ball, and (c) top.

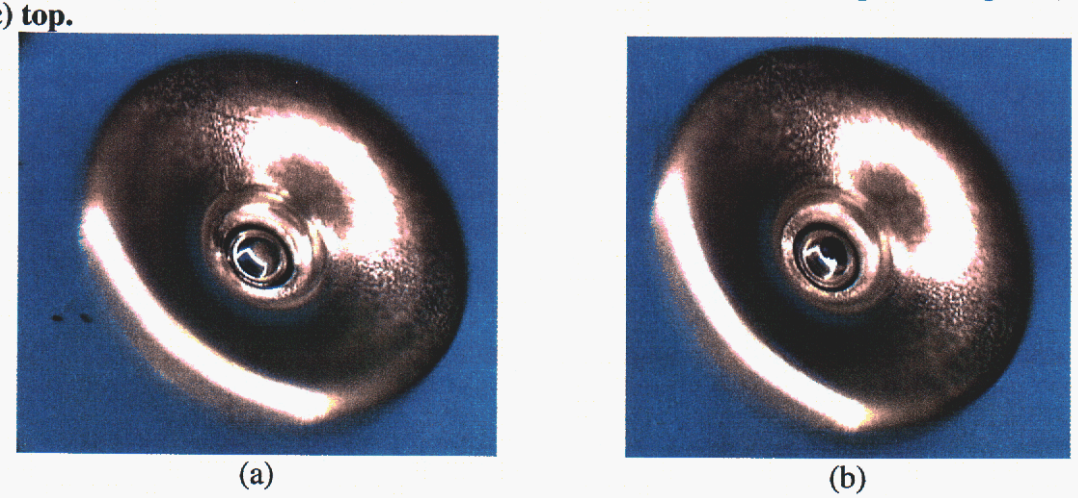

Figure 6. Photographs of endplates after dipping in electrolyte, drying in dry room for 15 minutes, storage in lab for 15 minutes, and cleaning - (a) vertical dip, (b) horizontal dip

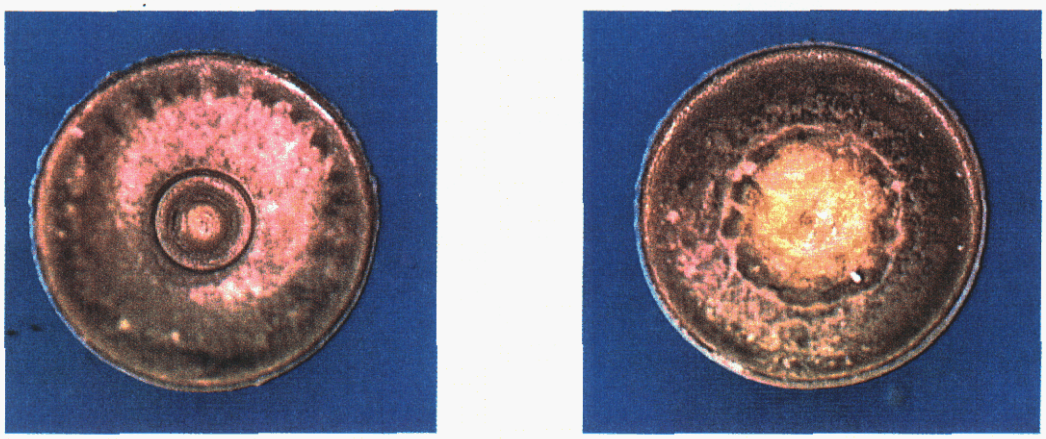

(a) (b)

Figure 7. Photographs of endplates after electrolyte contamination and drying in dry room for 15 minutes - (a) horizontal dip, (b) 0.01 ml drop.

Characterization of Solid in Electrolyte

We have been investigating the characterization of the previously isolated $[Cl_2Al(\mu\text{-}O_2SCl)]_2$ shown in Figure 8 This compound was isolated from the 1.5 M solution of $AlCl_3$ in SO_2Cl_2. We have reproduced the crystals by cooling the samples or allowing them to sit at glove box temperatures. The crystals can be redissolved by warming slightly and then re-cooling. The crystals tend to be very unstable at room temperature and often redissolve or form a gelatin-like mass upon warming slightly. This makes it difficult to characterize this compound fully.

Characterization of $[Cl_2Al(\mu\text{-}O_2SCl)]_2$

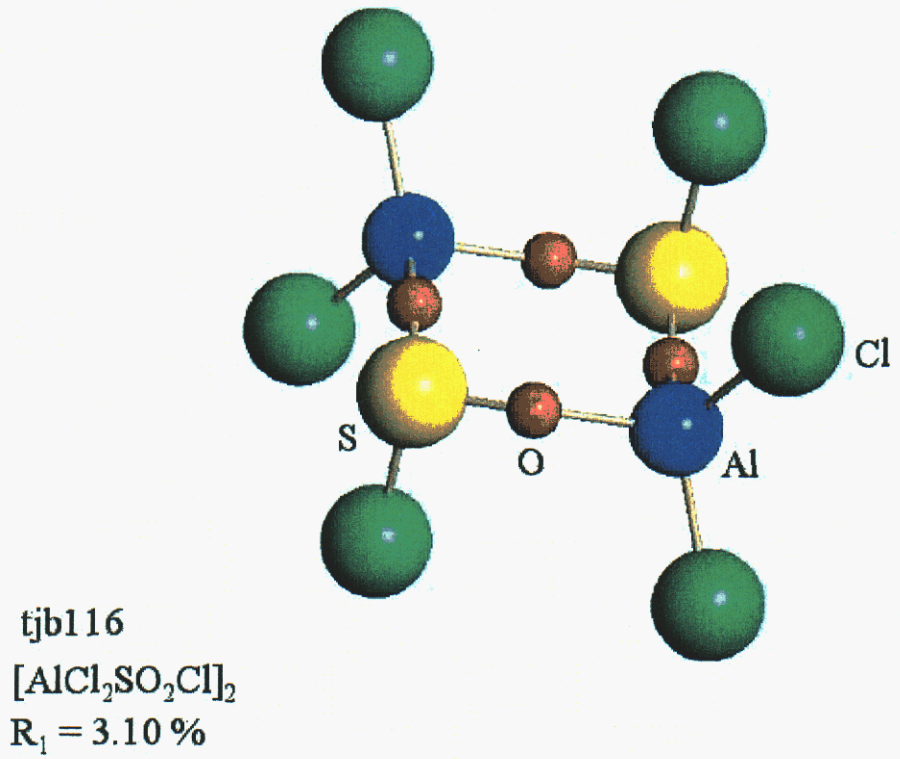

Figure 8. Proposed Composition of Solid in Electrolyte

Initially we determined the identity of the new crystalline material by mounting the crystals on the diffractometer, as done previously to generate the X-ray structure, and comparing unit cell dimensions (i.e., if the same compound is made, the unit cell parameters should match). Numerous samples were investigated in this manner and each sample was shown to be identical to $[Cl_2Al(\mu\text{-}O_2SCl)]_2$.

Several of the crystals isolated and characterized as above were transferred to an NMR tube wherein they remained in a crystalline material. The initially clear and colorless crystals turn dark brown upon this transfer, which is associated with decomposition of the crystalline $[Cl_2Al(\mu\text{-}O_2SCl)]_2$. Attempts to remove the brown material through selective solvent washes yielded a white, free-flowing powder. Solid state ^{27}Al Magic Angle Spinning (MAS) NMR data indicated that this material was identical to $AlCl_3$ (Figure 9a). Since this was inconsistent with the crystalline material, a ^{27}Al MAS NMR of crystalline material that was not washed was collected and is shown in Figure 9b. For $[Cl_2Al(\mu\text{-}O_2SCl)]_2$, the symmetry of the molecule argues for the presence of one ^{27}Al signal but we observe up to 3 signals. It should be noted, *none* of these signals are for $AlCl_3$. Since the crystalline material should dominate, the $[Cl_2Al(\mu\text{-}O_2SCl)]_2$ signal

should dominate and is tentatively assigned to the δ +102 ppm resonance. The remainder of the signals may correspond to other products, such as monomers, SO_2-defficient products, or mono-bridged ClSO(μ-O) species.

Interestingly, the solution state ^{27}Al NMR of the unaged species (shown in Figure 9c) are nearly identical to those observed for the solid sample. ^{27}Al NMR chemical shifts are very dependant on the environment (i.e., coordination), solvent, and concentration of the metal centers. Therefore, it appears that the solid state and solution state environments of the Al are the same; hence it appears that all of the $AlCl_3$ is converted to $[Cl_2Al(\mu\text{-}O_2SCl)]_2$ in solution. We can initiate the crystallization by lowering the temperature slightly (< 0 °C) or by lowering the solubility by increasing the concentration of the reaction mixture. The previous assignments ($AlCl_4^-$ and $AlOCl_4^-$ as determined by literature references) may not be accurate for this sample. Additional work on the hydrolysis and variable temperature experiments of both the standard solutions and $[Cl_2Al(\mu\text{-}O_2SCl)]_2$ are underway to study the changes that occur around the metal center. Unfortunately, there are very few NMR handles that can be investigated. Since a clear route exists to large amounts of crystal of $[Cl_2Al(\mu\text{-}O_2SCl)]_2$ we are attempting to get Infrared, ultraviolet, powder X-ray, and Raman data to completely characterize this compound.

Further preliminary experiments concerning this system have revealed two unusual results. First, due to unusual SO_2 insertion into the Al-Cl sigma bond, we investigated a representative number of metal chloride (MCl_x) species. For every sample investigated (< 10 MCl_x) none would dissolve at room temperature. In boiling SO_2Cl_2, only $NbCl_5$ dissolved; however, the structure of the resulting crystals proved to be $NbCl_5$. The surprising lack of reactivity was further studied by mixing $AlCl_3/SO_2Cl_2$ with the MCl_x and again no dissolution occurred. The unusual lability of the Al-Cl bond of $AlCl_3$ was therefore further studied using SO_2 gas. Again, quite unexpectantly, $AlCl_3$ became completely soluble in toluene merely by bubbling SO_2 gas through the mixture. Further studies on the product isolated are underway.

In summary, we have initiated the complete characterization of the $[Cl_2Al(\mu\text{-}O_2SCl)]_2$ product previously isolated. ^{27}Al MAS NMR data indicate that the solution and solid state species are nearly identical. This indicates that all the $AlCl_3$, upon dissolution in SO_2Cl_2, is converted to $[Cl_2Al(\mu\text{-}O_2SCl)]_2$. The SO_2 is facilely inserted and removed. At lower temperatures, this complex will fall out of solution, indicating that at even slightly reduced temperatures the functionality of a battery may be lower than expected. Comparisons of the analytical data obtained on this compound and the observed high temperature precipitate are underway. Initial thoughts are that the high temperature decomposition products are a different species; indicating problems with high temperature operations.

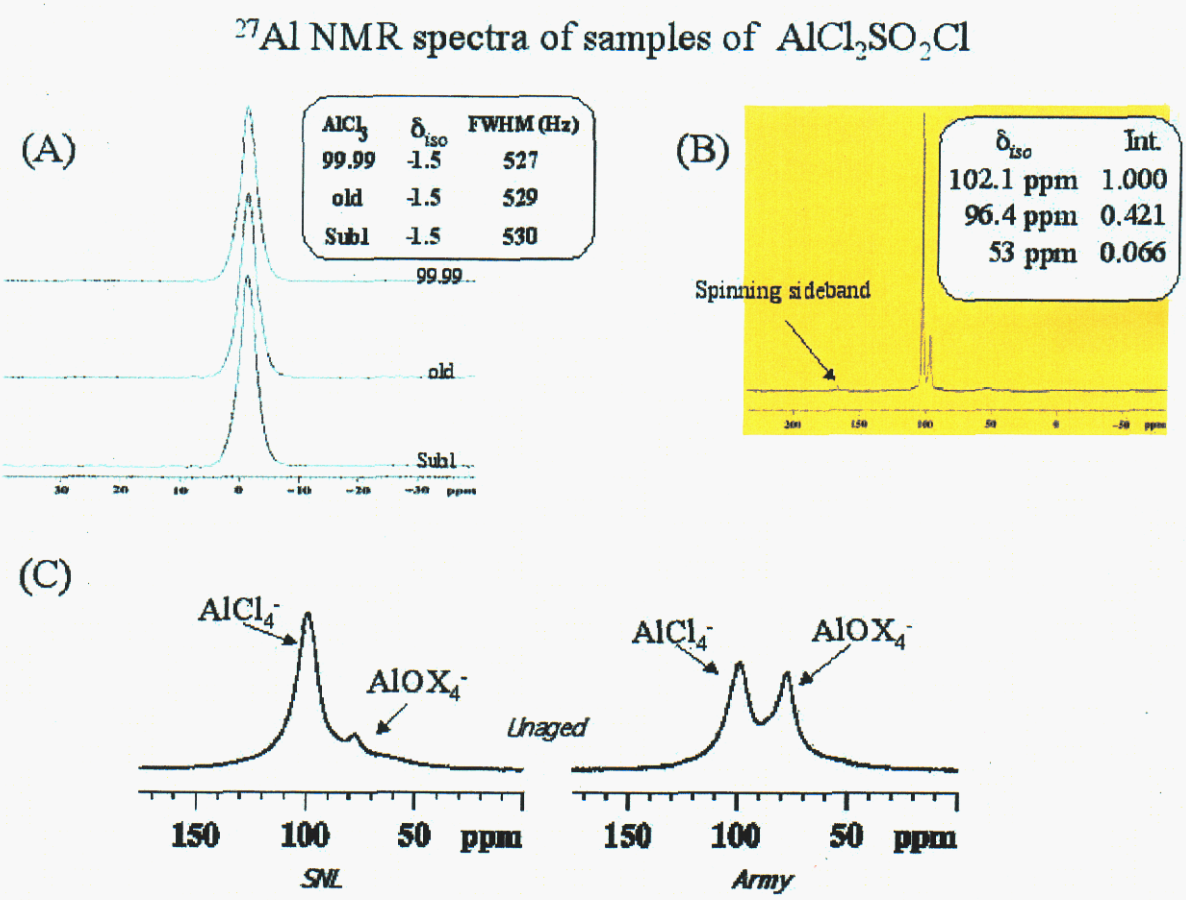

Figure 9. NMR Spectra of Solid Material after washing (a), unwashed (b) and NMR of Unaged Solution(c).

Electrolyte Performance at Temperature Extremes and in Thermal Cycling

Samples for the other three matrices that have yet to be fielded that utilize KDI electrolyte have not yet been prepared. However, the environmental chambers are currently being set up and calibrated. In addition, prior to fielding the higher temperature matrix, individual sample screenings will be done to determine how often samples should be withdrawn during the early part of the aging. The samples for performing these early screening experiments using the KDI electrolyte have been prepared.

If questions arise concerning any of the above items, please contact Nancy Clark at (505) 845-8056 or David Ingersoll at (505) 844-6099.

Distribution:
email Joe Donini, TACOM-ARDEC
email Ben Lagasca, TACOM-ARDEC
email Bill Vogt, OPM-CAS ARDEC
email Dean Booker OPM-CAS ARDEC
email Alan Goldberg, ARL
email Bruce Poese, ARL
email P. Butler, 2522
email N. Clark, 2522
email D. Doughty, 2521
email D. Ingersoll 2521
email L. Malizia 2525
email D. Tallant, 1822
email T. Boyle, 1846
email J. Braithwaite, 1832
email R. Sorensen, 1832
email T. Alam, 1811
MS 0614 Day File, 2522

19. Appendix G

Monthly Report
December 2002-January 2003

This memo summarizes the activity performed in December 2002-January 2003, on the Self-Destruct Fuze Reserve Battery Project for ARDEC.

Project Status

1. Aging Matrices

1.1 Electrolyte Aging Matrices – general comments

Three aging matrices are currently ongoing, and Table 1.1 summarizes the current status of these samples based on the number of characterization intervals during the aging process. Matrices 1 and 2 are currently being characterized and Matrix 3 will be removed early next week for characterization.

Table 1.1. Time duration for each aging interval for each matrix currently under test.

	Aging Duration/Days					
	Matrix 1 Reservoirs		Matrix 2 Full Factorial		Matrix 3 Large Matrix	
Characterization Completed	Time in Oven During This Interval	Cumulative Total Time in Oven	Time in Oven During This Interval	Cumulative Total Time in Oven	Time in Oven During This Interval	Cumulative Total Time in Oven
Baseline Analysis	0*	0	0*	0	0*	0
First Interval	28*	28	13*	13	14*	14
Second Interval	28*	56	15*	28	14*	28
Third Interval	56*	112	28*	56	31*	59
Fourth Interval			56*	112	29*	88
Fifth Interval					58	146
Sixth Interval						
Seventh Interval						

- - indicates that samples were withdrawn for characterization.

At the end of the third interval, there were no apparent gross physical changes in the samples of Matrix 1, the filled reservoirs. In every case the entrained gas bubble was freely mobile.

In the case of the samples associated with Matrix 2 at the end of the fourth interval, there was significant frosting of the NMR glass tube in several instances. (More will be said about this later.) A summary of the gross physical characteristics of these samples is given in Table 1.2.

Table 1.4. Summary of Visual Observations for Matrix 2 After 112 Days of Aging

Matrix 2 Visual Appearance After 112 Days at Temperature			
Matrix Element Number	Tim's Label	Aging Temp °C	Comments
1	100 H_2O/1.5 $AlCl_3$	65	Clear yellow

2	500 H_2O/1.5 $AlCl_3$	40	Clear yellow
3	0 H_2O/1.5 $AlCl_3$	74	Yellow – frosted*
4	500 H_2O/1.5 $AlCl_3$	74	Yellow – frosted*
5	0 H_2O/1.5 $AlCl_3$	74	Yellow – frosted*
6	100 H_2O/1.5 $AlCl_3$	65	Clear yellow
7	0 H_2O/1.5 $AlCl_3$	40	Clear yellow
8	500 H_2O/1.5 $AlCl_3$	40	Clear yellow
9	0 H_2O/1.5 $AlCl_3$	40	Clear yellow
10	500 H_2O/1. $AlCl_3$	74	Yellow – frosted*
11	100 H_2O/1.5 $AlCl_3$	65	Clear yellow

- - the frosted appearance corresponds to that portion of the tube in direct contact with the solution. When the tube is inverted in order to move the liquid to an unfrosted portion of the tube, the solution appears clear. (More will be said about this later.

1.2. "Frosting" of the Glass

As mentioned and as will be discussed further, we have observed a change in the opacity of the glass NMR tubes in some of the matrix samples in this latest sampling interval that makes it difficult, if not impossible to collect Raman spectra since it is so highly scattering. A one-word general description of the appearance of the glass is "frosted". At least two explanations for the source of this change in opacity are: 1) etching of the glass by the electrolyte present and/or 2) deposition of some material onto the inside wall of the tube. At this point it is difficult to say which, if either of these explanations is responsible for the change in appearance. In fact, we are considering opening selected tubes in order to make this determination as well as to attempt to identify the compound in the event that it is a deposit of some source. (Your input on this decision would be appreciated.) Regardless of the source for the increased opacity, in this report we will use the term "frosting" as a general description of the observation.

In addition, these observations are consistent with, and may provide an explanation for, other observations that we have previously reported for the reservoir samples. Recall that we have essentially three sets of reservoirs. These are: 1) reservoirs that had been received from B. Poesse some of which had evidence of a possible gel present; 2) new reservoirs that were received from KDI and that have been held at room temperature in the dark; and 3) new reservoirs as in item 2 that are being aged at the three different temperatures.

In the case of sample set 3, the new reservoirs that are being aged, we are seeing increased scattering from the window. In the event that the same process is occurring in the reservoirs that we are observing in the NMR tubes, we would also expect to see an increase in the scattering, and this has been observed. Bruce Poesse was wondering if the increased scatter in this case could be due to solids formation at the glass/solution interface. In that event and if these species were in fact Raman-active, then we would expect to see additional Raman bands when their concentration increased

to a sufficient level. At this point we have only seen an increase in the intensity of the bands due to the glass in the reservoir window, but we will continue to look for the appearance of bands due to a precipitating solid.

1.3 Characterization of Matrix Samples

In January, Raman spectra of the 12-week-aged Matrix 1 (reservoirs), Matrix 2 (Full factorial, NMR tubes), and the baseline Matrix 4 (extreme temperature, NMR tubes) samples were collected. However, only the data from the Matrix 2 samples has been processed at this point in time. Consequently, only results from Matrix 2 will be discussed here.

Raman Analysis of Matrix 2 Samples

The Raman spectra of the Matrix 2 samples were collected using the macroscopic, 90° scatter configuration. The Matrix 2 samples are in NMR tubes and a 785 nm laser was used for sample excitation. (Near-infrared excitation wavelengths tend to reduce background photoluminescence). The laser beam was focused into the solution in a horizontally mounted tube and Raman scattering was collected at 90° to the propagation direction of the laser beam. A triple spectrograph and charge-coupled-device (CCD) detector analyze and record the scattered light.

After 12 weeks of aging the glass of the NMR tubes maintained at 74°C shows evidence of increased opacity (frosting) where it is in contact with the solution. The frosting is bad enough that the laser beam used to excite the Raman signal is largely scattered at the glass/solution interface. We obtained Raman spectra of the 74°C-aged samples by tilting the sample tube so that the solution flowed to the (unfrosted) opposite end of the tube. The laser beam was then directed to this end of the sample tube. (It will be important to maintain the initial orientation of the NMR tubes in subsequent aging exposures, or we may not have an unfrosted portion of the NMR tubes for Raman analysis.)

In the 74°C-aged NMR tubes the solutions remain clear. The Raman spectra of the solutions from Matrix 2 still do not show any major changes since those occurring in the first two weeks of aging period. However, there is now some evidence for low-intensity, low-frequency (<200 cm^{-1}) features developing in the spectra. The source of these features is not yet apparent, but if these features intensify with additional aging we will have a reasonable chance of identifying their source.

We have not been able to identify any aging-related species at the frosted glass interface using the macroscopic Raman configuration with the solution drained to the far end of the NMR tube. The frosted glass region will be examined using the microscope accessory in the near future.

1.4 New Matrices

Several new matrices will be implemented soon, including those based on the KDI baseline electrolyte, a high temperature matrix and a cyclical temperature matrix. The samples for all of these matrices have been prepared, and the baseline (time 0) analyses have been completed.

1.4.1 High Temperature Environment - Preliminary Screening

All of the samples to be evaluated at 120°C, the highest temperature, have been prepared. In addition, the convection oven for this environment was received, installed in a fume hood, and calibrated. The final two preliminary issues were also completed, and these are discussed more fully below.

The first issue focuses on the compatibility of the NMR sample tube configuration at the elevated temperatures and resultant high internal pressures. We evaluated five separate sample tubes filled with the standard electrolyte, and five survived this environment for the duration of the tests, the longest of which was approximately one day.

The other issue focused on the question of sample withdrawal time. In the work so far completed at the other lower temperatures (40, 65 and 74 °C), it was determined that the initial sample withdrawal times described in the statement of work (i.e. one month intervals) was insufficient for capturing the kinetics of the reactions occurring in the sample tubes. What was observed was that after one-month at 65 and 74 °C , many of the species have reached equilibrium values. Based on these results, we shortened the sample withdrawal interval in these matrices so that we could observe the changes in the equilibrium of the various species present. Based on this previous work, we felt that a similar situation might exist for the 120 °C temperature regime, and that preliminary screening work to establish appropriate withdrawal times at the 120 °C was warranted.

The preliminary screening was done using electrolyte received from KDI. Four samples were placed into the 120°C environment, and at time intervals of 0.5 h, 1 h, 2 h, 4.5 h, and 21 h. Samples were removed and allowed to cool to room temperature. In the case of the samples placed into the oven for 2 h or less, the samples were immersed into a sandbath that had been equilibrated in the oven overnight. In the case of the remaining two samples, i.e. 4.5 h and 21 h, both samples were placed into the oven in air. The ^{27}Al NMR characterization of the samples has been completed, and Raman analysis will be completed next month.

NMR Results

Figure 1.4.1 shows the ^{27}Al NMR spectra for the KDI series as a function of aging time at 120 °C. These KDI sample have no water added. As is evident, there is a large change in the Al speciation following heating at 120 °C, with the largest variation being observed in the first 30 minutes.

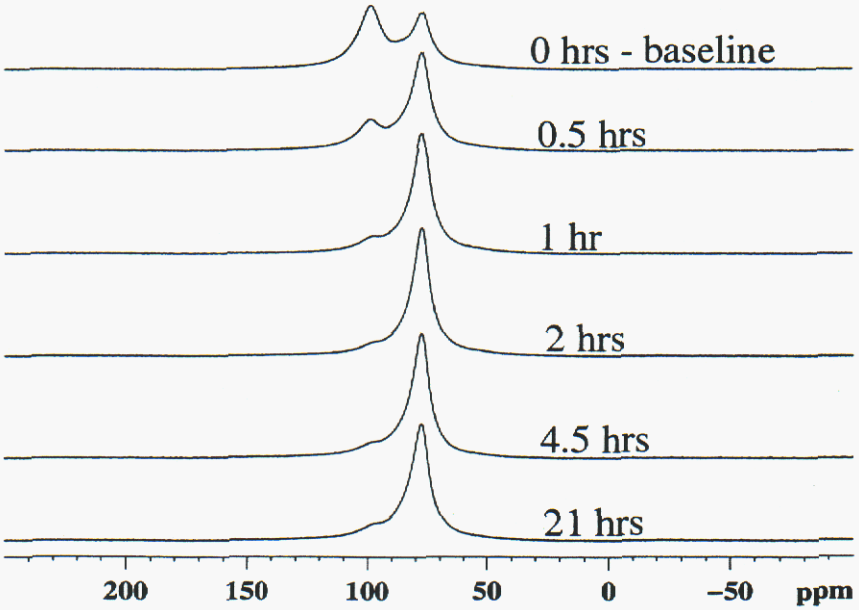

Figure 1.4.1. Comparison of NMR spectra of samples heated in oven at 120C for the time intervals shown.

Although preliminary in nature, these data, along with that previously collected, begin to provide us with an understanding of the evolution of the aluminum species over time. As seen above, there are two readily apparent aluminum species that predominate in the 0 hr baseline solution. (The 0 hr baseline solution in this case is the as-received KDI electrolyte). One of these species is found at about 100 ppm and the other is located at about 80 ppm. (In actuality, there are three aluminum species present, but for the sake of simplicity this discussion will focus on only the predominate two.) This baseline spectrum is similar to that observed and described in the July 2002 report for a different batch of the KDI electrolyte, where again the 80 and 100 ppm species predominate. The spectrum for that sample is shown in Figure 1.4.2, along with the spectrum collected from a freshly prepared solution 1.5 M $AlCl_3$ in SO_2Cl_2.

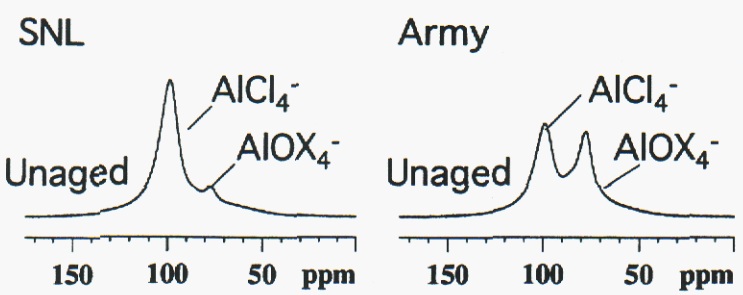

Figure 1.4.2. Comparison of NMR spectra of freshly prepared electrolyte and KDI supplied electrolyte first reported in July 2002.

As seen, the aluminum species at 100 ppm predominates in the fresh solution. At the time of these original observations, the reason for the observed differences was not apparent. However, at this point we can begin to describe the processes occurring, and the place to begin is by showing the spectra for representative samples from the aging matrices currently on test. Shown in Figure 1.4.3 are the NMR spectra for four different samples collected at various times during the aging process at four different temperatures. In the case of the samples aged at 40, 64 and 74 °C, these samples consist of freshly prepared electrolyte. The spectra shown for the 120 °C case was collected for the preliminary screening studies just described, and this sample was supplied by KDI as the most recent batch of electrolyte sample.

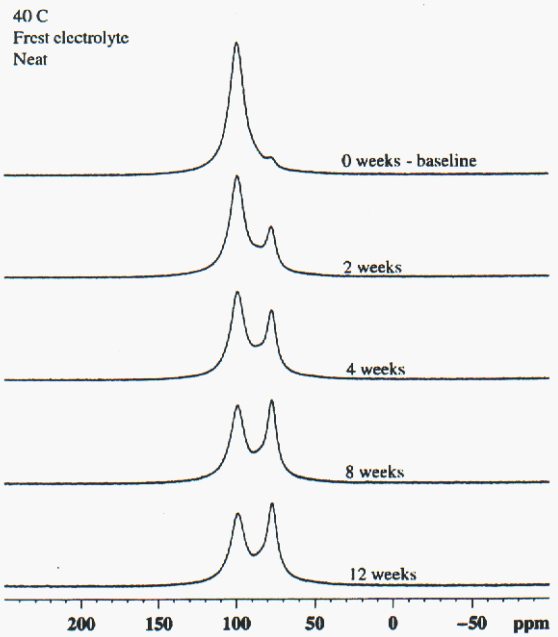
40 C
Frest electrolyte
Neat
0 weeks - baseline
2 weeks
4 weeks
8 weeks
12 weeks
200
150
100
50
0
-50
ppm

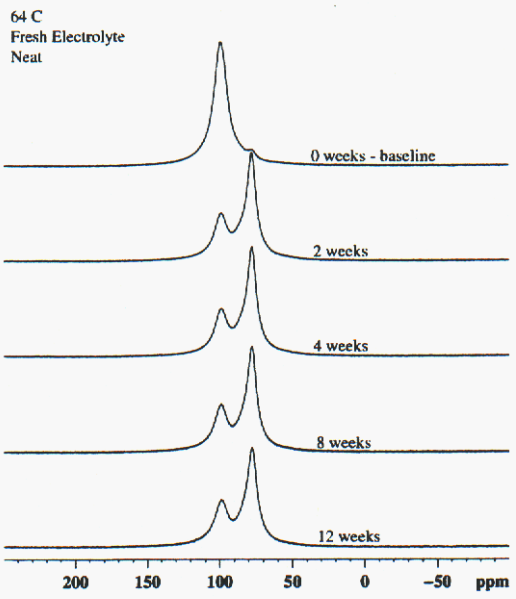
64 C
Fresh Electrolyte
Neat
0 weeks - baseline
2 weeks
4 weeks
8 weeks
12 weeks
200
150
100
50
0
-50
ppm

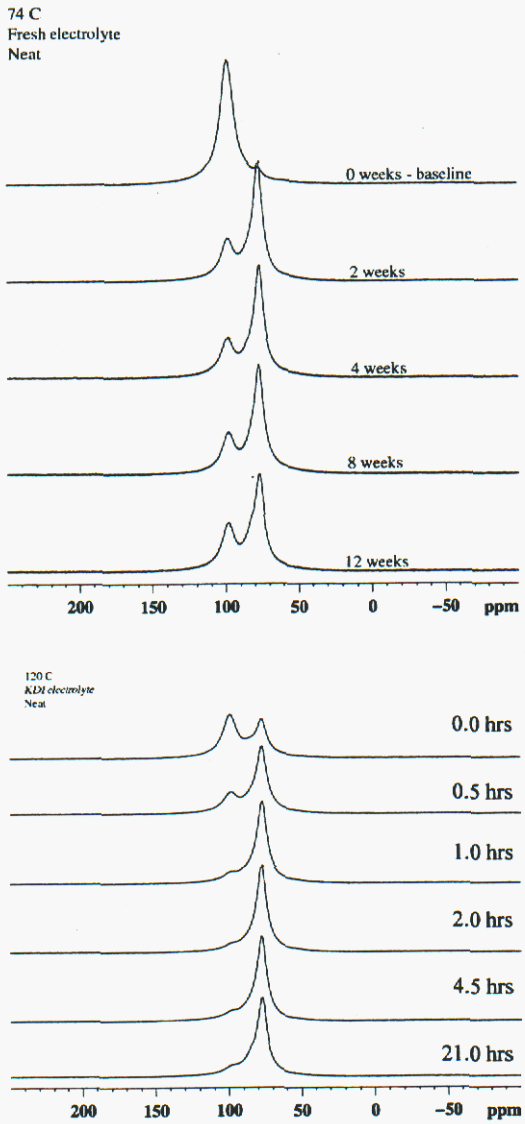

Figure 1.4.3. Comparison of NMR spectra for four different samples obtained at various time intervals during the aging process. In the case of the 40, 64, and 74 °C samples, these are freshly prepared electrolyte. In the case of the 120 °C samples, these are actually six separate samples of recently received KDI electrolyte. (Excess water was NOT added in any case.)

Based on these data it appears that the initial aluminum species found in a freshly prepared solution is that found at 100 ppm. On aging this species is converted to 80 ppm moiety at the expense of the 100 ppm species. It is also clear that this interconversion process is a function of both time and temperature. The interconversion is found to proceed to the greatest extent in the 120 °C. However, at this point it is not clear if the lower temperature samples will reach the same equilibrium values as that seen at the highest temperature.

Returning now to the discussion on the preliminary data obtained at 120 C, there are in fact three aluminum species present in the samples, and Table 1.4.1 summarizes the relative concentration of these three species for the various samples. It should be noted that the species having $\delta = 85$ and $\delta = 77$ ppm resonances are not well resolved, such that the deconvolution of these two resonances are problematic. Figure 1.4.4 shows a plot of these data.

Table 1.4.1: ^{27}Al NMR chemical shifts and relative concentrations of the different observed Al species in the KDI matrix following 120 °C aging.

Sample ID	δ (ppm)	f(i) %
Base line (no aging)	98.8	58.4
	85.6	4.8
	77.4	36.8
0.5 hrs 120 °C	99.1	27.0
	83.0	6.7
	77.3	66.3
1.0 hrs 120 °C	98.8	13.3
	85.6	6.5
	77.4	80.2
2.0 hrs 120 °C	98.4	12.5
	84.8	6.2
	77.5	81.3
4.5 hrs 120 °C	98.2	11.3
	83.0	23.2
	77.6	65.5
21 hrs 120 °C	98.1	9.6
	82.0	32.2
	77.5	58.3

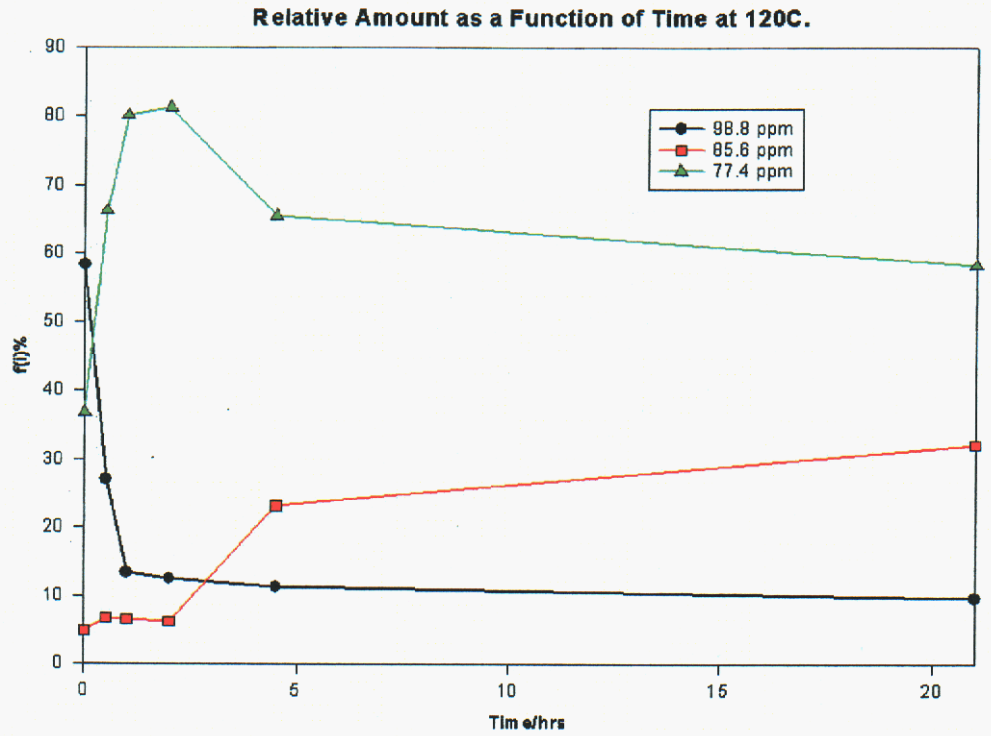

Figure 1.4.4. Plot of percent fraction as a function of time for the three different aluminum species found during the aging process.

2. Corrosion Task

2.1 Effect of Water Content

The matrix designed to identify the effect of water content on the corrosion characteristics of reservoir and ball-seal metals was initiated (see Table 2.1). As indicated, 18 glass vials were loaded with various combinations of five different metal couple combinations and KDI electrolyte at three different water levels. The vials were then hermetically sealed by flame and placed at the three temperatures specified in the table.

Table 2.1. Test Matrix for Water Contamination Corrosion Studies

EXPT NUMBER	METAL COUPLES					WATER CONC (PPM)			TEMPERATURE (°C)		
	304L	304L/ 440C	304L/ 316L	304L/ Ni	304L/ WC	0	100	200-500	25	40	74
1	X					X			X		
2	X					X				X	
3	X					X					X
4	X						X		X		
5	X						X			X	

6	X						X				X
7	X							X	X		
8	X							X		X	
9	X							X			X
10		X	X	X	X	X			X		
11		X	X	X	X	X				X	
12		X	X	X	X	X					X
13		X	X	X	X		X		X		
14		X	X	X	X		X			X	
15		X	X	X	X		X				X
16		X	X	X	X			X	X		
17		X	X	X	X			X		X	
18		X	X	X	X			X			X

The metal couples were formed by spot welding (in the case of the 304L-304L, 304L-316L, 304L-Ni, 304L-440C combinations) or banding together (in the case of the 304L-WC combination) 1-cm^2 coupons. This approach allowed formation of a tight crevice and galvanic couple. Photographs of two of the 18 vials now on test are shown in Figure 2.1. The electrolyte in all of the aging studies containing coupons other than just 304L (i.e. vials 10 -18) quickly discolored relative to the starting KDI material. The darkening began immediately after sealing of the vials and the level of the greenish discoloration appears to correlate primarily with aging temperature and not moisture content. Based on related work with the thionyl-chloride system, a probable cause for this observation is that a small amount of nickel was solubilized. Because the electrolyte in vials 1- 9 (which contain only 304L stainless steel) became only slightly darker, the source of the nickel was probably the nickel coupon itself and not the stainless steel.

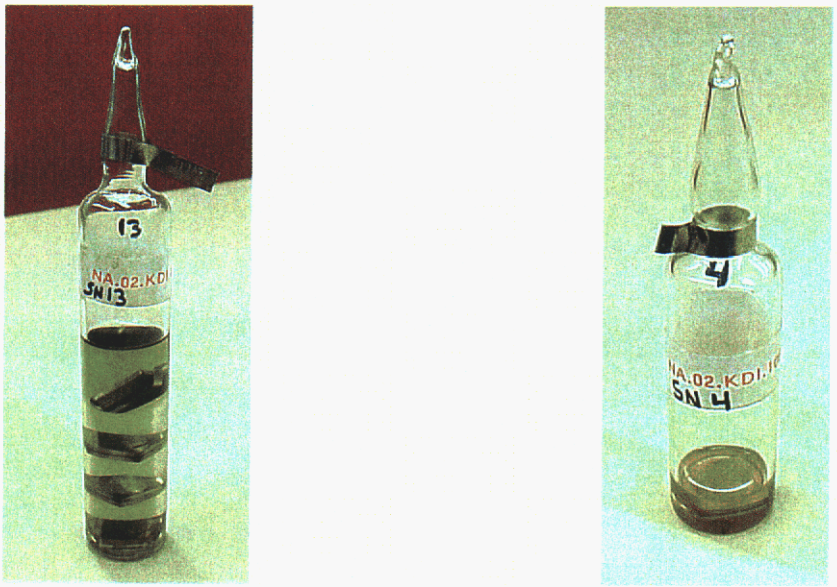

(a) (b)

Figure 2.1.Photographs of sealed glass vials containing KDI electrolyte and various metal couples: (a) 304L SS welded to 440C SS, 316L SS, Ni, and WC, respectively from bottom to top, and (b) 304L SS welded to 304L SS alone. In the multi-sample configuration shown in (a), the individual metal sandwiches are separated with a glass spacer ring. For both of these specific tests, the electrolyte was contaminated with 100 ppm of water, the aging temperature is ambient, and the test duration had reached approximately one month.

As it is currently defined, the Statement of Work calls for termination of all the storage tests after one year. At this time, the extent of corrosion will be determined using a combination of optical and SEM observation along with gravimetric (weight-loss) measurements. During the one-year period while the aging tests continue, we plan to visually inspect each of the 45 metal samples on a monthly basis. Photographs of some representative observations from our initial inspection are shown in Figures 2.2 and 2.3.

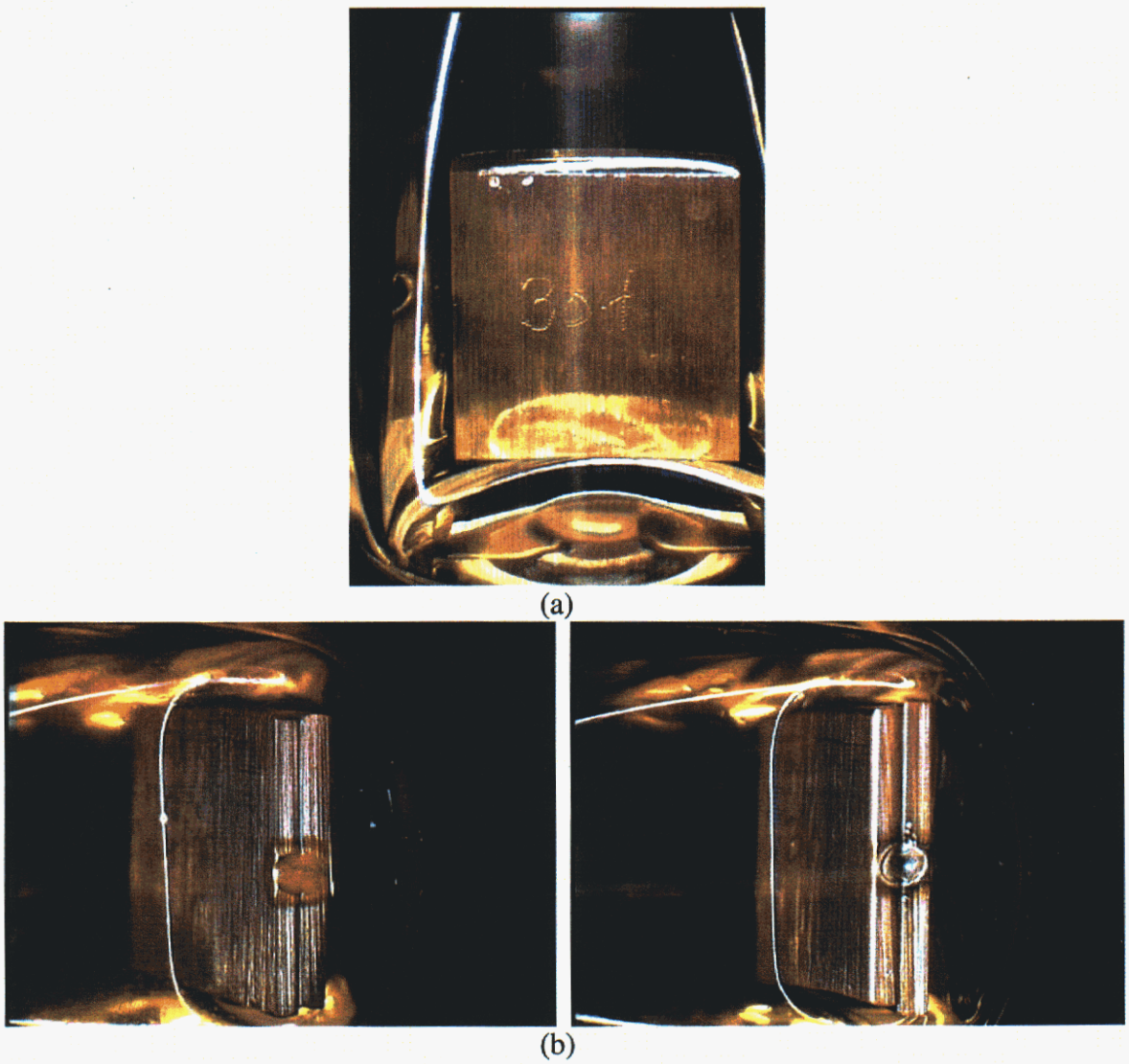

Figure 2.2. Photographs of features of 304L-304L couples that were aged in KDI electrolyte with 100 ppm H_2O for 4 weeks at 25°C: (a) a coupon face showing that no visible signs of corrosion, and (b) the slight rusty like corrosion that occurred around or on the welds on the edge of two separate couples. Also, the two edges of the samples that were cut with a band saw also experienced some general rusting. This edge corrosion probably occurred because of the presence of iron particles that were deposited during the sawing operation.

In general, the 304L, 316L, and nickel samples were relatively free from observable corrosion. The exception is that some small amount of corrosion is obvious on many of the fusion welds, and, in fact, they appeared rustlike in nature (Figure 2.2b and 2.2c). The existence of rust on these samples could imply that significant sensitization occurred in the stainless during the welding process that effectively produced non-stainless like characteristics. Alternatively, it is certainly possible that our traditional knowledge of stainless steel corrosion in chloride-containing aqueous media is not applicable in this case. That is, we expected that the prime vulnerability would be localized pitting of the surface and maybe the longer-term emergence of crevice corrosion. Possibly, the presence of this inorganic electrolyte can render the entire surface more active and permit general dissolution of the normally passivating layer that consists primarily of nickel and chromium oxides. In this situation corrosion of the base iron could occur resulting in formation of the typical rust layer. However, because the rust exists at the point primarily around the weld spot, a combination of both explanations could be applicable. It should be pointed out that at this point we cannot identify any significant correlation with water content except that the spot welds on the samples containing only 304L stainless that are being aged in the as-received KDI electrolyte showed no sign of corrosion. Clearly some degree of differentiation may become evident as the aging continues.

Evidence also exists (Figure 2.3b and 2.3d) that significant corrosion of the 440C stainless steel and some on the tungsten carbide occurred at 74 °C. It should be pointed out however, that the corresponding samples aged at the lower temperatures still appear unaffected except for a few "rust" spots on the 440C samples.

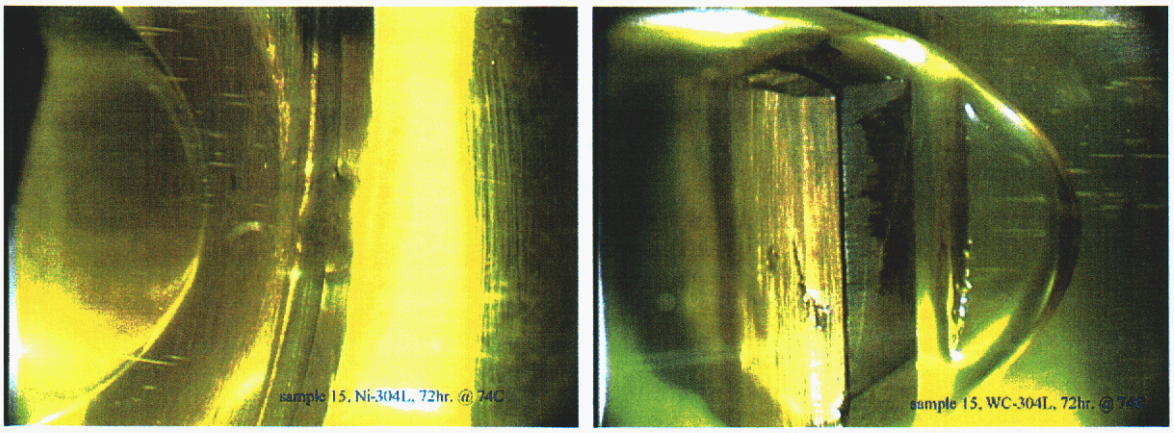

(a) (b)

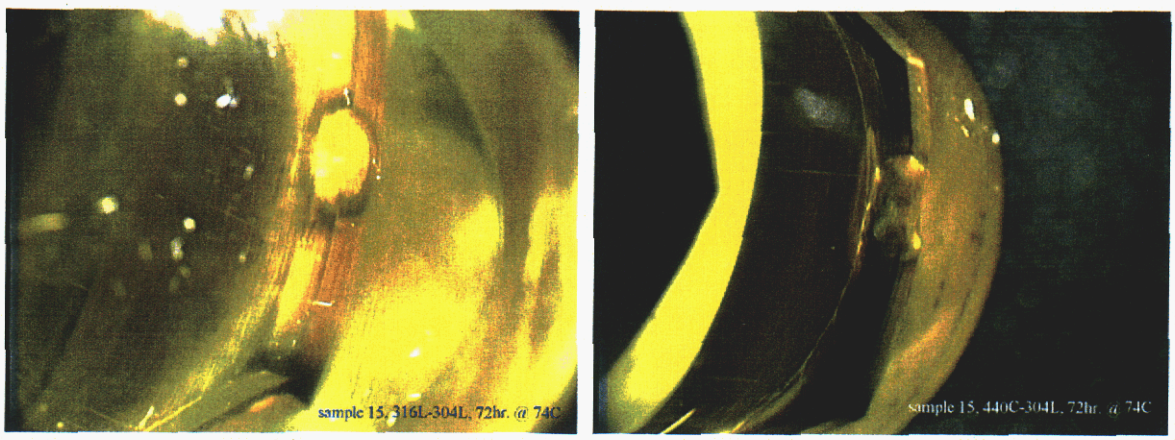

(c) (d)

Figure 2.3. Photographs of the base 304L – ball metal coupons after aging in the KDI electrolyte with 100 ppm H_2O for only 3 days at 74°C: (a) nickel, (b) tungsten carbide, (c) 316L, and (d) 440C. Some evidence of corrosion exists on the tungsten carbide (staining on the visible face of the right hand WC coupon) and the 440C sample (significant darkening of the entire surface – left coupon).

Martensitic stainless steels like 440C are in fact known to have inferior corrosion resistance relative to the 300-series austenitic formulations in chloride-containing aqueous environments. In addition, because the electrochemical potential of martensitic stainless steels is often lower (less noble) than that for 300-series steels, the direct electrical connection through the weld forms a galvanic cell that could, in effect, make the 440C corrode preferentially to the 304L. Although a galvanic series for the various metals has not been established in the $SOCl_2/AlCl_3$ electrolyte, consideration of the galvanic series for many metals measured in seawater is instructive (see Figure 2.4). In this figure, the gray and black boxes for each metal indicate the range of electrochemical potential that have been measured and reported in the literature. The gray boxes cover the potentials measured when the metals are in their normal passive state (the native oxide layer is providing substantial protection) and the black boxes indicate behavior when the oxide is not very protective. For reference, stainless steels can transition from their normal passive state to the active condition when the environment becomes more reducing in nature (a situation certainly possible in our situation). Using this figure, one can then observe the possible differences in potential and identify if a significant galvanic interaction is possible. As a general rule of thumb, corrosion engineers believe that a potential difference of about 250 mV is sufficient to effect galvanic-assisted corrosion. Importantly, the metal with the more negative potential will be the one whose corrosion rate can be accelerated. As seen in this figure (using stainless types 410 and 416 as analogs to the slightly higher Cr-containing 440C), the potential difference between 304L and 440C is about 250 to 500 mV depending on whether or not the surfaces of the steel are active or passive. As such, an appreciable galvanic current could result that would accelerate corrosion of the 440C. This general observation is substantiated in another table contained in Volume 13 of the ASM Metal Handbook (page 773) which shows that the coupling of a small area of a 16-18% Cr steel (e.g., a 440C ball) to a larger area of a 300 series stainless (e.g., an endplate) will "considerably increase" the corrosion of the Cr steel (again in seawater). Another conclusion that can be reached from the information in

Figure 2.4 is that the potential differences between 304L and 316L or nickel are not probably significant. Although we do not know of any potential measurements in seawater for the tungsten carbide, there is evidence that this material is active to austenitic stainless steels in this media (ASM Volume 13, pg 855). This behavior is consistent with our observation that corrosion probably has initiated in our high temperature exposure. Finally, because visible corrosion is definitely occurring at 74 °C after only a few days on the 440C stainless and the tungsten carbide samples, we may need to revisit the position of allowing all the samples to remain on test for a full year.

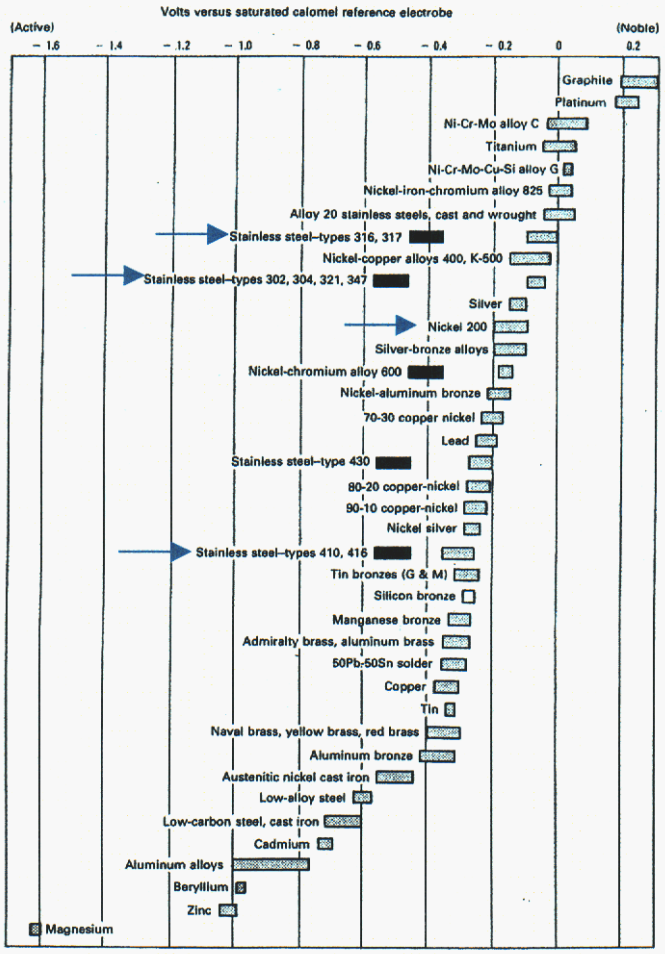

Figure 2.4. Galvanic series for various metals in seawater. Darker boxes indicate the range of observed potentials when the subject metal is in an electrochemically active state. The arrows point to the two primary stainless steels of interest. Note: this figure was copied from ASM Metals Handbook, Volume 13, p. 235.

Electrolyte contamination.

As reported last month, the matrix of corrosion experiments designed to study the effect of electrolyte contamination on the outside of the reservoir was initiated, (see Table 2.2). As specified, one set of replicate samples was removed from the 40 °C oven (experiment 11). For reference, relevant photographs of typical endplates taken prior to aging are shown in Figure 2.5. As described last month, we could not observe any corrosion on the endplate or the 440C ball following the sample preparation procedures (that is, prior to sealing in the hermetic enclosure). Figures 2.6 through 2.8 show photographs of the aged endplates: the top (or external) surfaces in Figures 2.6 and 2.7 for the two replicates (11A and 11) and then views of the internal surface in Figure 2.8 (only for sample 11A). All figures show photographs of the sample as it looked following extraction from the vessel and then following cleaning in the standard sodium-bicarbonate solution. Of note, the deposits were easily cleaned and had sufficient reactivity to still produce a noticeable quantity of off-gas products. Given that a real change in the physical appearance of the electrolyte residue had occurred during this period, we concluded that some environmental interactions (e.g., with either the occluded atmosphere or the metals) had proceeded. However, based on visual inspection of these endplates, it appears that if any corrosion had occurred, it was slight. There was some graying/dulling of the inner endplate surfaces near the ball seal, possibly some widespread but shallow pitting of the 440C ball, and no evidence of any crevice corrosion between the plate and the ball. This apparent lack of significant corrosion is certainly a positive initial result.

Table 2.2. Test matrix for the external electrolyte contamination corrosion studies (Experiment #11 was terminated this month)

Aging Expt #	*Material*	*Electrolyte Contamination*		*Dry room Exposure Time*	*Lab Exposure Time*	*Clean*	*Temp*	*Aging Time*
		Drop	*Dip*	*Minutes*	*Minutes*		*°C*	*Months*
Baseline conditions								
1	Endplate		X	15	--	--	40	6
2	Endplate		X	15	15	--	40	6
3	Endplate		X	15	15	yes	40	6
Alternate Contamination								
4	Endplate	X		15	--	--	40	6
5	Endplate	X		15	15	--	40	6
6	Endplate	X		15	15	yes	40	6
Dry Room Exposure Time								
7	Endplate		X	30	--	--	40	6
8	Endplate		X	120	--	--	40	6
Standard Laboratory Exposure Time								
9	Endplate		X	15	30	--	40	6
10	Endplate		X	15	120	--	40	6
Aging Time								
11	***Endplate***		***X***	***15***	***--***	***--***	***40***	***1***
12	Endplate		X	15	--	--	40	12
Welded Reservoir								
13	Reservoir		X	15	--	--	40	6
14	Reservoir		X	15	15	--	40	6
15	Reservoir		X	15	15	yes	40	6
Low Temperature								
16	Endplate		X	15	--	--	25	6
17	Endplate		X	15	15	--	25	6
18	Endplate		X	15	15	yes	25	6
High Temperature								
19	Endplate		X	15	--	--	74	6
20	Endplate		X	15	15	--	74	6
21	Endplate		X	15	15	yes	74	6

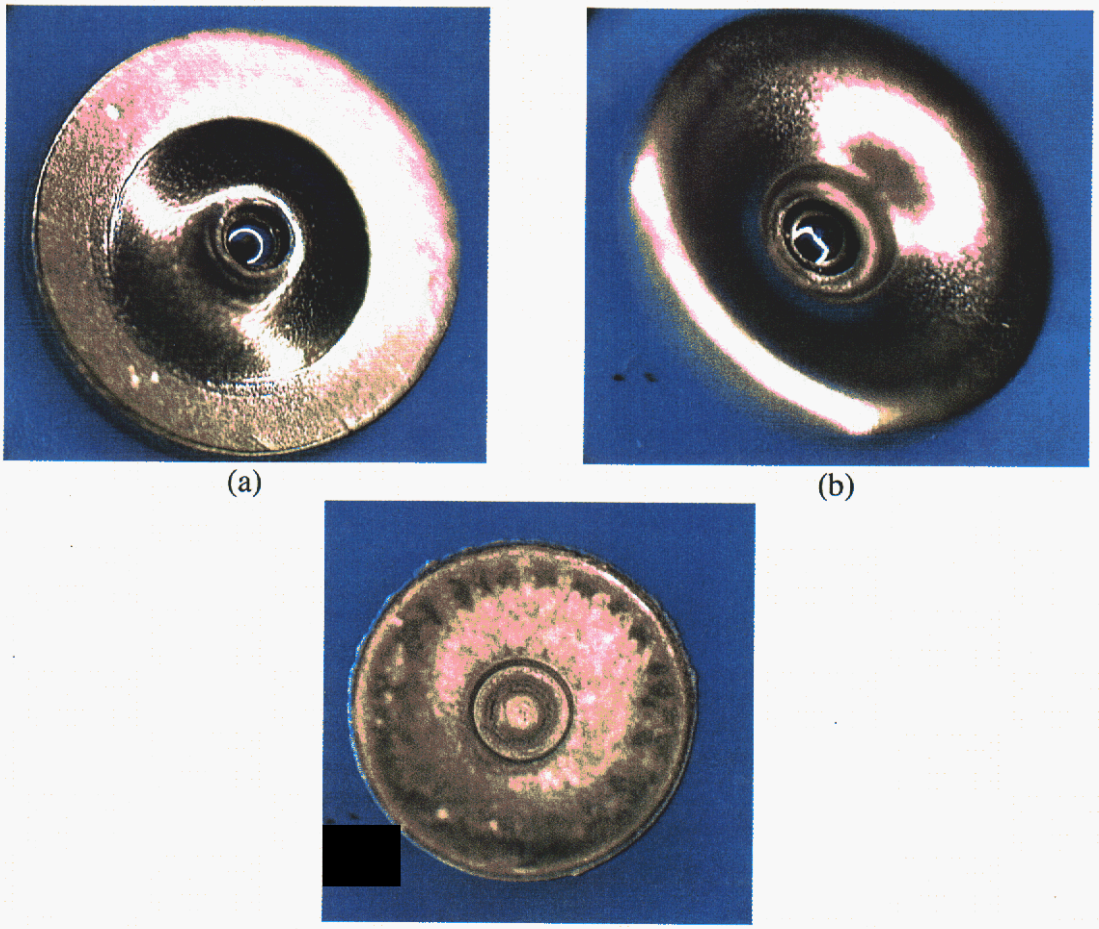

(a) (b)

(c)

Figure 2.5. Photographs of as-received endplates (a) bottom, (b) top. A photographs of an endplate after electrolyte contamination and drying in dry room for 15 minutes is shown in (c).For reference, photographs of endplates after dipping in electrolyte, drying in dry room for 15 minutes, storage in lab for 15 minutes, and cleaning appear similar to those shown in (a) and (b).

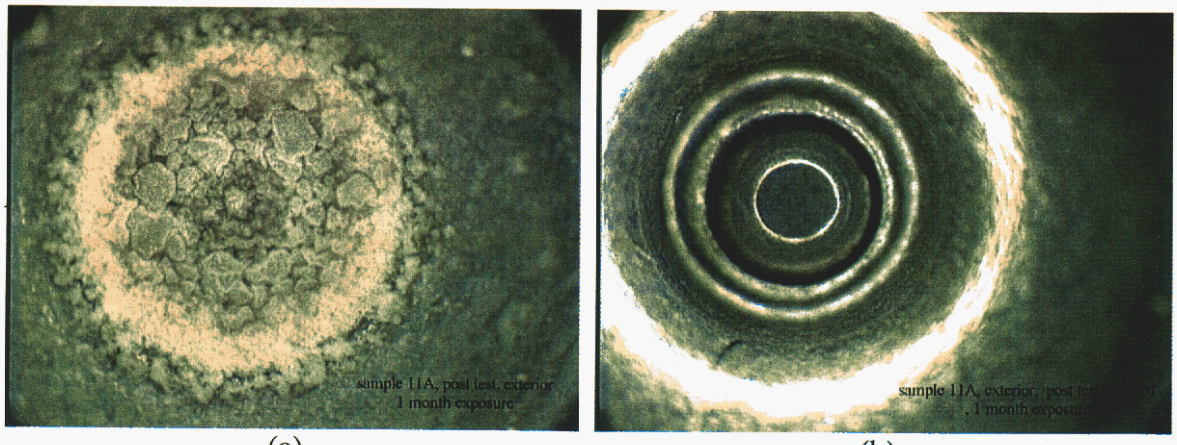

(a) (b)

Figure 2.6. Photographs of the outside surface of the endplate from Experiment 11a following one-month of aging at 40°C: (a) as removed from the hermetic enclosure, (b) after cleaning in the $NaHCO_3$ solution.

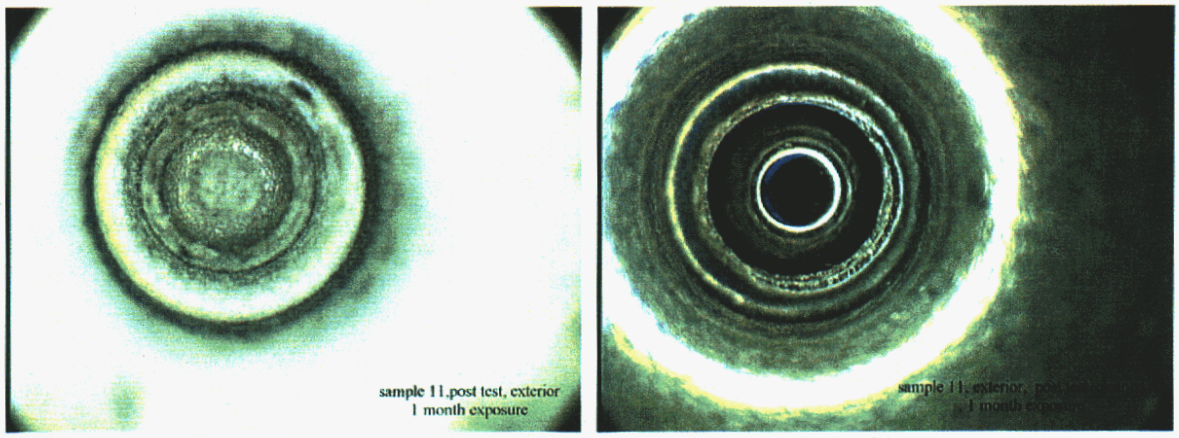

(a) (b)

Figure 2.7. Photographs of the outside surface of the endplate from Experiment 11 following one-month of aging at 40°C: (a) as removed from the hermetic enclosure, (b) after cleaning in the $NaHCO_3$ solution. This endplate is a replicate of the one shown in Figure 6.

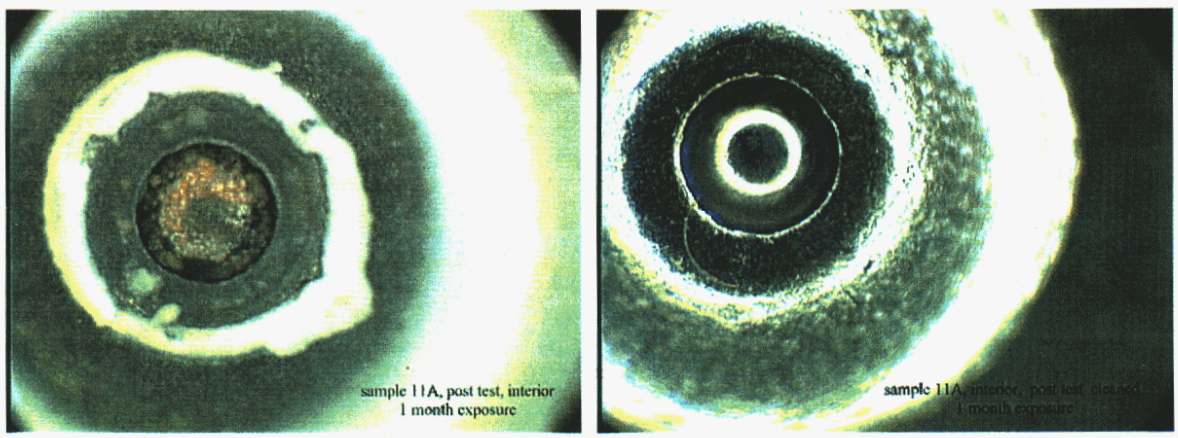

(a) (b)

Figure 2.8. Photographs of the inside surface of the endplate from Experiment 11a following one-month of aging at 40°C: (a) as removed from the hermetic enclosure, (b) after cleaning in the $NaHCO_3$ solution.

3. SDF Battery Reservoir Welding Study

The objective of this study was to evaluate laser welding of the end plate onto the reservoir.

3.1 Experimental Procedure and Results

Thirty reservoirs filled with electrolyte and sealed by pulse laser welding were received from KDI. Upon receipt, a visual inspection of all of the reservoirs was made. Electrolyte was then removed from the reservoirs by breaking the glass seal on the bottom of the reservoir in an inert environment. (The electrolyte recovered was utilized for another aspect of the program.) Residual electrolyte was removed from the reservoirs by flushing the reservoir with alcohol.

After removal of the electrolyte, microscopic examination of all of the welds on each reservoir was completed, and Figure 3.1 shows photomicrographs of the typical closure welds observed on two different reservoirs. As can be seen, the weld beads are uniform in width, and there did not appear to be excessive concavity in the bead. However, the solidification lines resulting from the pulsed laser source did show somewhat excessive pulse-to-pulse overlap. These observations were the same in every case, demonstrating good reproducibility.

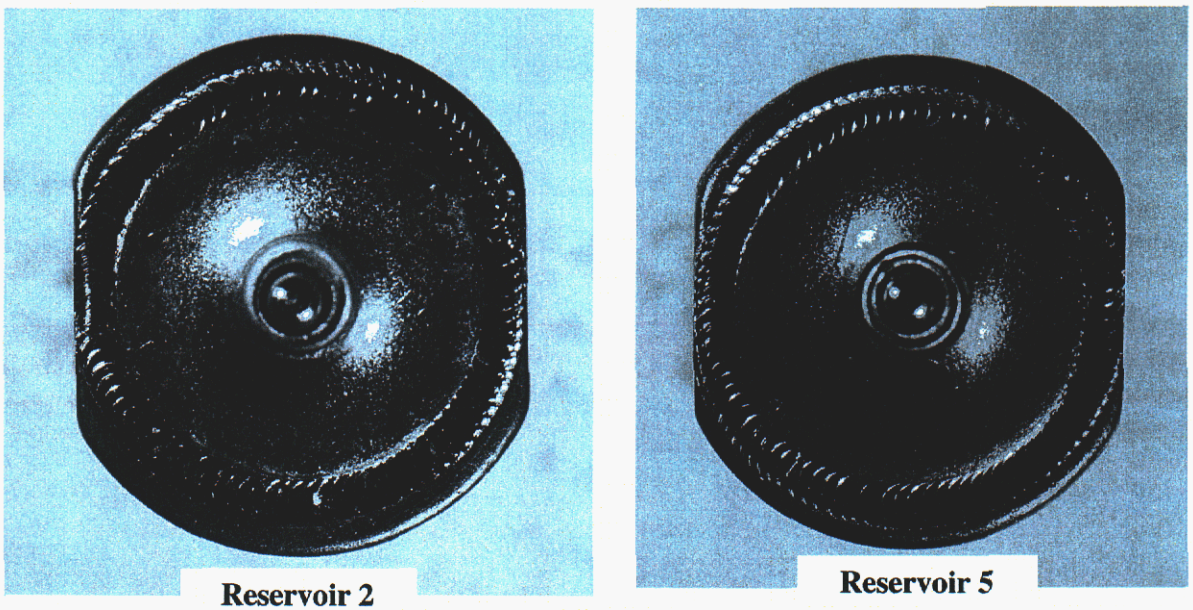

Figure 3.1. Photomicrographs of two different reservoirs showing typical laser weld.

The first twenty numerically sequenced reservoirs were selected for further metallurgical examination, and the remaining ten reservoirs were held in reserve. Metallurgical examination was done by microscopic examination of a cross-section through the weld. Sectioning of the reservoirs was done by first positioning the reservoir in a mount, and then grinding to the approximate middle of the reservoir. The ground samples were then polished and etched.

As seen in the photomicrographs of Figure 3.1, the welds themselves are circular in nature, and the outer circumference of the reservoir displays two flats diametrically opposed to one another along the perimeter. Since it is conceivable that the nature of the weld is different in these areas, two reservoirs were cross-sectioned through the flats and two reservoirs were cross-sectioned at 90-degrees to the flats. Figure 3.2 shows cross-

sectional photomicrographs of these four reservoirs. As seen, these welds were found to be essentially identical in every case, consequently the remaining 16 reservoirs were cross-sectioned through the welds at 90-degrees to the flats.

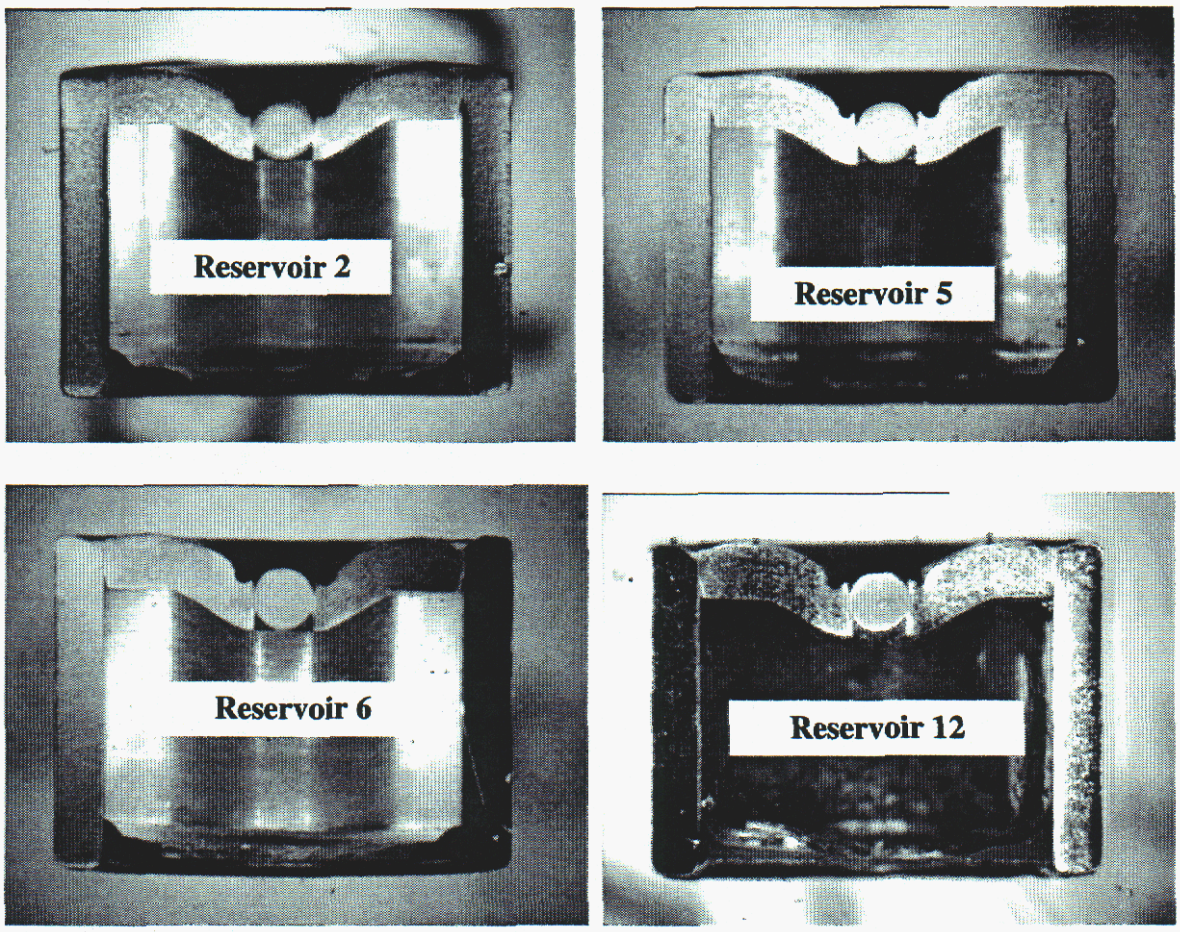

Figure 3.2. Cross sectional photomicrographs of the weld taken parallel and normal to the flat.

Figures 3.3 through 3.12 show photomicrographs of welds of various reservoirs. All of the photomicrographs were examined in detail, and several important weld measurements were made. These measurements including: 1) the weld depth, corresponding to the distance between the fusion lines on the surface; 2) the maximum weld depth, corresponding to the dimension of the deepest portion of the fusion zone; and 3) the effective weld depth corresponding to the minimum thickness of the weld at the joint between the cap and case. A tabular compilation of these dimensions for each reservoir is given in Table 3.1.

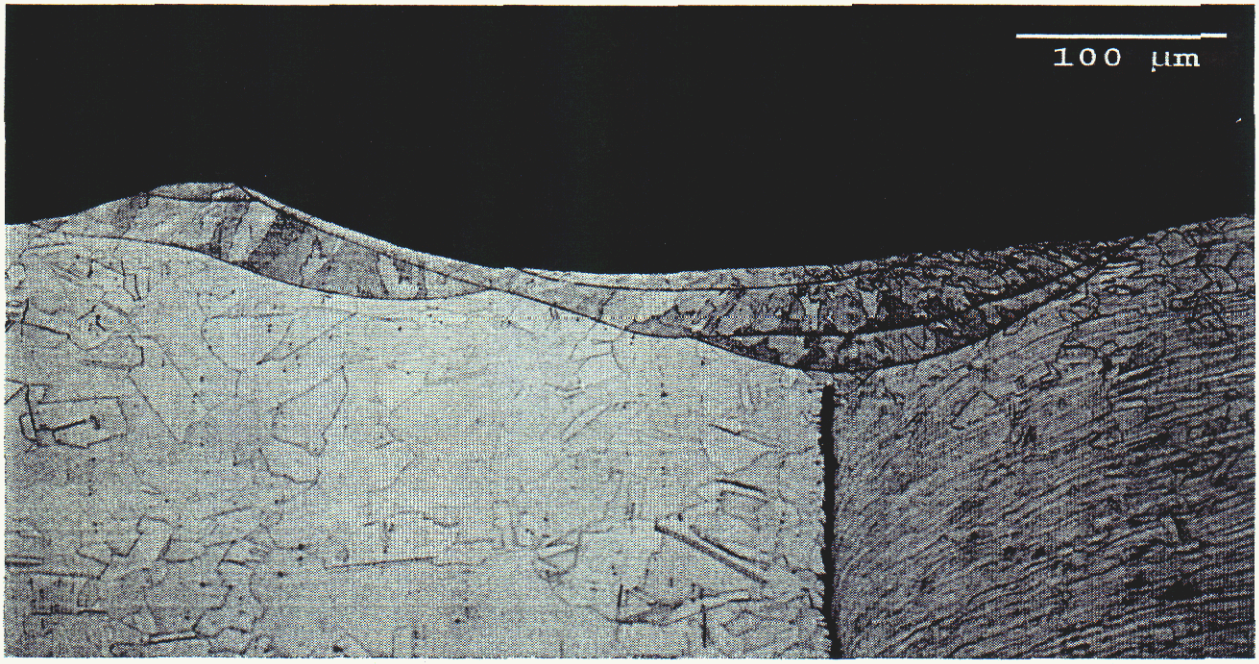

Figure 3.3 – Side 1 of Reservoir 2 Laser Weld Width = .017"; Max. Depth - .0041"; Eff. Depth - .0036"; Fusion Lines – 6.

Figure 3.4 – Side 2 of Reservoir 2 Laser Weld Width = .018"; Max. Depth - .0036"; Eff. Depth - .003"; Fusion Lines – 3. The weld is a slight amount of a root void that reduced the leak path.

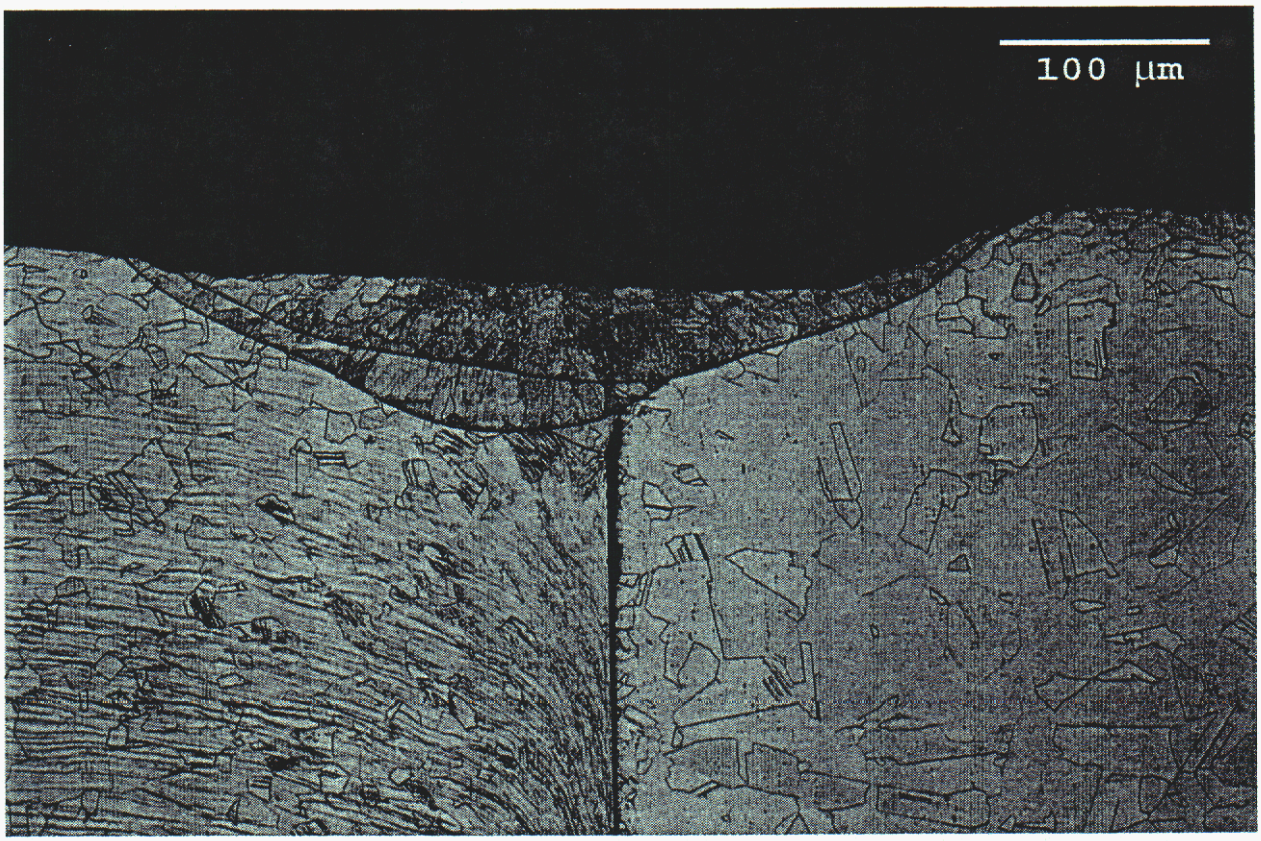

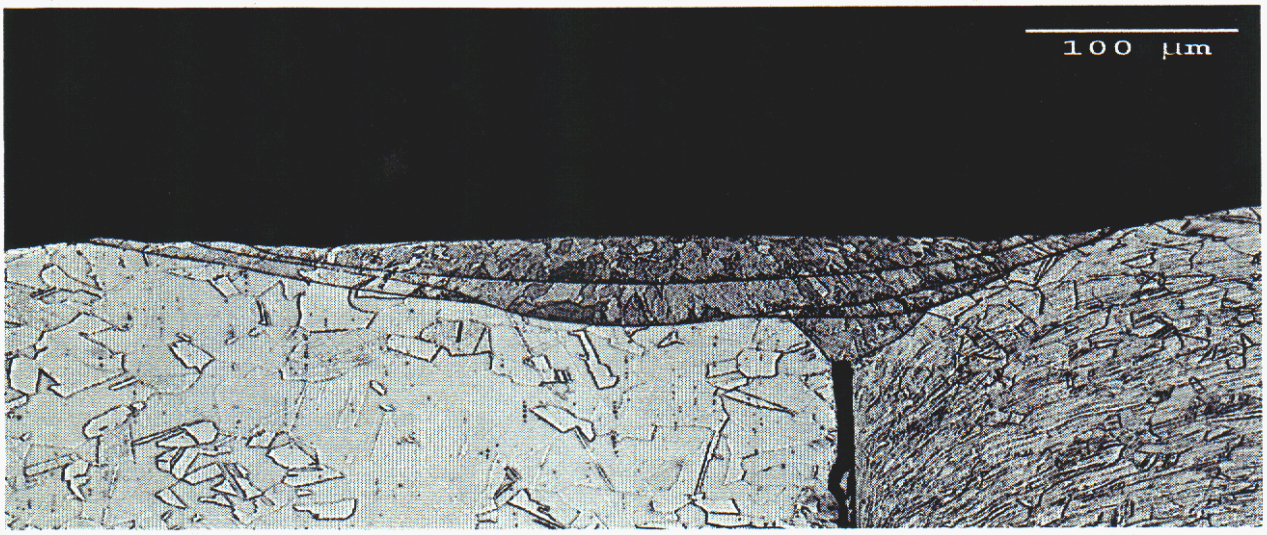

Figure 3.5 – Side 1 of Reservoir 5 Laser Weld Width = .020"; Max. Depth - .0044"; Eff. Depth - .0044"; Fusion Lines – 4. The weld is slightly off-center of the weld joint.

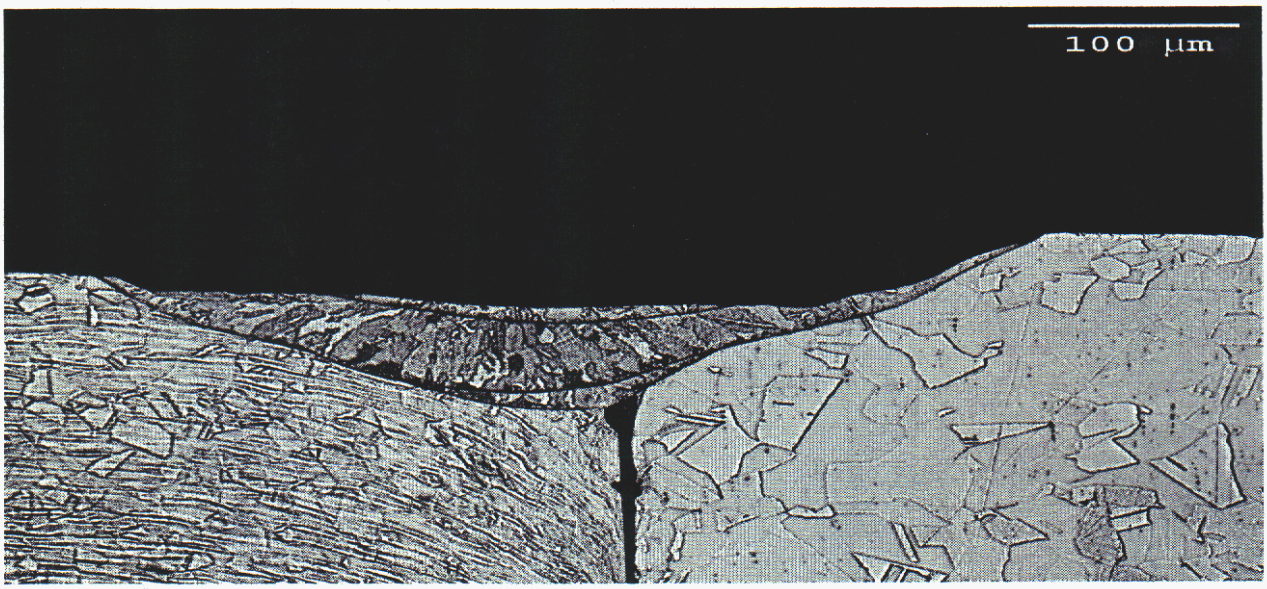

Figure 3.6 - Side 2 of Reservoir 5 Laser Weld Width = .018"; Max. Depth - .0041"; Eff. Depth - .0028"; Fusion Lines – 3. A small amount of root porosity is shown here.

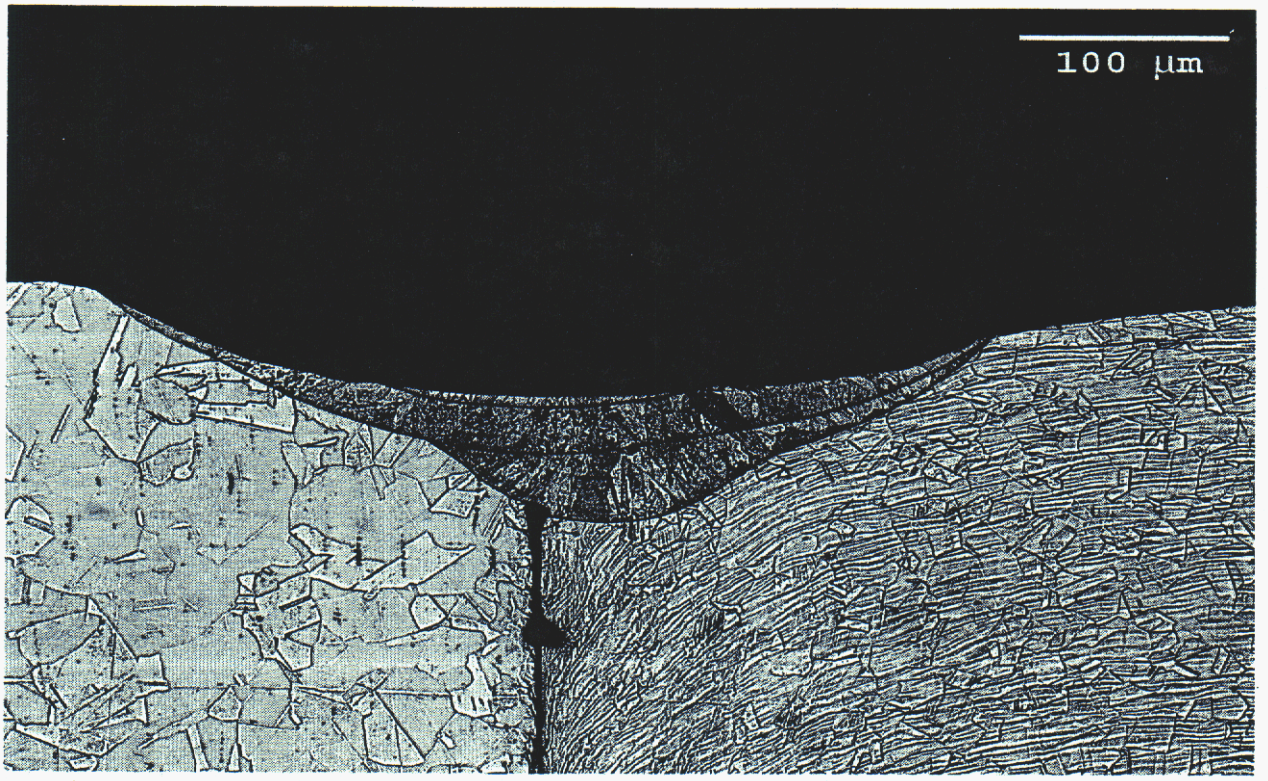

Figure 3.7 – Side 1 of Reservoir 6 Laser Weld Width = .018"; Max. Depth - .0030"; Eff. Depth - .0025"; Fusion Lines – 3. The weld is slightly off-center of the weld joint.

Figure 3.8 – Side 2 of Reservoir 6 Laser Weld Width = .020"; Max. Depth - .0052"; Eff. Depth - .0033"; Fusion Lines – 4. A large amount of root void/porosity can be seen in this cross-section.

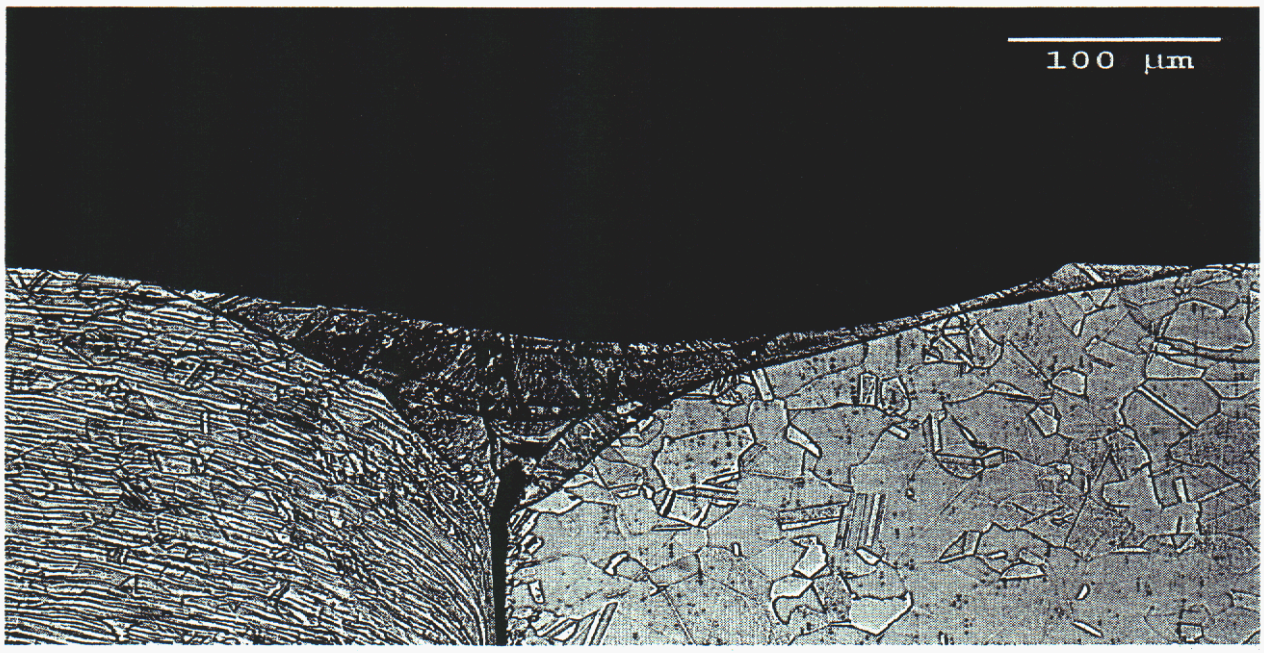

Figure 3.9 – Side 1 of Reservoir 12 Laser Weld Width = .021"; Max. Depth - .0030"; Eff. Depth - .0030"; Fusion Lines – 3 – 5. The number of fusion lines reflects a power ramp down area.

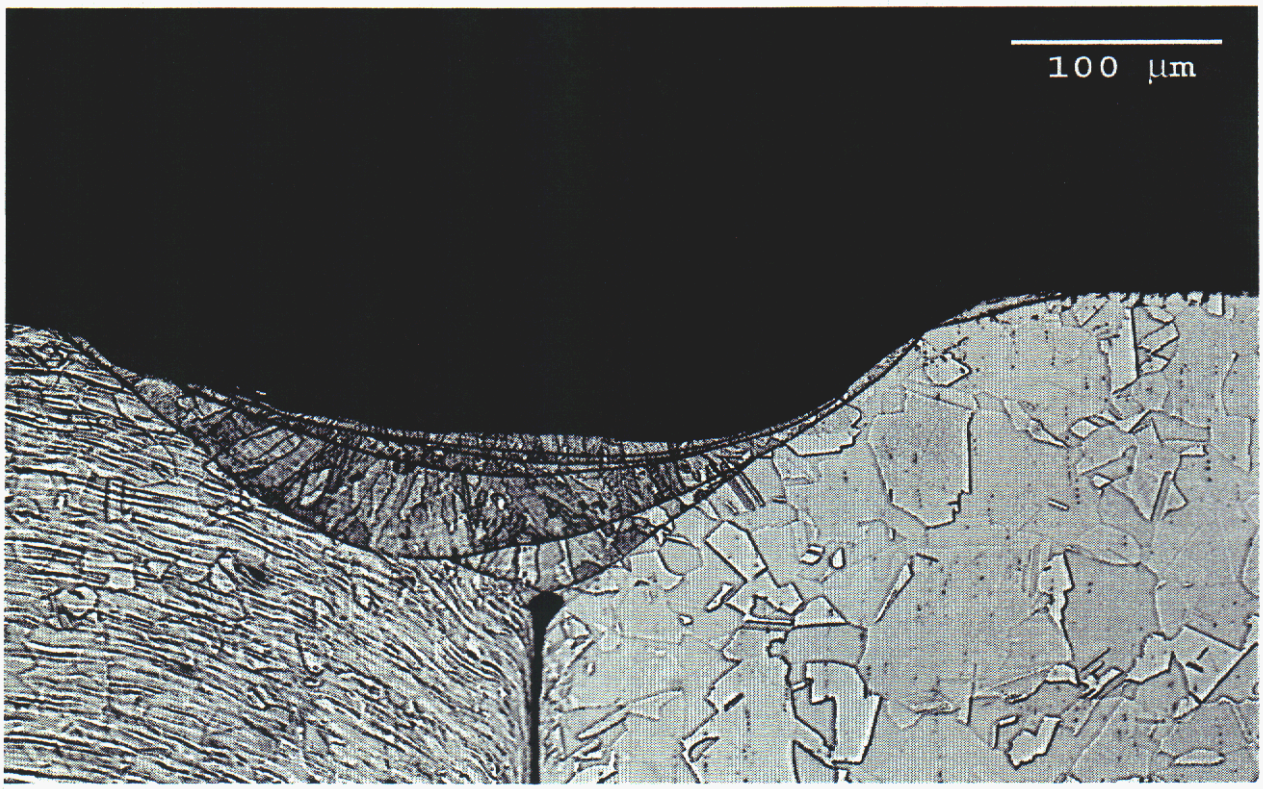

Figure 3.10 – Side 2 of Reservoir 12 Laser Weld Width = .019"; Max. Depth - .0044"; Eff. Depth - .0036"; Fusion Lines – 6. The number of fusion lines reflects a power ramp down area. Some root void/porosity can also be seen in this cross-section.

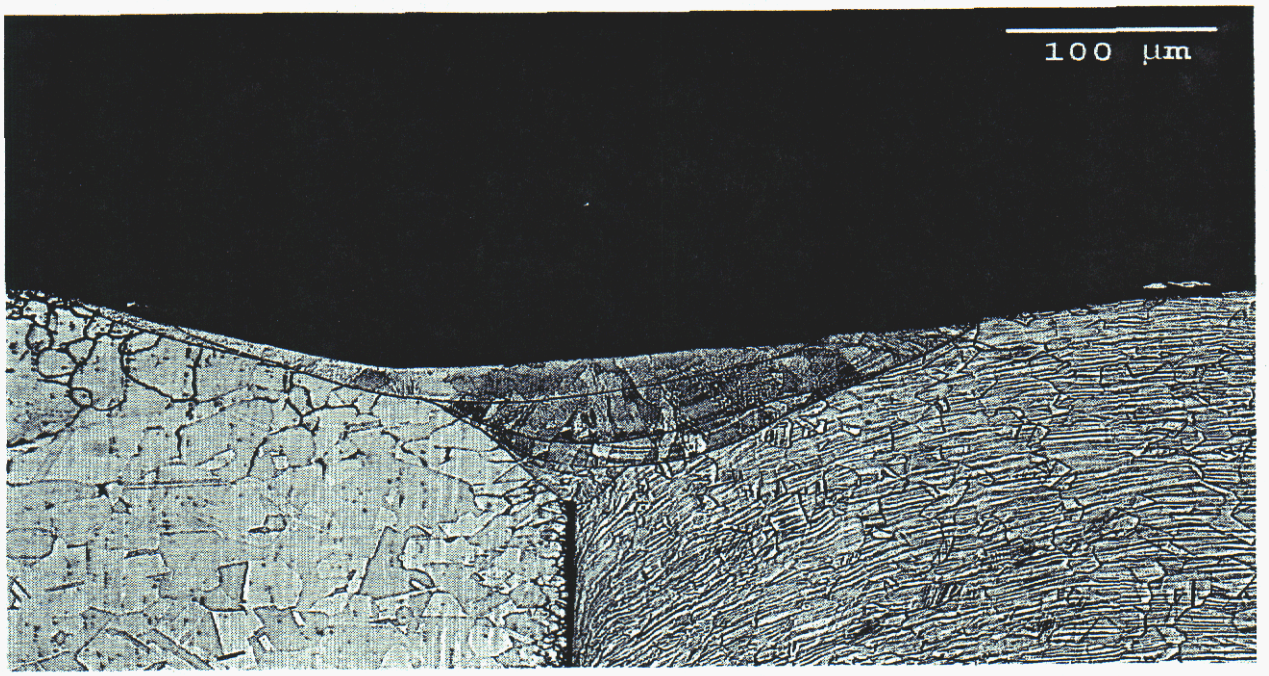

Figure 3.11 – Side 1 of Reservoir 14 Laser Weld Width = .018"; Max. Depth - .0038"; Eff. Depth - .0038"; Fusion Lines – 4. Areas of sensitization can be seen on the top & side of the case.

Figure 3.12 – Side 2 of Reservoir 14 Laser Weld Width = .017"; Max. Depth - .0041"; Eff. Depth - .0036"; Fusion Lines – 5. Areas of sensitization can be seen on the top & side of the case.

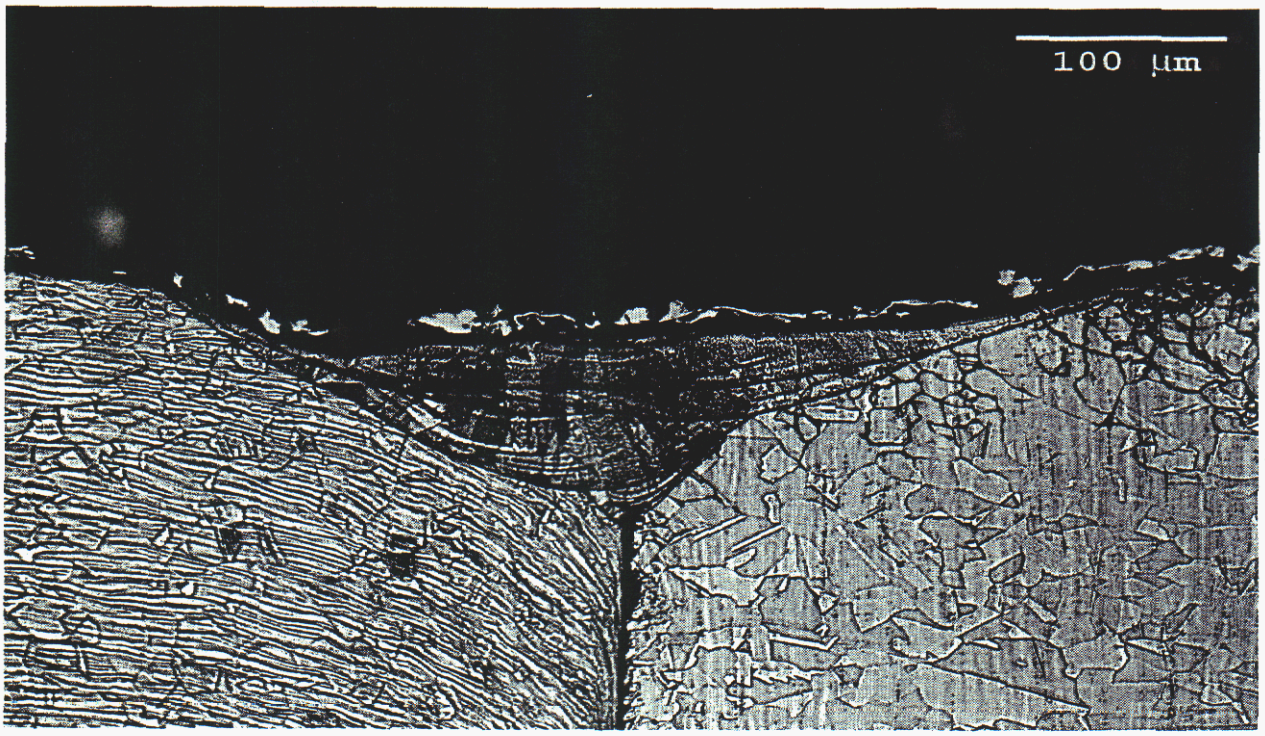

Table 3.1. Compilation of critical weld characteristics for each reservoir.

Sample #	Weld X-Section	Width	Maximum Depth	Effective Depth	# Of Fusion Lines
1	1	0.017	0.0041	0.0036	3
	2	0.019	0.0041	0.0041	5
2	1	0.018	0.0036	0.0033	6
	2	0.018	0.0036	0.0030	3
3	1	0.020	0.0059	0.0050	3
	2	0.018	0.0038	0.0033	3
4	1	0.020	0.0059	0.0041	4
	2	0.018	0.0038	0.0033	4
5	1	0.020	0.0044	0.0044	4
	2	0.018	0.0041	0.0028	3
6	1	0.018	0.0030	0.0025	3
	2	0.020	0.0052	0.0033	4
7	1	0.019	0.0030	0.0027	3
	2	0.018	0.0038	0.0036	3
8	1	0.018	0.0041	0.0027	3
	2	0.020	0.0050	0.0044	4
9	1	0.020	0.0030	0.0030	3
	2	0.018	0.0036	0.0036	3
10	1	0.018	0.0044	0.0038	3
	2	0.018	0.0038	0.0038	4
11	1	0.019	0.0041	0.0041	4
	2	0.021	0.0056	0.0047	3
12	1	0.021	0.0030	0.0030	3-5
	2	0.019	0.0044	0.0036	6
13	1	0.018	0.0046	0.0044	5
	2	0.019	0.0059	0.0056	3
14	1	0.018	0.0038	0.0038	4
	2	0.019	0.0044	0.0041	5
15	1	0.017	0.0030	0.0027	4
	2	0.018	0.0047	0.0047	3
16	1	0.019	0.0053	0.0038	4
	2	0.019	0.0036	0.0036	5
17	1	0.017	0.0030	0.0022	3
	2	0.017	0.0044	0.0044	3
18	1	0.017	0.0031	0.0024	3
	2	0.020	0.0050	0.0050	4
19	1	0.020	0.0056	0.0056	4
	2	0.018	0.0038	0.0030	3
20	1	0.017	0.0030	0.0030	3
	2	0.020	0.0071	0.0059	4
Average		**0.0186**	**0.0043**	**0.0037**	
STD Dev.		**0.0012**	**0.0010**	**0.0009**	

Discussion

1. The condition of the welds from a metallurgical perspective was very good. There were no cracks, porosity or other anomalies found in the main portion of the weld bead in any of the cross-sections. Also, the grain structure was very good and similar to that of the base metal.

However, there was a possible effect of a minor amount of electrolyte (moisture) being present in the weld joint prior to welding. In the root (bottom of the weld) of reservoir 1 - welds 1 and 2, reservoir 3 - weld 1, reservoir 4 - weld 1, reservoir 5 - weld 2 and reservoir 6 - weld 2, to list several of the examples, there was a minor amount of root porosity.

In all likelihood, this root porosity can be attributed to small amounts of moisture being vaporized. This vapor created a bubble-shaped void in the root weld metal. Alternatively this amount of root porosity could be attributed to weld metal shrinkage that can sometimes occur in these type welds.

Regardless of the cause, the root porosity that was found is considered minor. However, it could be a future production concern. Problems could arise if variations occur either in the fit of the end plate into the case or in the electrolyte level that allows sufficient moisture to be present such that it creates a blowout.

2. The welding parameters (power, pulse length & rate, travel speed, etc.) used to make the welds appear to be good. These parameters are producing a very consistent conductive (low depth to width ratio) weld. As shown in Table 3.1, the average width of the welds is .0186" with a standard deviation (STD) of .0012"; the average maximum penetration depth is .0043" with an STD of .001"; and the effective depth (leak path) average is .0037" with an STD of .0009".

However, there is margin in the parameters to reduce the heat input by lowering the welding pulse rate or increasing the welding speed. The photomicrographs, Figures 3.3 and 3.7 for example, show 3-5 solidification lines in the cross-section of each weld. This number of solidification lines is an indication that there is too much overlap, by as much as 75%, of the individual pulses. Normal overlap is around 50% and results in 2-3 solidification lines. Too much overlap adds unnecessary heat input to the weld & reservoir.

3. There were no signs of sensitization as a result of welding in any of the cases. However, in one case, reservoir 14, sensitization of the reservoir is evident on the container itself and well removed from the weld areas. This is seen in Figures 3.11 and 3.12. Based on the location of the areas of sensitization, this undoubtedly occurred prior to welding. Since we do not have information regarding the production process up to this

point, we cannot definitively say when the sensitization occurred. However, one likely production process to consider is the glassing step. Furthermore, an assessment of the effect that these areas have on corrosion processes should be considered. It should be reemphasized that the welding of this sensitized base metal is unaffected by the prior sensitization, and in fact this weld is as good as any of the other nineteen reservoirs.

4. Two reservoirs, 2 and 12, have six fusion lines in one of the weld sections. This number of fusion lines indicates that the sectioning was in a ramping up or ramping down region of the weld. In a ramp up/down the power of the laser is raised or lowered in a series of incremental changes to or from the required weld power level. There were no anomalies found in these welds.

5. There were no signs of degradation of the welds due to the electrolyte in the reservoir.

Conclusions and Recommendations

1. Overall metallurgical weld quality was very good.

2. With regards to the weld strength, no mechanical testing was performed. However, if the .003" - .005" penetration is acceptable based on past performance of the units, no additional parameter development is needed to increase the weld strength via increased penetration.

3. It is recommended that the weld parameters need to be adjusted to reduce the pulse-to-pulse overlap from ~75% to 50% to reduce the heat input. Reduction in the amount of overlap will not affect the penetration depth but will lower the excess heat input.

4. It is recommended that the end plate geometry and weld be changed. If the present weld strength, based on .003" - .005" penetration, is sufficient for unit performance, the end plate thickness can be reduced to .005" instead of the .020" thickness. Reducing the thickness to .005" will enable the plug to be stamped so that it can form a cap rather than a plug. The cap outer diameter should be slightly smaller in diameter than the case as shown in Figure 3.13.

The seal weld can then be made around the edge of the cap producing a meltdown type fillet weld. This type of weld is easy and results in a low-stress joint. This type of weld will eliminate the 'coalescence' problem when there is a gap in the 'butt' weld (plug/case). Also, it will reduce the effect of electrolyte in the root of the joint. There should not be any electrolyte present as the weld is being made to the outer portion of the end of the case rather than the inner portion where the electrolyte is present.

This option provides the opportunity of being able to increase the amount of electrolyte in the reservoir by ~15% when the end plate thickness is reduced. The increase can be seen in the calculations shown with Figure 3.13. This additional electrolyte may be beneficial to battery performance.

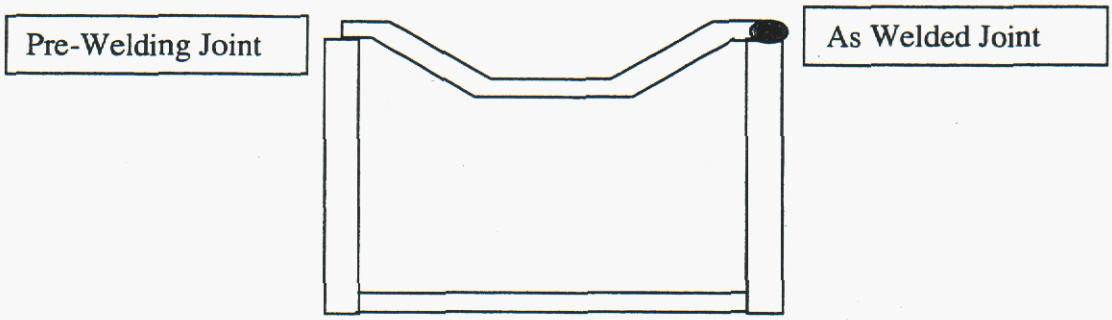

Figure 3.13. Proposed Endplate to Case Weld

By reducing the endplate thickness from .020" to .005" the interior volume of the reservoir can be increased by approximately 15%, according to the calculations below.

OD of Reservoir =	.21"
ID of Reservoir =	.16"
Case Wall Thickness =	.023"
Present Depth of Electrolyte = (Based on bottom of endplate)	.083"
Additional Electrolyte from Thinner Endplate	.098"

$$\text{Volume} = \pi r^2 h$$

$$\text{Present Volume} = (3.14)\,(.08")^2(.083") = .0017\ \text{in}^3$$

$$\text{New Volume} = (3.14)\,(.08")^2(.098") = .0020\ \text{in}^3$$

$$\text{Additional Volume} = .003/.017 = \sim 17\%$$

Allowing for a little less electrolyte, a 15% increase is possible.

Acknowledgements

Garry Bryant, Alice Kilgo and Robert Wright were responsible for the preparing and photographing the metallographic sample.

20. Appendix H

Executive Summary

Executive Summary

Analytical Investigation of $AlCl_3/SO_2Cl_2$ for Fuze Reserve Batteries

Todd M. Alam, David R. Tallant, Timothy J. Boyle

The fundamental chemical behavior of the electrolyte $AlCl_3/SO_2Cl_2$ system for the ARDEC Self-Destruct Fuze Reserve Battery Project was investigated using a variety of analytical tools including infrared absorption (FTIR), Raman, and ^{27}Al NMR spectroscopy. From these investigations, it was determined that all electrolyte samples, either the so-called "commercial electrolyte" synthesized from commercial precursors at Sandia National Laboratories (SNL) or the "KDI electrolyte" supplied by KDI, possessed the same chemical species in solution; however, there are differences in the relative concentrations of these species. This variation was attributed to the different extent of aging, concentration, and storage temperature, each of which controls the kinetics of this complex reaction system. FTIR studies revealed that very little water (<20 ppm) is present in as-received (or prepared) neat SO_2Cl_2, the commercial electrolyte or the KDI electrolyte. Raman spectroscopic studies showed that $SO_2(g)$ and $Cl_2(g)$ are present in a quasi-equilibrium with SO_2Cl_2. However, in solutions containing $AlCl_3$, the amount of $SO_2(g)$ is much lower, apparently because of a reaction with $AlCl_3$. The ^{27}Al NMR experiments show the presence of 4 tetrahedrally (T_d) bound Al-species in the electrolyte, the major peak of which is consistent with $[AlCl_3]_2$, an equilibrium product of $AlCl_3$ in solution. The other three minor species are complexes with SO_2Cl_2 described below. Single crystal X-ray diffraction studies revealed that an adduct formed at low temperatures which was identified as $[Cl_2Al(\mu\text{-}O_2SCl)]_2$. Chemical investigations indicate that this adduct can reversibly eliminate/insert SO_2. Bands believed to be associated with the adduct species, $[Cl_2Al(\mu\text{-}O_2SCl)]_2$, are present in Raman spectra of unaged SO_2Cl_2 solutions containing $AlCl_3$, but they disappear by the end of two weeks of aging. The ^{27}Al NMR studies found that the concentration of the major Al species, $[AlCl_3]_2$, diminished with time and temperature, while the concentration of the minor Al species increased. Again, for the minor species, the Al is Td coordinated, but the chemical shifts argue for an increase in the degree of oxygen coordination. Further, over time it was noted that the electrolyte solutions gel or precipitate with increasing aging time (3 months or more). Raman spectroscopic studies show this gel or precipitate has a component that is consistent with $SOCl_2$. Combined, these data imply the adduct may be transformed to a polymeric species with Al-O-Al bonds coordinated by $SOCl_2$. Hydrolysis has been eliminated as a mechanism since both the ^{27}Al NMR and Raman investigations reveal that water does not alter the number, or concentration, of the electrolyte's chemical species. At higher temperatures (120 °C) the gelation or precipitation occurs rapidly (< 2 weeks conversion is complete). In summary, the attached scheme is a representation of the chemistry elucidated from this study. It appears that while storing the electrolyte at low temperature may result in a precipitate, identified as the adduct $[Cl_2Al(\mu\text{-}O_2SCl)]_2$, this may be preferred since it will prevent the formation of the polymeric species during additional aging, but, upon warming above room temperature, the formation of this adduct is reversible and will not effect the overall capacity of the electrolyte. At higher temperatures and extended aging periods, a gel or

precipitant will irreversibly form and ultimately this will inhibit the flow characteristics (and therefore the functionality) of the electrolyte.

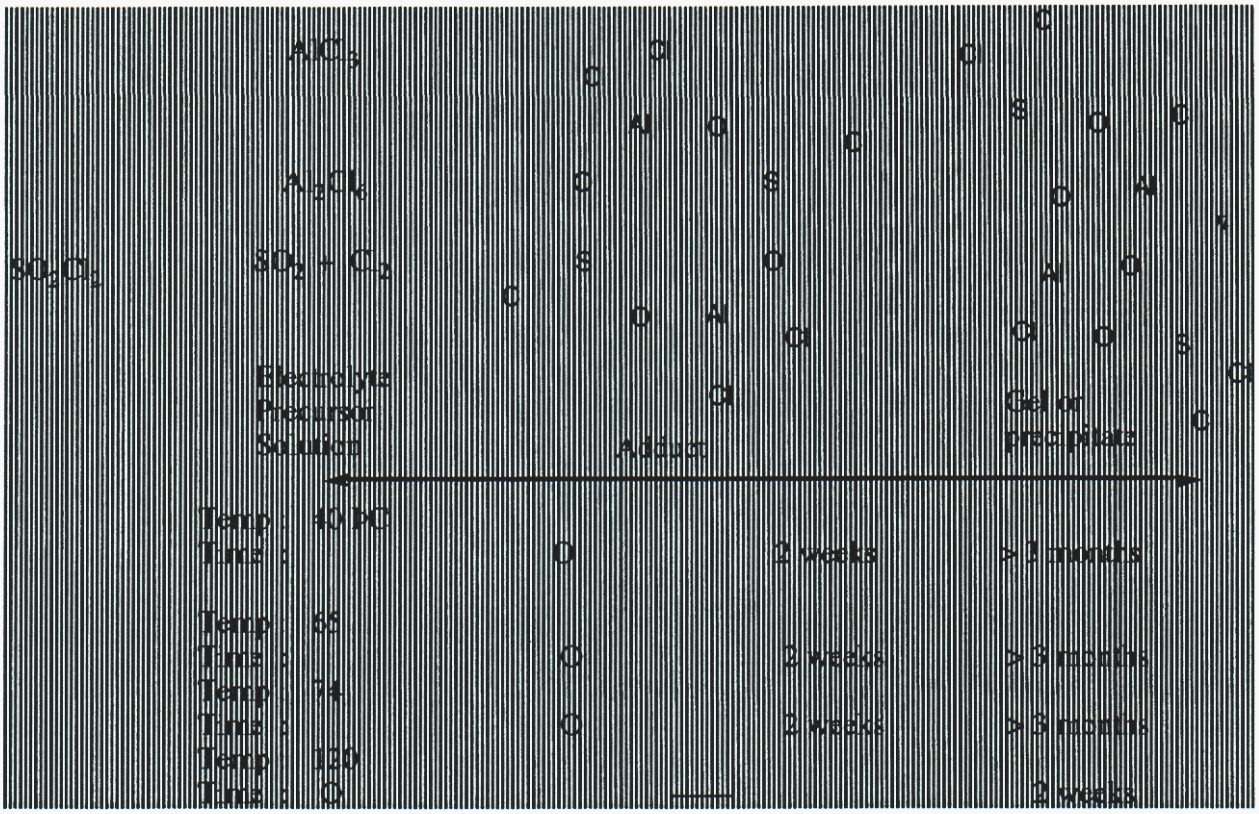

21. Appendix I

Data Collection Information for **1.**

$[AlCl_2(\mu\text{-}O)_2SCl]_2$

Code: TJB116

Experimental

A colorless crystal was mounted on a thin glass fiber using fluorolube. The crystal, which was mounted from a pool of fluorolube, was then immediately placed under a liquid N_2 stream on a Bruker AXS diffractometer. The radiation used was graphite monochromatized Mo Kα radiation (λ=0.71073 A). The lattice parameters were optimized from a least-squares calculation on ~500 centered reflections. Lattice determination and data collection were carried out using SMART Version 5.054 software. Data reduction was performed using SAINT+ 6.02 (7/13/99) software. Structure solution was performed using SHELXTL 5.1 (10/29/98) software. The structure refinement was performed using XSHELL 4.1 (11/08/2000) software. The data was corrected for absorption using the program SADABS within the SAINT+ package. Data collection parameters are given in Table 1.

Structure Solution and Refinement

The structure was solved in the space group P-1 using Direct methods. This solution yielded the entire molecule with the Cl atoms properly identified. Subsequent refinements enabled proper identification of Al, S, and O atoms. The final refinement included anisotropic thermal parameters on all atoms, and converged to R1=0.0294 and R2w=0.0732.

Table 1. Crystal data and structure refinement for [AlCl2(u-O)2SCl]2.

Identification code	tjb116s
Empirical formula	Al2 C16 O4 S2
Formula weight	394.78
Temperature	168(2) K
Wavelength	0.71073 A
Crystal system, space group	Triclinic, P-1

Unit cell dimensions

a = 6.188(7) A	alpha = 94.202(17) deg.
b = 7.351(8) A	beta = 106.616(16) deg.
c = 7.816(8) A	gamma = 109.251(15) deg.
Volume	316.0(6) A^3

Z, Calculated density	1, 2.074 Mg/m^3
Absorption coefficient	1.810 mm^-1
F(000)	192
Crystal size	.11 x ? x .34 mm
Theta range for data collection	2.77 to 25.70 deg.
Limiting indices	-7<=h<=7, -8<=k<=8, -9<=l<=9
Reflections collected/unique	2434 / 1199 [R(int) = 0.0235]
Completeness to theta = 25.70	99.2 %
Absorption correction	SADABS
Refinement method	Full-matrix least-squares on F^2
Data / restraints / parameters	1199 / 0 / 64
Goodness-of-fit on F^2	1.076
Final R indices [I>2sigma(I)]	R1 = 0.0294, wR2 = 0.0732
R indices (all data)	R1 = 0.0371, wR2 = 0.0768
Largest diff. peak and hole	0.433 and -0.339 e.A^-3

Table 2. Atomic coordinates (x 10^4) and equivalent isotropic displacement parameters (A^2 x 10^3) for [AlCl2(u-O)2SCl]2. U(eq) is defined as one third of the trace of the orthogonalized Uij tensor.

	x	y	z	U(eq)
				A
l(1)	2939(1)	8017(1)	11563(1)	23(1)
S(1)	3863(1)	7537(1)	7728(1)	25(1)
O(1)	3820(3)	7677(3)	9637(2)	31(1)
O(2)	5814(3)	9379(3)	7692(2)	29(1)
Cl(1)	4622(1)	6720(1)	13551(1)	33(1)
Cl(2)	-812(1)	7169(1)	10891(1)	37(1)
Cl(3)	771(1)	7971(1)	6379(1)	49(1)

Table 3. Bond lengths [A] and angles [deg] for [AlCl2(u-O)2SCl]2.

Al(1)-O(1)	1.769(2)
Al(1)-O(2)#1	1.790(3)
Al(1)-Cl(2)	2.086(3)
Al(1)-Cl(1)	2.0867(17)
S(1)-O(2)	1.496(2)
S(1)-O(1)	1.496(2)
S(1)-Cl(3)	2.043(2)
O(2)-Al(1)#1	1.790(3)
O(1)-Al(1)-O(2)#1	103.75(9)
O(1)-Al(1)-Cl(2)	112.20(8)
O(2)#1-Al(1)-Cl(2)	106.55(7)
O(1)-Al(1)-Cl(1)	108.10(10)
O(2)#1-Al(1)-Cl(1)	109.14(9)
Cl(2)-Al(1)-Cl(1)	116.32(6)
O(2)-S(1)-O(1)	106.28(11)
O(2)-S(1)-Cl(3)	102.61(11)
O(1)-S(1)-Cl(3)	102.09(9)
S(1)-O(1)-Al(1)	161.63(13)
S(1)-O(2)-Al(1)#1	143.44(12)

S
ymmetry transformations used to generate equivalent atoms:
#1 -x+1,-y+2,-z+2

Table 4. Anisotropic displacement parameters (A^2 x 10^3) for [AlCl2(u-O)2SCl]2. The anisotropic displacement factor exponent takes the form:

$$-2\pi^2 [h^2 a^{*2} U11 + \ldots + 2 h k a^* b^* U12]$$

	U11	U22	U33	U23	U13	U12
Al(1)	22(1)	27(1)	22(1)	7(1)	8(1)	9(1)
S(1)	30(1)	24(1)	23(1)	4(1)	10(1)	11(1)
O(1)	34(1)	37(1)	24(1)	7(1)	13(1)	12(1)
O(2)	31(1)	29(1)	28(1)	6(1)	13(1)	11(1)
Cl(1)	41(1)	39(1)	25(1)	13(1)	10(1)	21(1)
Cl(2)	22(1)	42(1)	47(1)	8(1)	11(1)	11(1)
Cl(3)	31(1)	68(1)	43(1)	18(1)	3(1)	17(1)

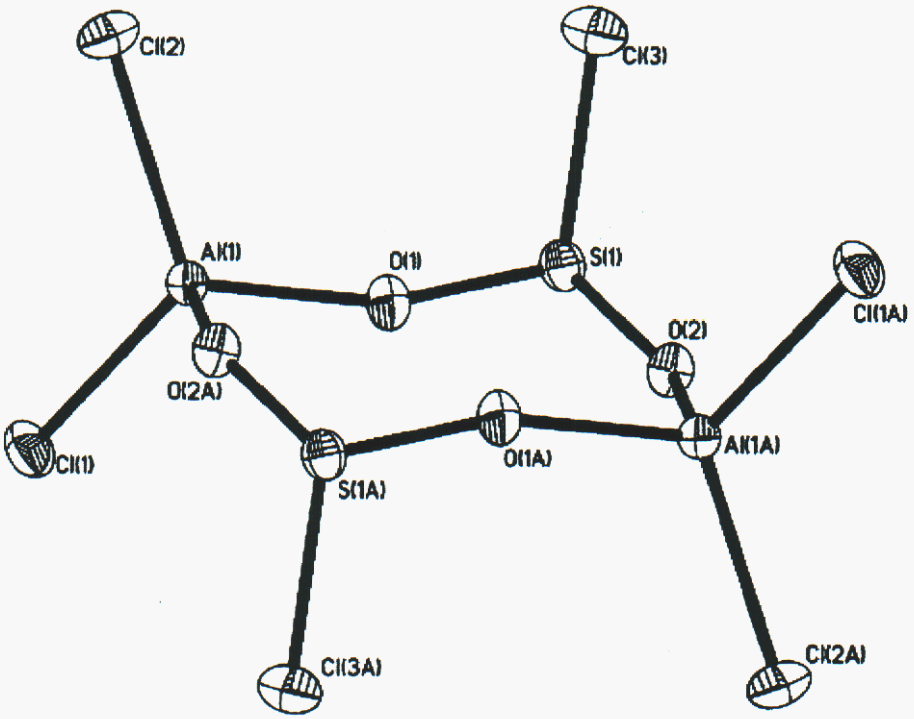
Cl(2)
Cl(3)
Al(1)
O(1)
S(1)
Cl(1A)
O(2)
O(2A)
Cl(1)
S(1A)
O(1A)
Al(1A)
Cl(3A)
Cl(2A)

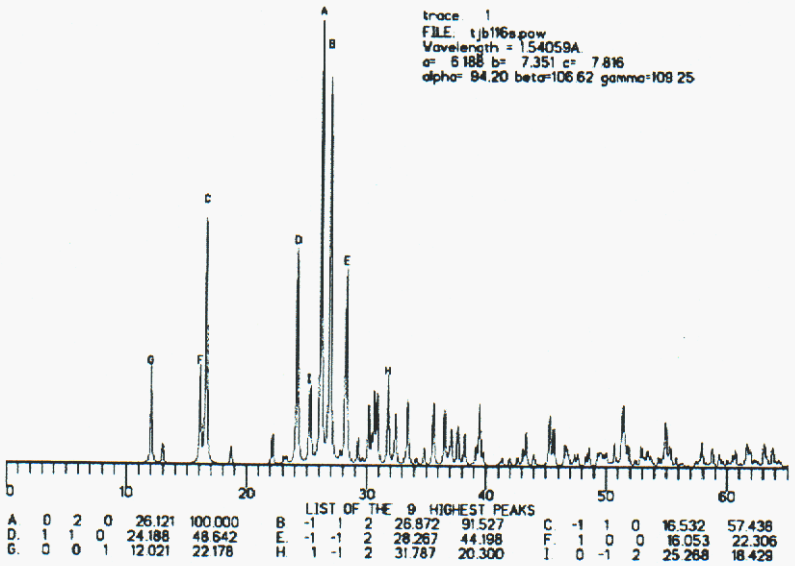
trace 1
FILE: tjb116a.pow
Wavelength = 1.54059A
a= 6.188 b= 7.351 c= 7.816
alpha= 84.20 beta=106.62 gamma=109.25
A
B
C
D
E
F
G
H
I
0
10
20
30
40
50
60
LIST OF THE 9 HIGHEST PEAKS
A 0 2 0 26.121 100.000
B -1 1 2 26.872 91.527
C -1 1 0 16.532 57.438
D. 1 1 0 24.188 48.642
E. -1 -1 2 28.267 44.198
F. 1 0 0 16.053 22.306
G. 0 0 1 12.021 22.178
H 1 -1 2 31.787 20.300
I 0 -1 2 25.268 18.429

14. Distribution List

Personnel	Group	Mail stop	Copies
Timothy J. Boyle	01846	1349	2
Nancy Clark	02522	0614	5
Louis A Malizia, Jr.	02525	0613	2
David Ingersoll	02521	0613	4
Paul Butler	02522	0614	2
David R. Tallant	01822	1411	4
Todd M. Alam	01811	0888	3
Brian Cherry	01811	0888	1
Roger Clough	01811	0888	1
Mark A. Rodriguez	01822	1411	2
Jun Liu	01846	1411	2
William F. Hammetter	01846	1349	1
Dick Salzbrenner	01801	0889	1
Michael Cieslak	01800	0887	1
Central Technical Files	8945-1	9018	1
Technical Library	9616	0899	2